

Combined short and long-term heat storage with sodium acetate trihydrate for solar combi-systems

Gerald Englmaier



**Combined short and long-term heat storage with sodium acetate
trihydrate for solar combi-systems**

Gerald Englmaier

PhD Thesis



28/02/2019

Department of Civil Engineering

Supervisors:

Jianhua Fan, Associate Professor, Department of Civil Engineering, Technical University of Denmark

Simon Furbo, Associate Professor, Department of Civil Engineering, Technical University of Denmark

Zhifeng Wang, Professor, Institute of Electrical Engineering, Chinese Academy of Sciences

Assessment Committee:

Toke Rammer Nielsen, Associate Professor, Department of Civil Engineering, Technical University of Denmark

Jørgen M. Schultz, Senior Sustainability Consultant, Steensen Varming Aps, Denmark

Wilhelmus G. J. van Helden, Group leader Thermal Energy Storage, AEE INTEC Institute for Sustainable Technologies, Austria

Combined short and long-term heat storage with sodium acetate trihydrate for solar combi-systems

Copyright: © 2019, Gerald Englmaier

Cover photos: *Gerald Englmaier*

Publisher: Department of Civil Engineering,

Technical University of Denmark,

Brovej, Building 118,

2800 Kgs. Lyngby, Denmark

ISBN: 9788778775078

ISSN: 1601-2917

Preface

This thesis was submitted as fulfilment of the requirements for the Degree of Doctor of Philosophy at the Department of Civil Engineering, Technical University of Denmark. The thesis is the result of research on **combined short and long-term heat storage with sodium acetate trihydrate for solar combi-systems**.

Part of the studies has been carried out at the Chinese Academy of Sciences, Institute of Electrical Engineering (CAS IEE) in Beijing, China.

This research was funded by the PhD program of the Sino-Danish Center for Education and Research (SDC). The work was also supported by the European Commission (Grant Agreement N_295568) as part of the Seventh Framework Programme of the European Community for Research, Technological Development and Demonstration Activities under the “Collaborative Project” funding scheme through the COMTES consortium.

This page is intentionally left blank.

Acknowledgement

My journey started ten years ago, after working for several years as a young agricultural engineer, when I decided to study renewable energy technologies. Although this decision was driven by the perspective of utilizing biomass for heat and power generation, I learned soon that utilization of solar energy, in particular the storage of solar energy, is one of the key challenges for sustainable development worldwide. During this time, I met and learned from a number of brilliant researchers, which I would like to thank:

The group for appropriate technologies at the Vienna University of Technology, led by Robert Wimmer, for their support during my internship and for the inspiration for research they gave me within further collaboration during my Master studies.

The team of the Austria Solar Innovation Center at the Upper Austrian University of Applied Sciences, for introducing me to research on solar energy. In particular I would like to thank Bernhard Zettl, who supported me as teacher, supervisor, and later as colleague and mentor in research on compact thermal energy storage.

The organizers of SolNet courses on solar energy (led by Ulrike Jordan) for the possibility to meet young researchers from various European countries. This was a great motivation for me to enter a PhD study.

During my PhD project at DTU Byg I had the pleasure to learn from the leading researches on solar energy in Denmark. I would like to thank the whole solar group, former members and visiting fellows: Elsabet Nielsen, Jakob Brinkø Berg, Junpeng Huang, Jie Deng, Ioannis Sifnaios, Janne Dragsted, Bengt Perers, Mark Dannemand, Adam Rasmus Jensen, Weiqiang Kong, Fabienne Salaberry, Yakai Bai, Gang Wang, Federico Bava, Zhiyong Tian and Daniel Tschopp for the nice intellectual discussions and “hyggelig” social gatherings. I would like to address my special thanks to my supervisors Simon Furbo and Jianhua Fan for their critical review of my work, for the opportunity to conduct research in Denmark and in China and (most important) to always find time for talks when needed.

I would like to thank the research technicians Claus Aagaard and Troels Kristensen for their practical support in building up experiments and recording data. In this context, I would also like to thank Jakob Brinkø Berg for the excellent collaboration in installing measurement equipment, discussions on system control strategy and for programming. I would also like to thank Yiliang Jiang and Andrea Hernandez Pedrero for their help for experimental work.

I would like to thank the colleagues from TU Graz, Hermann Schranzhofer and Christoph Moser, for their collaboration. It was a delight to work together and to bridge a distance of about 900 km with interesting discussions during project meetings and joint dissemination work. Further, I would like to thank our project partners from Nilan A/S for the good collaboration. I would also like to thank all co-authors of papers for the excellent collaboration and for their permission to reuse text and figures in this thesis.

I would like to express my gratitude to Professor Zhifeng Wang, Ming Yang and all other researches from my host institute in China, CAS IEE. Thank you for the friendly welcome, for involving me in social events and for explaining me the Chinese culture. I would also like to thank the PhD students at CAS IEE for their great help in organizing life in Beijing, in particular Choi, Mengdi, Carl and Yakai Bai.

Of course, my stays in China would not have been possible without the support of my SDC colleagues (Bozidar, Elizabeth, Martin). Thank you for joining forces in finding apartments and our way to the city of Beijing.

I need to thank all my dear friends in Denmark, which helped me to settle down in this country.

To my wonderful family: Thank you for supporting me on every step on my way. You never questioned my decision to conduct research in Denmark and you provide me with the security of a second home in Austria. And to Kathrine: You gave me extra power to finalize this work. Thank you for your support and for reminding me from time to time that life is more than just research.

Gerald Englmaier

Kgs. Lyngby, February 28th, 2019.

Gerald Englmair,

Ing., MSc.

Technical University of Denmark

Department of Civil Engineering

DK-2800 Kongens Lyngby

Abstract

With increasing utilization of energy from renewable sources, solar heating has become a promising technology for reducing fossil fuel consumption in the building sector. Due to the mismatch of solar energy resources and the demand patterns of single family houses in central and northern Europe, long-term heat storage is essential for solar combi-systems that cover hot water supply and heating with a solar fraction larger than 50%.

Therefore, a concept for combined short and long-term heat storage utilizing stable supercooling of sodium acetate trihydrate (SAT) was examined for its applicability in combi-systems. The concept enables use of the sensible heat capacity of liquid SAT composites while preserving its heat of fusion at room temperature. Thus, loss-free heat storage is achieved, which can be utilized for on-demand supply in periods without solar irradiation available. The research objective was to develop a heat storage prototype and to test it in a full scale laboratory solar heating system. Findings were used in system simulation as well as to design inexpensive heat storage units.

SAT composites containing thickening agents and liquid polymers were identified to be suitable heat storage materials. Their heat of fusion, available in supercooled state at 20 °C, was determined to be in the range of 205–216 kJ/kg. Material tests showed that SAT composites in glass bottles supercool down to temperatures of about –24 °C, and crystallized in the range of –9 °C to –15 °C in contact with steel. Thus, devices employing mechanical seed crystal injection and local cooling by Peltier elements or evaporating carbon dioxide were applicable to initiate crystallization of supercooled SAT composites when heat was on demand.

Four heat storage units, each containing 200–220 kg of SAT composites, and a 735 L water tank formed a segmented heat storage prototype. A system control strategy was developed for charging the heat storage with an array of 22.4 m² (aperture) evacuated tubular solar collectors and to enable hot water supply and space heating. System demonstration with heat demand patterns of a Passive House in Danish climate and verified control parameters proved applicability of the heat storage concept. System simulations for a solar heating system for the house with a yearly heat demand of 3977 kWh with optimized component specifications and 1 m³ of SAT composites and 22.4 m² (aperture) collector area resulted in a yearly solar fraction of 71%. The system was found to perform best with SAT composite volumes below 1 m³, heat storage units of 200 L, a 0.6 m³ water tank and with collector areas of 12.8–22.4 m² with a collector tilt of 70°. Inexpensive tank-in-tank units, built with standard components of water stores, could be applied in the system. Laboratory tests showed that their heat transfer properties were sufficient for hot water supply and space heating with liquid SAT composite, whereas discontinuous discharge would be needed during solidification.

For the first time, a solar heating system utilizing stable supercooling of SAT composites was demonstrated. This work will provide reference for solar heating in energy efficient buildings with solar fractions above 70%. Further studies are needed to elucidate optimal application of the heat storage concept for different climates considering different collector types, improved heat storage units and electric grid stabilization via power-to-heat conversion.

Resumé

Med en stigende udnyttelse af vedvarende energi i byggesektoren, har solenergi udviklet sig til en lovende teknologi til at reducereforbruget af fossile brændstoffer. I Central- og Nordeuropa er der et misforhold mellem den sæsonmæssige tilgængelighed af solenergi og energiefterspørgslen i enkeltfamiliehuse. Derfor er det essentielt at udvikle solvarme-kombianlæg med langtidslagring af varme, der kan dække varmtvandsforsyningen og rumopvarmning med en dækningsgrad over 50%.

Således er et koncept til anvendelse i kombianlæg undersøgt, der kombinerede kort- og langtidslagring af varme ved brug af stabil underafkøling af natriumacetat trihydrat (SAT). Konceptet muliggør brugen af varmfylden af flydende SAT blandinger, imens smeltevarmen af SAT ved stuetemperatur bibeholdes. Herved er det muligt tabsfrit at lagre varme, som kan bruges ved behov i perioder uden solstråling. Formålet var, at udvikle en prototype på et varmelager og teste det i et solvarmeanlæg i laboratoriet. Resultaterne blev brugt i systemsimuleringer såvel som til at designe billige varmelagerenheder.

SAT blandinger, der indeholder fortykningsmidler og flydende polymerer, blev fundet egnede til konceptet. Deres smeltevarme, tilgængelig i underafkølet tilstand ved 20 °C, blev bestemt til 205–216 kJ/kg. Undersøgelser viste at SAT blandingerne i glasbeholdere underafkøler til temperaturer omkring –24 °C og til rækkevidden af –9 °C til –15 °C ved kontakt med stål. Således kan mekanisk tilføjelse af krystaller, lokal afkøling ved Peltier elementer eller fordampning af kuldioxid, benyttes til at initiere krystallisering af underafkølet SAT blandinger ved behov for varme.

Et solvarmeanlæg bestående af 22,4 m² vakuumrørsolfangere og et varmelager med fire varmelagerenheder, hver indeholdende 200–220 kg SAT blanding, og en 735 L vandtank blev afprøvet. Anlægget blev afprøvet i laboratoriet med et årligt simuleret varmebehov på 3977 kWh svarende til varmebehovet for et Passivt Hus i Dansk klima. Simuleringsberegninger viste at anlægget med en optimal udformning, blandt andet med en solfangerhældning på 70°, kan nå en årlig dækningsgrad på 71%. Billige tank-i-tank varmelagre, bygget med standard komponenter af vandtanke, kan med fordel bruges i anlægget. Laboratorietests viste at deres varmeoverføringsegenskaber var tilstrækkelige for varmtvandsforsyning og rumopvarmning med flydende SAT blandinger, hvorimod diskontinuert afladning af varmelageret vil være nødvendig under storkning.

Dette er den første demonstration af et solvarmeanlæg, der udnytter stabil underafkøling af SAT blandinger. Dette arbejde vil bidrage som basis for videreudvikling af langtidsvarmelagre og af solvarmeanlæg til bygninger med årlige dækningsgrader over 70%. Fremtidige studier er nødvendige for at bestemme optimale udformninger af solvarmeanlæg med langtidsvarmelagre til forskellige klimaer. Undersøgelserne bør inkludere forskellige solfangertyper, forbedrede varmelagerenheder og stabilisering af det elnettet via kraft-til-varme konvertering.

摘要

随着可能生能源的应用和推广，太阳能光热利用正逐步成为一种建筑能源领域至关重要的化石能源替代技术。由于太阳能资源禀赋和建筑用能需求不匹配的矛盾，在欧洲中部和北部地区应用时，迫切需要大力发展长周期储能技术，以满足建筑采暖和生活热水用能需求，实现50%以上的高太阳能保障率。

因此，本文基于三水醋酸钠溶液稳定过冷特性，提出了一种长周期短周期结合的蓄热技术，并对技术适应性进行了深入研究。该蓄热技术的原理是，充分利用液态材料显热储能特性的同时，在室温环境下保存相变材料潜热能，以达到长期、无损耗储能的目的；在太阳能匮乏的冬季，存储的潜热能可根据需求释放并加以利用。本文旨在开发储能器模型，并在全尺寸太阳能采暖示范系统上进行测试。基于实验研究，进一步开展系统仿真建模和经济性储能器的研发工作。

经过增稠剂和液体高分子材料改性后，三水醋酸钠是一种非常合适的相变储能材料，在20℃室温条件下稳定过冷时保存的潜热能在205 - 216kJ/kg范围内。实验室研究表明，三水醋酸钠在玻璃容器中可稳定过冷到约-24℃，在铁制容器中可稳定过冷到-9 - -15℃。因此，在有热需求时，需要采用相变激活技术激发相变材料结晶，如直接加入晶粒或采用Peltier器件、液态二氧化碳蒸发进行局部低温冷却。

本文构建了一个模块化储能器模型，由一个735升的蓄热水箱和四个相变材料储能器模块组成，单个相变材料储能器模块材料装填量为200 - 220kg。储能器模型经22.4m²（透光面积）的太阳能集热器进行加热，以满足生活热水和采暖用能需求。示范系统模拟丹麦气候环境下被动房的用能特性。本文开发了系统控制策略，确定了主要控制参数，验证了蓄热系统的适应性。模拟分析结果表明，对于一个年用热负荷为3977kWh的建筑，若采用1m³的相变材料和22.4m²的集热器，系统的太阳能保障率是71%。最佳的系统参数是相变材料容积小于1m³，单个蓄热体体积200升，蓄热水箱体积0.6m³，集热器面积12.8-22.4m²，安装倾角70°。系统中相变材料储能器可由标准化水箱部件组装而成，以降低储能器造价，提高系统经济性。实验研究表明，储能器具有足够高的换热系数，通过结晶过程中间断的可控的放热操作，可充分满足生活热水和建筑采暖用能负荷。

本文开创性地研究示范了一种基于三水醋酸钠稳定过冷特性的太阳能供热系统。研究结果为低能耗建筑技术中大规模应用推广太阳能采暖，实现太阳能保障率的大幅提升（大于70%），提供了技术参考。后续有必要继续深入研究不同气候特征区域、不同集热器类型对系统性能的影响，改进优化储能器的设计，并结合电热转换技术和控制技术，研究大规模应用时对电网稳定性的贡献。

List of papers

This thesis is based on the following publications:

- [1] W. Kong, M. Dannemand, J. B. Johansen, J. Fan, J. Dragsted, **G. Englmair**, and S. Furbo, “Experimental investigations on heat content of supercooled sodium acetate trihydrate by a simple heat loss method,” *Solar Energy*, vol. 139, pp. 249–257, 2016.
- [2] **G. Englmair**, Y. Jiang, M. Dannemand, C. Moser, H. Schranzhofer, S. Furbo, and J. Fan, “Crystallization by local cooling of supercooled sodium acetate trihydrate composites for long-term heat storage,” *Energy and Buildings*, vol. 180, pp. 159–171, 2018.
- [3] **G. Englmair**, C. Moser, S. Furbo, M. Dannemand, and J. Fan, “Design and functionality of a segmented heat-storage prototype utilizing stable supercooling of sodium acetate trihydrate in a solar heating system,” *Applied Energy*, vol. 221, pp. 522–534, 2018.
- [4] **G. Englmair**, S. Furbo, W. Kong, M. Dannemand, J. Fan, and Z. Wang, “Performance Evaluation of a Demonstration System with PCM for Seasonal Heat Storage: Charge with Evacuated Tubular Collectors,” *ISES Solar World Congress - IEA SHC International Conference on Solar Heating and Cooling for Buildings and Industry 2017, Proceedings*, 2017
- [5] **G. Englmair**, W. Kong, J. B. Berg, S. Furbo, and J. Fan, “Demonstration of a solar combi-system utilizing stable supercooling of sodium acetate trihydrate for heat storage”, submitted to *Applied Thermal Engineering*, in review.
- [6] **G. Englmair**, C. Moser, H. Schranzhofer, J. Fan, and S. Furbo, “A solar combi-system utilizing stable supercooling of sodium acetate trihydrate for heat storage: numerical performance investigation”, *Applied Energy*, vol. 242, pp. 1108–1120, 2019
- [7] **G. Englmair**, S. Furbo, M. Dannemand, and J. Fan, “Experimental investigation of a tank-in-tank heat storage unit utilizing stable supercooling of sodium acetate trihydrate”, submitted to *Applied Thermal Engineering*, in review.

Publications that were part of the PhD study, but not included in the thesis:

- [8] **G. Englmair**, M. Dannemand, J. B. Johansen, W. Kong, J. Dragsted, S. Furbo, and J. Fan, “Testing of PCM Heat Storage Modules with Solar Collectors as Heat Source,” *Energy Procedia*, vol. 91, pp. 138–144, 2016.
- [9] **G. Englmair**, C. Moser, S. Furbo, H. Schranzhofer, and J. Fan, “Combined short- and long-term heat storage with Sodium Acetate Trihydrate for solar heat supply in buildings,” *Proceedings of the International Sustainable Energy Conference (ISEC) 2018*, pp. 617–618.
- [10] C. Moser, **G. Englmair**, H. Schranzhofer, and A. Heinz, “Simulation Study of a Novel Solar Thermal Seasonal Heat Storage System Based on Stable Supercooled PCM for Space Heating and Domestic Hot Water Supply of Single Family Houses,” *Appl. Mech. Mater.*, vol. 887, pp. 650–658, 2019.
- [11] J. B. Johansen, **G. Englmair**, M. Dannemand, W. Kong, J. Fan, J. Dragsted, B. Perers, and S. Furbo, “Laboratory Testing of Solar Combi System with Compact Long Term PCM Heat Storage,” *Energy Procedia*, vol. 91, pp. 330–337, 2016.
- [12] W. Kong, M. Dannemand, J. B. Berg, J. Fan, **G. Englmair**, J. Dragsted, and S. Furbo, “Experimental investigations on phase separation for different heights of sodium acetate water mixtures under different conditions,” *Appl. Therm. Eng.*, vol. 148, pp. 796–805, 2019.

Contents

| | |
|-----------------------|------|
| Preface..... | I |
| Acknowledgement..... | III |
| Abstract..... | VI |
| Resumé..... | VII |
| Chinese abstract..... | VIII |
| List of Papers..... | IX |

Part A: Summary

| | |
|---|----|
| 1. Introduction..... | 3 |
| 1.1. Background..... | 3 |
| 1.2. State of the Art..... | 4 |
| 1.2.1. Phase separation theory..... | 4 |
| 1.2.2. Sodium acetate trihydrate composites..... | 5 |
| 1.2.3. Crystallization theory..... | 6 |
| 1.2.4. Controlled initialization of SAT crystallization..... | 7 |
| 1.2.5. Heat stores utilizing stable supercooling of SAT..... | 7 |
| 1.3. Research objective..... | 9 |
| 2. Concept of combined short and long-term heat storage..... | 10 |
| 3. Material investigations..... | 13 |
| 3.1. Heat content of SAT composites in supercooled state..... | 13 |
| 3.2. Visual study of phase separation mechanisms..... | 15 |
| 3.3. Liquid polymeric solutions as additive..... | 17 |
| 3.4. Initialization of crystallization by local cooling..... | 19 |
| 3.5. Recycling and material handling..... | 22 |
| 4. System development..... | 23 |
| 4.1. Design..... | 23 |
| 4.2. PCM heat storage..... | 24 |
| 4.3. Control..... | 26 |
| 4.4. Demonstration..... | 27 |
| 4.5. Investigation of PCM units after system demonstration..... | 30 |
| 5. System simulation..... | 33 |
| 5.1. Method..... | 33 |

| | |
|--|----|
| 5.2. Sensitivity analysis | 34 |
| 5.3. Annual system performance | 35 |
| 6. Inexpensive heat storage units..... | 37 |
| 6.1. Tank-in-tank design | 37 |
| 6.2. Experimental method | 38 |
| 6.3. Performance | 39 |
| 7. Measurement uncertainty..... | 41 |
| 8. Conclusions..... | 45 |
| 9. Perspectives..... | 47 |
| 9.1. Material development..... | 47 |
| 9.2. Heat storage development..... | 47 |
| 9.3. System development..... | 48 |
| 9.4. Life cycle aspects | 49 |
| References..... | 51 |

Part B: Appended papers

- Paper 1:** Experimental investigations on heat content of supercooled sodium acetate trihydrate by a simple heat loss method
- Paper 2:** Crystallization by local cooling of supercooled sodium acetate trihydrate composites for long-term heat storage
- Paper 3:** Design and functionality of a segmented heat-storage prototype utilizing stable supercooling of sodium acetate trihydrate in a solar heating system
- Paper 4:** Evaluation of a Demonstration System with PCM for Seasonal Heat Storage: Charge with Evacuated Tubular Collectors
- Paper 5:** Demonstration of a solar combi-system utilizing stable supercooling of sodium acetate trihydrate for heat storage
- Paper 6:** A solar combi-system utilizing stable supercooling of sodium acetate trihydrate for heat storage: numerical performance investigation
- Paper 7:** Experimental investigation of a tank-in-tank heat storage unit utilizing stable supercooling of sodium acetate trihydrate

This page is intentionally left blank.

PART A: Summary

Nomenclature

Symbols

| | |
|------------|--|
| A | collector aperture area (m ²) |
| c_p | specific heat capacity (kJ/kg K) |
| C | energy storage capacity (kWh) |
| Δh | specific heat of fusion during solidification from supercooled state (kJ/kg) |
| ΔH | heat of fusion during solidification from supercooled state (kJ) |
| HXCR | heat exchange capacity rate (W/K) |
| I | inclination (°) |
| L | latent heat (kJ/kg) |
| Q | thermal energy, heat (kWh) |
| \dot{Q} | thermal power (kW) |
| T | temperature (°C) |
| \bar{T} | average temperature (°C) |
| ΔT | temperature difference (K) |
| u | Standard uncertainty (K, %) |
| V | volume (m ³) |
| \dot{V} | volume flow rate (L/min) |

Greek letters

| | |
|----------|------------------------------|
| ρ | density (kg/m ³) |
| σ | standard deviation (% , K) |

Abbreviations

| | |
|-----------------|---|
| E_{aux} | auxiliary heating element |
| amb | ambience |
| AMPS | 2-Acrylamido-2-methylpropane sulfonic acid |
| CI | confidence interval |
| CMC | carboxymethyl cellulose |
| CO ₂ | carbon dioxide |
| DHW | domestic hot water |
| EDTA | ethylenediaminetetraacetic acid |
| HTF | heat transfer fluid |
| LabVIEW | laboratory virtual instrument engineering workbench |
| PCM | phase change material |
| %wt. | percent of weight |
| SA | sodium acetate |
| SAT | sodium acetate trihydrate |
| SF | solar fraction |
| SH | space heating |
| TRNSYS | transient system simulation tool |
| X | measurand |
| X-gum | xanthan rubber |

1. Introduction

1.1. Background

In Europe, the energy consumption in buildings accounts for 40% of the total energy supply [1]. Since heating accounts for the largest share, a near-zero energy consumption is required by all new buildings as stated in the EU Energy Performance of Buildings Directive in 2010 [2] from 31st December 2020. With increasing utilization of energy from renewable sources, solar heating has become one of the most promising technologies for reducing fossil fuel consumption in the building sector. Due to the mismatch of solar energy resources and the demand patterns of thermal household services, efficient heat storage is pivotal [3].

To develop a well-performing solar heating system for space heating (SH) and domestic hot water (DHW) supply in buildings with compact heat storage, recent findings on solar combi-systems and long-term heat storage were applied.

Solar combi-systems

Solar combi-systems, consisting of a solar collector circuit and a heat storage, enables solar heat supply for SH and DHW in buildings [4]. A backup heating system is connected to the heat store to ensure continuous heat supply.

Research has focused on how a large solar fraction (SF) of heat supply (net utilized solar energy divided by SH and DHW demand) can be achieved. Energy-efficient building envelopes and optimal DHW supply temperatures are the basis for good system performance. The Danish code of practice for domestic water supply, DS 439 [5], recommends a hot water temperature of 45 °C as sufficient to fulfil comfort requirements. The optimal collector tilt required to optimize SF, depends primarily on latitude, it needs to increase, to best utilize solar irradiation during the heating season [6]. Detailed investigations were conducted on storage tanks in terms of discharge from different levels [7], inlet stratifiers [8], and degrees of stratification efficiency [9]. Thür [10] developed a compact system focused on minimizing temperature to reduce heat losses and to increase the efficiency of the solar collectors.

Overall, efficient heat storage has been identified as the key component for well-performing solar heating systems [11]. Long-term heat storage is necessary to cover heat demand with solar fractions higher than 50% in central and northern Europe. Water tanks have been used for this purpose [12], [13], but large storage volumes were necessary to compensate sensible heat losses.

Long-term heat storage concepts

[This section is based in part on Paper 6]

Research on novel materials and processes for more efficient heat storage over long periods have been collected and discussed in the International Energy Agency - Solar Heating and Cooling Task 42 on compact

thermal energy storage [14]. The following heat storage concepts have recently been tested for solar heating application:

Sorption systems with zeolites or composites of zeolite and salt as storage material can store solar heat during summer for heat supply in winter [15]. Open reactors have been demonstrated in laboratory scale [16]. Zettl et al. developed a process with solar air collectors for regeneration of zeolite pebbles [17], which can be utilized for heat supply via a rotating drum-reactor [18]. A closed sorption system in realistic system scale (33%), utilizing 12 m² of evacuated tube collectors for regeneration of 2 m³ zeolites and charge of a 660 L water tank was tested [19]. It achieved a solar fraction of 83.5% during laboratory testing with demand patterns of an Austrian single family house in winter. Evacuated tubular solar collectors can also be used for regeneration in a liquid sorption heat storage with sodium hydroxide [20], the concept was proved by Fumey et al. [21].

Sodium acetate trihydrate (SAT) is a phase change material (PCM) which has the ability to supercool stably to ambient temperatures while preserving its heat of fusion [22]–[24]. After melting and heating to a temperature above 77 °C sensible heat can be discharged until room temperature is reached. Subsequently, the crystallization of the supercooled solution can be initiated by seed crystal injection [25] and the preserved heat of fusion will be released as it crystalizes. This heat storage concept dates back to initial research in the late 1920s [26] and was later identified to enable a more efficient solar heat supply of low-energy buildings in summer and transitional seasons [27]. A numerical model for a solar combi-system for the Danish climate with an ideal seasonal PCM heat storage with SAT has been used to calculate the possible annual solar fraction of a solar heating system in a low-energy house [28], [29]. It was calculated that solar fractions in the range of 80–100% could be achieved when the PCM storage volume is subdivided into segments. Individual control with respect to charging, discharging and the initialization of solidification would make it possible to utilize a small storage volume to match small heat demands while conserving the remaining energy.

1.2. State of the Art

1.2.1. Phase separation theory

As an incongruently melting salt hydrate, SAT suffers from phase separation over repeated heating and cooling cycles and over long periods in supercooled state. The solubility of SAT in water was experimentally measured by Green [30] and Sidgwick and Jentle [31], their data was utilized in a phase diagram, see Figure 1, published by Araki et al. [32]. The solubility of sodium acetate (SA) in the corresponding crystal water at 58 °C (the melting point of SAT) is not high enough to dissolve all anhydrous salt. To avoid phase separation, Furbo and Svendsen [33] suggested adding extra water to the salt hydrate. The necessary amount is related to the solubility curve of SAT. Based on its molar ratio, SAT contains 39.7%wt. of crystal water. At least 5.3%wt. of water has to be added to avoid phase separation when melted SAT is supercooled

to room temperature (293–298 K), when a maximum SA-concentration of about 55% can be dissolved in water.

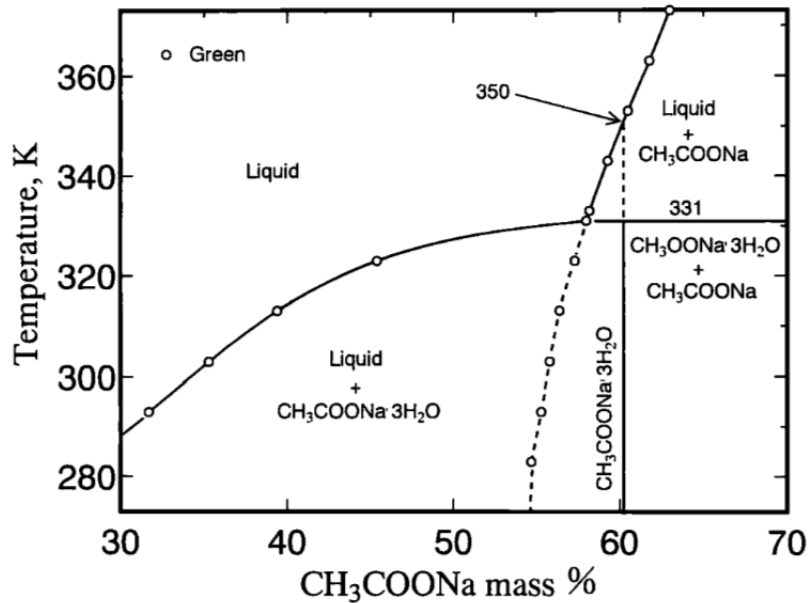


Figure 1. Phase diagram of SA-water mixtures [32].

Phase separation is caused by the density difference between SA and saturated salt water. Mechanical stirring and rotating storage devices can be applied to hold the suspension of unsolved salt. When SA molecules settle down at the bottom of a SAT volume and a leaner salt-water solution remains in the upper part of the volume, full reformation of SAT crystals can no longer be achieved [34]. This effect reduces the material's heat storage capacity. Kong et al. [35] investigated phase separation for different heights of SA-water mixtures under different conditions. Water content in certain positions, especially at the bottom of containers, was identified as a key factor. However, even with extra water added to the samples, repeated heating and cooling resulted in phase separation. Tests without mechanical stirring of SA-water mixtures in prototype storage units [36], [37] showed a decrease in heat capacity after a number of storage cycles.

1.2.2. Sodium acetate trihydrate composites

[This section is based in part on Paper 2]

SAT (chemical formula CH₃COONa·3H₂O) is a salt hydrate with a melting point of 58 °C. SAT is attractive for domestic heat storage applications because of its relatively high heat of fusion (264 kJ kg⁻¹ [24]), its high density, its rather high specific heat capacities in both liquid and solid phases [32], the low price (industrial purity typically below 0.5 €/kg) and its non-toxic properties. The density of solid SAT in a closed sample that has solidified from supercooled state has been determined to be 1.24–1.28 kg L⁻¹ [38]. Reviews on thermal energy storage with PCM [39], [40] therefore list SAT among the most suitable salt hydrates

identified for domestic applications.

To overcome phase separation, thickening agents were used to increase the viscosity of the liquid solution and avoid sodium acetate (SA) to settle at the bottom of storage units. Carboxymethyl cellulose (CMC) and Xanthan rubber were investigated by Cabeza et al. [41] and Dannemand et al. [15] for this purpose. Liquid polymer solutions have also been identified as additives able to reduce the phase separation effect by increasing the solubility of SAT in the liquid solution [43]. A thermal conductivity in the range of 0.5–0.65 W/mK was found for solid SAT with CMC and Xanthan rubber as additives [42]. As for most PCMs, this is considered as a limitation for heat transfer.

For utilization of SAT composites in domestic heat stores, volumes of several cubic meters are needed for solar heating systems. For economic reasons chemically pure SAT cannot be used. Instead, SAT of food grade (European standard 262i) from industrial supply [44] was applied during the PhD project.

1.2.3. Crystallization theory

[This section is based in part on Paper 2]

Nucleation is the birth of new crystal nuclei. Mullin [45] defined two kinds of nucleation: either from solution (primary nucleation) or in the presence of existing crystals (secondary nucleation).

For primary nucleation, Mullin defined the formation of crystal nuclides from a homogenous fluid as homogeneous nucleation. This is not a common event, because supercooled solutions are probably seeded without our knowledge by the presence of atmospheric dust during material preparation. Because the rate of nucleation of a solution can be affected considerably by the presence of such impurities, this so-called heterogeneous nucleation leads to “spontaneous” nucleation events, the mechanisms of which are not fully understood [46]. A supersaturated solution nucleates much more readily when crystals of the solute are already present or added [45]. Seed crystal injection into a supercooled SAT solution is a secondary nucleation method, which has proved reliable even at low degree of supercooling [32].

As soon as stable nuclei have been formed in a supersaturated solution, they begin to grow into crystals of visible size. Dietz et al. [47] and Munakata and Nagata [48] have measured the crystal growth rate of supercooled SA-aqueous solutions in tubes. The growth rates were found to be dependent on the solution concentration and the degree of supercooling. Measured and calculated crystal growth rates have been evaluated by Ma et al. [49], but parameters for the degree of supercooling or models for crystal growth of melted SAT composite material are still not available.

1.2.4. Controlled initialization of SAT crystallization

[This section is based in part on Paper 2]

To use stable supercooling of SAT heat stores reliable nucleation mechanisms are needed. Several possibilities were tested in laboratory-scale experiments, fewer in setups with volumes of 100 L or more:

- Adding seed crystals is a common method of initializing the crystallization in SAT in laboratory-scale setups [25], [32], [47]. Crystallization with seed crystals works as long as the crystals do not melt and become inactive [50].
- Triggering crystallization using ultrasonic waves has been reported as successfully tested [51], but other researchers [52] have stated that it failed.
- Local cooling of SAT in liquid phase down to its crystallization temperature (primary, heterogeneous nucleation). Previous studies have shown that SAT will spontaneously crystallize between $-15\text{ }^{\circ}\text{C}$ and $-25\text{ }^{\circ}\text{C}$ [25]. Evaporation of liquid CO_2 in a 100 ml chamber, welded to the outside of flat prototype heat storage units, was reported to initialize crystallization of supercooled SAT [37]. A setup with a double-element Peltier device reached $-30\text{ }^{\circ}\text{C}$ and may be able to trigger crystallization [53].

1.2.5. Heat stores utilizing stable supercooling of SAT

[This section is based in part on Paper 3]

Various designs have been developed for domestic heat storage units using PCMs. The performance of heat exchangers with large PCM volumes in metal containers with an internal bundle of tubes has been studied by López-Navarro et al. [54]. Shell-and-tube heat exchangers [55] and macro encapsulated PCM in water vessels [56] have been tested for sensible-latent heat storage. Moreno et al. [57] have investigated the corrosion of metal and metal alloy containers in contact with PCMs.

Experiments with rectangular and cylindrical PCM containers with SA-water and CMC composites have been reported by Zhou and Xiang [58]. Their results show that more stable supercooling could be achieved with longer charging periods (to ensure the full melting of all SAT crystals), a relatively low cooling rate, and a lower inner surface roughness in PCM containers. The bending of rough metal surfaces might be an uncontrolled activation mechanism during cooling [50].

In previous work at the Technical University of Denmark (DTU), various heat storage designs [59], each based on a flat box with SAT and additives as the heat storage material, have been tested. A functioning design was identified as consisting of either steel or stainless steel units with room for PCM expansion in the box. Its thermal behaviour was then further investigated by using numerical models [60], [61]. Figure 2 a presents a photo of the final design. Its characteristics with SAT as the heat storage material were investigated by Dannemand et al. under laboratory conditions [37]. It was proved and documented that the stable supercooling of SAT composites in flat boxes and cylindrical vessels [36] is enabled by: a) avoiding pressure changes in the PCM container (e.g. by using a membrane expansion vessel), b) smooth inner container surfaces, and c) heating up the whole material volume to a minimum temperature of ~ 77 °C. Later, the concept of stable supercooling has been successfully applied in cylindrical prototype heat storage [36], see Figure 2 b, and in the mantle of hot water tanks [62].

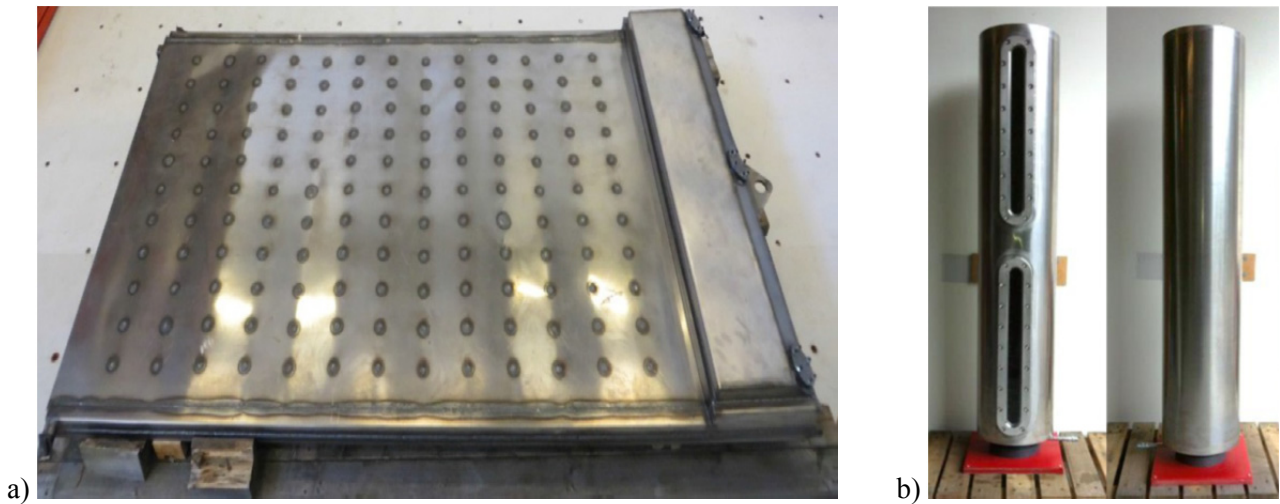


Figure 2. Heat storage prototypes a) Flat design [37]; b) Cylindrical design [36].

1.3. Research objective

As illustrated by Figure 3 the aim of the PhD project was to develop a solar combi-system utilizing stable supercooling of SAT, supported by further development of SAT composites and heat storage units. Thus, multidisciplinary methods were used for technology development.

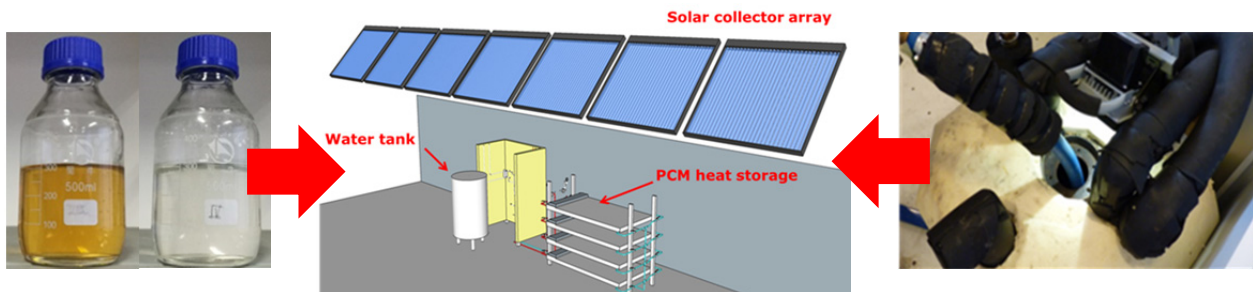


Figure 3. System development supported by material investigations and component tests.

In this thesis, the heat storage concept, material investigations, system development, system simulation and potential improvements have been subsequently elaborated. The following research hypotheses were defined as goals for technology development:

- SAT, extra water and liquid polymers forms a composite enabling convective heat transfer in liquid state and can supercool to room temperature without phase separation occurring
- Heat of fusion can be utilized on-demand for building heat supply, utilizing seed crystal injection or local cooling in heat storage units containing SAT composites
- Heat storage units with heat transfer limitations can be integrated in a solar combi-system by means of appropriate hydraulic design and control
- Utilization SAT composites in a solar combi-system will result in high solar fractions of domestic hot water and space heating supply in a Danish Passive House
- Inexpensive heat storage units utilizing stable supercooling of SAT composites can be built with standard components of water heat stores

Hypotheses a–b were examined in laboratory experiments and by later application of developed SAT composites and nucleation devices in heat storage prototypes. Hypothesis c was examined by a system development with previously developed flat heat storage units [37]. System simulation with a model of the developed solar combi-system was used to verify hypothesis d. Finally, a tank-in-tank heat storage unit was built and tested for its heat transfer properties to verify hypothesis e.

The summary of this work includes the methods applied and main results from research papers, as well as additional investigations which were not included in papers.

2. Concept of combined short and long-term heat storage

Quinnel and Davidson [63] investigated utilization of absorption and desorption of water in aqueous calcium chloride. They found that the sensible heat capacity of the salt solution can be utilized without disturbing the stored reaction potential of a concentrated solution. In this way, absorption reaction enthalpy would be available after utilizing stored sensible heat, which is potentially advantageous for domestic heat storage applications.

Analogous, stable supercooling enables utilization of the sensible heat capacity of liquid SAT while preserving the heat of fusion. Long-term heat storage is achieved by storing heat of fusion at ambient temperature, while the sensible heat capacity of SAT is used for short-term heat storage. For domestic application, the energy storage capacities are calculated as follows:

- a) The temperature-dependent specific heat capacities of pure SAT have been determined by Araki et al. [32]. They found Equation 1, for the solid state (30–58 °C), and Equation 2, for the liquid state (30–80 °C), respectively, where $T_{absolute}$ is the temperature of SAT in K:

$$c_{p,solid} \left(\frac{kJ}{kg K} \right) = 0.811 + 4.06 * 10^{-3} * T_{absolute} \quad (1)$$

$$c_{p,liquid} \left(\frac{kJ}{kg K} \right) = 1.56 + 4.27 * 10^{-3} * T_{absolute} \quad (2)$$

Assuming sensible heat storage is utilized from 30–80 °C in liquid state, the short-term energy storage capacity of SAT ($C_{SAT \text{ short-term}}$) is 177 kJ/kg.

- b) The long-term energy storage capacity of SAT ($C_{SAT \text{ long-term}}$) is depending on its heat of fusion. The latent heat of fusion (L) at 58 °C has been determined by differential scanning calorimetry to be 264 kJ/kg [24]. The released heat of fusion during solidification from supercooled state (Δh) is temperature-dependent. It is based on L, reduced by the difference of c_p in between liquid and solid states during supercooling. By employing Equations 1–2 and a supercooling temperature of 20 °C, Δh is resulting in 215 kJ/kg. Experimental investigations on Δh of SAT composites have been conducted with a simple heat loss method and are presented in Section 3.1.
- c) As a result, the total energy storage capacity of pure SAT is 392 kJ/ kg.

Figure 4 presents the specific energy contents of pure SAT over temperature. For passivation of nucleation seeds, the liquid phase of SAT is required to exceed 77 °C [32] in order to supercool to ambient temperature.

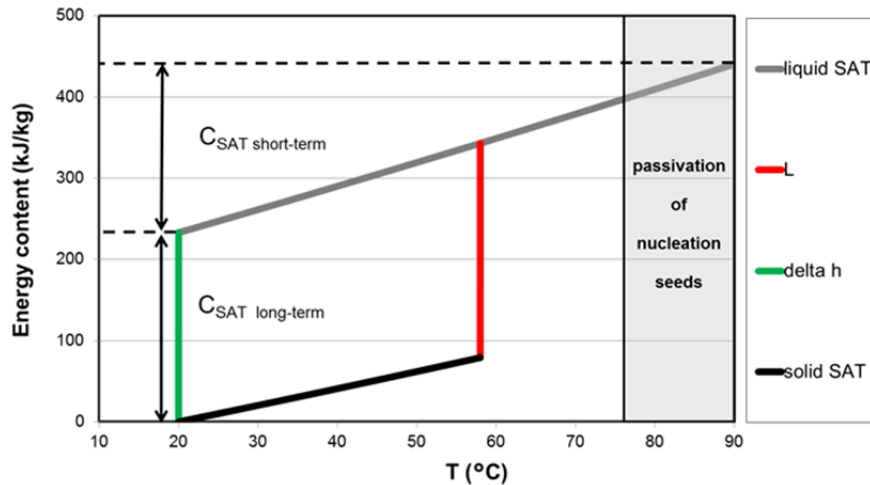


Figure 4. Specific energy contents of SAT (Paper 7).

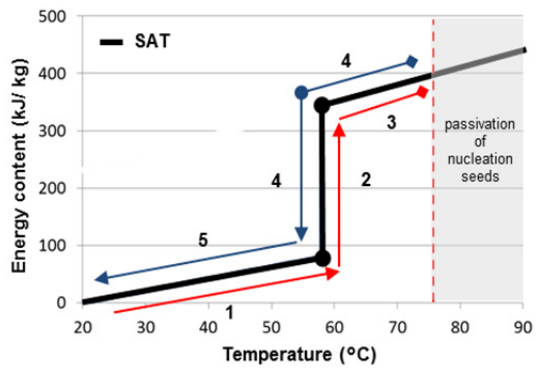
[The following section is based on Paper 3]:

SAT composites in closed containers can be utilized for heat storage with or without stable supercooling. In the temperature range of 20–90 °C, SAT has an average specific heat capacity of 2.9 kJ/kgK in liquid and supercooled state [32] and an average density of 1280 kg/m³ in liquid phase [64]. This results in a specific, volumetric heat capacity of 3.71 kJ/LK – a value close to that of water (4.18 kJ/LK [65]). The thermal conductivity of liquid SAT (~0.4 W/mK) [32]) is lower than for water (~0.64 W/mK [66]) in the mentioned temperature range. These material properties make SAT also suitable for sensible heat storage applications.

Operation states are defined by the specific energy content and temperature of SAT at atmospheric pressure. Figure 5 shows the three different storage principles (a–c) which can be combined for the short-term and long-term storage of heat:

- Its high heat-storage capacity at melting point is utilized (as latent heat storage) when no passivation of nucleation seeds is achieved during the charging of SAT composites.
- Most of the heat of fusion can be transferred to a lower temperature level, reducing heat losses to the environment. When SAT composites supercool at ambient temperature, no heat loss due to heat transfer to the environment occurs until crystallization is initialized. Only changes within the material composition, such as phase separation, can reduce the potential of conserved heat.
- When SAT composites remain in liquid state below their melting point, it is possible to utilize sensible heat storage without phase change.

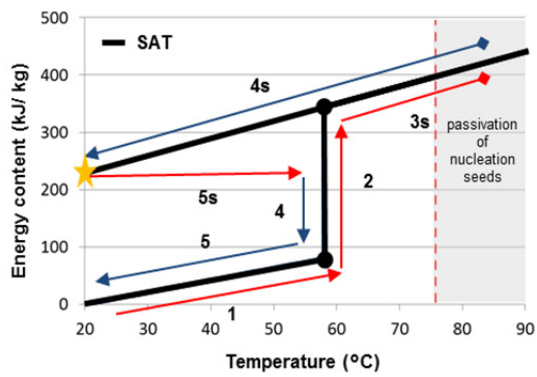
Storage principles (a) and (c) are relevant for short heat-storage periods (hours, days), while the utilization of stable supercooling (b) is beneficial for long-term storage (weeks, months).



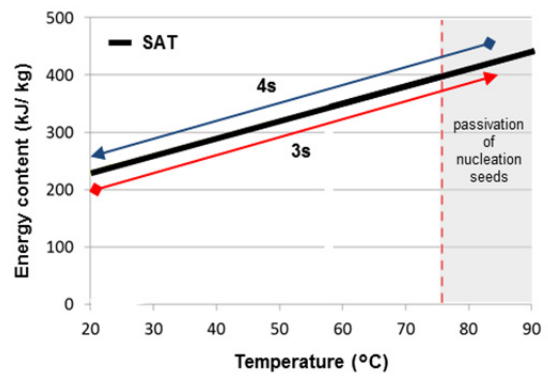
a) Heat of fusion and sensible heat capacity without supercooling

Heat storage operation states:

- 1 Charge of solid material
- 2 Melting
- 3 Charge of liquid material, nucleation seeds remain
- 3s Charge of liquid material, passivated seeds
- 4 Discharge from liquid state with solidification
- 4s Discharge of liquid material without solidification
- 5 Discharge of solid material
- 5s Initialization of crystallization



b) Heat of fusion and sensible heat capacity with stable supercooling



c) Sensible heat capacity of supercooled, liquid phase

Figure 5. Heat storage operation states with SAT composites (Paper 3).

3. Material investigations

3.1. Heat content of SAT composites in supercooled state

[This section is based in part on Paper 1]

The aim was to identify well-performing SAT composites in terms of heat of fusion released during solidification from supercooled state. A wide variety of SAT composites with extra water, thickening agents, solid and liquid polymers as additives have been tested for their values on Δh .

Figure 6 a shows the temperature development of a SAT composite sample, where the heat content was evaluated as the thermal energy dispersed to the ambience (green area). Similar glass jars, see Figure 6 b, containing different SAT composites of approximately the same volume, placed in well-insulated boxes, were tested in parallel. The heat loss coefficient (W/K) of the glass jar was determined with reference tests containing hot water. Glass jars were equipped with three thermocouples (Type TT) on their outside surfaces; the ambient temperature was measured outside the box.

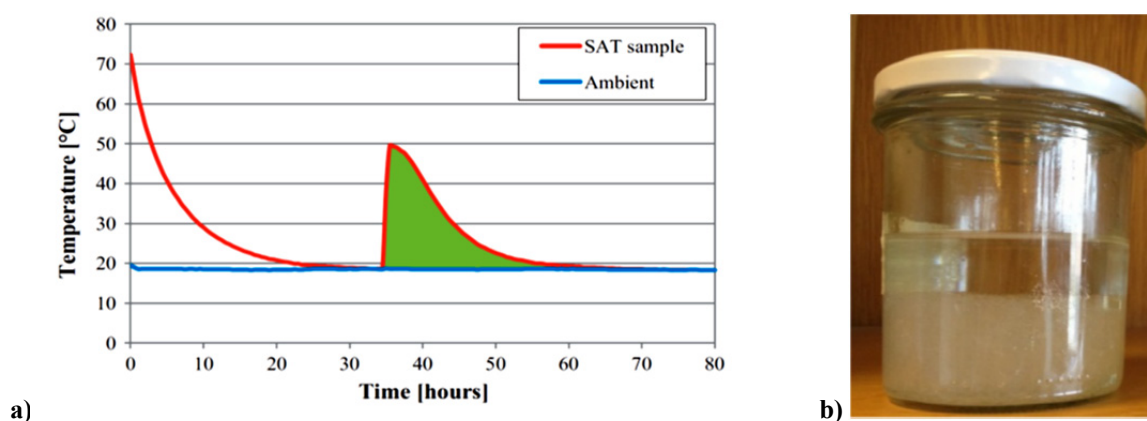


**Figure 6. a) An example of a cooling process of an SAT composite sample (Paper 1);
b) Glass jar containing supercooled SAT (Paper 1).**

Figure 7 presents an overview of measured heat contents of samples containing SAT and SAT composites. The red section of the bars indicates the variation of heat contents with different concentrations of additives. It was found that the heat content of samples containing SA-aqueous solutions was significantly lower than the theoretical Δh of SAT (Section 2). Glycero, AquaKeep and tartaric acid had limited effect on increasing the heat content, and were therefore found to be inappropriate for application in SAT composites. Composites of SAT containing 0.5–2%wt. CMC, 0.3–0.5 %wt. Xanthan rubber (X-gum) and 1–2%wt. of liquid polymeric solutions showed a heat content approximately 30% higher than SAT. Determined Δh values of these SAT composites were close to the theoretical value of SAT, considering their mass fraction of SAT. Liquid polymers HD 200, HD 310 and HD 500, developed by the Chinese company Suzhou Hongde Co. Ltd., showed best performance among polymeric additives with a mass fraction of 1%wt.

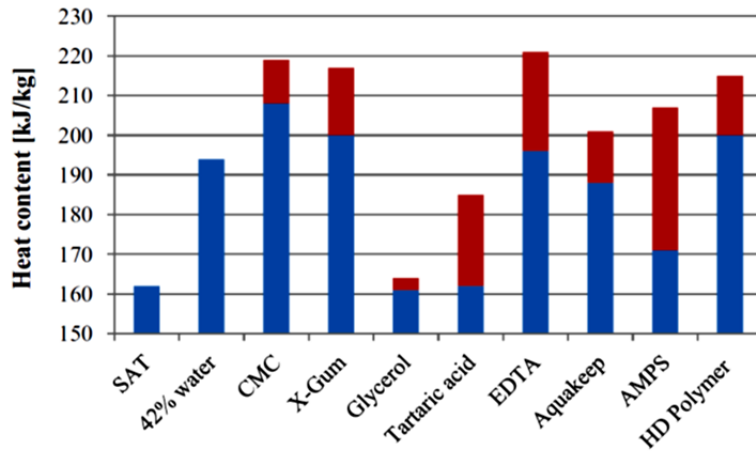


Figure 7. Determined Δh of SAT with and without different additives (Paper 1).

SAT composites with thickening agents and graphite have been reported with increased thermal conductivity [42], which is advantageous for heat transfer during solidification. During supercooling of SAT however, liquid additives are considered to be advantageous because natural convection improves the heat transfer of the heat exchanger. Thickening agents have been successfully applied in heat storage prototypes (Section 1.3). To verify the applicability of SAT composite containing HD 310 polymer, it was applied in tests of an inexpensive heat store (Paper 7).

Figure 8 presents specific energy contents of SAT composite with 2 % extra water and 3 % HD 310, as determined by heat storage testing (Paper 7). Evaluation of 12 test cycles resulted in a value of 207 kJ/kg for Δh , which was in accordance with results from previous investigations (Figure 7). The energy content of the SAT composite in liquid state deviated from pure SAT. The specific heat capacity (c_p) of the SAT composite could be calculated with Equation 3:

$$c_{p,liquid} \left(\frac{kJ}{kg K} \right) = 1.56 + 3.65 * 10^{-3} * T_{absoute} \quad (3)$$

SAT in food grade was used, which had a purity >98.5%. By employing energy storage capacity calculations, L was determined to be 238 kJ/kg SAT. This result corresponds to reference investigations of SAT containing 1% of nucleating agents, where L was found to be 237–243 kJ/kg SAT [41]. This indicated that the presence of impurities decreased L in comparison to pure SAT, which was used in differential scanning calorimetry investigations.

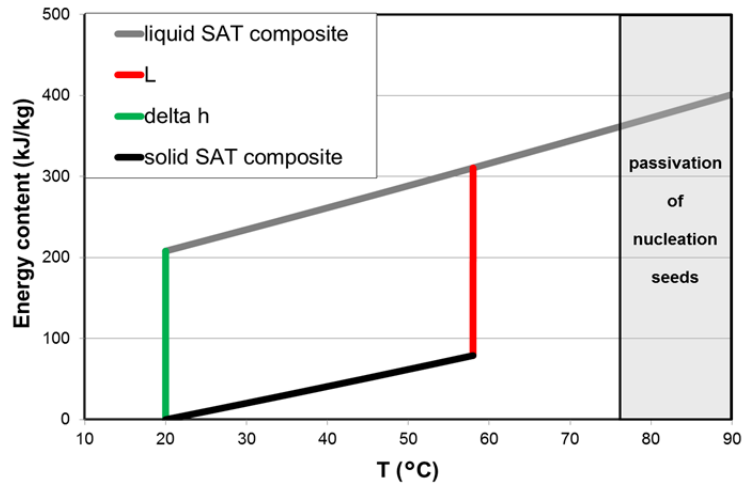


Figure 8. Specific energy contents of SAT composite with 2 % extra water & 3 % HD 310.

3.2. Visual study of phase separation mechanisms

Phase separation of SAT has been investigated visually in a transparent cylinder (\varnothing : 9 cm, height: 30 cm). The cylinder was glued on a flat, transparent plate. The top was covered by another plate and sealed with rubber. Cylinder and plates were made of polyethylene with temperature stability to 90 °C. A sequence of melting, supercooling and solidification of SAT was applied:

- 1) Melted SAT was filled in the cylinder to a height of 24 cm. Then, the cylinder was heated in an oven for 24 hours at 85 °C. After heating, the SA-water mixture contained water vapour bubbles, which were moving upwards (Figure 9 a). Their release on top of the SA-water mixture caused formation of a layer of jelly material. It is assumed that the layer consisted of anhydrous SA and SA, which was dissolved in its crystal water. As a consequence, longer periods with high temperature lead to reduced water content of the SA-water mixture. This enhances phase separation. However, water vapor condensed on the inner surfaces on top of the closed cylinder. Water drops were formed and fell down during cool-down of the cylinder. Therefore it can be assumed that, by mechanical mixing or convective movements of the SA-water mixture, the majority of the evaporated water can be regained.
- 2) Next, the cylinder cooled down for 12 hours to a temperature of 20 °C. Because of contact to the table and due to heat transfer to the upper volume of the cylinder, the SA-water mixture cooled down fastest at the bottom of the cylinder (Figure 9 a). Therefore, a suspension of an anhydrous SA and SA dissolved in water started from the bottom to the top. So, falling temperatures of the SA-water mixture were indicated by change from transparent to dull properties. Figure 1 b shows that, at 20 °C, the mixture was homogeneously hazy. At the bottom of the cylinder (Figure 9 d) the texture of the anhydrous SA phase, meaning a network of white lines, was visible. This indicated that the full volume consisted of SA, dissolved in its crystal water and a finely distributed phase of anhydrous SA. According to Paper 1, this phase separation leads to reduced heat content of the material, in comparison to SAT composites. Because of its higher density, the anhydrous SA had the tendency to settle down at the bottom of the cylinder.

- 3) Solidification was initialized by a seed crystal, inserted from the top of the cylinder. Crystallization of SAT caused a milky colour. Figure 9 c shows the cylinder when crystallization started in three quarters of the volume.
- 4) After full solidification was reached (solid SAT at room temperature), a photo was taken from the bottom of the cylinder. The colour-contrast of liquid and solid phases was increased by using a black background and a light-source at the side. A phase of solidified SAT and the previously observed SA-phase were also visible after full solidification. In Figure 9 e the SAT is in light yellow and the anhydrous SA phase is in darker colour.

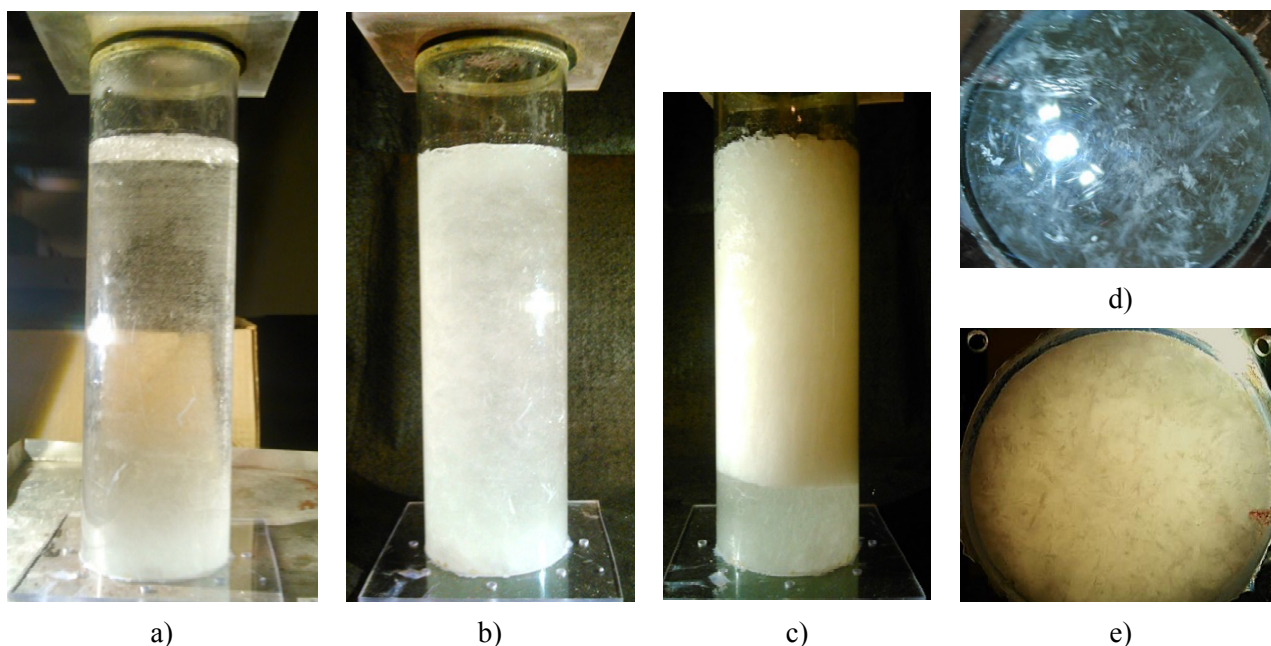


Figure 9. Visual properties of SAT in different states: a) Initial supercooling; b) Stable supercooling at 20 °C; c) During solidification; d) Texture at the bottom of supercooled phase at 20 ° C; e) Texture at the bottom after solidification.

Mechanical stirring or convection movements are needed to avoid phase separation of incongruently melting SAT. Formation of water vapor in supercooled, liquid phase leads to decrease of water content over time and enhances therefore phase separation.

A network of white lines became visible when anhydrous SA was formed in the supercooled SA-water mixture. Therefore, increasing degree of supercooling of SAT was visible by change of transparent to hazy properties. Because of differences in light reflection, contrast of phases was also visible after solidification.

In conclusion, visual properties can be used to investigate the effect of different liquid polymeric solutions, which are transparent, on phase separation of SA-water mixtures.

3.3. Liquid polymeric solutions as additive

Based on the successful application of the liquid polymer solutions in SAT composites, Suzhou Hongde Co., Ltd. developed new solutions, which had to be tested for its applicability:

- HD 310-1, which consists of longer molecules than HD 310, resulting in a thicker consistency
- HD 310-2, which consists of shorter molecules than HD 310, resulting in a thinner consistency
- HD 110-1, which is not comparable to previously tested solutions

Samples of SAT containing 1 and 2%wt. of each liquid polymeric solution, with and without 1%wt. of extra water were prepared in glass bottles (Table 1). The preparation procedure was similar to that one described in Paper 2. Subsequently, samples were heated for 12 hours to 85 °C. Afterwards, they were placed in the laboratory for cool-down at room temperature for three days, before a seed crystal was inserted to initiate crystallization. The procedure was repeated three times. A picture was taken from each sample. Next, the samples were reheated and rested in supercooled state for 9 months at room temperature before new pictures were obtained. Visual properties of the different samples were evaluated in accordance to Section 3.2.

Table 1. Overview of investigated samples.

| material | sample | SAT [g] | additive [%wt.] | water [%wt.] |
|----------|--------|------------|--------------------|-----------------|
| HD 310-1 | 1 | 400 | 1 | 0 |
| HD 310-1 | 2 | 400 | 2 | 0 |
| HD 310-1 | 3 | 400 | 1 | 1 |
| HD 310-1 | 4 | 400 | 2 | 1 |
| HD 310-2 | 5 | 400 | 1 | 0 |
| HD 310-2 | 6 | 400 | 2 | 0 |
| HD 310-2 | 7 | 400 | 1 | 1 |
| HD 310-2 | 8 | 400 | 2 | 1 |
| HD 110-1 | 9 | 400 | 1 | 0 |
| HD 110-1 | 10 | 400 | 2 | 0 |
| HD 110-1 | 11 | 400 | 1 | 1 |
| HD 110-1 | 12 | 400 | 2 | 1 |

The liquid polymer solution HD 110-1 was identified to be caustic. The PET bottle, which contained the solution, became porous after 9 months. Therefore it is assumed that metal and polymer containers will degrade when using HD 110-1 for SAT composites. Used glass bottles were identified to be not air-tight, therefore water vapor losses occurred. However, no crystallization occurred when anhydrous SA was built on top of supercooled SAT composites.

Figure 10 shows the conditions of the samples in supercooled state after 3 heat storage cycles as well as following 4 heat storage cycles with additional 9 months of resting at room temperature in supercooled state:

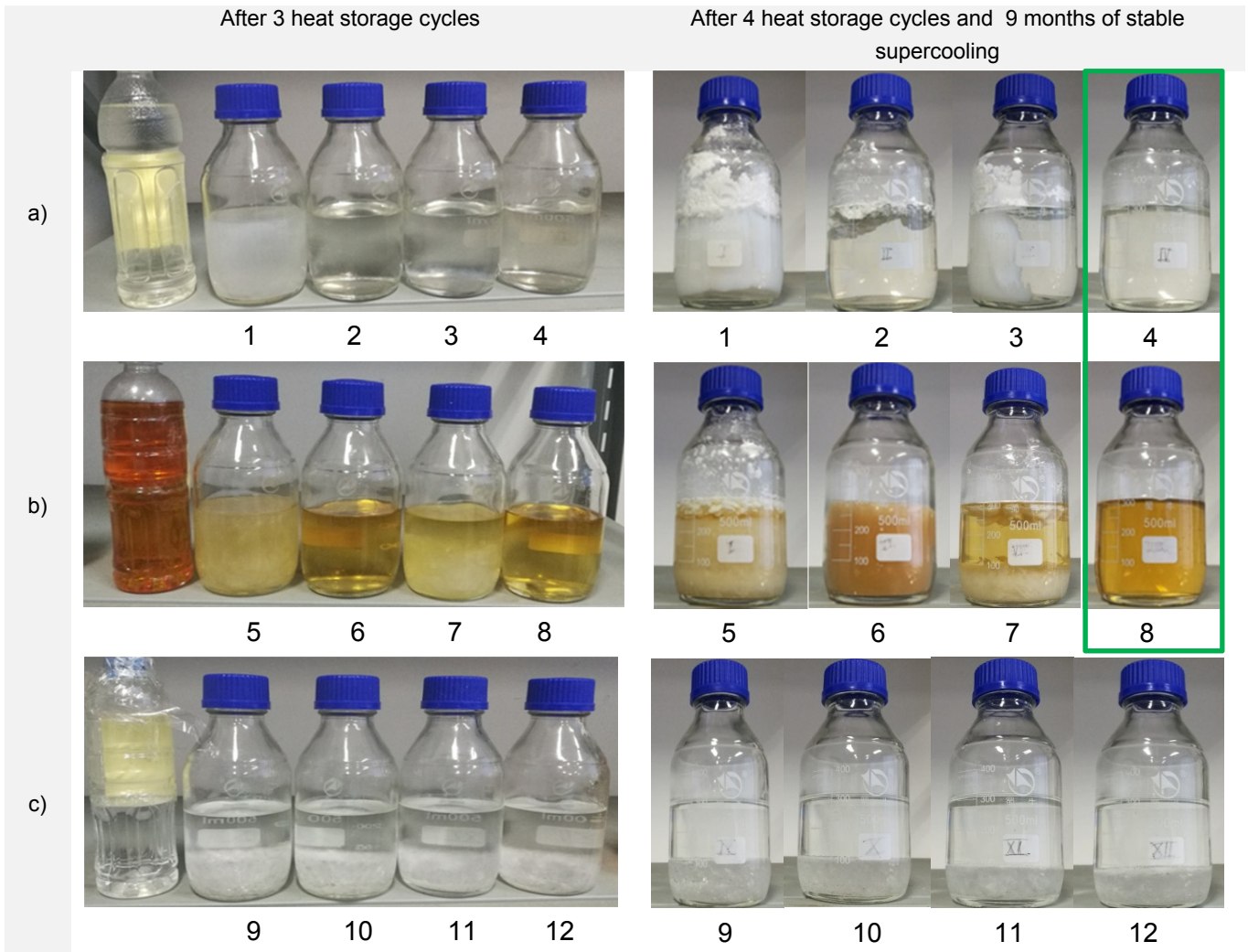


Figure 10. Visual properties of samples: a) Samples 1-4, containing HD 310-1; b) Samples 5-8, containing HD 310-2; c) Samples 9-12, containing HD 110-1.

It was found that the resting period had a significant influence on visual properties of samples:

- HD 310-1; 3 heat storage cycles applied: Without extra water, SAT composite with 1%wt. of liquid polymer (no. 1) was hazy, indicating undissolved SA in the mixture. The composite containing 2%wt. of liquid polymer (no. 2) was fully transparent, which also applied to both samples (no. 3, 4) containing 1%wt. of extra water.
- HD 310-1; 4 heat storage cycles and 9 months of supercooling applied: Water vapor losses in samples 1–3 led to formation of anhydrous SA on top of the mixture, which did not happen in sample 4. This sample had the highest concentration of liquid polymer and water. Part of the volumes in samples 1 and 3, both with 1%wt. of liquid polymer, were hazy. So, after a long resting period, enhanced by water vapor losses, undissolved SA was also observed in sample 3.

- HD 310-2; 3 heat storage cycles applied: In samples containing 1%wt. of liquid polymers (no. 5, 7) phase separation occurred, while samples containing 2%wt. of liquid polymers (no. 6, 8) were fully transparent.
- HD 310-2; 4 heat storage cycles and 9 months of supercooling applied: Anhydrous SA settled down in samples containing 1%wt. of liquid polymers (no. 5, 7), which also showed anhydrous SA on top. Sample 6 crystallized due to a defect of the glass bottle. Sample 8, containing 2%wt. liquid polymer and 1%wt. extra water was stable.
- HD 110-1; 3: After 3 heat storage cycles, phase separation was visible in all samples. Undissolved SA settled down and reached equally high levels after 9 months of stable supercooling. No anhydrous SA was observed on top of the samples, which is assumed to be a result of enhanced phase separation.

In conclusion, SAT composite with the liquid polymer solution HD 310-1 showed best properties with the investigated concentrations. With 2%wt. and 1%wt. of extra water, no undissolved SA was observed after four heat storage cycles and after 9 months of stable supercooling at room temperature. Employing these concentrations, also application of HD 310-2 led to a stable SAT composite. A minimum of 2%wt. and 1%wt. of extra water is suggested to be used in order to achieve stable SAT composites in heat storage applications. Such concentrations enabled higher solubility of SA in water and it can potentially compensate water vapor losses, occurring in melted state.

Based on manufacturer information, the previously applied liquid polymer solution HD 310 (Paper 1) is of similar molecular formula, with medium length of molecules, in comparison to HD 310-1 and HD 310-2. This study implies that the chosen concentration of additives (3%wt. HD 310, 2%wt. extra water) was sufficiently high.

3.4. Initialization of crystallization by local cooling

[This section is based in part on Paper 2]

To utilize heat of fusion on-demand for domestic heating, a reliable method for initializing the solidification of supercooled SAT composites is needed. The crystallization temperatures of SAT composites during cooling were therefore determined. CMC, extra water, liquid polymer HD 310, metal-based graphite flakes, and silicone oil were applied as additives to form the different SAT composites.

Figure 11 a presents a drawing (intersection) of insulated glass jars, filled with approximately 60 g SAT composite, used for supercooling samples in a freezer. The sample temperature was measured by a thermocouple wire (type TT). Figure 11 b shows a glass jar filled with SAT containing extra water and steel profiles. Cooling tests were conducted with and without rusty steel profiles to investigate their influence regarding supercooling stability and crystallization temperature. Furthermore, the period of stable supercooling at room temperature prior to cool-down in the freezer was varied.

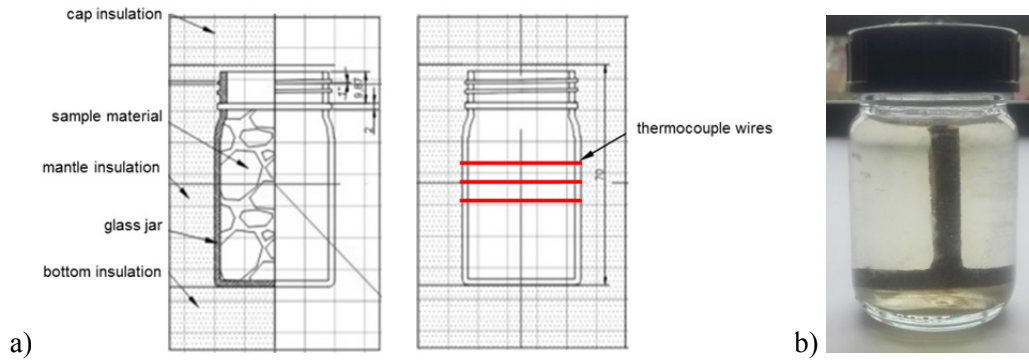


Figure 11. a) Sample containment for cooling tests; b) Glass jar with SAT and sliced steel profile (Paper 2).

Figure 12 presents the temperature development of samples containing different SAT composites with and without and steel profiles during cool-down in the freezer. When no steel profiles were applied, the following temperatures were required for initialization of crystallization of SAT composites:

- $-24\text{ }^{\circ}\text{C}$ for SAT and SAT with 9%wt. water added
- $-18\text{ }^{\circ}\text{C}$ for SAT with 5% CMC and 3% of HD 310 added
- $-15\text{ }^{\circ}\text{C}$ for all SAT composites in closed steel containers

The presence of steel profiles led to more homogeneous and higher crystallization temperatures. All the investigated SAT composites supercooled to temperatures below $-8\text{ }^{\circ}\text{C}$, which means that they can be utilized for long-term heat storage by stable supercooling in households. This effect is considered useful for application of cooling devices to initiate SAT composite crystallization on-demand.

Composites with thickening agents and liquid polymers demonstrated highest temperature peaks during crystallization, which is in correspondence to previous investigations on Δh (Section 3.1).

A second minor temperature peak occurred below $-20\text{ }^{\circ}\text{C}$ in the SAT composites with no stabilizers added, and the samples cooled further after the first crystallization. This indicates that due to the very low temperature, further exothermic crystallization was enabled. It can be assumed that corresponding reaction enthalpy only can be utilized when the SA-water mixtures (full volume) are exposed to low temperatures, as in the freezer ($-30\text{ }^{\circ}\text{C}$).

Figure 13 shows the two devices developed to initialize SAT composite solidification in heat storage units by local cooling. The CO_2 evaporation device (Figure 13 a) was tested on a flat heat storage prototype unit containing SAT with extra water and a SAT composite with CMC. A device using Peltier elements (Figure 13 b) was tested on a small-scale flat heat storage prototype containing SAT with extra water. Evaporating CO_2 in a chamber adjacent to supercooled SAT composite worked reliably. The device with Peltier elements generated local cooling to sufficiently low temperatures for crystallization after the SA-water mixtures had been supercooled below $30\text{ }^{\circ}\text{C}$. With both methods, local cooling was achieved rapidly, so that crystallization was initiated 2–5 minutes after the experiments were commenced.

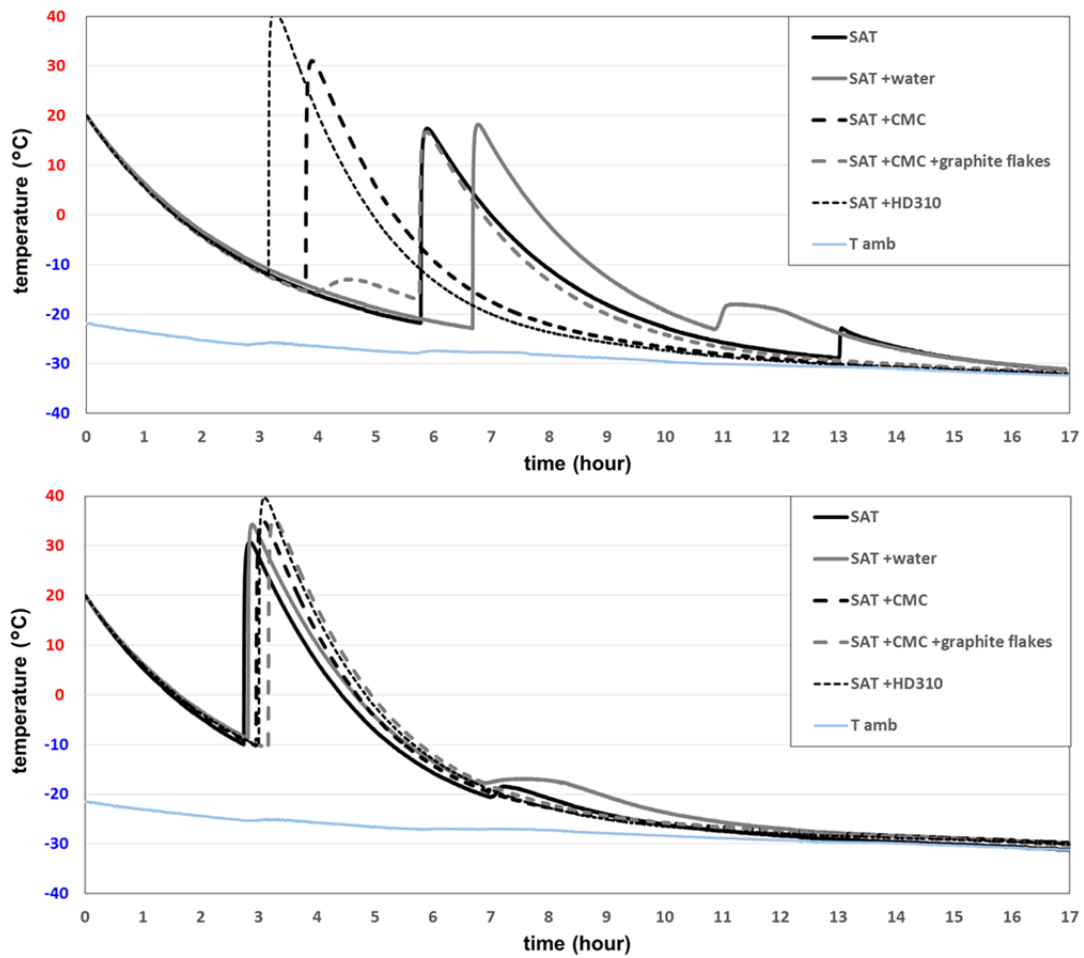


Figure 12. Temperature development of samples containing different SAT composites without steel profiles (top) and with steel profiles (bottom) during cool-down (Paper 2).

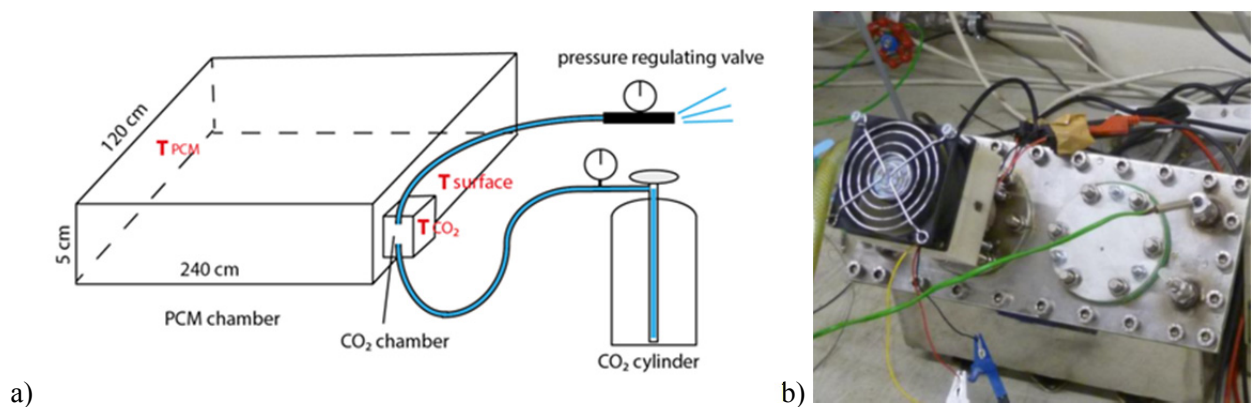


Figure 13. Devices to initialize SAT composite solidification on demand: a) Principle diagram of using cooling with CO₂ (Paper 2); b) Diagram of the Peltier device mounted on a small-scale heat storage prototype (Paper 2).

3.5. Recycling and material handling

[This section is based in part on the following publication: J. Jänchen, W. Wagner, H. Schranzhofer, P. Gantenbein, X. Daguene-frick, G. Englmaier, M. Dannemand, S. Furbo, T. Badenhop, EU-COMTES project report about the materials handling & recycling path, no. 2.5, <http://comtes-storage.eu/publications/reports/>]

Recycling of SAT after heat storage application is not a simple task, because of the necessity of pure SAT in the majority of its applications. Pure SAT can be easily dissolved in water and removed through the drainage system. The environmental effects of a highway deicer containing sodium acetate have been assessed by Bang and Johnston [67], who concluded that negative effects on both aquatic and terrestrial ecosystems are minimal. However, the recycling process may include a costly chemical process separating the components, in case of additives applied. It depends on the additives in question as well as amount of material involved. Aspects of material handling and proposed material path for selected additives, applied in SAT composites, are summarized below:

- CMC is a commonly used material in food and pharmaceutical industries, as well as in various products as toothpaste, detergents and water-based plants as a thickener or stabilizer emulsion. It is a non-toxic material, which could potentially damage the skin, eyes, respiratory- and digestive system, in case of human contact. CMC usually ends in wastewater treatment plants or in the environment, due to the fact that it degrades completely at slow rate [68].
- Graphite is a commonly used material in several industrial applications, especially in thermochemical processes, due to its high thermal conductivity. It is a slightly hazardous material, toxic for the respiratory- and cardiovascular system. The most damaging impact on the environment from the use of graphite consists in the mining industry. [69]
- Paraffin oil has also a wide industrial application and as a cosmetic additive. It is hazardous for the respiratory system, which calls for safety when handled. It does not cause highly harmful environmental effects: both terrestrial and aquatic organisms are not severely affected. Moreover, it is expected to be biodegradable on a long-term scale. [69]
- Ethylenediaminetetraacetic acid (EDTA) is a material mainly used in industries, for instance in the textile industry and in pulp and paper industries, to sequester metal ions in aqueous solutions. It is also used in medicine. EDTA exhibits low acute toxicity. It has been found to be both cytotoxic and weakly genotoxic in laboratory animals. The longevity of EDTA can pose serious issues in the environment because its degradation is slow. EDTA elimination can be achieved at about 80% using microorganisms. [70]

After utilization in heat storage units, a minimal requirement suggested is the separation of graphite from SAT composites before the disposal. SAT can be dissolved in water and removed through the drainage system, while CMC and paraffin oil are biodegradable. Composites containing EDTA or liquid polymeric additives (no information available for prototype solutions from Suzhou Hongde Co., Ltd) must be handled with care.

4. System development

4.1. Design

Figure 14 presents the layout of a novel solar combi-system consisting of a solar collector circuit, a segmented PCM heat storage and a tank-in-tank water heat storage.

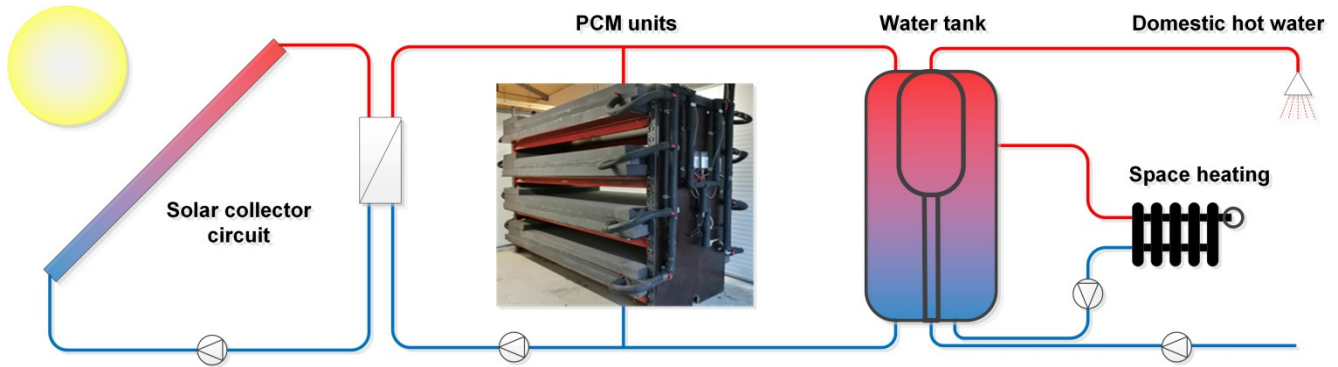


Figure 14. Diagram of the developed solar combi-system utilizing stable supercooling of SAT (Paper 6).

The system was built in the prototype test facility at the Technical University of Denmark (northern latitude: 55.8°). Its operation was monitored and controlled via a LabVIEW (Laboratory Virtual Instrument Engineering Workbench) program.

The collector array (Figure 15 a) was formed with 7 panels (in total 22.4 m² of aperture area) of heat pipe evacuated tubular collectors, type Thermomax HP 450 from Kingspan Renewables. The collectors were mounted with an inclination of 45° and an azimuth angle of 12° towards east. The panels were connected in 2 parallel circuits, with 4 panels and 3 panels in series, respectively. The water tank (Figure 15 b) had a volume of 735 L. It was designed as a tank-in-tank heat storage with an electrical resistor for auxiliary heating.



**Figure 15. a) Solar collector array (Paper 3);
b) Water tank and LabVIEW interface for live data reading (Paper 3).**

4.2. PCM heat storage

[This section is based in part on Paper 3]

Flat PCM units (length: 2.4 m; width: 1.2 m) with a height of 5 cm inside the enclosed PCM container (volume: 150 L) were constructed by the Danish company Nilan A/S. Figure 16 a presents a diagram of a unit. Its air expansion chamber was connected via the left flange to an membrane expansion vessel (50 L) to minimize any pressure change during material expansion (about 10% [42]) from solid to liquid state. An activation device was mounted on the right flange of the air expansion chamber. Using this device, solid SAT crystals were injected by a needle into the supercooled SAT composite. A thermocouple inside a hollow metal cylinder was mounted on the central flange to allow temperature measurement of the SAT composite.

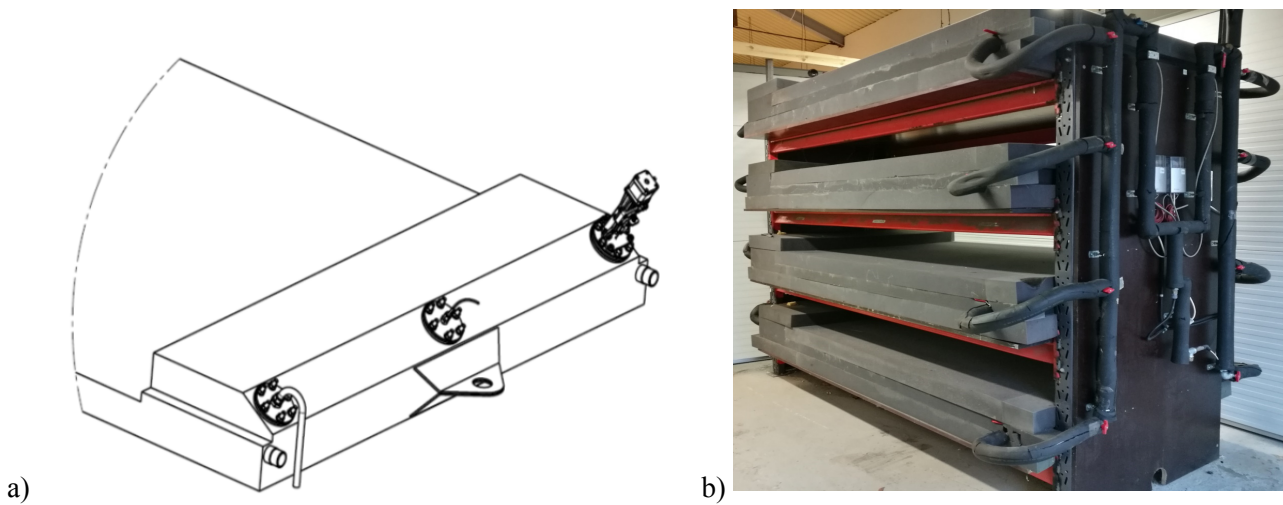


**Figure 16. a) Perspective drawing of a PCM unit (Paper 3);
b) Photograph of the segmented PCM storage (Paper 3).**

Four flat units were stacked to form the PCM heat storage. Two units (2 and 3) were made of stainless steel, while the other two were made of steel (1 and 4). A two-metre-high assembly (Figure 16 b) with sufficient space for maintenance between the units was built. To investigate their performance separately, each PCM unit was insulated with 10 cm foam and separately connected to the hydraulic circuit. Water was used as the HTF. Motor valves were mounted at the inlet of each unit to control the HTF flow.

Table 2 presents the SAT composite fillings in PCM units. SAT with 1%wt of CMC (as in units 1 and 2) and 1%wt (unit 3) or 2%wt (unit 4) of EDTA, were applied. Unit 3 needed 1%wt extra water to achieve a fully dissolved solution during melting. Moreover, highly conductive graphite powder and paraffin oil were added in unit 1. The PCM container of unit 4 was damaged and refilled before the installation. During refill no exact weight measurement was carried out.

| | Unit 1 | Unit 2 | Unit 3 | Unit 4 |
|----------------------|--|-----------------|-----------------------------------|------------------|
| PCM composition | SAT + 1%wt. CMC + 2%wt. graphite + 5 L oil | SAT + 1%wt. CMC | SAT + 1%wt. water + 1%wt. EDTA | SAT + 2%wt. EDTA |
| PCM mass | 202 kg | 220 kg | 202 kg | unknown |
| Δh (Paper 1) | 211 kJ/kg* | 211 kJ/kg | 216 kJ/kg** | 215 kJ/kg |
| ΔH unit | 40759 kJ | 46420 kJ | 42004 kJ | - |

*Value for SAT with 1%wt. CMC, added graphite and oil was assumed to be additional non-reactive mass

**Value for SAT with 1%wt. EDTA without extra water in the composition

Table 2. SAT composites in PCM units (Paper 3).

Functionality tests showed that:

- For charging with solar heat, a sequence for the combined operation of the water tank and a variable number of PCM units enabled control of HTF temperatures in the operation range. Melting of the PCM with temperatures above 90 °C was possible.
- Discharge of sensible heat from liquid and supercooled SAT composite was achieved in PCM units 1–3 without causing solidification. As presented in Figure 17 a, thermal power during the discharge of a single unit reached 32 kW with a PCM temperature of ~80 °C. Furthermore, rapid unit charging in supercooled state did not cause spontaneous crystallisation. This allows for utilization of melted PCM as short-term sensible heat storage.
- Initialization of crystallization by mechanical seed crystal injection worked in initial tests. However, the materials used for the activation device could not withstand repeated cycles of charging and discharging.
- Figure 17 b presents discharge power during solidification. By continuous discharging with a HTF flow rate of 2.13 L/min, thermal power reached 4 kW. With a start and stop strategy, and a HTF flow rate of 5 L/min, thermal power reached 8 kW. This “pulsed-flow” also yielded higher flow temperatures.

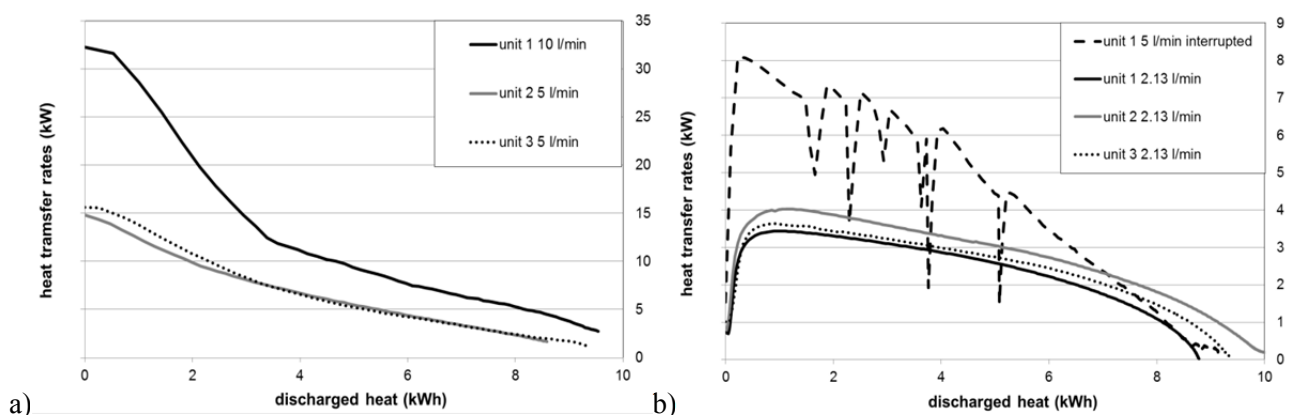


Figure 17. Development of thermal power during discharging (Paper 3): a) Discharge of sensible heat; b) Discharge during solidification of supercooled PCM (Paper 3).

4.3. Control

[This section is based on Paper 6]

Settings of seven operation modes (A–G) have been developed and their control parameters have been verified in system tests. The solar combi-system was operated in the following way:

- System standby (mode A): Water tank coverage is sufficient for DHW and SH supply.
- Water tank charging (mode B, Figure 18 a): The mode starts when the collector outlet temperature ($T_{\text{collector}}$) is 10 K higher than T_1 and the temperature in the middle of the water tank (T_2) is below 50 °C. During operation, $T_{\text{collector}}$ must be at least 2 K higher than the temperature at the bottom of the water tank (T_1). Water tank charging stops when T_2 reaches 60 °C.
- PCM heat storage charging (mode C, Figure 18 b): A total irradiance on the tilted collector plane of at least 150 W/m² is required, or a $T_{\text{collector}}$ of minimum 70 °C. The mode starts when T_2 is above 60 °C and it is interrupted by water tank charging (mode B) when T_2 falls below 50 °C. Units with a PCM temperature (T_{PCM}) below 80 °C are subject to charge, where the warmest unit has priority. Charging starts with a single unit; the next warmer unit is charged in parallel if the flow temperature ($T_{\text{secondary}}$) exceeds 95 °C. When $T_{\text{secondary}}$ falls below 85 °C, the coldest unit is removed from the charging circuit. The mode stops when the PCM in all units reaches a temperature of at least 80 °C.
- Additional water tank charging (mode D, Figure 18 a): When all PCM units are fully charged and $T_{\text{collector}}$ is 10 K higher than T_1 , additional water tank charging takes place. It stops when $T_{\text{collector}}$ is less than 2 K higher than T_1 , or if stagnation conditions occur.
- PCM discharge of sensible heat (mode E, Figure 18 c): Without collector power available and a temperature at the middle of the tank (T_2) below 45 °C, heat from the warmest PCM unit is transferred to the water tank. When T_{PCM} falls below 50 °C the next warmest unit is discharged. The mode stops when either T_2 reaches 45 °C, or all PCM temperatures become too low.
- PCM discharge of heat of fusion (mode F, Figure 18 c): When threshold conditions for mode E are reached, but PCM unit temperatures are too low, SAT composite solidification of the warmest, supercooled unit is initialized by means of seed crystal injection. Heat transfer fluid flow starts when T_{PCM} rises to 58 °C. When T_{PCM} is lower than 50 °C, the procedure is repeated with the next warmest, supercooled unit. The mode stops when either T_2 reaches 45 °C, or when all PCM temperatures become too low.
- Auxiliary heating (mode G): When no collector power is available, T_2 and T_3 (top of the tank) are below 45 °C, PCM temperatures are below 50 °C and SAT composites are in solid state, an auxiliary heating element (E_{aux}) is switched on in the water tank. The mode stops when T_3 reaches 45 °C.

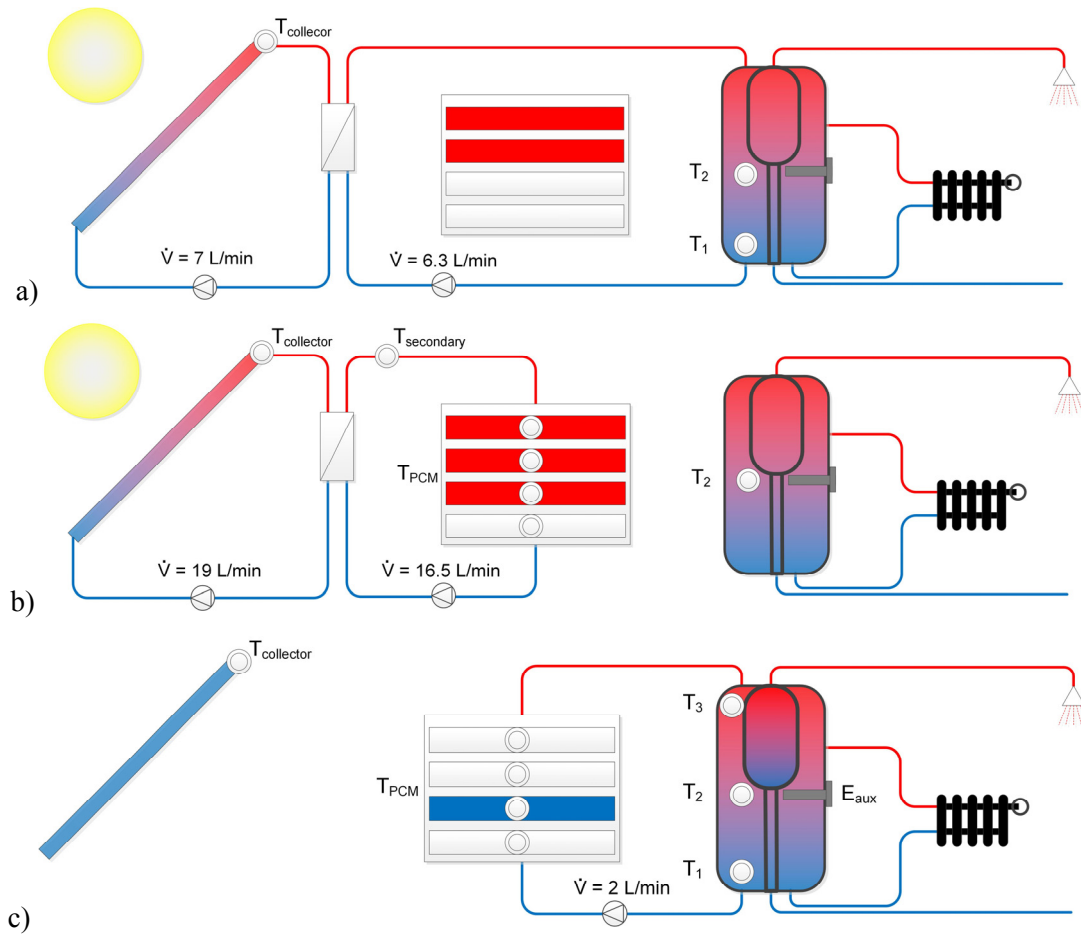


Figure 18. Diagram of operation schemes: a) Modes B and D; b) Mode C; c) Modes E and F.

4.4. Demonstration

[This section is based in parts on Papers 3, 4 and 5]

The system was operated from August 2015 until April 2017. Manual settings were applied to test functionality of components and control parameters. The system operated automated for most of the year 2016.

The dependency of SH loads on solar irradiation and ambient temperature has been determined by B. Johansen et al. [71] by simulation of a space heating system in a 130 m² building in Denmark, built to Passive House Standard [72]. The annual SH demand was 15 kWh/m². The building model included south-orientated windows. During demonstration, SH demand was applied from 15th October to 31st March. Heat-draw was enabled in intervals of 6 hours. In this way, it was possible to calculate heat demand for six hours based on measured ambient conditions. DHW consumption was calculated based on a daily consumption of 113 L of hot water at 45 °C and a cold water temperature of 10 °C, considering the comfort requirements of 3.5 users and efficient use of water [5]. This resulted in daily loads of 4.6 kWh. Three hot water draw-offs a day (7:00 h, 12:00 h, 19:00 h), with 1.53 kWh of heat each draw-off, were applied to simulate user behaviour.

Figure 19 presents heat transfer data of automated system charging during a sunny day. The daily solar irradiation on the solar collector array was 135 kWh, defined as the solar potential. 76 kWh (53 % of the solar potential) of heat was stored. Most heat was transferred to the PCM units (46 kWh) in the period from 10:30 h to 16:00 h. For charge of the water tank (buffer charge), the highest share of energy (25 kWh) was transferred until 10:00 h, while the rest was transferred later, in four short periods. Daily heat losses of 9 kWh in the collector circuit and 3 kWh in charging circuits, respectively, occurred.

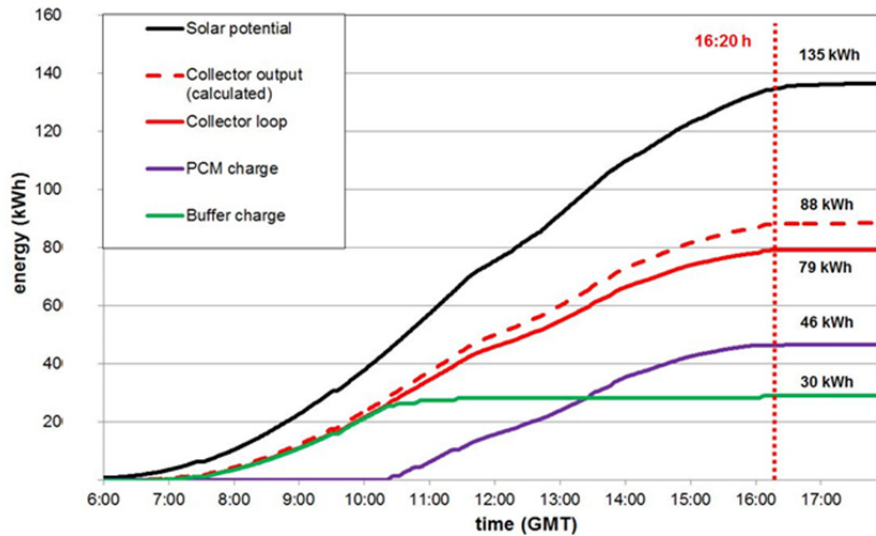


Figure 19. Development of heat transfer during the 9th of September 2015 (Paper 4).

Figure 20 shows the development of the SAT composite temperature in the PCM unit 2 in autumn 2015. During September the unit was repeatedly charged and discharged and it therefore served as a sensible heat storage, additionally to the water tank. The SAT composite remained in liquid state for 57 days until crystallization was initiated on the 11th of November. In this way, solar heat from early October was utilized for domestic heat supply in mid-November.

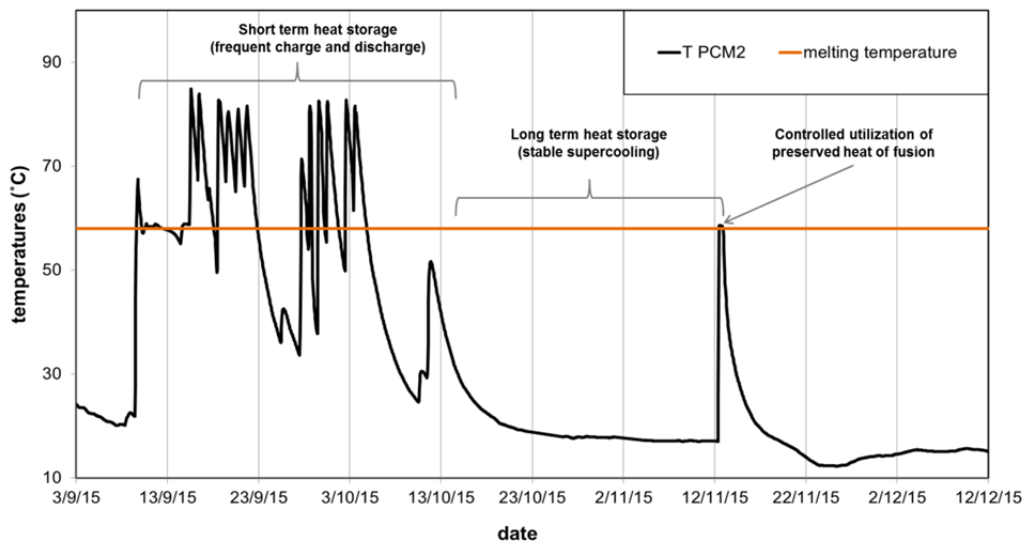


Figure 20. Operation sequence with PCM unit charging and discharging in 2015 (Paper 3).

Figure 21 shows the system behavior during a sunny period of eight days in March, when five different operation modes occurred. At the beginning of the period, auxiliary heating was needed to enable DHW and SH supply. On 16th March, T_2 reached 60 °C during charging of the water tank, leading to activation of PCM storage charging (mode C). PCM storage charging was interrupted once by repeated water tank charging in the afternoon. During mode shifts, and when PCM units were added or removed from the PCM charging circuit, heat transfer rates of up to 36 kW were measured. During the following days, charging of the water tank was typically followed by charging of the PCM units. Discharge of sensible heat (mode E) was activated to transfer heat from the PCM units to the water tank when the collector array could not fully cover the heat demand. On 22nd and 23rd March, the water tank was mainly heated in this way.

Further system operation data showed that PCM units were frequently charged and discharged in spring and autumn. HTF temperatures closely followed the collector outlet temperature during water tank charging and were kept between 70 and 95 °C during PCM unit charging, to ensure good heat transfer to the SAT composites. During continuous operation, heat transfer rates were below 16 kW, but peaked up to 36 kW when PCM units were added to the charging circuit. An observation period of five minutes was proved a practical way to avoid frequent mode changes.

The applicability of the concept of combined short and long-term heat storage was proven. Mode F for discharging heat of fusion on demand was included in the control strategy. However, composite crystallization needed to be initialized manually, and thus studying the annual system performance was impossible.

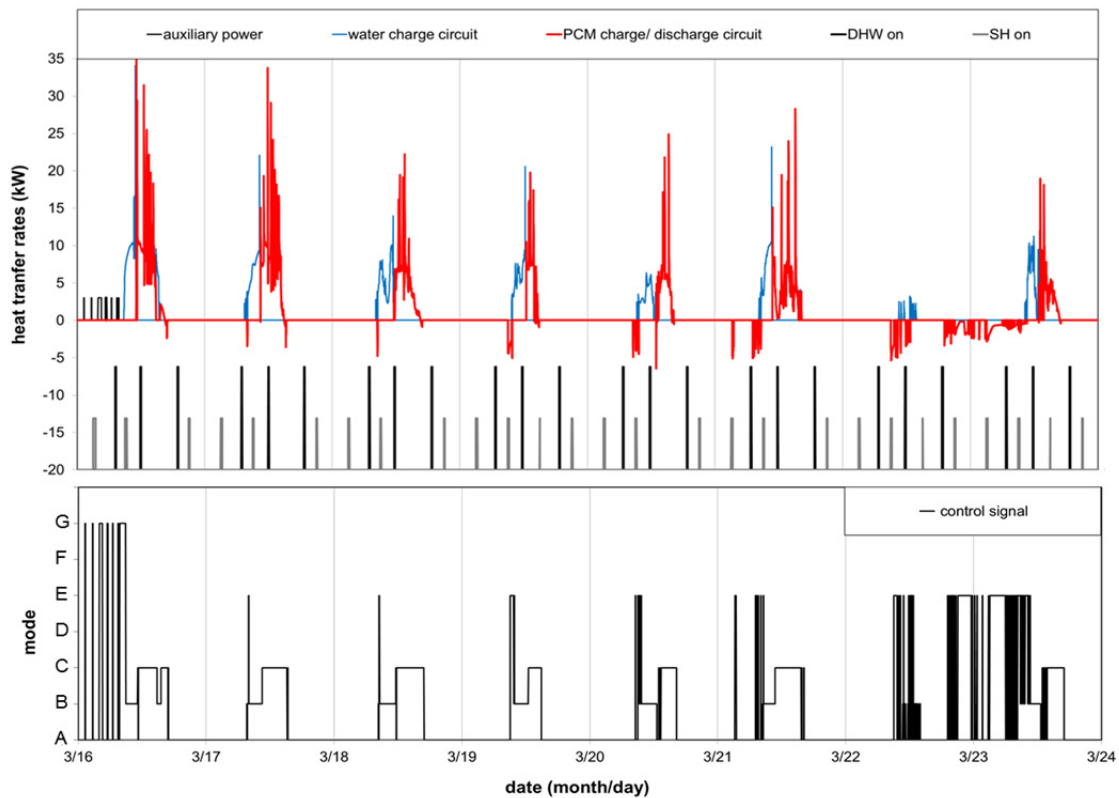


Figure 21. Storage heat transfer, SH and DHW demand patterns, and control signals in March 2016 (Paper 5).

4.5. Investigation of PCM units after system demonstration

The applied SAT composites represented the state of art in spring 2015, when the system was built. During system demonstration, all PCM units were exposed to frequent charge and discharge. In periods with sunshine the composites were heated for several days to temperatures up to 90 °C. This occurred multiple times during two years, meaning that a stress test of SAT composites was performed.

Prior to installation into the system, PCM units were used in laboratory tests [37]: Unit 1 was subject to 20 test cycles with SAT and 9%wt. extra water in the laboratory. After the laboratory testing, unit 1 was emptied from its SA-water mixture and flushed with water before it was filled with the new SAT composite used in system demonstration. Unit 2 was tested in the laboratory with SAT and 1%wt. CMC, unit 2 was subject to 11 test cycles. Both short (2–3 days) and long (5 weeks/ 2 months) test cycles were carried out for both units. Unit 1 was tested over approximately 9 months and unit 2 over 6 months. Unit 3 and unit 4 were used for cyclic tests with different SA-water mixtures at the Technical University of Graz, before they were filled with composites containing EDTA for system demonstration.

Method

PCM units were checked after dismantling the demonstration system. SAT composites were investigated in solid state via open flanges on top of their PCM expansion chamber. Material was extracted by drilling of holes with 34 mm in diameter. The following aspects were checked:

- Visual examination of the expansion chamber (Figure 22)
- Filled height and visual examination of composites by means of drilled holes below flanges (Figure 23)
- Condition of extracted SAT composites in different levels of the filling (Figure 24)

Observations and their interpretation

Unit 1 contained 202 kg composite of SAT with 1%wt. CMC and 2%wt. graphite powder and 5 L oil. Evaporated oil stuck on the steel container surfaces and bedewed the top layer of the SAT composite. A material layer depth of 5.7 cm was measured. Black composite material in the bottom layer showed that graphite powder settled down. The light-brown color of the extracted composite on the top of the layer is considered to be a result of adding oil.

Unit 2 contained 202 kg composite of SAT with 1%wt. CMC. Clean container surfaces of stainless steel indicated no oxidation reaction. The composite contracted during solidification, showing the regular texture of SAT containing CMC on the side. The top layer was covered with crusts of dry material due to water vapor losses. A material layer depth of 7.1 cm was measured. The extracted material was amber colored, characteristically for SAT containing CMC. In the central layer traces of black material were found. This could be either due to dust particles, present before filling of the container, or due to thermal degradation of the CMC.

Unit 3 contained 220 kg composite of SAT with 1%wt. extra water and 1%wt. EDTA. Clean surfaces of stainless steel indicate that no oxidation reaction happened. The composite contracted during solidification. The top layer was covered with a hard shell of dry material. A material layer depth of 8 cm was measured. The extracted material had a homogeneous texture. Traces of brown particles at the bottom of the layer are considered to be a result of dust particles, present before filling.

Unit 4 contained SAT with 2%wt. EDTA. Unit 4 never achieved stable supercooling. Steel surfaces of the container were heavily oxidized. This is considered to be a result of the presence of oxygen, water vapor which was released by the SAT and as result of the chemical properties of EDTA, which is assumed to accelerate corrosion. A material layer depth of only 4 cm was measured. Extracted material was black in the bottom and red at the top of the layer. Black color is assumed to be a result of corroded steel, settling down in melted state. The red color is assumed to be a result of traces of ferrite (iron).

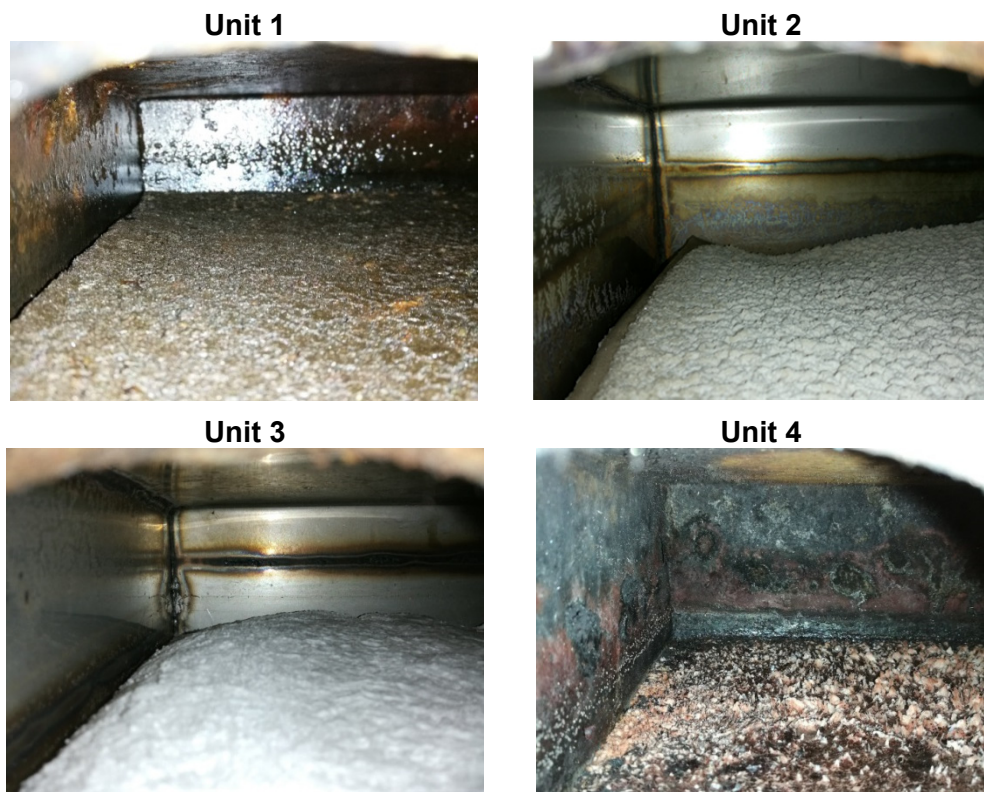


Figure 22. PCM expansion chambers after system demonstration.

Material layers in unit 1–3 were higher than the PCM chamber (5 cm). This indicates that they were sufficiently filled, while unit 4 was not fully filled. This means that, after reparation of unit 4 in 2014, filling of the unit in spring 2015 failed. It can be concluded that unit 4 was broken before it was utilized in the system.

Two years after unit filling, in spring 2017, supercooling of PCM units 1, 2 and 3 was recorded. Afterwards unit 1 solidified spontaneous, while supercooling of unit 2 and unit 3 was stable. It can thus be concluded

that, with the tested SAT composites, flat plate prototype units of stainless steel showed advantages over units in steel. No comparison was possible because container materials were not tested with the same SAT composite.

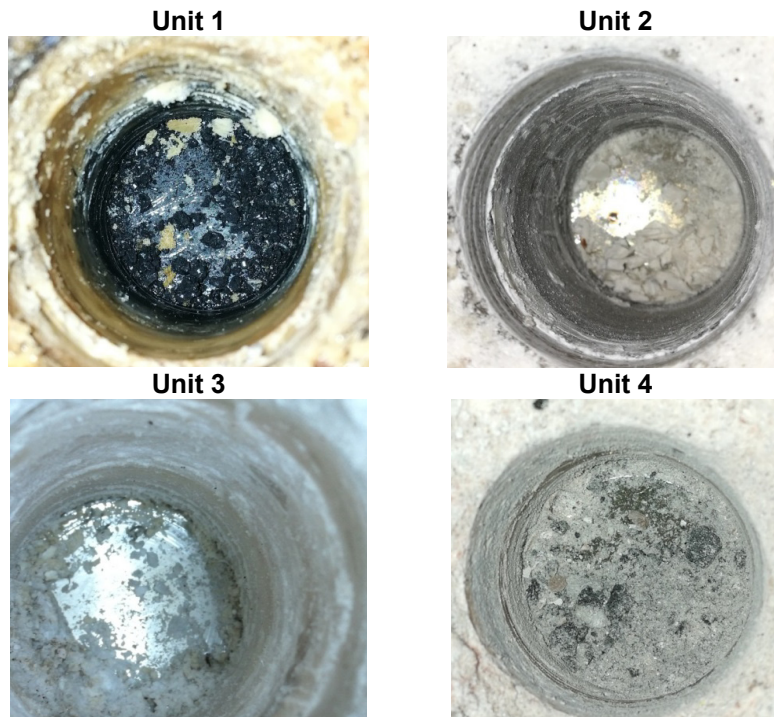


Figure 23. Drilled holes in solidified SAT composites after system demonstration.



Figure 24. Extracted sample material (from bottom to the top) after system demonstration.

5. System simulation

[This section is based on Paper 6]

5.1. Method

A numerical model was built in the TRNSYS 17 environment. The water tank model (type 8893) the multiple flat PCM unit model (type 8888) the controller of PCM units (type 8889) and the system controller (type 8896) have been previously developed at the Technical University of Graz within the EU-COMTES project. The system control strategy (Section 4.3) was implemented in type 8896. The collector array was modeled with type 538. Minute-based weather data from 2016, measured at the DTU climate station [73], was used for annual system simulation. The annual, global irradiation on a horizontal plane was measured to 1010 kWh/m², similar to the Danish reference year (1038 kWh/m²).

The generated data from system demonstration was used for model validation. Table 3 presents the comparison of measured to simulated heat transfer of system components. For the collector circuit a period of 42 days was compared. For water tank charge, SH and DHW consumption as well as PCM charge and discharge, single days were analysed. All component models were found to be valid with minor deviations.

Table 3. Simulated and measured heat transfer in collector circuit, water tank and PCM heat storage.

| | Measurement (kWh) | Simulation (kWh) | Deviation (kWh) | Deviation (%) |
|--|-------------------|------------------|-----------------|---------------|
| Collector circuit (March 17 th – April 28 th 2016) | 1146 | 1168 | 22 | 1.9 |
| Water tank charge | 25.2 | 25.6 | 0.4 | 1.7 |
| Space heating consumption | 10.4 | 10.2 | 0.2 | 1.9 |
| Hot water consumption | 4.76 | 4.83 | 0.07 | 1.5 |
| PCM unit charge | 28.09 | 27.91 | 0.18 | 0.6 |
| PCM unit discharge | 8.87 | 9.09 | 0.23 | 2.6 |

Simulation results were evaluated by employing yearly energy balances. They were calculated using periodic integration of heat transfer rates in the hydraulic circuits. The net utilized solar heat (Q_{solar}) resulted from the sum of the domestic hot water and space heating minus auxiliary energy use:

$$Q_{solar} (kWh) = \int (\dot{Q}_{SH} + \dot{Q}_{DHW} - \dot{Q}_{auxiliary}) * dt \quad (4)$$

The solar fraction (SF) of heat supply was calculated as the fraction of Q_{solar} on SH and DHW consumption, employing Equation 5:

$$SF (\%) = \left[1 - \frac{\int (\dot{Q}_{auxiliary}) * dt}{\int (\dot{Q}_{SH} + \dot{Q}_{DHW}) * dt} \right] * 100 \quad (5)$$

Q_{solar} and SF were determined at the water tank.

The performance of the system with demonstrator specifications, including shading of the collector array due to buildings and trees, resulted in an annual SF of 56 %. SH and DHW patterns of a Danish single-family Passive House with a yearly heat demand of 3723 kWh were applied. The DHW demand was fully covered

by solar heat from April to September, due to the relatively large collector array (22.4 m² aperture area). From October to March space heating caused higher heat demand, which was partly covered by heat transfer from the PCM heat storage.

The performance potential of the system was studied in an optimized scenario. Compact PCM heat storage design was assumed by increased insulation of the PCM units. Reduced water tank heat losses were considered by reduced tank dimensions, resulting in a water volume (V_{water}) of 0.6 m³, and increased insulation. A daily DHW consumption of 130 L at 45 °C (5.175 kWh daily loads) was applied. SH and SHW patterns resulted in a yearly heat demand of 3977 kWh.

5.2. Sensitivity analysis

The sensitivity of competent sizing on Q_{solar} was analysed for the optimized scenario. Figure 25 presents the relative change of Q_{solar} by variation of solar collector array and PCM heat storage parameters based on a reference setting; collector aperture area (A) of 16 m², collector inclination (I) of 70°, SAT composite volume (V_{PCM}) of 1 m³ and 200 L PCM units.

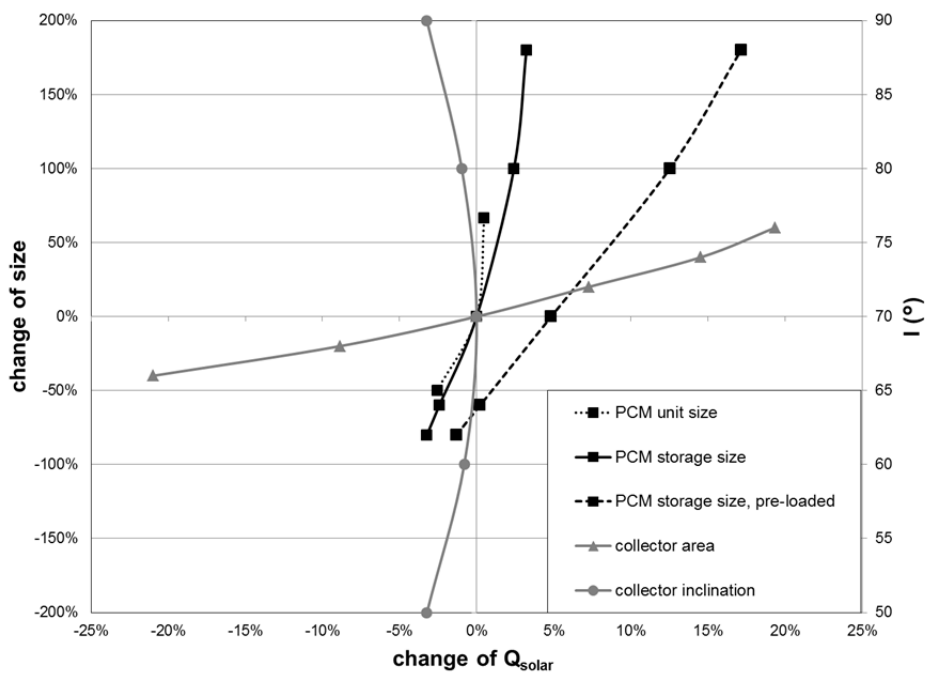


Figure 25. Annual Q_{solar} in dependency of PCM heat storage and collector array parameters (Paper 6).

PCM units of 200 L were found to perform better than units of 150 L. The optimal solar collector array tilt was determined to be 70°. Collector array sizing had the highest impact on Q_{solar} , where relative changes of +/- 20% were calculated with a 60% larger and respectively 40% smaller aperture area. Relatively small changes of Q_{solar} (+/- 3%) were determined for PCM heat storage sizes 180% larger and 80% smaller. Assuming full storage charge at the beginning of the year (pre-loaded PCM heat storage), Q_{solar} would be 5% higher with $V_{\text{PCM}}=1 \text{ m}^3$ and 14% higher with $V_{\text{PCM}}=2.8 \text{ m}^3$, respectively.

5.3. Annual system performance

Table 4 presents the influences of the collector area, the PCM volume (200 L units) and the water tank volume on the annual SF. SF ranged from 47.5% ($V_{\text{water}}=0.6 \text{ m}^3$, $A=9.6\text{m}^2$; $V_{\text{PCM}}=0.2 \text{ m}^3$) to 76.7% ($V_{\text{water}}=1 \text{ m}^3$, $A=25.6 \text{ m}^2$; $V_{\text{PCM}}=2.8 \text{ m}^3$). SF changed moderately (about 4%) by variation of V_{PCM} . Collector area increase from $A=9.6 \text{ m}^2$ to $A=25.6 \text{ m}^2$ increased SF by approximately 25% points throughout all storage sizes. The performance difference was most pronounced between $A=9.6\text{m}^2$ and $A=12.8\text{m}^2$, respectively, between three and four collector panels.

Table 4. Parametric study on annual SF (Paper 6).

| $V_{\text{PCM}} (\text{m}^3)$ | 0.2 | 0.4 | 1 | 2 | 2.8 |
|-------------------------------|---------------------------------------|------|------|------|------|
| No. of units | 1 | 2 | 5 | 10 | 14 |
| A (m^2) | SF (%) with 0.6 m^3 water | | | | |
| 9.6 | 47.5 | 47.9 | 49.1 | 50.3 | 50.3 |
| 12.8 | 54.8 | 55.2 | 56.5 | 57.8 | 59.3 |
| 16 | 60.2 | 60.4 | 62.2 | 63.7 | 64.3 |
| 19.2 | 64.8 | 64.8 | 66.2 | 67.7 | 68.5 |
| 22.4 | 68.9 | 68.9 | 71.2 | 72 | 72.7 |
| 25.6 | 72.7 | 73.8 | 74.2 | 75.1 | 76.1 |

The system was found to perform best with collector aperture areas in between 12.8 and 22.4 m^2 , with $V_{\text{PCM}} < 1 \text{ m}^3$ and when additional storage charge at the beginning of the year was assumed. With $A=22.4 \text{ m}^2$, approximately 1000 kWh heat demand would be covered by 1 m^3 SAT composite and its heat storage capacity would be utilized 5.5 times per year, those of the water tank 116 times per year respectively.

Full-charge of a single 200 L PCM unit and a 0.6 m^3 water tank enabled heat supply of 2 days in January, which increased to 18 days when 2.8 m^3 of SAT composite was charged. The heat storage of the system could be charged several times during winter in periods with surplus of wind energy and in summer, spring and autumn by solar collectors.

As presented in Figure 26, the system could reveal a SF of 71% and additionally utilize wind power generation peaks in winter, whereas only a relatively small storage volume would be required.

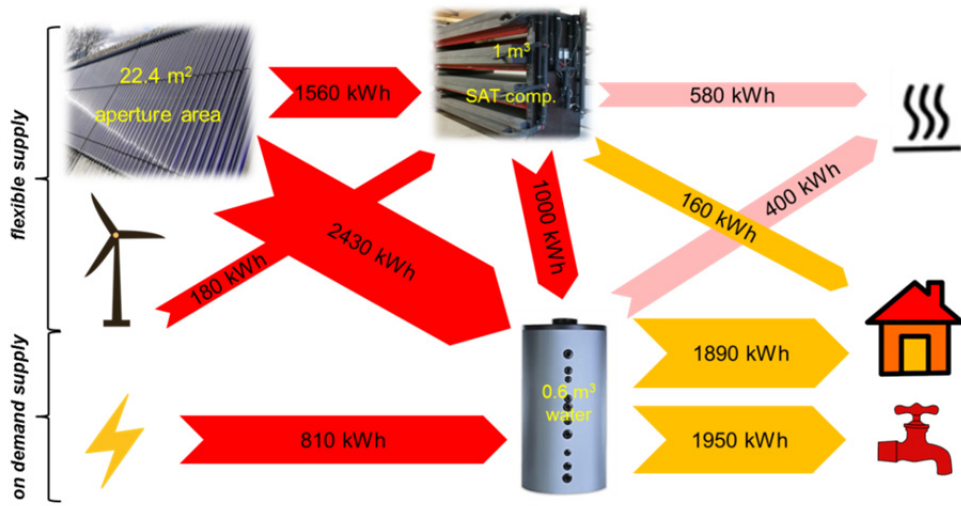


Figure 26. Annual heat flux scenario (supply in red, demand in orange, heat loss in pink) with a SF of 71% (Paper 6).

6. Inexpensive heat storage units

[This section is based on Paper 7]

6.1. Tank-in-tank design

The development of inexpensive heat storage units was based on the following aspects:

- Due to their thermo-physical properties, SAT composites in liquid state enabled good heat transfer in vessels by allowing convection. During solidification, thermal conductivity decreases and no convective heat transfer is possible.
- Rathgeber et al. [74] found that acceptable energy storage capacity costs of heat stores in buildings ranged from about 1 €/kWh for seasonal heat storage to 429 €/kWh for daily utilization. For industrial use SAT is available in large quantities, with market prices typically below 0.5 €/kg. For heat storage units containing 200 kg SAT composites in solar combi-systems, monthly utilization of a heat storage capacity in the range of 15 – 27.4 kWh could be assumed. Thus, acceptable costs would be 100 – 460 €/heat storage unit. Therefore, an inexpensive design of heat exchanger and PCM container is warranted.

A cylindrical heat storage prototype in tank-in-tank design, based on standard components of water heat stores was developed (scheme in Figure 27 a, specification in Table 5). It was manufactured by the Danish company NILAN A/S. A steel tank contains SAT composite and an internal steel spiral heat exchanger. It is centred in an outer steel tank to realize heat exchange via its outer surface (mantle heat exchanger). An installer friendly modular design was realized by rectangular shaped foam insulation and a metal cabinet with sufficient space for piping (Figure 27 b). An expansion vessel can be placed on top of the cabinet.

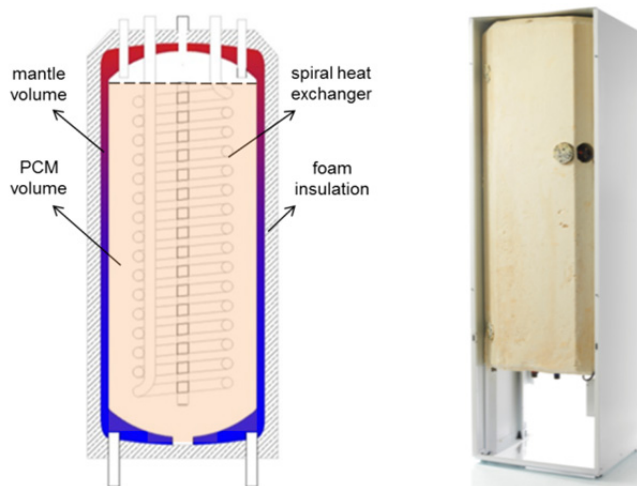


Figure 27. a) Schematic drawing of the intersection (Paper 7);
b) Photograph of the cylindrical heat storage (Paper 7).

| Specifications of the heat store | |
|----------------------------------|---------------------|
| PCM filling | 200 kg |
| Inner tank diameter | 0.45 m |
| Inner tank height | 1.20 m |
| Outer tank diameter | 0.50 m |
| Outer tank height | 1.25 m |
| Heat transfer area | 3.40 m ² |
| PCM volume | 158 L |
| Water volume | 59 L |
| Steel tank mass | 140.8 kg |

Table 5. Specification of the heat store.

6.2. Experimental method

Figure 28 presents the test setup. It was used to investigate whether the concept of stable supercooling can be utilized with the prototype heat store, and furthermore, whether the heat transfer with spiral- and mantle heat exchangers is sufficient for DHW and SH supply in buildings. Energy storage capacities for full charge, short and long-term heat storage were determined with a series of test cycles. The heat transfer properties of the store filled with water or the SAT composite were studied.

A hydraulic circuit with two parallel lines for the spiral and the mantle heat exchanger was built. An electric heater (9 kW) for charge and a plate heat exchanger for cooling via a cooling unit were connected. Water was used as HTF. Performance evaluation was based on measurements of heat transfer fluid flow rates as well as inlet and outlet temperatures in both lines.



Figure 28. Test setup with graphical LabVIEW interface for live data reading.

For this work, a composite containing food-grade SAT (European standard 262i, IG Chemicals GmbH, Germany) 3 %wt. liquid polymer solution HD 310 (Suzhou Hongde Co. Ltd., China) and 2%wt. of extra water was chosen as PCM. Solidification of supercooled SAT composite was initiated by seed crystals which were inserted by an opening to the inner tank. The temperature of the SAT composite was measured with 12 thermocouples, distributed in the inner tank.

The heat exchange capacity rate (HXCR) was used to evaluate the ability to transfer thermal energy between the HTF and the SAT composite:

$$HXCR \left(\frac{W}{K} \right) = \dot{V} * c_p * \rho * \ln \left(\frac{T_{in} - \bar{T}_{PCM}}{T_{out} - \bar{T}_{PCM}} \right) \quad (6)$$

Where the average SAT composite temperature (\bar{T}_{PCM}) was determined with a volume-based weight-model for inner tank measurements.

6.3. Performance

During all 12 test cycles, low supercooling temperatures were achieved, although temperature measurement devices and corrosion on the inner tank surface influenced supercooling stability.

The development of thermal power (\dot{Q}) and heat content of the store (Q_{store}) during a representative test cycle is presented in Figure 29. After charging (orange area) the SAT composite supercooled to ambient temperature and rested for a period of 12 hours (grey area). During SAT composite solidification (blue area) \dot{Q} peaked at approximately 5 kW. The energy storage capacity of the store was measured to be 27 kWh for heat-up from 25 °C to 90 °C, whereas 15.5 kWh of heat was discharged in liquid state and 11.5 kWh of heat was stored in the supercooled PCM. The capacity of the composite was determined to be 21.3 kWh, which was 76 % higher than with water filled in the tank.

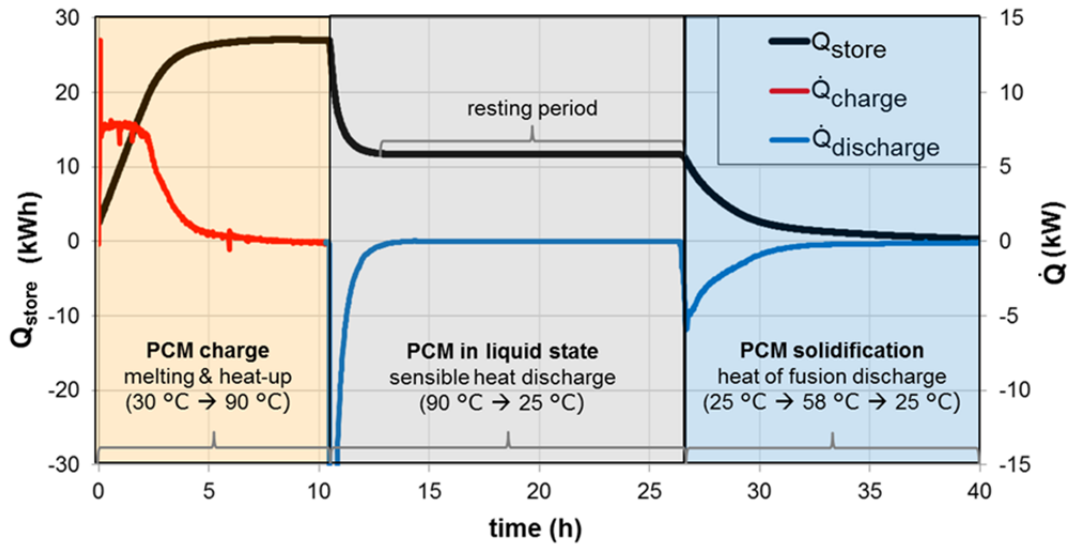


Figure 29. Development of heat transfer rates and heat content during a selected test cycle (Paper 7).

HXCRs during charging and discharging of SAT composite did not change in the flow rate range of 3–10 L/min. This shows that the heat transfer was limited by the SAT composite. For charging, an average HXCR of 298 W/K was found, which was a factor of four lower than for water with a flow rate of 10 L/min.

Combined use of a spiral and a mantle heat exchanger with a flow rate of 2 L/min was advantageous during discharging of liquid SAT composite. Thermal stratification was utilized in the mantle, resulting in outlet temperatures (T_{out}) higher than \bar{T}_{PCM} . During solidification thermal power and outlet temperatures were rather low, and the effectiveness of heat transfer was reduced by a factor of three in comparison to liquid state (further explanations in Paper 7).

Figure 30 presents data from a test cycle with discontinuous discharge. In liquid SAT composite state (grey area) T_{out} was higher than \bar{T}_{PCM} until a heat content of 15 kWh was remaining. Then discharge was interrupted for the first time. Subsequently, discharge was conducted in seven parts, with intervals of 2–24 hours. Thus, it was possible to utilize heat of fusion with thermal power up to 4 kW (flow rate of 2 L/min) and with outlet temperatures close to that of the SAT composite. T_{out} exceeded 30 °C during all discharge parts, which is considered as requirement for SH and DHW supply in domestic dwellings.

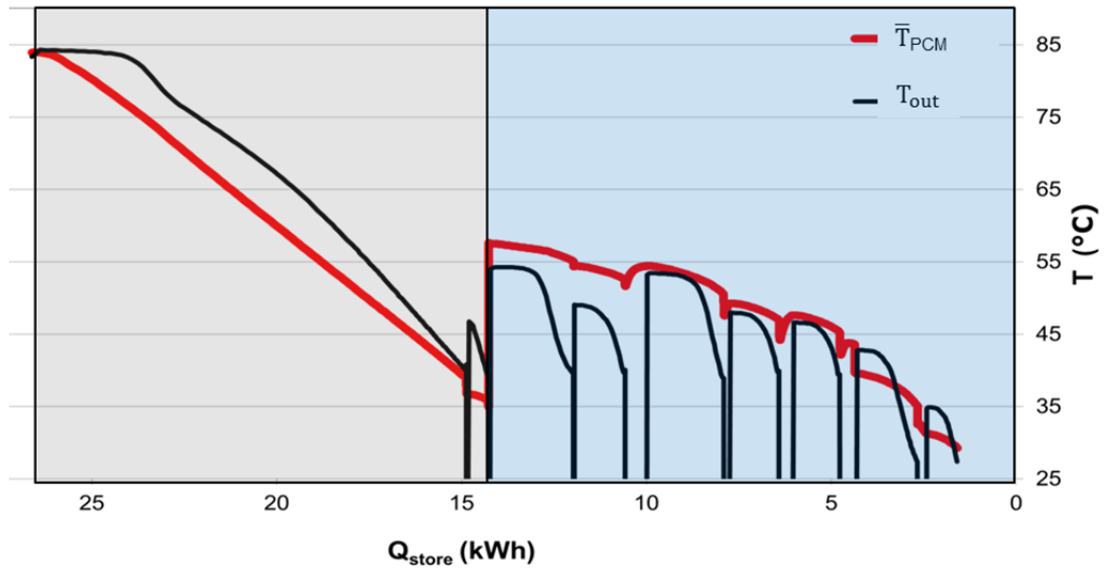


Figure 30. Development of \bar{T}_{PCM} and T_{out} during discontinuous discharge.

7. Measurement uncertainty

The measurement equipment used in the system demonstration and heat storage testing consisted of the following main components:

- Thermocouples TT-type (copper-constantan)
- Thermopiles TT-type (5-junction-sets)
- Flow meters (class 2, European norm 1434): Kamstrup Ultraflow 5400 sensors were applied for heat storage testing and Brunata HGQ sensors for system demonstration, respectively.
- National Instruments data acquisition system with 16-channel modules no. 9214 for thermocouple and thermopile readings and 32-channel digital input/output modules no. 9403 for flow meter readings.
- A LabVIEW programme was used to monitor data in real time. During system demonstration, averaged measurement values were logged in time intervals of 10 sec, 1 minute and 1 hour, whereas a time interval of 1 minute was chosen for heat storage testing.

Prior to installation, systematic error values of temperature sensors and flow meters have been determined and design principles of hydraulic circuits were applied. Flow meters have been calibrated as recommended by the manufacturer. Systematic error values were compensated by applying correction factors during data processing. Flow meter and temperature sensor readings were tested for their variation, resulting from random measurement error. Measurement accuracy calculations were based on the approach of the Guide to the expression in Uncertainty in Measurements (GUM) [75]: Variations of readings were quantified and the combined uncertainty of thermal power (\dot{Q}) was calculated in Matlab. This allowed for evaluation of confidence interval (CI) of measurements, with \dot{Q} as main quantity of interest. A typical state of charge and resulting shares of measurand readings on the uncertainty budget were evaluated. Finally, accuracy of heat loss tests was evaluated.

To calculate the standard uncertainties (u) associated with a measurand X , probability distributions (a–c) of factors influencing the standard uncertainty were considered:

- a) Normal probability distribution (2σ ; the variation of temperature sensors):

$$u^2(X) = \left(\frac{u_{effect}}{2}\right)^2 \quad (7)$$

- b) Normal probability distribution (σ ; the variation of flow meter readings):

$$u^2(X) = u_{effect}^2 \quad (8)$$

- c) Uniform distribution (fluid property calculation, data acquisition system):

$$u^2(X) = \frac{u_{effect}^2}{3} \quad (9)$$

Where the effective uncertainty value (u_{effect}) represents the half value of the CI of the measurand, in which 95.4% (a), 68.2% (b) and all (c) measured values occur. In the normal probability distribution, the standard deviation (σ) equals the half value of the CI. Thus, given u_{effect} for σ equals half the value of u_{effect} for 2σ .

The share of a measurand (X_i) on the uncertainty budget for an objective quantity Y (e.g. thermal power) can be calculated by employing Equation 10:

$$u\%(X_i) = \frac{\left(\frac{\partial Y}{\partial X_i}\right)^2 * u^2(X_i)}{u^2(Y)} * 100 \quad (10)$$

The uncertainty shares were used to determine the impact of sensors to the uncertainty budget of \dot{Q} , which was calculated with Equation 11:

$$\dot{Q}(T_{out}, \Delta T, \dot{V}) = \rho(T_{out}) * \dot{V} * c_p \left(\frac{(T_{out} - \Delta T) + T_{out}}{2} \right) * \Delta T \quad (\text{W}) \quad (11)$$

Table 6 presents a summary of all considered uncertainty factors. Experimental data analysis is based on 1-minute-averaged values. Effective uncertainty values of fluid property formulas corresponded to the IAWPS standard [76].

Table 6. Summary of uncertainty factors.

| Uncertainty factor | Effective uncertainty value | Distribution | Source |
|-------------------------------|-------------------------------|----------------------|--------------------------------|
| ρ | 0.02 (%) | uniform | Zirkel Hofer et al. [77] |
| c_p | 0.02 (%) | uniform | Zirkel Hofer et al. [77] |
| \dot{V} | reference precision: 0.5 (%) | normal (σ) | Calibration, manufacturer [78] |
| T_{out} (incl. datalogger) | reference precision: 0.3 (K) | normal (2σ) | Experimental data analysis* |
| ΔT (incl. datalogger) | reference precision: 0.15 (K) | normal (2σ) | Experimental data analysis |

*: Furbo[79] reported a maximum variation of 0.42 K of TT-thermocouple readings.

Single measurement uncertainty

A typical operation state during charge with a single heat exchanger was used to determine variation of \dot{Q} . The following measurand mean values were chosen:

- HTF flow: 2 L/min
- HTF ρ : 983.35 kg/m³
- ΔT : 30 K
- HTF c_p : 4.1901 kJ/kg K

Probability distributions of measurands were implemented in Matlab via a high number of calculated random observations (150000). This approach was possible, because all effective uncertainty values of measurands were determined as combined values of sensor and data acquisition system.

Figure 31 shows histograms of the defined measurand properties (blue) and resulting variation of \dot{Q} (red). The effective uncertainty values of the reference scenario (Table 6) were used.

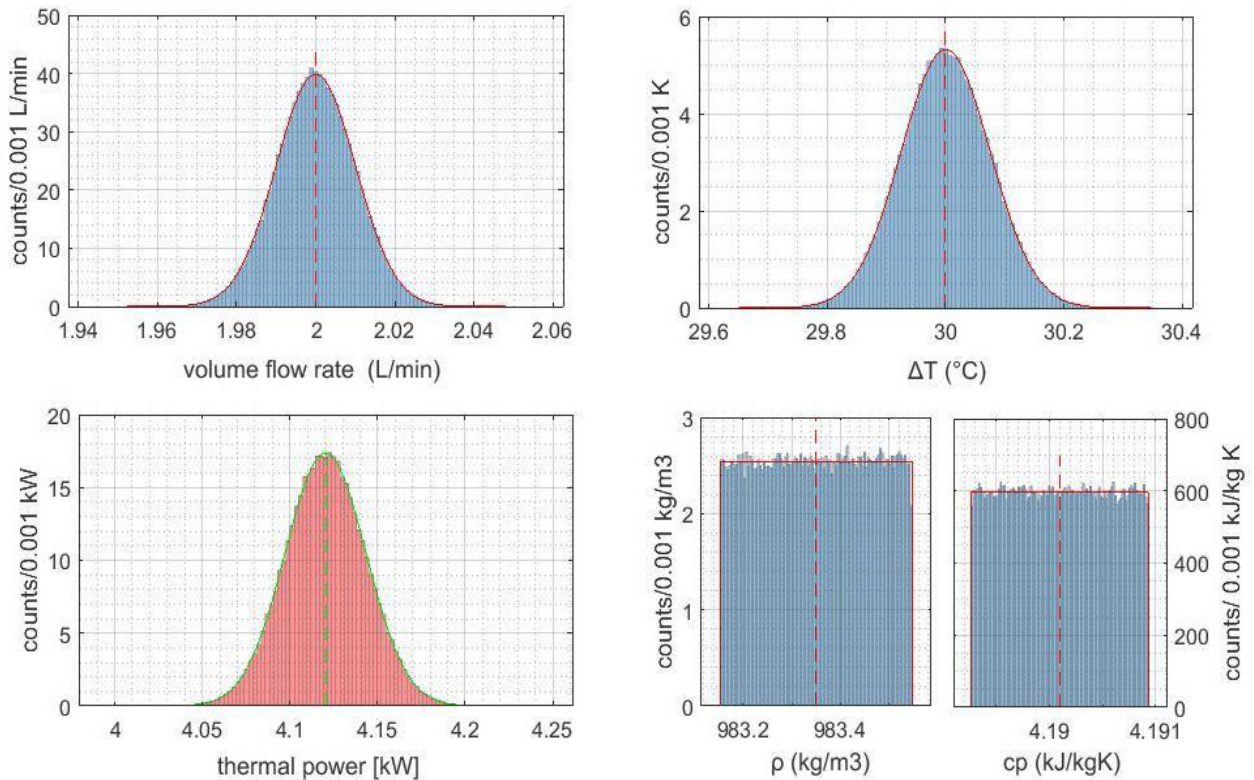


Figure 31. Evaluation of a single measurement.

The mean thermal power was 4.12 kW and results were normally distributed with a standard deviation (σ) of $\pm 0.56\%$ (± 23 W). The combined measurement accuracy in the 95.4% CI was $\pm 1.12\%$ and ± 46 W, respectively.

In accordance with Equation 10 the share of measurands on the uncertainty budget was evaluated. The standard deviation of \dot{Q} was used as reference. For the investigated state of charge, flow meter readings accounted for 80% and thermopile readings for 20% of the measurement uncertainty budget. The share of fluid property calculations on the uncertainty budget was negligible small.

As found in calibration tests, the flow meter readings displayed a constant, *relative* variation over the full operation range. Temperature readings however showed constant *absolute* variations. Therefore, with increasing state of charge/discharge, the uncertainty budget of \dot{Q} became highly dependent on thermopile readings (ΔT). Figure 32 shows the development of CIs of \dot{Q} dependent on ΔT , where a constant HTF flow rate of 2 L/min was assumed. Decreasing ΔT led to significantly higher standard deviations of \dot{Q} ($\pm 0.562\%$ for 30 K; $\pm 0.9\%$ for 10 K; $\pm 7.5\%$ for 1 K).

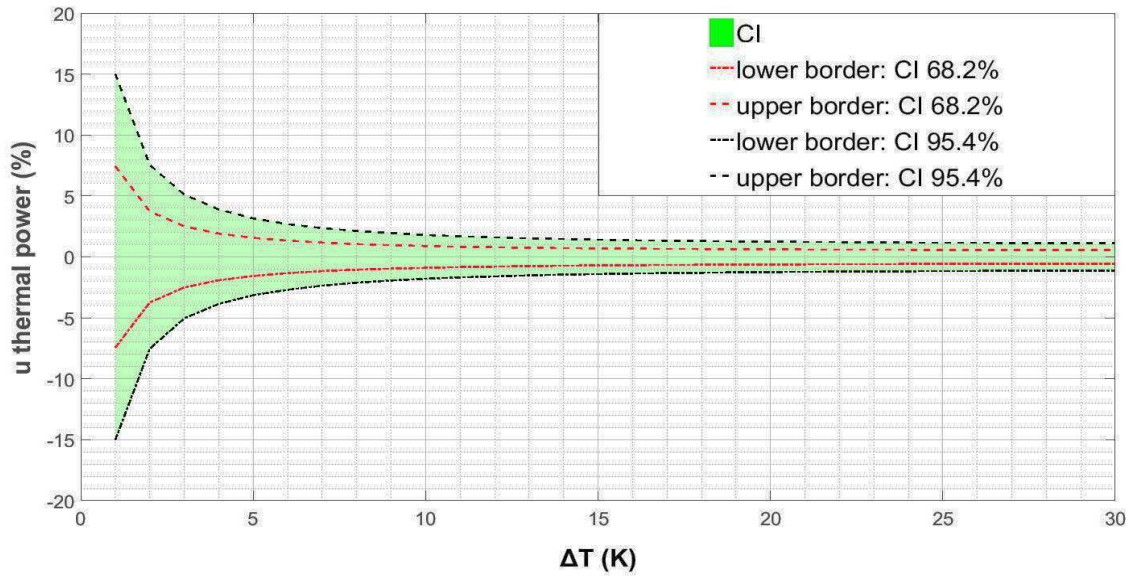


Figure 32. \dot{Q} in dependency of ΔT .

Determination of steady state heat losses

A steady state heat loss test with the following mean measurand values was analyzed:

- HTF flow: 2 L/min
- HTF ρ : 978 kg/m³
- ΔT : 0.45 K
- HTF c_p : 4.1863 kJ/kg K

With given values \dot{Q} was calculated to be 61 W with a standard deviation of $\pm 18\%$ (± 11 W).

Figure 33 presents the evaluation of one heat loss test where measurements were taken for 120 minutes. With 120 observations (random variation assumed) its mean value was determined to be 60.8 W. Although measurements were unprecise, the determined heat loss became relatively accurate. Smaller uncertainty could be achieved by using a lower flow rate, which would result in higher ΔT .

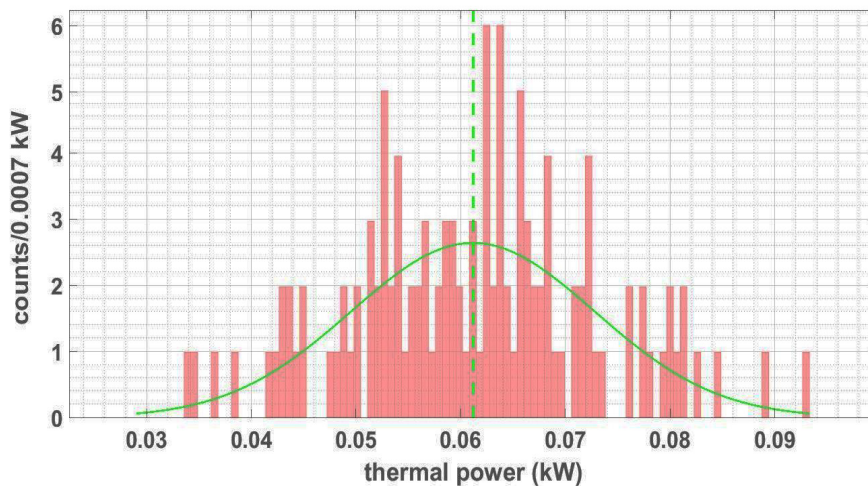


Figure 33. Variation of \dot{Q} during a heat loss test with 120 observations.

8. Conclusions

For the first time, a solar combi-system utilizing stable supercooling of SAT composited was demonstrated. Its development resulted in:

- SAT composites with thickening agents and liquid additives were identified to be suitable for heat storage with stable supercooling. Their heat of fusion available in supercooled state at 20 °C was:
 - 210–216 kJ/kg with 0.5–2%wt. of carboxymethyl cellulose and 0.3–0.5%wt. xanthan gum
 - 205–216 kJ/kg with 1–2%wt. of EDTA and liquid polymeric solutions
- In steel containers SAT composites supercool to temperatures below -8 °C, whereas sodium acetate water mixtures in glass jars supercooled down to -24 °C.
- To efficiently use heat storage units in a solar combi system, their sensible heat capacity in liquid state should be utilized for short heat storage periods (hours, days), and their heat of fusion for long-term heat storage (weeks, months), respectively.
- Devices can be used to initiate crystallization of supercooled composites in heat storage units on demand:
 - Mechanical seed crystal injection via a hollow needle
 - Local cooling by evaporating carbon dioxide in a chamber adjacent to PCM units
 - Local cooling with Peltier elements mounted on PCM units
- The heat storage concept worked in a solar combi-system by means of a novel control strategy. The PCM heat storage needed to consist of several PCM units. It can be built with flat units containing 200 kg SAT composite each, resulting in an effective energy storage density of 48 kWh/m³.
- For efficiency, solar collectors firstly charged the water tank and then the PCM heat storage. The number of PCM units is needed to be varied during charging to match their limited heat transfer capacity with the fluctuating collector power.
- Heat transfer fluid flow rates of ~ 16 L/min were suitable to charge flat PCM units up to 90 °C, whereas discharge flow rates of 2 L/min were needed to heat the water tank. In this way, about 80% of conserved heat of fusion was utilized during discharge from stable supercooled SAT composite.
- Validated component models and verified control parameters were applicable for system simulation in a Danish Passive House scenario. The system was found to perform best with PCM volumes below 1 m³, PCM units of 200 L, a 0.6 m³ water tank and with collector aperture areas of 12.8–22.4 m², with an inclination angle of 70°. A scenario with 1 m³ of SAT composites, optimized component specifications, 22.4 m² (aperture) collector area and 3977 kWh of total heat demand resulted in a solar fraction of 71%.
- Inexpensive tank-in-tank heat storage units, built with standard components of water stores were able to utilize SAT composite with liquid polymers. Heat transfer with liquid SAT composite was sufficient for hot water supply and space heating, whereas pulsed discharge would be needed during solidification.

Table 7 presents the summarized conclusion to the examination of research hypotheses.

Table 7. Conclusions to the investigations of research hypotheses.

| Hypothesis | Conclusion |
|---|---|
| <p>a) SAT, extra water and liquid polymers forms a composite enabling convective heat transfer in liquid state and can supercool to room temperature without phase separation occurring</p> | <p>True. Analysis of heat storage tests showed that SAT containing 3%wt. HD 310 and 2%wt. water provided a heat of fusion 207 kJ/kg in supercooled state at 25 °C. Its latent heat of fusion (58 °C) was determined to be 238 kJ/kg SAT, which corresponds to impure SAT. During 12 test cycles the heat content did not change. Convection improved heat transfer in liquid state.</p> |
| <p>b) Heat of fusion can be utilized on demand for building heat supply, utilizing seed crystal injection or local cooling in heat storage units containing SAT composites</p> | <p>True. A control logic including a mode for discharge of heat of fusion was verified during system demonstration. Activation devices utilizing mechanical seed crystal injection worked in initial tests. The functionality of devices for local cooling utilizing CO₂ evaporation or Peltier elements was verified by tests on heat storage prototype units.</p> |
| <p>c) Heat storage units with heat transfer limitations can be integrated in a solar combi-system by means of appropriate hydraulic design and control</p> | <p>Largely True. Sequences of water tank charge and parallel charge of PCM units enabled continuous operation of the solar collector circuit. During discharge of flat PCM units, thermal power and flow temperatures were sufficiently high to cover space heating demands. However, further system and PCM unit development is needed to enable hot water supply via stored heat from supercooled SAT composite.</p> |
| <p>d) Utilization SAT composites in a solar combi-system will result in high solar fractions of domestic hot water and space heating supply in a Danish Passive House</p> | <p>True. The heat storage concept was verified in system demonstration. System simulation showed that in spring and autumn, up to three PCM units were subject to repeated charge and discharge, while additional PCM units were utilized as seasonal storage from summer to winter. In this way, solar fractions above 70% could be achieved with a relatively large collector area and a relatively small heat storage volume.</p> |
| <p>e) Inexpensive heat storage units utilizing stable supercooling of SAT composites can be built with standard components of water heat stores</p> | <p>Largely true. Combined short and long-term heat storage was demonstrated with a tank-in-tank heat store, manufactured in steel. During 12 test cycles over 19 months low supercooling temperatures were achieved. However, in seven test cycles uncontrolled crystallization occurred. Potential reasons were identified; improvement of the heat store is needed.</p> |

The concept of combined long- and short term heat storage was proved to be applicable in solar combi-systems. This work will form the basis for development of solar heating systems for energy efficient buildings with solar fractions above 70%.

9. Perspectives

9.1. Material development

As elaborated in Paper 2, SAT in food grade differs in water content. Extra water was needed to fully dissolve the delivered SAT during melting. It can be assumed that: a) For heat storage application 1–2%wt. of extra water is needed to compensate water vapor losses during melting; b) Water vapor condenses and returns to liquid SAT during supercooling.

As elaborated in Section 4.5, the condition of SAT composites changed during two years of application in flat heat storage units: No visual change was observed for the composite containing EDTA. Graphite powder and oil was demixed from the SAT composite containing CMC. It can therefore be assumed that this composition is not durable. Also, CMC showed potential signs of degradation, which needs to be systematically investigated.

The SAT composite containing the liquid polymer HD 310 and extra water was performing well after 12 test cycles in the tank-in-tank store. Tests with a high number of heat storage cycles, considering long durations of heating at 90 °C are needed to prove its applicability in metal heat storage units. Tests of several units for several years would be necessary. This would require a lot of personnel and material resources. A company with commercial interest could potentially raise such resources, accompanied by scientific guidance.

Machida et al. [46] found a relationship between supercooling stability and solution structure in SA-aqueous solutions by means of scanning electron microscopy. They concluded that the slow aggregation process of molecule clusters is the reason for the high supercooling degree of melted SAT. As elaborated in Paper 2, during cooling of SA-water mixtures a second exothermic reaction was observed, which did not appear during cooling of SAT composites containing thickening agents or liquid polymers. In this context, a full explanation of how thickening agents and liquid polymers overcome phase separation is missing. Microscopy of SAT composites, crystallized from supercooled solution, could therefore be of interest. Further, x-ray diffraction could be used to investigate potential differences in crystal structures.

9.2. Heat storage development

As elaborated in Section 6.1, acceptable heat storage unit costs (~200 kg SAT composite) would be in the range of 100–460 €/unit assuming monthly utilization of its energy storage capacity. For economic assessments SAT, additives, container, heat exchanger, hydraulics and devices for controlled activation of crystallization need to be taken into account. Considering thickening agents or liquid polymers, costs of SAT composites of approximately 100 €/unit result. To build heat storage units with activation devices below 460 €, the following aspects could be considered:

- Cylindrical unit design potentially allows material reduction and application of cheaper heat exchangers in comparison to flat units. Also, a smaller surface-volume ratio is required for efficient sensible heat storage.

- To withstand repeated cycles of charging and discharging, the mechanical seed crystal injection device would need to be manufactured in a more temperature-resistant material. However, the device was rather complex. Sealing membranes could fail, which means a potential risk of unwanted spontaneous solidification of supercooled composites. In contrast, local cooling using CO₂ evaporation or Peltier elements can be done without any moving parts in the supercooled SAT and without penetrating the chamber containing the PCM. Local cooling is therefore considered a potentially more durable and cost-efficient solution.
- PCM units in stainless steel did not show corrosion. PCM units in steel (flat and cylindrical) however showed corrosion of surfaces which were in contact with SAT composite and air. This is considered as a source of unwanted nucleation of supercooled SAT composite. Because stainless steel is expensive, two potential solutions for inexpensive PCM units could be investigated: a) Containers and heat exchangers in steel and using oil as filling material. This could also result in improved heat transfer by filling cavities, which occur during SAT solidification; b) Using polymeric vessels and heat exchangers. Potentially attractive materials could be polymers used in solar collectors (e.g. used to heat swimming pools), which are durable in terms of temperature. However, it must be investigated if the water permeability of polymeric vessels is sufficiently low to not interfere supercooling stability and to avoid long-term change of the SAT composition.
- Container and heat exchanger could be built with lower thickness than for water heat stores if the static pressure of the heat transfer fluid could be maintained close to atmospheric conditions.

9.3. System development

The solar combi-system prototype could be improved by considering the following aspects:

- The units were installed in such a way that they could be tested individually. Better thermal insulation and a more compact arrangement of PCM units are needed to reduce sensible heat losses.
- The system prototype could be improved by shortening pipework lengths.
- Control logic to avoid PCM units cooling during charging should be considered.
- About 80% of the conserved heat of fusion was utilized during discharge from stable supercooled PCM units. However, with the present storage configuration, hot water supply must be realised with a backup heater to ensure supply temperatures above 45 °C. To overcome heat transfer limitations of PCM units, larger heat exchangers and additives for thermal conductivity enhancement of SAT composites would be required. Both measures would cause costs. As an alternative, application of several inexpensive stores (tank-in-tank design) in parallel could enable heat supply in buildings utilizing discontinuous discharge of single stores. Pulsed-flow must be then included in the control logic.

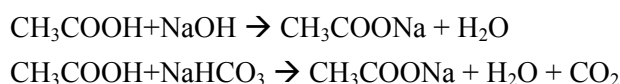
Energy storage is needed to overcome the mismatch between renewable electricity generation and hot water, heating and cooling demand [80]. Finck et al. [81] investigated demand flexibility of water tanks, PCM and solid sorption as heat storage. The study of a Danish Passive House with a solar combi-system utilizing on-demand crystallization of SAT showed potential for decentralized electrical grid stabilization in regions with a large wind power generation capacity in winter. This could be an interesting aspect for future research activities.

For better economy, application of PCM units with a high number of annual storage cycles is needed. Reduction of collector area lowers system costs in solar combi-systems, but reduces applicability of SAT composites. Further studies elucidating optimal application of PCM units are therefore needed. Investigations may include the following aspects:

- Applicability of flat plate solar collectors, which are less expensive than evacuated tubular collectors.
- System performance in different climates. It can be assumed that the system performs more efficient in locations with increased heat demand and solar irradiation in winter time. Typical meteorological years of attractive locations, for example Switzerland or China (Hebei, Tibet) could be used in system simulation. Concerning heating patterns Chinese locations seem to be especially attractive: Direct solar irradiation is well distributed over the year; High heating loads of building occur in winter; The cooling demand in summer is high and could be covered by thermally-driven chillers employing sorption processes.
- Adaption of control logic will be required when changing collector types and demand patterns.
- For this work, PCM units were modelled by using thermo-physical properties of SAT composites, steel and water. Instead, the heat transfer properties of novel heat storage units could be implemented in system simulation by data sets. As reported in Paper 7, with a constant HTF flow rate the heat content of a store corresponds to a specific average SAT composite temperature, thermal power and heat exchange capacity rate. Heat transfer properties could be therefore described in dependency of the state of charge/discharge.

9.4. Life cycle aspects

Within the German project “Speicher-LCA” novel heat storage materials were evaluated by a life cycle assessment [82]. Sodium acetate is industrially produced by reacting sodium hydroxide, sodium carbonate or sodium bicarbonate with acetic acid:



The reaction occurs in a static mixer, the reactants are in aqueous solution. Acetic acid and sodium hydroxide are diluted with water and then fed into the mixer. The SA solution is stored in a storage tank. When sodium carbonate is used as a reactant, gaseous carbon dioxide is emitted. In the final step, water is added to the SA solution to achieve SAT.

For global warming potential calculation, different market shares of primary product productions are considered. Further, the calculation also includes the energy mix in electricity and heat supply in relevant locations of production. The study concluded that the global warming potential of a SAT composite including CMC and graphite flakes, as developed by Dannemand et al. [42], is 2.0 kg CO₂ equivalent per kilogram composite [83]. SAT accounted to 83.7% and additives (CMC, graphite) accounted to 14.1 % of this number.

Because attributional approach was used, the full production impact accounted to SAT. Potential recycling was not investigated. In heat storage application, the global warming potential of SAT composites could be compensated by increasing the efficiency of renewable energy supply systems (e.g. in a solar combi-system). Thus, the more annual heat storage cycles can be achieved, the more ecological is the application of SAT.

References

- [1] European Parliament, Directive 2012/27/EU of the European Parliament and of the Council of 25 October 2012 on energy efficiency, amending Directives 2009/125/EC and 2010/30/EU and repealing Directives 2004/8/EC and 2006/32/EC. Official Journal of the European Union, 315, pp. 1–56, 2012.
- [2] European Parliament, Directive 2010/31/EU of the European Parliament and of the Council of 19 May 2010 on the energy performance of buildings. Official Journal of the European Union, 153, pp. 13–35, 2010.
- [3] L. F. Cabeza, L. Miró, E. Oró, A. de Gracia, V. Martin, A. Kroenauer, C. Rathgeber, M. M. Farid, H. O. Paksoy, M. Martínez, and A. I. Fernández, “CO₂ mitigation accounting for Thermal Energy Storage (TES) case studies,” *Appl. Energy*, vol. 155, pp. 365–377, 2015.
- [4] Weiss W. (Ed.), *Solar Heating Systems for Houses, a Design Handbook for Solar Combisystems*. James & James Ltd., UK, 2003.
- [5] DS 439, “Norm for vandinstallationer – Code of Practice for domestic water supply,” Danish Standards, 75 pp., 2009.
- [6] W. Streicher, R. Heimrath, and C. Bales, “Analysis of System Reports of Task 26 for Sensitivity of Parameters,” December 2003 (revised February 2007).
- [7] S. Furbo, E. Andersen, A. Thür, L. J. Shah, and K. D. Andersen, “Performance improvement by discharge from different levels in solar storage tanks,” *Sol. Energy*, vol. 79, no. 5, pp. 431–439, 2005.
- [8] L.J. Shah, E. Andersen, and S. Furbo, “Theoretical and experimental investigations of inlet stratifiers for solar storage tanks,” *Appl. Therm. Eng.*, vol. 25, no. 14–15, pp. 2086–2099, 2005.
- [9] M.Y. Haller, E. Yazdanshenas, E. Andersen, C. Bales, W. Streicher, and S. Furbo, “A method to determine stratification efficiency of thermal energy storage processes independently from storage heat losses,” *Sol. Energy*, vol. 84, no. 6, pp. 997–1007, 2010.
- [10] A. Thür, “Compact solar Combi-system – High Efficiency by Minimizing Temperatures,” PhD thesis, Technical University of Denmark, Department of Civil Engineering report no. R-160, 2007.
- [11] S. Colclough and T. McGrath, “Net energy analysis of a solar combi system with Seasonal Thermal Energy Store,” *Appl. Energy*, vol. 147, pp. 611–616, 2015.
- [12] W. Kramer, A. Oliva, G. Stryi-Hipp, S. Kobelt, D. Bestenlehner, H. Drück, J. Bühl, and G. Dasch, “Solar-active-houses – Analysis of the building concept based on detailed measurements,” *Energy Procedia*, vol. 48, pp. 895–903, 2014.
- [13] A. Oliva, G. Stryi-Hipp, S. Kobelt, D. Bestenlehner, H. Drück, and G. Dasch, “Solar-Active-Houses - Dynamic System Simulations to Analyze Building Concepts with High Fractions of Solar Thermal Energy,” *Energy Procedia*, vol. 70, pp. 652–660, 2015.
- [14] A. Ristić, S. Furbo, C. Moser, H. Schranzhofer, A. Lazaro, M. Delgado, C. Peñalosa, L. Zalewski, G. Diarce, C. Alkan, S.N. Gunasekara, T. Haussmann, S. Gschwander, C. Rathgeber, H. Schmit, C. Barreneche, L. Cabeza, G. Ferrer, Y. Konuklu, H. Paksoy, H. Rammelberg, G. Munz, T. Herzog, J. Jänchen, and E.P. del Barrio, “IEA SHC Task 42 / ECES Annex 29 WG A1: Engineering and Processing of PCMs, TCMs and Sorption Materials,” *Energy Procedia*, vol. 91, pp. 207–217, 2016.
- [15] B. Mette, H. Kerskes, H. Drück, and H. Müller-Steinhagen, “New highly efficient regeneration process for thermochemical energy storage,” *Appl. Energy*, vol. 109, pp. 352–359, 2013.
- [16] T. Nonnen, S. Beckert, K. Gleichmann, A. Brandt, B. Unger, H. Kerskes, B. Mette, S. Bonk, T. Badenhop, F. Salg, and R. Gläser, “A Thermochemical Long-Term Heat Storage System Based on a Salt/Zelite Composite,” *Chem. Eng. Technol.*, vol. 39, no. 12, pp. 2427–2434, 2016.

- [17] B. Zettl and H. Kirchsteiger, "An open sorption heat storage application," in Proceedings of the International Sustainable Energy Conference (ISEC) 2018, pp. 605–611, 2018.
- [18] B. Zettl, G. Englmaier, and G. Steinmaurer, "Development of a revolving drum reactor for open-sorption heat storage processes," *Appl. Therm. Eng.*, vol. 70, no. 1, pp. 42–49, 2014.
- [19] R. Köll, W. van Helden, G. Engel, W. Wagner, B. Dang, J. Jänchen, H. Kerskes, T. Badenhop, and T. Herzog, "An experimental investigation of a realistic-scale seasonal solar adsorption storage system for buildings," *Sol. Energy*, vol. 155, pp. 388–397, 2017.
- [20] R. Weber and V. Dorer, "Long-term heat storage with NaOH," *Vacuum*, vol. 82, no. 7, pp. 708–716, 2008.
- [21] B. Fumey, R. Weber, and L. Baldini, "Liquid sorption heat storage – A proof of concept based on lab measurements with a novel spiral fined heat and mass exchanger design," *Appl. Energy*, vol. 200, pp. 215–225, 2017.
- [22] J. Xu, R. Z. Wang, and Y. Li, "A review of available technologies for seasonal thermal energy storage," *Sol. Energy*, vol. 103, pp. 610–638, 2013.
- [23] T. Kousksou, P. Bruel, a. Jamil, T. El Rhafiki, and Y. Zeraouli, "Energy storage: Applications and challenges," *Sol. Energy Mater. Sol. Cells*, vol. 120, no. PART A, pp. 59–80, 2014.
- [24] B. Zalba, J.M. Marín, L.F. Cabeza, and H. Mehling, "Review on thermal energy storage with phase change: materials, heat transfer analysis and applications," *Appl. Therm. Eng.*, vol. 23, no. 3, pp. 251–283, 2003.
- [25] M.A. Rogerson and S.S.S. Cardoso, "Solidification in heat packs: I. Nucleation rate," *AIChE J.*, vol. 49, no. 2, pp. 505–515, 2003.
- [26] G.A. Lane, *Solar heat storage latent heat material, Volume 1: Background and Scientific Principles*. CRC, 1983.
- [27] J.M. Schultz and S. Furbo, "Investigation of heat of fusion storage for solar low energy buildings," *Proc. Sol. World Congr. 2005 Bringing Water To World, Incl. Proc. 34th Ases Annu.*, vol. 3, pp. 1833–1838, 2005.
- [28] J. Schultz and S. Furbo, "Solar heating systems with heat of fusion storage with 100% solar fraction for solar low energy buildings," in *ISES Solar World Congress 2007 Proceedings*, 2007, pp. 2721–2725.
- [29] M. Dannemand, J. M. Schultz, J. B. Johansen, and S. Furbo, "Long term thermal energy storage with stable supercooled sodium acetate trihydrate," *Appl. Therm. Eng.*, vol. 91, pp. 671–678, 2015.
- [30] W. F. Green, "The 'Melting-Point' of Hydrated Sodium Acetate : Solubility Curves," *J. Phys. Chem.*, vol. 12, pp. 655–660, 1908.
- [31] N. V. Sidwick and J. A. Jentle, "The solubilities of alkali formats and acetates in water.," *J. Chem. Soc.*, pp. 1837–1843, 1922.
- [32] N. Araki, M. Futamura, A. Makino, and H. Shibata, "Measurements of Thermophysical Properties of Sodium Acetate Hydrate," *International J. Thermophys.*, vol. 16, no. 6, pp. 1455–1466, 1995.
- [33] S. Furbo and S. Svendsen, "Report on heat storage in a solar heating system using salt hydrates," Technical University of Denmark, Thermal Insulation Laboratory, report no. 70, 1977.
- [34] H. Kimura and J. Kai, "Phase change stability of sodium acetate trihydrate and its mixtures," *Sol. Energy*, vol. 35, no. 6, pp. 527–534, 1985.
- [35] W. Kong, M. Dannemand, J.B. Berg, J. Fan, G. Englmaier, J. Dragsted and S. Furbo, "Experimental investigations on phase separation for different heights of sodium acetate water mixtures under different conditions," *Appl. Therm. Eng.*, vol. 148, pp. 796–805, 2019.
- [36] M. Dannemand, J.B. Johansen, W. Kong, and S. Furbo, "Experimental investigations on cylindrical latent heat storage units with sodium acetate trihydrate composites utilizing supercooling," *Appl. Energy*, vol. 177, pp. 591–601, 2016.

- [37] M. Dannemand, J. Dragsted, J. Fan, J.B. Johansen, W. Kong, and S. Furbo, "Experimental investigations on prototype heat storage units utilizing stable supercooling of sodium acetate trihydrate mixtures," *Appl. Energy*, vol. 169, pp. 72–80, 2016.
- [38] M. Dannemand, M. Delgado, A. Lazaro, C. Penalosa, C. Gundlach, C. Trinderup, J.B. Johansen, C. Moser, H. Schranzhofer, and S. Furbo, "Porosity and density measurements of sodium acetate trihydrate for thermal energy storage," *Appl. Therm. Eng.*, vol. 131, pp. 707–714, 2018.
- [39] A. Sharma, V. V Tyagi, C. R. Chen, and D. Buddhi, "Review on thermal energy storage with phase change materials and applications," *Renew. Sustain. Energy Rev.*, vol. 13, no. 2, pp. 318–345, 2009.
- [40] J. Pereira da Cunha and P. Eames, "Thermal energy storage for low and medium temperature applications using phase change materials – A review," *Appl. Energy*, vol. 177, pp. 227–238, 2016.
- [41] L. F. Cabeza, G. Svensson, S. Hiebler, and H. Mehling, "Thermal performance of sodium acetate trihydrate thickened with different materials as phase change energy storage material," *Appl. Therm. Eng.*, vol. 23, no. 13, pp. 1697–1704, 2003.
- [42] M. Dannemand, J.B. Johansen, and S. Furbo, "Solidification behavior and thermal conductivity of bulk sodium acetate trihydrate composites with thickening agents and graphite," *Sol. Energy Mater. Sol. Cells*, vol. 145, Part 3, pp. 287–295, 2016.
- [43] H. W. Ryu, S. W. Woo, B. C. Shin, and S. D. Kim, "Prevention of supercooling and stabilization of inorganic salt hydrates as latent heat storage materials," *Sol. Energy Mater. Sol. Cells*, vol. 27, no. 2, pp. 161–172, 1992.
- [44] IG Chemicals, Specification sheet SAT E262i. Bad Salzufen, Germany, 2015.
- [45] J.W. Mullin, *Crystallization*, 4th Edition, Oxford: Butterworth-Heinemann, 2001.
- [46] H. Machida, T. Sugahara, and I. Hirasawa, "Relationship between supercooling stability and solution structure in sodium acetate aqueous solution," *J. Cryst. Growth*, vol. 475, pp. 295–299, 2017.
- [47] P.L. Dietz, J.S. Brukner, and C.A. Hollingsworth, "Linear Crystallization Velocities of Sodium Acetate in Supersaturated Solutions," *J. Phys. Chem.*, vol. 61, no. 7, pp. 944–948, 1957.
- [48] T. Munakata and S. Nagata, "Electrical initiation of solidification and preservation of supercooled state for sodium acetate trihydrate," in *Proceedings of the International Heat Transfer Conference*, 2010.
- [49] Z. Ma, H. Bao, and A. P. Roskilly, "Study on solidification process of sodium acetate trihydrate for seasonal solar thermal energy storage," *Sol. Energy Mater. Sol. Cells*, vol. 172, pp. 99–107, 2017.
- [50] M. A. Rogerson and S. S. S. Cardoso, "Solidification in heat packs: III. Metallic trigger," *AIChE J.*, vol. 49, no. 2, pp. 522–529, 2003.
- [51] K. Seo, S. Suzuki, T. Kinoshita, and I. Hirasawa, "Effect of Ultrasonic Irradiation on the Crystallization of Sodium Acetate Trihydrate Utilized as Heat Storage Material," *Chem. Eng. Technol.*, vol. 35, no. 6, pp. 1013–1016, 2012.
- [52] M. A. Rogerson and S. S. S. Cardoso, "Solidification in heat packs: II. Role of cavitation," *AIChE J.*, vol. 49, no. 2, pp. 516–521, 2003.
- [53] L. Wei and K. Ohsasa, "Supercooling and Solidification Behavior of Phase Change," *ISIJ Int.*, vol. 50, no. 9, pp. 1265–1269, 2010.
- [54] A. López-navarro, J. Biosca-Taronger, J.M. Corberán, C. Peñalosa, A. Lázaro, P. Dolado, and J. Payá, "Performance characterization of a PCM storage tank," *Appl. Energy*, vol. 119, pp. 151–162, 2014.
- [55] C. Zauner, F. Hengstberger, B. Mörzinger, R. Hofmann, and H. Walter, "Experimental characterization and simulation of a hybrid sensible-latent heat storage," *Appl. Energy*, vol. 189, pp. 506–519, 2017.
- [56] A. Frazzica, M. Manzan, A. Sapienza, A. Freni, G. Toniato, and G. Restuccia, "Experimental testing of a hybrid

sensible-latent heat storage system for domestic hot water applications,” *Appl. Energy*, vol. 183, pp. 1157–1167, 2016..

- [57] P. Moreno, L. Miró, A. Solé, C. Barreneche, C. Solé, I. Martorell, and L. F. Cabeza, “Corrosion of metal and metal alloy containers in contact with phase change materials (PCM) for potential heating and cooling applications,” *Appl. Energy*, vol. 125, pp. 238–245, 2014.
- [58] G. Zhou and Y. Xiang, “Experimental investigations on stable supercooling performance of sodium acetate trihydrate PCM for thermal storage,” *Sol. Energy*, vol. 155, pp. 1261–1272, 2017.
- [59] S. Furbo, J. Fan, E. Andersen, Z. Chen, and B. Perers, “Development of seasonal heat storage based on stable supercooling of a sodium acetate water mixture,” *Energy Procedia*, vol. 30, pp. 260–269, 2012.
- [60] M. Dannemand, J. Fan, S. Furbo, and J. Reddi, “Validation of a CFD Model Simulating Charge and Discharge of a Small Heat Storage Test Module based on a Sodium Acetate Water Mixture,” *Energy Procedia*, vol. 57, pp. 2451–2460, 2014.
- [61] J. Fan, S. Furbo, E. Andersen, Z. Chen, B. Perers, and M. Dannemand, “Thermal behavior of a heat exchanger module for seasonal heat storage,” *Energy Procedia*, vol. 30, pp. 244–254, 2012.
- [62] J. Deng, S. Furbo, W. Kong, and J. Fan, “Thermal performance assessment and improvement of a solar domestic hot water tank with PCM in the mantle,” *Energy Build.*, vol. 172, pp. 10–21, 2018.
- [63] J. A. Quinnell and J. H. Davidson, “Heat and mass transfer during heating of a hybrid absorption/sensible storage tank,” *Sol. Energy*, vol. 104, pp. 19–28, 2014.
- [64] H. Mehling and L. F. Cabeza, “Materials used as PCM in thermal energy storage in buildings: A review,” *Renew. Sustain. Energy Rev.*, pp. 1675–1695, Apr. 2011.
- [65] K.N. Marsh (Editor), *Recommended Reference Materials for the Realization of Physicochemical Properties*. Oxford: Blackwell Scientific Publications, 1987.
- [66] J.V. Sengers and J.T.R. Watson, “Improved International Formulations for the Viscosity and Thermal Conductivity of Water Substance,” *Journal of Physical and Chemical Reference Data*, vol. 15, no. 4, pp. 1291–1314, 1986
- [67] S. S. Bang and D. Johnston, “Environmental effects of sodium acetate/formate deicer, ice shear,” *Arch. Environ. Contam. Toxicol.*, vol. 35, no. 4, pp. 580–587, 1998.
- [68] C. G. van Ginkel and S. Gayton, “The biodegradability and nontoxicity of carboxymethyl cellulose (DS 0.7) and intermediates,” *Environ. Toxicol. Chem.*, vol. 15, no. 3, pp. 270–274, 1996.
- [69] R. Orlando, “Phase Change Material Heat Storage using Stable Supercooling,” Master thesis, Department of Civil Engineering, Technical University of Denmark, 2015.
- [70] Wikipedia-the free Encyclopedia, “Ethylenediaminetetraacetic acid.” [Online]. Available: https://en.wikipedia.org/wiki/Ethylenediaminetetraacetic_acid#Industry. [Accessed: 19-Nov-2018].
- [71] J. B. Johansen, G. Englmair, M. Dannemand, W. Kong, J. Fan, J. Dragsted, B. Perers, and S. Furbo, “Laboratory Testing of Solar Combi System with Compact Long Term PCM Heat Storage,” *Energy Procedia*, vol. 91, pp. 330–337, 2016.
- [72] Passive House Institute, “Passive House Institute.” [Online]. Available: <https://passivehouse.com>. [Accessed: 31-Oct-2018].
- [73] Department of Civil Engineering, “DTU Climate Station Data, climate data from the Technical University of Denmark.” [Online]. Available: <http://climatestationdata.byg.dtu.dk/> [Accessed: 30-Sept-2018].
- [74] C. Rathgeber, E. Lävemann, and A. Hauer, “Economic top-down evaluation of the costs of energy storages- A simple economic truth in two equations,” *J. Energy Storage*, vol. 2, pp. 43–46, 2015.
- [75] JCGM. Joint committee for guides in metrology: evaluation of measurement data – Guide to the expression of uncertainty in measurement (GUM); JCGM 100; 2008.
- [76] The International Association for the Properties of Water and Steam, *The IAPWS Industrial Formulation 1997*

for the Thermodynamic Properties of Water and Steam, IAPWS R7-97 (2012).

- [77] A. Zirkel-Hofer, S. Perry, S. Fahr, K. Kramer, A. Heimsath, S. Scholl, and W. Platzler, “Improved in situ performance testing of line-concentrating solar collectors: Comprehensive uncertainty analysis for the selection of measurement instrumentation,” *Appl. Energy*, vol. 184, pp. 298–312, 2016.
- [78] Kamstrup A/S, Technical Description of Ultraflow sensors, [Online]. Available: <https://products.kamstrup.com/index.php>. [Accessed: 27-Feb-2019].
- [79] S. Furbo “Varmelagring til solvarmenanlæg,” Technical University of Denmark, Thermal Insulation Laboratory report no. 162, 1984.
- [80] A. Arteconi, N.J. Hewitt, and F. Polonara, “State of the art of thermal storage for demand-side management,” *Appl. Energy*, vol. 93, pp. 371–389, 2012.
- [81] C. Finck, R. Li, R. Kramer, and W. Zeiler, “Quantifying demand flexibility of power-to-heat and thermal energy storage in the control of building heating systems,” *Appl. Energy*, vol. 209, pp. 409–425, 2018
- [82] R. Horn, M. Burr, D. Fröhlich, S. Gschwander, M. Held, J. P. Lindner, G. Munz, B. Nienborg, and P. Schossig, “Life Cycle Assessment of Innovative Materials for Thermal Energy Storage in Buildings,” *Procedia CIRP*, vol. 69, pp. 206–211, 2018.
- [83] B. Nienborg , S. Gschwander, D. Fröhlich, T. Helling, R. Horn, F. Klinker, G. Munz, P. Schossig, and H. Weinläder, “Life Cycle Assessment of thermal energy storage materials and components,” *Energy Procedia*, vol. 155, pp. 111–120, 2018.

This page is intentionally left blank.

PART B: Appended papers

This page is intentionally left blank.

Paper 1: W. Kong, M. Dannemand, J. B. Johansen, J. Fan, J. Dragsted, G. Englmair, and S. Furbo, “Experimental investigations on heat content of supercooled sodium acetate trihydrate by a simple heat loss method,” *Solar Energy*, vol. 139, pp. 249–257, 2016. <http://dx.doi.org/10.1016/j.solener.2016.09.045>

This page is intentionally left blank.

Experimental investigations on heat content of supercooled sodium acetate trihydrate by a simple heat loss method

Weiqiang Kong*, Mark Dannemand, Jakob Berg Johansen, Jianhua Fan, Janne Dragsted, Gerald Englmaier, Simon Furbo

Technical University of Denmark, Department of Civil Engineering, Kgs. Lyngby 2800, Denmark

Abstract

Sodium acetate trihydrate is a phase change material that can be used for long term heat storage in solar heating systems because of its relatively high heat of fusion, a melting temperature of 58°C and its ability to supercool stable. In practical applications sodium acetate trihydrate tend to suffer from phase separation which is the phenomenon where anhydrous salt settles to the bottom over time. This happens especially in supercooled state. The heat released from the crystallization of supercooled sodium acetate trihydrate with phase separation will be lower than the heat released from sodium acetate trihydrate without phase separation. Possible ways of avoiding or reducing the problem of phase separation were investigated. A wide variety of composites of sodium acetate trihydrate with additives including extra water, thickening agents, solid and liquid polymers have been experimentally investigated by a simple heat loss method. The aim was to find compositions of maximum heat released from the crystallization of supercooled sodium acetate trihydrate samples at ambient temperature. It was found that samples of sodium acetate trihydrate with 0.5% to 2% (wt.%) Carboxy-Methyl Cellulose, 0.3% to 0.5 % (wt.%) Xanthan Gum or 1% to 2% (wt.%) of some solid or liquid polymers as additives had significantly higher heat contents compared to samples of sodium acetate trihydrate suffering from phase separation.

Keywords: Sodium acetate trihydrate, Supercooling, Heat content measurement, Phase separation, Phase change material

1. Introduction

Solar energy along with other renewable energy sources can play an important role in clean energy utilization in modern society. However, solar energy has the characteristic of being intermittent on a daily basis and has an uneven seasonal distribution. Heat storage is one possible and effective way of solving the mismatch between heat demand and solar energy supply. Solar energy systems combined with long term heat storage are being widely studied in many projects. For example in the four EU funded projects (Helden, 2013) (SAM.SSA, MERITS, SOTHERCO, COMTES), and in IEA SHC Task 42 and IEA ECES Annex 29. Phase change materials (PCMs) are considered as promising heat storage materials due to their latent heat of fusion which can possibly increase storage density compared to

sensible heat storages. In some PCMs the latent heat of fusion can be preserved without heat loss for a long term storage period via the principle of stable supercooling (Kousksou et al., 2014; Xu et al., 2013; Zalba et al., 2003)

1.1. Sodium acetate trihydrate as heat storage material

Sodium acetate trihydrate (SAT), $\text{NaCH}_3\text{COO}\cdot 3\text{H}_2\text{O}$, consisting of 60.3% (wt.%) sodium acetate and 39.7% (wt.%) water, has the ability to supercool stable to ambient temperatures and has relatively high latent heat of fusion of 264 kJ/kg at the melting temperature of 58°C (Zalba et al., 2003). Once the solidification of the supercooled SAT is activated the latent heat of fusion from the phase change will be released. This energy can be used for space heating and domestic hot water preparation. The ways of activating the solidification are easy and flexible such as cooling a part of the SAT to its maximum degree of supercooling by either evaporating liquid CO_2 (Furbo et al., 2012) or by a Peltier element cooling or by mechanically introducing a seed crystal. Therefore SAT is a promising phase change material which can be used for long term heat storage.

Fig. 1(a) shows one sample of supercooled sodium acetate water mixtures which have been in supercooled state for more than 2 years at indoor temperatures. Even impurities such as rusty iron immersed in the supercooled sodium acetate water mixture did not influence the stability of the supercooling, as can be seen in Fig. 1(b).

1.2. Limitations of the material

Phase separation/segregation is a key problem of using SAT for heat storage. It causes the heat content of the supercooled SAT to decrease over time (Kimura and Kai, 1985). It is caused by the fact that SAT is an incongruently melting salt hydrate. An incongruently melting salt hydrate consists of an anhydrous salt with corresponding crystal water. The solubility of the anhydrous salt in water, which is given in (Furbo and Svendsen, 1977) is not high enough at the melting point of 58°C to dissolve all the anhydrous salt in the corresponding crystal water of the trihydrate composition. Therefore the molten salt hydrate at a temperature just above the melting point consists of a saturated salt solution and some anhydrous salt undissolved in the water (Kimura and Kai, 1985). When nothing is done to prevent it, the anhydrous salt settles to the bottom of the container as sediment due to its higher density, which can be seen in Fig. 1(a). In supercooled state below the melting point, even less anhydrous salt will be

dissolved and the problem increases. This can be realized by observing the phase diagram for the sodium acetate - water system (Araki et al., 1995). When the crystallization of a sample is initiated, the anhydrous salt at the bottom is unable to bind with the water in the top of the container. Therefore only a part of the anhydrous salt is active during phase change. The solidified salt hydrate with phase separation consists of three parts: At the bottom the solid salt hydrate crystals with additional anhydrous salt, in the middle a layer of salt hydrate crystals, and at the top the salt hydrate crystals with some additional water in which some salt dissolves in. The amount of sediment increases with repeated cycles, and the heat storage capacity will therefore decrease with each melting/crystallization cycle. Therefore phase separation has to be avoided.

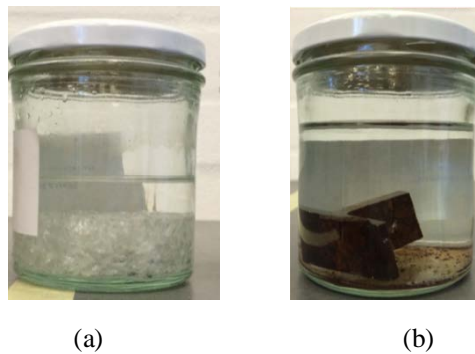


Fig. 1. Long term supercooled samples of (a) SAT with extra water (b) SAT with extra water and immersed steel

1.3. Solutions

Different possible ways of avoiding or reducing phase separation were investigated in previous studies. For example, the problem does not occur for the incongruently melting Glauber's salt, $\text{Na}_2\text{SO}_4 \cdot 10\text{H}_2\text{O}$, if the height of the container is smaller than 0.9 cm according to Kaufmann (K. Kauffman and Pan, 1972). Glauber's salt has a much larger difference between the salt solubility at the melting point and the content of anhydrous salt in the salt hydrate compared to the difference between the salt solubility at the melting point and the content of anhydrous salt in SAT. Therefore it could be possible that a low material height can avoid phase separation. Adding extra water is suggested a way to avoid phase separation and was studied by Furbo and Svendsen (Furbo and Svendsen, 1977). The stored energy in SAT with extra water has however shown to decrease after a number of cycles in tests with prototype heat storage units with a PCM heights of 5 cm (Dannemand et al., 2015b; Dannemand and Furbo, 2014). Phase separation can also be reduced by adding thickening agents which were

widely investigated in the literature. Peng Hu et al. (Hu et al., 2011) presented the mixture of SAT with 4 % Carboxy-Methyl Cellulose (CMC) as thickening agent and 5 % AIN nanoparticles as nucleating agent which had a high latent heat and avoids the supercooling. Similarly, Garay Ramirez et al. (Garay Ramirez et al., 2013) used 0.5% AgNPs to reduce the supercooling and mixing silica gel with CMC to avoid phase separation and yielded an increment in the stability of the phase change behaviour. Nearly 95% of the latent heat of SAT was recovered in this study. In a study by Cabeza et al. (Cabeza et al., 2003), bentonite, starch and Cellulose were investigated for the thickening effect on SAT and they found an enthalpy decrease between 20% and 35% depending on the type and amount of thickening agents used. In a study by Ryu et al. (Ryu et al., 1992), a super-absorbent polymer (SAP) made from acrylic acid copolymer and CMC-Na was investigated as thickening agent to avoid phase separation, together with K_2SO_4 as the nucleating agents. The combination of SAT with 1% SAP, 2% CMC-Na and 2% K_2SO_4 was used in a study by Choi et al. of heat storage systems (Choi et al., 1996).

Studies (Cabeza et al., 2003; Choi et al., 1996; Garay Ramirez et al., 2013; Haillet et al., 2012, 2011; Hu et al., 2011; Ryu et al., 1992) focused on short term heat storage in which supercooling of the storage materials has to be avoided. Therefore nucleating agents, which reduce the degree of supercooling, were used in those studies. For seasonal heat storage using the principle of stable supercooling, nucleating agents should be avoided and therefore the total mass of the PCM material is reduced. That's one of the advantages of utilizing long term supercooling.

Suggested ways of reducing phase separation can be summarized in the following ways:

- Low height of material
- Adding extra water
- Adding thickening agent

1.4. Measurement techniques

Differential thermal analysis (DTA) and differential scanning calorimetry (DSC) methods (Höhne et al., 2003) are conventional method for determining the latent heat of fusion and the specific heat of PCMs. However, DTA and DSC measurement facilities are complicated and expensive and the tested samples are usually very small (1-10 mg), which does not represent the bulk PCMs in actual storages (Zalba et al., 2003). Zhang (Yinping et al., 1999) proposed the T-history method, as a simple alternative to the DTA and DSC methods, to determine the melting point, heat of fusion, specific heat

and thermal conductivity of the bulk PCMs with additives in a sealed tube. The T-history method was then widely recognized and used in studies. Further modification and improvement for the T-history method were proposed by researchers in order to remove unstable phase change, enhance the measurement accuracy and enlarge the range of applications (Hong et al., 2004, 2003; Peck et al., 2006).

In this study, possible additives for reducing phase separation including extra water, thickening agents, solid and liquid polymers were investigated. Adding extra water will allow for more anhydrous salt to dissolve. Thickening agents can increase the viscosity of the solution and suspend the anhydrous salt in the container so that it does not settle to the bottom of the container. Other solid or liquid additives can work in such a way that the salt solubility is increased so much that phase separation is avoided.

1.5. The heat loss method

A simple heat loss method was used to determine the heat contents of supercooled SAT samples by measuring the heat released after the solidification of supercooled SAT samples with and without additives at ambient temperature. The method was designed specifically for measuring heat released from supercooled samples and it resembles the way the material is intended to be used in supercooled thermal energy storage (Dannemand et al., 2016b, 2015c). The results are used for comparison of different combinations of SAT and additives and to find mixtures with high heat contents.

The heat loss method has many advantages compared to conventional test method. First the heat loss method is simple in operation. There are no precision instruments. The equipment is cheap and easy to set up. Second, the bulk samples can be made as the same height as in the applications, for example 5 cm in (Dannemand et al., 2015a). Then the mathematical calculation process is simple. The data logger only records the sample and ambient temperatures. The heat content is easy to calculate. Finally, the well-insulated box provide low and stable heat loss coefficient for the whole test process which is the guarantee for obtaining accurate results. The detailed description can be seen in section 2.1.

2. Heat content measurement method

2.1. The heat loss test method

The heat content measurement of SAT samples were carried out by a simple heat loss method. Glass jars with metal lids were used to contain the samples as shown in Fig. 2(a). The glass jars were placed in well insulated boxes to cool down, see Fig. 2(b). There were four boxes tested at the same time. The boxes were located in an underground room where the diurnal temperature variation was minimal.

There were four thermocouple (Type T) temperature sensors for each box. Three of them were fixed outside of glass jar for measuring the temperature of the sample, see Fig. 2(c) and the fourth to measure the ambient temperature nearby.

The temperature sensors were connected to an Agilent data logger and the test data were recorded on a PC. See Fig. 3.

2.1.1. Determining heat loss coefficient of well insulated boxes

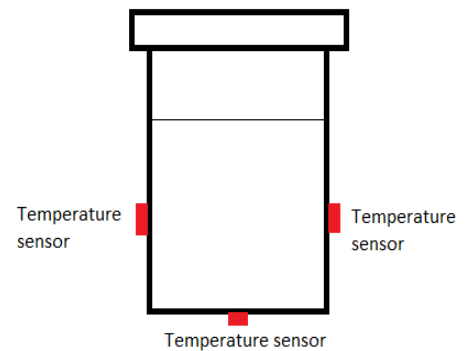
The main assumption of the method is that the heat loss coefficient UA (W/K) of glass jar in the well-insulated box can be determined by having hot water cool down because the properties of water are known. Heated reference samples with water were set to cool down towards the ambient temperature of the room.



(a)



(b)



(c)

Fig. 2 (a) Glass jar with lid (b)The well-insulated box (c)Locations of temperature sensors



Fig. 3 Test facilities of heat loss test method

The heat loss process of glass jar inside the box can be described by the differential equation of Eq. (1). After solving Eq. (1), a logarithmic equation was derived for calculating UA , see Eq. (2).

$$mc \frac{dT}{dt} = -UA \cdot (T - T_a) \quad (1)$$

$$UA = \frac{mc}{\Delta t} \ln \frac{T_e - T_a}{T_b - T_a} \quad (2)$$

Where mc (J/K) is the total heat capacity of the reference consisting of glass, water and lid, T (K) is water temperature, T_b (K) and T_e (K) are start and end temperature of water, T_a (K) is ambient temperature, t (s) is time and Δt (s) is time period.

The UA value calculated by Eq. (2) is the average heat loss coefficient of the temperature range from T_b to T_e during the time interval Δt . UA values were obtained for all temperature steps, a continuous UA curve was regressed by the scatter of UA values. A quadratic equation described the UA development. Equation for each box was determined. One example is shown in Fig. 4. The blue points are the UA values. Each point was calculated during the time interval of 60 min. The curve was regressed based on UA values and a trend line was obtained with R-square value. The quadratic equation was the UA curve based on reference sample temperatures.

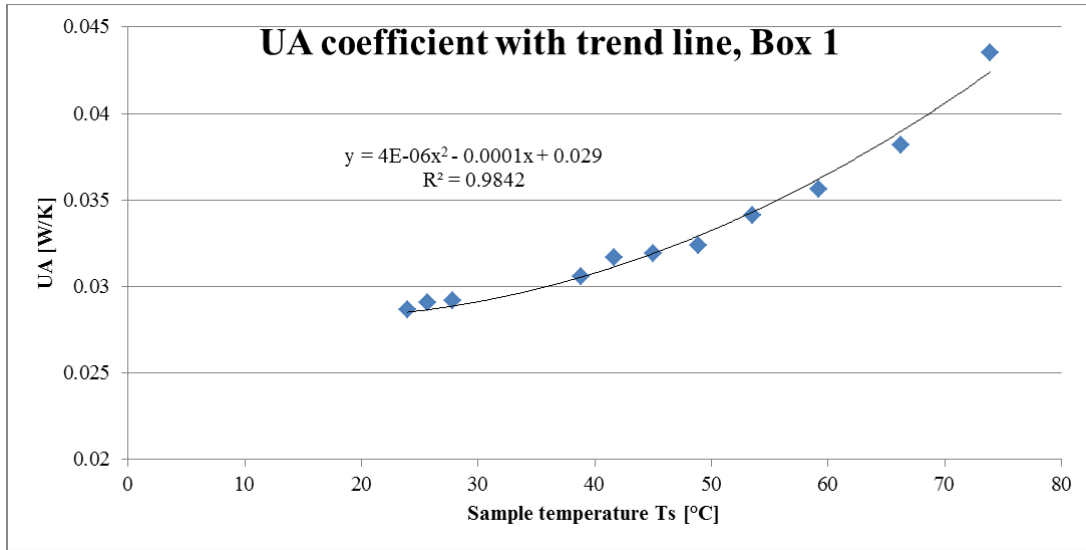


Fig. 4 An example of UA coefficient regression

2.1.2. Measuring procedure for SAT samples

The heat released from the supercooled SAT samples after solidification is considered the heat content of the supercooled sample. The heat content of SAT mixtures inside glass jar cooling down after solidification from supercooled state can then be calculated by using the heat loss coefficient UA of the boxes. The heat content measurement procedure of SAT samples can be summarized as follows:

1. The SAT samples were fully melted in the glass jars and then cooled down to the ambient temperature of the room of the test facility leaving them in supercooled state.
2. The samples were placed in the boxes and the solidification was initiated by dropping a SAT crystal into them. The temperature development during the cooling process was recorded. The samples cooled back down to the ambient temperature of the test facility room.
3. The heat contents E (kJ/kg) of the SAT samples were determined by using the heat loss coefficient and the recorded temperatures. See Eq. (3), where T_s is the SAT sample average temperature, m is the mass of the SAT sample.

$$E = \int_t^{t+\Delta t} UA(t) \cdot [T_s(t) - T_a(t)] \cdot dt / m \quad (3)$$

Fig. 5 shows the temperature development of a SAT sample cooling down to ambient temperature to supercooled state followed by activation of solidification, the rapid increase in temperature and the

cooling down to ambient temperature again. The green area is the heat content measured by this heat loss method.

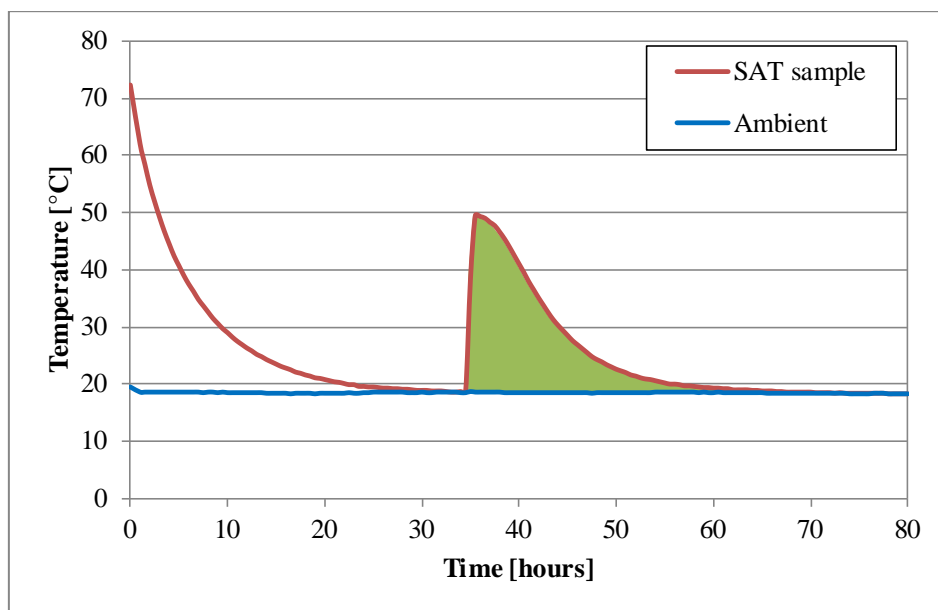


Fig. 5 An example of cooling process of PCM

The heat loss method is closely related to the T-history method but not the same. The T-history method compares the cooling or heating over time of a water sample as a reference and the investigated sample simultaneously. Whereas the heat loss method uses a water sample as a reference to determine the heat loss coefficient of a well-insulated box. Afterwards the investigated sample is then placed in the box to cool down. This heat loss coefficient used to calculate the heat released from the investigated sample and thereby determine its heat content.

2.2. Materials

Possible additives for reducing phase separation including extra water, thickening agents, solid and liquid polymers are investigated. The masses of additives in the following paragraphs are given in weight percentages.

The following materials were used:

Sodium acetate trihydrate (analytical degree, purity>99%) produced by Shijiazhuang Haosheng Chemical Co. Ltd in China.

A variety of additives were tested including,

- Thickening agents provided as samples by the company of CP Kelco
 - Carboxymethyl Cellulose (CMC) under the product name CEKOL[®] 30000
 - Xanthan Gum (X-Gum) under the product name Keltrol[®] Advance Performance

The thickening agents CMC and X-Gum are widely used in the food industry. The thickening effect can increase the viscosity of the SAT and suspend the anhydrous salt in the container so that phase separation is reduced or avoided.

A selection of other additives with various effects on the phase separation was investigated. Effect on some of the additives could be to increase the solubility of anhydrous sodium acetate in crystal water.

- Acid modifier, tartaric acid (CAS number: 526-83-0);
- Glycerol (C₃H₅(OH)₃) (CAS number: 56-81-5);
- Chelating agent, EDTA. Disodium Ethylenediaminetetraacetic acid (CAS number: 139-33-3);
- Solid polymer AMPS. 2-Acrylamido-2-methylpropane sulfonic acid (CAS number: 15214-89-8);
- AquaKeep (10SH-NF) produced by SUMITOMO SEIKA Chemicals Co., Ltd.
- Liquid polymers HD 200 (PH: 4.5), HD 310 (PH: 4.0) and HD 500 (PH: 4.0) are liquid polymers with different lengths of molecular chains provided by Suzhou Hongde Co., Ltd. Jiangsu, China.

2.3. Sample preparation

The heat content measurements were carried out with SAT and three types of additives; (1) different quantities of extra water, (2) thickening agents and (3) polymer additives. All the samples were prepared with a height of 5 cm in liquid phase. All heat content results (kJ/kg) were calculated by considering the total mass of SAT including additives. The water used in experiments was distilled water.

SAT contains approximately 40% water. Samples of sodium acetate water mixtures with the water content of 40% (205g SAT), 42% (196g SAT+7.8g water), 45% (185g SAT+17.8g water) and 46% (180g SAT+21g water) were prepared. Three repetitions of each sodium acetate water mixture, in total of 12 samples were made.

Samples of 200 g SAT with 0.1% to 2% CMC and Xanthan Gum were prepared. A proper mixing method was necessary for adding thickening agents into the SAT, especially Xanthan Gum. The Xanthan Gum powder binds very fast with the water when it is mixed into a sample and will easily form jelly chunks in the sample instead of dispersing evenly in the sample. To achieve uniformly mixed samples 90% of the SAT was melted in an oven, the remaining 10% of the SAT was in cold solid granular state mixed with the thickening agent powder before it was added to the melted SAT little by little while mixing with an overhead stirrer. Mixing at hot state will easily trap unwanted air bubbles inside the mixture therefore the mixing was done carefully to avoid this (Dannemand et al., 2016a).

Samples of 200g SAT with different quantities of liquid or solid polymers were prepared. The liquid or solid polymers were added little by little into the melted SAT while stirring with an electronic stirrer.

2.4. Relating of the latent heat of fusion to the heat content

The heat content of a supercooled SAT sample is defined in this paper as the thermal energy dispersed to the ambient environment by the natural cooling process towards the ambient temperature after solidification of the supercooled SAT sample at ambient temperature (The green area in Fig. 5).

The definition of the latent heat of fusion is the enthalpy change resulting from heating a given quantity of a substance to change its state from a solid to a liquid at the temperature of the melting point (G.F.S., 1922).

The latent heat of fusion at the melting point is therefore somewhat different but related to the heat content of a supercooled sample. The heat loss method measures the heat content.

The following theory (Dannemand and Furbo, 2014) explains the theoretical heat content of SAT in a simplified way as if the SAT behaves as an ideal compound which changes from solid to liquid phase at a specific melting temperature.

Eq. (4) and Eq. (5) show the theoretical change of thermal energy over a temperature increase where the melting temperature is passed for a heating and a cooling process.

$$E_{heating} = (T_{melt} - T_{start}) \cdot c_p(s) + L + (T_{max} - T_{melt}) \cdot c_p(l) \quad (4)$$

$$E_{cooling} = (T_{max} - T_{melt}) \cdot c_p(l) + L + (T_{melt} - T_{end}) \cdot c_p(s) \quad (5)$$

where T_{melt} is the melting point of 58°C, T_{start} is the PCM temperature at the start of the charge, $c_p(s)$ is the specific heat of SAT in solid phase, $c_p(l)$ is the specific heat of SAT in liquid phase, L is the heat of

fusion, T_{max} is the maximum temperature of the PCM during heating, T_{end} is the temperature of the PCM after the cooling.

When the SAT cools down to T_{end} without crystalizing, assuming that the specific heat of the supercooled SAT has the same properties as the liquid SAT, then the stored thermal energy in the supercooled PCM is:

$$E_{supercooled} = E_{heating} - c_p(l) \cdot (T_{max} - T_{end}) \quad (6)$$

If T_{start} and T_{end} are equal, then $E_{heating}$ and $E_{cooling}$ are also equal. When the temperature of the supercooled SAT and the end temperature are the same, then the thermal energy stored at supercooled state is:

$$E_{supercooled} = L - (T_{melt} - T_{end}) \cdot [c_p(l) - c_p(s)] \quad (7)$$

The heat content measured by the heat loss method is theoretically equal to $E_{supercooled}$ which is lower than the heat of fusion. $E_{supercooled}$ can be calculated according to Eq. (7). Assuming that T_{end} is 20 °C, the latent heat of fusion is 264 kJ/kg, the specific heat capacity $c_p(l)$ and $c_p(s)$ are 2.8 kJ/(kg·K) and 1.9 kJ/(kg·K), respectively (Araki et al., 1995). In reality the specific heat capacities are temperature dependant but for this calculations average values over the representative intervals are used. The theoretical heat content of SAT at 20 °C is calculated to 230 kJ/kg. The heat content at the supercooled state is lower than the latent heat of fusion due to the different heat capacities of the liquid and the solid state of the material and depends on the supercooled and end temperature of the SAT sample.

2.5. Error analysis

The deviation between measured heat content and the theoretical heat content mainly comes from two parts.

The first is from the change of ambient temperature. During one test, the variation of ambient temperature was within 0.5 K but among all the tests the maximum difference of ambient temperature was up to 7 K. Assuming that $c_p(l)$ is the specific heat capacity of the supercooled SAT and $c_p(s)$ is the specific heat capacity of SAT in solid state and the two heat capacities are constant when the ambient temperature changes 7 K. The theoretical heat content is 230 kJ/kg. The relative error of this term can be estimated as

$$\frac{\Delta Q}{E} = \frac{[c_p(l) - c_p(s)] \Delta T_{end}}{E} = \frac{(2.8 - 1.9) \cdot 7}{230} = 2.3\% \quad (8)$$

The second deviation comes from the temperature measurement method. The average temperature of three temperature sensors fixed outside of glass jar for representing the sample temperature was lower than the actual material temperature. The error can be estimated by the Biot number (Bi) for long cylinder heat exchange object which is shown in Eq. (9), in which h ($\text{W}/\text{m}^2\cdot\text{K}$) is the surface heat loss coefficient, R is the cylinder diameter and λ ($\text{W}/\text{m}\cdot\text{K}$) is the thermal conductivity of SAT-additives. h can be calculated by UA/A_s , where A_s is the surface area. Since UA is a function of temperature varying around 0.029-0.035 from 20 °C to 55 °C and λ has a value from literature with large variations 0.17-1.1(Dannemand et al., 2016a), the Biot number can be calculated as a range of 0.04-0.34 which is shown in Eq. (9). In theory, only if the Biot number is smaller than 0.05, the outside average temperature can represent the whole sample temperature (Yang and Tao, 1998).

$$Bi = \frac{hR}{2\lambda} = \frac{UA/A_s \cdot R}{2\lambda} = \frac{(0.029 \sim 0.034) / 0.01 \cdot 0.034}{2(0.17 \sim 1.1)} = 0.04 \sim 0.34 \quad (9)$$

3. Results and discussion

The heat contents measured by the simple heat loss method for samples of SAT with extra water, SAT with thickening agents and SAT with polymer additives are presented in the following subsections. All results are shown as specific heat content. The masses used in calculations are for total PCM mass including SAT and additives.

3.1. Heat content measurement of SAT with extra water

The 40%, 42%, 45% and 46% water content SAT-water samples were tested with different durations of the supercooled period: Less than 14 days, 41 days and 100 days. The tests with the period of less than 14 days were repeated three times. Fig. 6 shows the samples after 100 days of supercooling. It can be seen from the figure that both the 40% and 42% samples have a visible salt crystal layer at the lower part of the sample. The crystal layer of the 42% sodium acetate water mixture appeared looser compared to the 40% mixture. Both the mixtures of 45% and 46% were transparent without any visible segregation.



Fig. 6 The 40%, 42%, 45% and 46% salt water mixtures from right to left after 100 days supercooling

The measured heat contents are plotted in Fig. 7. It can be seen from the figure that:

- For the short supercooled periods, the 42% mixture had the highest heat content of 194 kJ/kg.
- With a supercooled period of 41 days, the heat content for the 42% mixture was reduced to 162 kJ/kg, while the heat content for the other mixtures were almost the same as for the short supercooled periods.
- For the samples which were supercooled for 100 days, the heat content of both the 40% and 42% mixtures were lower than for the short supercooled period. The heat content of the 45% and 46% mixtures were not further decreased.

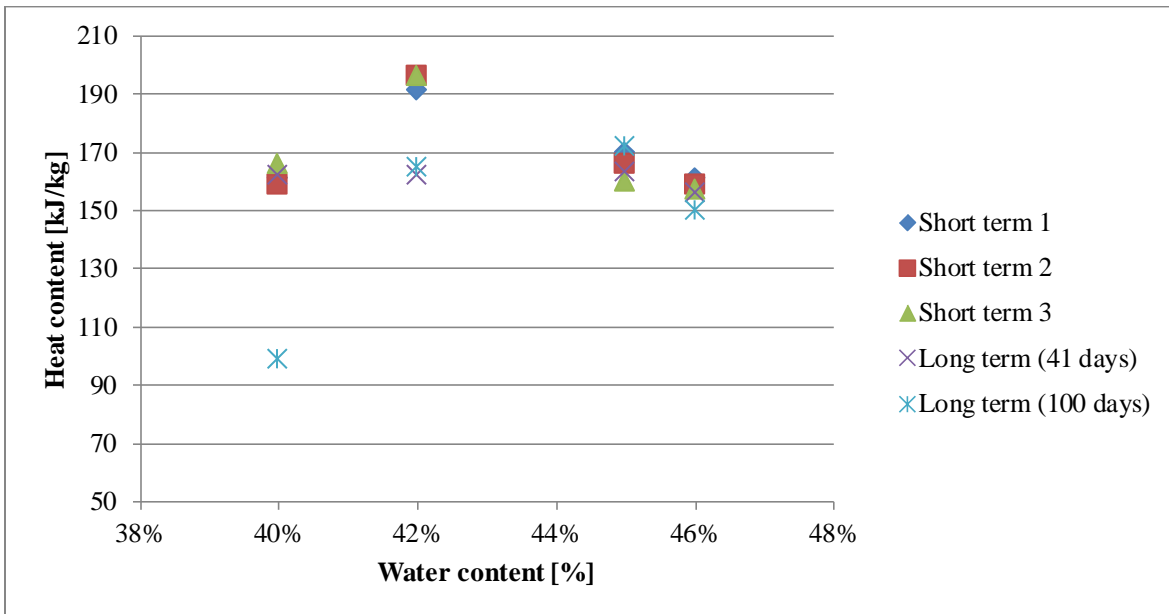


Fig. 7 Heat content of the 40%, 42%, 45% and 46% water salt mixtures

3.2. Heat content measurement of SAT with thickening agent

Table 1 and Table 2 show the measured heat content for SAT with different quantities of Xanthan Gum and CMC. All the samples were tested after short term supercooling period - less than 7 days. The heat content of SAT with 0.1% and 0.2% Xanthan Gum was 183-195 kJ/kg. SAT samples with 0.3% - 0.5% Xanthan Gum had the highest heat contents with an average of 214 kJ/kg. Samples with 1% to 2% Xanthan Gum had heat contents of 204-208 kJ/kg.

The heat contents of SAT with CMC were for all mixtures above 200 kJ/kg. Samples with 0.3% and 2% CMC had heat contents of 213-216 kJ/kg which was a slight improvement compared to SAT with 0.1% to 0.2% CMC.

Table 1. Heat content of SAT with different quantities of Xanthan Gum

| SAT | Heat content (kJ/kg) | | | | SAT | Heat content (kJ/kg) | | | |
|--------------|----------------------|--------|--------|---------|--------------|----------------------|--------|--------|---------|
| | Test 1 | Test 2 | Test 3 | Average | | Test 1 | Test 2 | Test 3 | Average |
| + 0.1% X-Gum | 179 | 185 | 184 | 183 | + 0.5% X-Gum | 213 | 216 | 214 | 214 |
| + 0.2% X-Gum | 196 | 196 | 192 | 195 | + 1.0% X-Gum | 205 | 214 | 205 | 208 |
| + 0.3% X-Gum | 213 | 217 | 214 | 215 | + 1.5% X-Gum | 205 | 208 | 204 | 206 |
| + 0.4% X-Gum | 210 | 217 | 215 | 214 | + 2.0% X-Gum | 208 | 206 | 206 | 207 |

Table 2. Heat content of SAT with different quantities of CMC

| SAT | Heat content (kJ/kg) | | | | SAT | Heat content (kJ/kg) | | | |
|------------|----------------------|--------|--------|---------|------------|----------------------|--------|--------|---------|
| | Test 1 | Test 2 | Test 3 | Average | | Test 1 | Test 2 | Test 3 | Average |
| + 0.1% CMC | 194 | 201 | 206 | 200 | + 0.5% CMC | 208 | 210 | 217 | 212 |
| + 0.2% CMC | 208 | 212 | 209 | 210 | + 1.0% CMC | 209 | 212 | 211 | 211 |
| + 0.3% CMC | 210 | 215 | 214 | 213 | + 1.5% CMC | 211 | 213 | 214 | 213 |
| + 0.4% CMC | 216 | 216 | 207 | 213 | + 2.0% CMC | 219 | 215 | 215 | 216 |

It needs to be noted that the thickening agents did not work together with extra water. When extra water was added, the thickening agents had no effect of increasing heat content because extra water has the dilution effect. Table 3 illustrates the phenomenon which shows the heat content of 42% SAT-water mixtures with 0.1% to 0.4% CMC. The average heat content was around 190 kJ/Kg which was similar to the heat content of 42% salt water mixture without additives and far below the heat content of SAT with 0.1% to 0.4% CMC. This shows that for the short test periods there is no phase separation occurring in the 42% samples and the thickening agent therefore has no effect. In longer test periods the thickening agent may help to avoid decrease in heat content as reported in Fig 7.

Table 3. Heat contents of 42% water content salt water mixture with 0.1% to 0.4 % CMC

| 42% water content salt water mixture | Heat content (kJ/kg) | | | |
|---|----------------------|--------|--------|---------|
| | Test 1 | Test 2 | Test 3 | Average |
| + 0.1% CMC | 198 | 200 | 186 | 195 |
| + 0.2% CMC | 187 | 193 | 192 | 191 |
| + 0.3% CMC | 189 | 191 | 187 | 189 |
| + 0.4% CMC | 188 | 189 | 195 | 191 |

3.3. Heat content measurement of SAT with polymer additives

Through heat content experiments, it was found that glycerol, AquaKeep and tartaric acid had limited effect on increasing the heat content of SAT-additive mixtures, see Table 4. All the samples were tested after short term supercooling period - less than 7 days. The heat content of SAT-glycerol, SAT-AquaKeep and SAT-tartaric was up to 164 kJ/kg, 201 kJ/kg and 185 kJ/kg, respectively.

Table 4. Heat content of SAT with different quantities of Glycerol, Aquakeep and Tartaric acid

| SAT | Heat content (kJ/kg) | SAT | Heat content (kJ/kg) |
|------------------------------------|----------------------|---------------------------------------|----------------------|
| +1% Glycerol | 161 | +1.5% Aquakeep+3% H ₂ O | 192 |
| +2% Glycerol | 161 | +2% Aquakeep+3% H ₂ O | 201 |
| +2% Glycerol +1% H ₂ O | 162 | +1% Tartaric acid | 166 |
| +3% Glycerol +1% H ₂ O | 164 | +2% Tartaric acid | 172 |
| +0.5% Aquakeep | 191 | +1% Tartaric acid+4% H ₂ O | 185 |
| +1% Aquakeep | 193 | +2% Tartaric acid+2% H ₂ O | 176 |
| +0.5% Aquakeep+2% H ₂ O | 188 | +2% Tartaric acid+6% H ₂ O | 162 |
| +1% Aquakeep+3% H ₂ O | 201 | +4% Tartaric acid+6% H ₂ O | 166 |

On the other hand, the solid additives EDTA, AMPS and the liquid polymer HD 200, HD 310 and HD 500 significantly increased the heat content of SAT-additive mixtures compared to SAT without additives. Typically an increase of 30% of heat content was observed. Through the heat content experiments with different compositions of SAT and additive mixtures it was found that SAT with 1% to 2% polymer additives had high heat contents of up to 216 kJ/kg. The promising polymer additives and the results are listed in Table 5. It can be seen from Table 5 that the heat contents of all the SAT-additive combinations were above 200 kJ/kg. Some samples of SAT with EDTA or HD had heat contents even higher than 210 kJ/kg.

Table 5. Heat contents of SAT with 1% or 2% polymer additives

| SAT | Heat content (kJ/kg) | | | |
|-------------|----------------------|--------|--------|---------|
| | Test 1 | Test 2 | Test 3 | Average |
| + 1% EDTA | 214 | 215 | 218 | 216 |
| + 2% EDTA | 213 | 212 | 221 | 215 |
| + 1% AMPS | 205 | 207 | 206 | 206 |
| + 2% AMPS | 205 | 204 | 205 | 205 |
| + 2% HD 200 | 217 | 216 | 216 | 216 |
| + 2% HD 310 | 215 | 215 | 217 | 216 |
| + 2% HD 500 | 212 | 212 | 215 | 213 |

Table 6 shows the heat contents of SAT with polymer additives and extra water. It can be seen from the table that the samples of SAT with polymer additives and extra water had lower heat contents than the samples of SAT with polymer additives in Table 5 but higher heat content compare to samples of SAT with phase separation and SAT with extra water.

Table 6. Heat contents of SAT with polymer additives with extra water

| SAT | Heat content (kJ/kg) | | |
|-----------------------|----------------------|--------|--------|
| | Test 1 | Test 2 | Test 3 |
| +3% EDTA + 4% H2O | 203 | 203 | - |
| +3% AMPS + 2% H2O | 197 | 200 | - |
| +2.6% HD200 +1.7% H2O | 200 | 198 | 196 |
| +2% HD310 +1.9% H2O | 200 | 199 | 200 |
| +2.6% HD500 +1.5% H2O | 203 | 200 | 201 |

3.4 Discussion

Fig. 8 gives an overview of all results of heat content ranges for the SAT samples with different additives. The first column is the heat content of SAT suffering from phase separation, followed by SAT with extra water, thickening agents CMC and X-Gum, and the solid and liquid additives presented in section 2.1. Each column represents the heat contents of the tested samples. The blue part of the column is the lowest heat content and the red part is the measured heat content fluctuation which was caused by different quantities of additives in SAT.

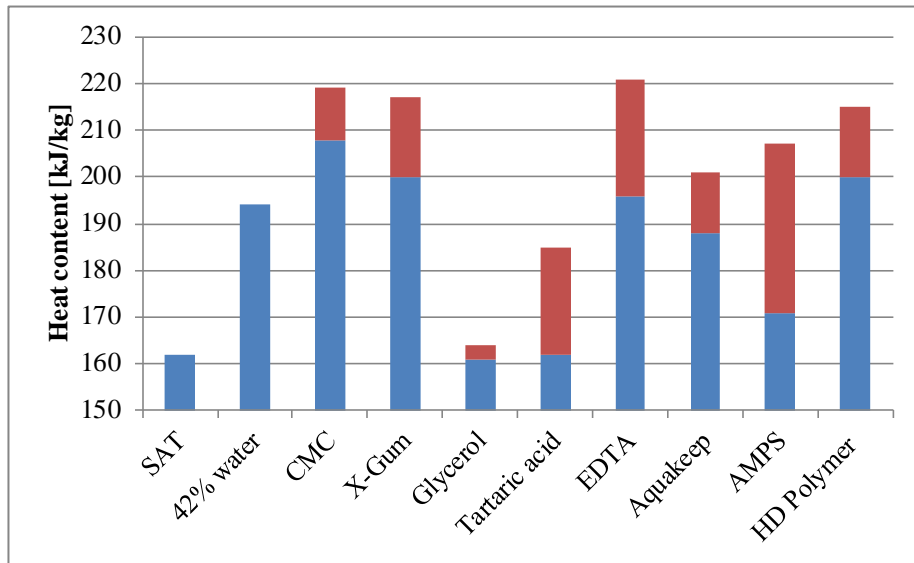


Fig. 8 Full scope of measured heat contents of SAT with and without different additives

Adding extra water into SAT is the easiest way to reduce phase separation since all the sodium acetate can be dissolved in water. However, in comparison of results it can be seen that the heat content of SAT-water (up to 194 kJ/kg) was lower compared to other SAT-additive compositions.

Adding thickening agents into SAT is an effective way of reducing phase separation by increasing the viscosity of SAT solution. There was a trend that for increased quantities of additives, the measured heat content increased. However, too large quantities of the additives will significantly increase the viscosity of the heat storage material and solid materials may be difficult to fully melt during the heating process, especially for SAT with Xanthan Gum. In addition, the specific heat content will be reduced by large quantities of additive and increasing material cost is another concern.

The solid and liquid polymer materials also showed to increase the heat content of SAT-polymer mixtures but the working principle is not clear. They do not increase the viscosity of the PCM as the thickening agents does. One theory is that the polymer materials increase the solubility of anhydrous sodium acetate in the water and in such a way that phase separation is avoided. Another theory could be that the chelating effect such as EDTA performs which may “keep” anhydrous salt dissolved in the solution by its hexadentate (“six-toothed”) structure resulting in an increased solubility.

The comparison of heat content of SAT with thickening agents and extra water shown in Table 3 and heat content of SAT with polymer additives and extra water shown in Table 6 also verified that the

working principle of increasing the heat content of SAT-additive mixture is different by the two kinds of additives.

4. Conclusions

The heat content measurements for samples of SAT with different additives with a height of 5 cm in liquid phase have been carried out in order to elucidate how best to reduce the phase separation and maximize the heat content for SAT composites in supercooled state.

The theoretical heat content of supercooled SAT at 20 °C was calculated to be 230 kJ/kg by applying the latent heat of fusion of 264 kJ/kg, the liquid and solid SAT specific heat capacity of 2.8 kJ/(kg·K) and 1.9 kJ/(kg·K). Based on heat content measurements the heat released after solidification of a supercooled sample of SAT without additives was 162 kJ/kg. The lower value is due to the phase separation in the SAT.

For samples of SAT and extra water, the highest measured heat content was 194 kJ/kg which was obtained in 42% water content salt water mixture. It was found that SAT and SAT-water mixtures with water contents lower than or equal to 42% suffered from phase separation. SAT-water mixtures with water contents higher than 42% did not suffer from the phase separation under the tested conditions. However, the heat content of SAT-water mixtures was decreased by the extra water and by a long supercooled period.

Adding thickening agent was an efficient way to reduce phase separation and thereby increased the energy released from heat storage material. SAT with 0.5%-2% CMC and SAT with 0.3% to 0.5% Xanthan Gum properly dispersed in the sample are promising seasonal heat storage materials which had the heat content of about 30% higher than SAT with phase separation. Experiments showed that the heat contents of the above mentioned compositions were higher than 210 kJ/kg and up to 216 kJ/kg.

The solid polymer materials EDTA and AMPS and the liquid polymer material HD series are also potential additives for SAT based heat storage materials since the SAT-polymer compositions had high heat contents above 200 kJ/kg and they were also working with extra water. The heat contents of SAT with 1% to 2% EDTA, AMPS, HD polymers were between 205-216 kJ/kg.

All in all, the optimal SAT and additive composite should be carefully selected and tested for cycling stability in order to find the best performing SAT composite for heat storage applications.

ACKNOWLEDGEMENT

This project was co-funded by the European Commission as part of the Seventh Framework Programme of the European Community for Research, Technological Development and Demonstration Activities under the funding scheme of “Collaborative Project” through the COMTES consortium and H.M. Heizkörper GmbH & Co. KG.

References

- Araki, N., Futamura, M., Makino, A., Shibata, H., 1995. Measurements of thermophysical properties of sodium acetate hydrate. *Int. J. Thermophys.* 16, 1455–1466.
- Cabeza, L.F., Svensson, G., Hiebler, S., Mehling, H., 2003. Thermal performance of sodium acetate trihydrate thickened with different materials as phase change energy storage material. *Appl. Therm. Eng.* 23, 1697–1704. doi:10.1016/S1359-4311(03)00107-8
- Choi, J.C., Kim, S.D., Han, G.Y., 1996. Heat transfer characteristics in low-temperature latent heat storage systems using salt-hydrates at heat recovery stage. *Sol. Energy Mater. Sol. Cells* 40, 71–87. doi:10.1016/0927-0248(95)00084-4
- Dannemand, M., Dragsted, J., Fan, J., Johansen, J.B., Kong, W., Furbo, S., 2015a. Experimental investigations on prototype heat storage modules utilizing stable supercooling of sodium acetate trihydrate mixtures. *Appl. Energy* 169, 72–80. doi:10.1016/j.apenergy.2016.02.038
- Dannemand, M., Furbo, S., 2014. Test of thermobatterie heat storage module. Report number R 308. Department of Civil Engineering, Technical University of Denmark.
- Dannemand, M., Johansen, J.B., Furbo, S., 2016a. Solidification behavior and thermal conductivity of bulk sodium acetate trihydrate composites with thickening agents and graphite. *Sol. Energy Mater. Sol. Cells* 145, 287–295. doi:10.1016/j.solmat.2015.10.038
- Dannemand, M., Johansen, J.B., Kong, W., Furbo, S., 2016b. Experimental investigations on cylindrical latent heat storage units with sodium acetate trihydrate composites utilizing supercooling. *Appl. Energy* 177, 591–601. doi:10.1016/j.apenergy.2016.02.038
- Dannemand, M., Kong, W., Fan, J., Johansen, J.B., Furbo, S., 2015b. Laboratory Test of a Prototype Heat Storage Module Based on Stable Supercooling of Sodium Acetate Trihydrate. *Energy Procedia* 70, 172–181. doi:10.1016/j.egypro.2015.02.113
- Dannemand, M., Schultz, J.M., Johansen, J.B., Furbo, S., 2015c. Long term thermal energy storage with stable supercooled sodium acetate trihydrate. *Appl. Therm. Eng.* 91, 671–678. doi:10.1016/j.applthermaleng.2015.08.055

- Furbo, S., Fan, J., Andersen, E., Chen, Z., Perers, B., 2012. Development of seasonal heat storage based on stable supercooling of a sodium acetate water mixture. *Energy Procedia* 30, 260–269.
doi:10.1016/j.egypro.2012.11.031
- Furbo, S., Svendsen, S., 1977. Report on heat storage in a solar heating system using salt hydrates. Report no. 70. Thermal Insulation Laboratory, Technical University of Denmark. (BOOK).
- G.F.S., 1922. Latent heat of fusion. *J. Franklin Inst.* 193, 656. doi:10.1016/S0016-0032(22)90585-X
- Garay Ramirez, B.M.L., Glorieux, C., Martin Martinez, E.S., Flores Cuautle, J.J. a, 2013. Tuning of thermal properties of sodium acetate trihydrate by blending with polymer and silver nanoparticles. *Appl. Therm. Eng.* 61, 838–844. doi:10.1016/j.applthermaleng.2013.09.049
- Hailot, D., Goetz, V., Py, X., Benabdelkarim, M., 2011. High performance storage composite for the enhancement of solar domestic hot water systems. Part 1: Storage material investigation. *Sol. Energy* 85, 1021–1027. doi:10.1016/j.solener.2011.02.016
- Hailot, D., Nepveu, F., Goetz, V., Py, X., Benabdelkarim, M., 2012. High performance storage composite for the enhancement of solar domestic hot water systems. Part 2: Numerical system analysis. *Sol. Energy* 86, 64–77. doi:10.1016/j.solener.2011.09.006
- Helden, W. van, 2013. COMTES: Combined development of compact seasonal thermal energy storage technologies. RHC Conf.
- Hong, H., Kim, S.K., Kim, Y.S., 2004. Accuracy improvement of T-history method for measuring heat of fusion of various materials. *Int. J. Refrig.* 27, 360–366. doi:10.1016/j.ijrefrig.2003.12.006
- Hong, H., Park, C.H., Choi, J.H., Peck, J.H., 2003. Improvement of the T-history Method to Measure Heat of Fusion for Phase Change Materials. *Int. J. Air-Conditioning Refrig.* 11, 32–39.
- Hu, P., Lu, D.J., Fan, X.Y., Zhou, X., Chen, Z.S., 2011. Phase change performance of sodium acetate trihydrate with AlN nanoparticles and CMC. *Sol. Energy Mater. Sol. Cells* 95, 2645–2649.
doi:10.1016/j.solmat.2011.05.025
- Höhne, G., Hemminger, W., Flammersheim, H.J., 2003. *Differential Scanning Calorimetry*. Springer.
- K. Kauffman, Pan, Y., 1972. *Thermal Energy Storage in Sodium Sulfate Decahydrate Mixtures*. University of Pennsylvania.
- Kimura, H., Kai, J., 1985. Phase change stability of sodium acetate trihydrate and its mixtures. *Sol. Energy* 35, 527–534. doi:10.1016/0038-092X(85)90121-5
- Kousksou, T., Bruel, P., Jamil, a., El Rhafiki, T., Zeraouli, Y., 2014. Energy storage: Applications and challenges. *Sol. Energy Mater. Sol. Cells* 120, 59–80. doi:10.1016/j.solmat.2013.08.015
- Peck, J.H., Kim, J.J., Kang, C., Hong, H., 2006. A study of accurate latent heat measurement for a PCM with a low melting temperature using T-history method. *Int. J. Refrig.* 29, 1225–1232.

doi:10.1016/j.ijrefrig.2005.12.014

- Ryu, H.W., Woo, S.W., Shin, B.C., Kim, S.D., 1992. Prevention of supercooling and stabilization of inorganic salt hydrates as latent heat storage materials. *Sol. Energy Mater. Sol. Cells* 27, 161–172. doi:10.1016/0927-0248(92)90117-8
- Xu, J., Wang, R.Z., Li, Y., 2013. A review of available technologies for seasonal thermal energy storage. *Sol. Energy* 103, 610–638. doi:10.1016/j.solener.2013.06.006
- Yang, S., Tao, W., 1998. *Heat transfer*, 3rd ed. Higher Education Press, Beijing.
- Yinping, Z., Yi, J., Yi, J., 1999. A simple method, the -history method, of determining the heat of fusion, specific heat and thermal conductivity of phase-change materials. *Meas. Sci. Technol.* 10, 201–205. doi:10.1088/0957-0233/10/3/015
- Zalba, B., Marin, J.M., Cabeza, L.F., Mehling, H., 2003. Review on thermal energy storage with phase change: materials, heat transfer analysis and applications. *Appl. Therm. Eng.* 23, 251–283. doi:10.1016/s1359-4311(02)00192-8

[2] G. Englmaier, Y. Jiang, M. Dannemand, C. Moser, H. Schranzhofer, S. Furbo, and J. Fan, “Crystallization by local cooling of supercooled sodium acetate trihydrate composites for long-term heat storage,” *Energy and Buildings*, vol. 180, pp. 159–171, 2018. <https://doi.org/10.1016/j.enbuild.2018.09.035>

This page is intentionally left blank.

Crystallization by local cooling of supercooled sodium acetate trihydrate composites for long-term heat storage

Gerald Englmaier^a, Yiliang Jiang^a, Mark Dannemand^a, Christoph Moser^b, Hermann Schranzhofer^b, Simon Furbo^a and Jianhua Fan^{a*}

¹Department of Civil Engineering, Technical University of Denmark, Brovej 118, 2800 Kgs. Lyngby, Denmark

²Institute of Thermal Engineering, Graz University of Technology, Inffeldgasse 25/B, 8010 Graz, Austria

Highlights

- Crystallization of supercooled SAT composites started between -9 °C and -24 °C
 - Sodium acetate-water mixtures released heat in two stages during crystallization
 - Higher, more uniform crystallization temperatures in samples with rusty steel profiles
 - Carboxymethyl cellulose and polymeric additives improved heat release during crystallization
 - Proof of applicability of CO₂ evaporation and Peltier element devices to initiate crystallization
-

Abstract

Sodium acetate trihydrate (SAT) can be used for long-term heat storage in buildings by utilizing its ability to supercool stably to ambient temperatures while preserving its heat of fusion. Additives are used to stabilize the SAT and avoid phase separation. A reliable method for initializing the solidification of supercooled SAT composites is needed to operate a heat storage unit based on supercooled SAT. The crystallization temperatures of SAT composites during cooling were therefore investigated and experiments carried out using methods applying local cooling in a small part of prototype heat storage units to initialize crystallization. To find the crystallization temperatures of SAT composites, supercooled samples were cooled down in a freezer. The influence of rusty metal parts submerged in melted SAT composite samples and various periods at rest in a supercooled state were investigated with regard to supercooling stability and crystallization temperature. Carboxymethyl cellulose, extra water, liquid polymer HD 310, metal-based graphite flakes, and silicone oil were applied as additives to form the different SAT compositions. Samples with 60 g SAT in glass jars were subject to repeated heating and cooling cycles. It was found that samples containing steel profiles crystallized in the range of -9 to -15 °C, while SA-water mixtures without steel profiles cooled down to -24 °C before crystallizing. Furthermore, samples with carboxymethyl cellulose and liquid polymer HD 310 showed a greater temperature rise during crystallization, which is in accordance with previous findings on heat contents. SA-water mixtures showed a second minor temperature peak at temperatures below -20 °C, when the sample was cooled down again after the first temperature rise. Devices were developed to initialize the crystallization of supercooled SAT composites in prototype heat storage units using rapid local cooling of the SAT composite. We successfully initialized crystallization by evaporating pressurized liquid carbon dioxide in a small chamber on one side of the PCM container and by using Peltier elements. Our experiments showed that the controlled initialization of crystallization by cooling is feasible for all the SAT composites investigated.

Keywords: Sodium acetate trihydrate, stable supercooling, long-term heat storage, CO₂ evaporation, Peltier elements.

Nomenclature

Dimensional variables

| | |
|---|------------------|
| T | temperature (°C) |
| m | mass (kg) |
| t | time (min) |

Greek letters

| | |
|------------|----------------------------|
| ΔT | temperature difference (K) |
|------------|----------------------------|

Subscripts

| | |
|-----------------|---|
| C | cooling |
| CR | crystallization |
| Ref | reference |
| Steel plate | steel plate attached to a Peltier element |
| Heat sink | heat sink attached to a Peltier element |
| PCM | phase change material |
| Surface | the surface of the PCM container |
| CO ₂ | carbon dioxide evaporation chamber |

Abbreviations

| | |
|-----------------|---------------------------|
| CMC | carboxymethyl cellulose |
| SA | sodium acetate |
| SAT | sodium acetate trihydrate |
| CO ₂ | carbon dioxide |
| PCM | phase change material |
| wt. | weight |

1. Introduction

1.1. Long-term heat storage with sodium acetate trihydrate

Due to the mismatch between solar energy resources and the demand of thermal household services, long-term storage of heat is essential for solar heating systems that aim to cover the heat demand with solar fractions in the range of 80–100%. The concept of a novel compact seasonal heat store based on supercooling of Sodium Acetate Trihydrate (SAT) has therefore been defined in previous research activities at the Technical University of Denmark [1].

SAT, chemical formula $\text{CH}_3\text{COONa}\cdot 3\text{H}_2\text{O}$, is a salt hydrate with a melting point of 58 °C. It has been identified as a potential heat storage material due to its relatively high heat of fusion (264 kJ kg⁻¹ [2]; 237–243 kJ kg⁻¹ [3];) and its relatively high specific heat capacities in both liquid and solid phases [4]. The density of solid SAT in a closed sample that has solidified from supercooled state has been determined to be 1.24–1.28 kg L⁻¹ [5]. SAT is attractive for domestic heat storage applications because of its high volumetric heat storage capacity (~500 kJ L⁻¹ from 20 °C in solid state to 80 °C in liquid state), the low price and its non-toxic properties. Reviews on thermal energy storage with PCM [6], [7] therefore list SAT among the salt hydrates identified for domestic applications.

Supercooling is a phenomenon in which a substance in liquid state cools below its solidifying temperature without solidifying. SAT can be used for long-term heat storage because of its ability to supercool stably to ambient temperatures while preserving its heat of fusion [2], [8], [9]. Once heat is in demand, the solidification of the supercooled solution can be triggered and the preserved heat of fusion will be released as it crystallizes. This has been demonstrated by Dannemand et al. with both flat [10] and cylindrical [11] prototype heat storage units. Flat units have also been used to demonstrate a segmented heat storage in a solar heating system for domestic heat supply [12]. Deng et al. [13] have investigated the performance of a hot water tank that makes use of the stable supercooling of SAT in the mantle.

1.2. Sodium acetate trihydrate composites

For utilization of SAT in domestic heat stores, volumes of several cubic meters are needed for solar heating systems with yearly solar fractions close to 1 [1]. For economic reasons chemically pure SAT cannot be used. Instead, industrial SAT products were successfully applied in previous research [10], [12], [14].

Additives are needed to stabilize the SAT in its liquid phase. The solubility of sodium acetate (SA) in the corresponding crystal water at 58 °C (the melting point of SAT) is not high enough to dissolve all anhydrous salt (experimentally measured by Green [15]). Moreover, as an incongruently melting salt hydrate, SAT suffers from phase separation over repeated heating and cooling cycles and over long periods in supercooled state. Phase separation is caused by the density difference between SA and salt water. When SA molecules settle down to the bottom of a SAT volume and a leaner salt-water solution remains in the upper part of the volume, full reformation of SAT crystals can no longer be achieved [16]. This effect reduces the material's heat storage capacity.

To overcome phase separation, Furbo and Svendsen [17] suggested adding extra water to the salt hydrate. However, tests with prototype storage units [10], [11] showed a decrease in heat capacity after a number of storage cycles had been applied. Thickening agents were therefore used to increase the viscosity of the liquid solution and avoid SA to settle at the bottom of storage units. Carboxymethyl cellulose (CMC) and Xanthan rubber were investigated by Cabeza et al. [3] and Dannemand et al. [15] for this purpose. Liquid polymer solutions have also been identified as able to

reduce the phase separation effect by increasing the solubility of SAT in the liquid solution [19]. A detailed study on the stability and the heat content of supercooled SAT with various additives was conducted by Kong et al. [14]. Composites containing CMC and the liquid polymer solution HD 310 were found to provide the highest heat of fusion.

Graphite flakes for thermal conductivity enhancement have also been investigated [18]. Oils (paraffin, silicone) that do not mix with SAT have been added to increase heat transfer by filling insulating cavities formed during the solidification and contraction of the SAT composition.

1.3. *Crystallization of sodium acetate trihydrate*

To use SAT as a heat storage material, we need greater understanding of the factors that influence supercooling stability, nucleation mechanisms and crystal growth.

1.3.1. *Supercooling stability*

The crystallization process from pure SA aqueous solution to SAT requires a large degree of supercooling; earlier research found a crystallization temperature of $-15\text{ }^{\circ}\text{C}$ [20]. The behaviour of SA aqueous solutions has been experimentally investigated and can be explained using phase diagrams [4], [15].

The difference between the actual concentration and the solubility concentration of a solution at a given temperature is called the supersaturation. When an SA aqueous solution supercools, it becomes supersaturated without forming crystals. Supersaturation is the driving force for solution crystallization processes, so a supercooled SA aqueous solution stays in a meta-stable state until nucleation takes place (start of the crystallization process).

In most latent heat storage applications, this phenomenon is unwanted [6], [21]. Measures have even been developed to deliver nucleation centres in order to reduce the supercooling of SAT [22], [23]. Nevertheless, for long-term heat storage, the utilization of supercooled salt hydrates has been studied since the late 1920s [24].

Additives were used to overcome phase separation in liquid SAT and to increase the thermal conductivity of solid SAT. Since pure SAT is too expensive for heat storage applications, impure low-cost SAT products were used to realize large heat storage units in a cost-effective way. And it may well be that the available information on the crystallization properties of SAT, such as phase diagrams, does not apply to SAT composites.

1.3.2. *Nucleation*

Nucleation is the birth of new crystal nuclei. Mullin [25] defined two kinds of nucleation: either from solution (primary nucleation) or in the presence of existing crystals (secondary nucleation).

For primary nucleation, Mullin defined the formation of crystal nuclei from a homogenous fluid as homogeneous nucleation. This is not a common event, because supercooled solutions are probably seeded without our knowledge by the presence of atmospheric dust during material preparation. Because the rate of nucleation of a solution can be affected considerably by the presence of such impurities, this so-called heterogeneous nucleation leads to “spontaneous” nucleation events, the mechanisms of which are not fully understood [26].

A supersaturated solution nucleates much more readily when crystals of the solute are already present or added [25]. Seed crystal injection into a supercooled SAT solution is a secondary nucleation method, which has proved reliable even where there is less supercooling [4], [12].

1.3.3. Crystal growth

As soon as stable nuclei have been formed in a supersaturated solution, they begin to grow into crystals of visible size. Dietz et al. [27] and Munakata and Nagata [28] have measured the crystal growth rate of supercooled SA-aqueous solutions in tubes. The growth rates were found to be solely a function of the solution concentration and the degree of supercooling. Measured and calculated crystal growth rates have been evaluated by Ma et al. [29], but we do not yet have parameters for the degree of supercooling or models for crystal growth of melted SAT composite material.

1.4. Mechanisms for the controlled initialization of crystallization

Heat storage applications that make use of the stable supercooling of SAT need reliable mechanisms for starting crystallization. Several possibilities were tested in laboratory-scale experiments, fewer in setups with volumes of 100 L or more:

- Adding seed crystals is a common method of initializing the crystallization in SAT in laboratory-scale setups [4], [20], [27]. Crystallization with seed crystals works as long as the crystals do not melt and become inactive [30]. Seed crystal injection in large storage units has been demonstrated by some of the present authors [12].
- Triggering crystallization using ultrasonic waves has been reported as successfully tested [31], but other researchers [32] have stated that it failed.
- Local cooling of SAT in liquid phase down to its crystallization temperature (primary, heterogeneous nucleation). We demonstrated how the cooling power resulting from the endothermic process of evaporating carbon dioxide (CO₂) could supply a temperature low enough to initiate nucleation in supercooled SAT composites in prototype storage units. Previous studies have shown that SAT will spontaneously crystallize between $-15\text{ }^{\circ}\text{C}$ and $-25\text{ }^{\circ}\text{C}$ [20]. The phase diagram of CO₂ shows a triple point at 5.1 bars at $-57\text{ }^{\circ}\text{C}$. At atmospheric pressure, the phase change is directly from solid to gas at $-78\text{ }^{\circ}\text{C}$. This indicates that the temperatures resulting from evaporating CO₂ may be low enough to reach the temperature where SAT will crystallize. Dannemand et al. have previously tested prototype heat storage units utilizing the stable supercooling of SAT composites. In their laboratory investigations, they initiated nucleation of SAT in storage units by evaporating CO₂ in a small chamber on one side of the PCM unit [1], [10], [33]. The method of using evaporation of CO₂ is also used in plumbing to freeze water in pipes to make temporary plugs of ice to enable repairs without draining the entire system.
- Local cooling of SAT in liquid phase using Peltier elements. A setup with a double-element Peltier device reached $-30\text{ }^{\circ}\text{C}$ and may be able to trigger crystallization [34].

Controlled seed crystal injection requires a rather complex device [12]. If the sealing membranes of the triggering units fail, there could be a risk of unwanted spontaneous solidification in supercooled storage material. In contrast, local cooling of SAT composites using CO₂ evaporation or Peltier elements can be done without any moving parts in the supercooled SAT and without penetrating the chamber containing the PCM and is therefore considered a potentially more durable and cost-efficient solution for closed PCM containers.

1.5. *Scope*

Local rapid cooling of a small part of a PCM storage unit has the potential to be used as a way to initiate the crystallization of supercooled SAT composites. It is therefore crucial to know the temperature at which relevant SAT composites crystallize during cooling. Apart from the additives in the SAT, the vessel containing the SAT composite may work as an impurity, affecting both the behaviour and the crystallization temperature of the SAT. So we investigated and determined the crystallization temperature of various promising SAT composites and of SAT in contact with steel. We also observed whether the length of time that the supercooled SAT composites were kept at 20 °C had any influence of the crystallization temperature. SAT composites with extra water, CMC, liquid polymeric solution, graphite flakes, and silicone oil were used for the experiments. The results of such investigations have not previously been reported in the literature.

Furthermore, this article includes the measurements and evaluations of two different methods of applying local rapid cooling of a part of the SAT composite volume in supercooled PCM prototype heat storage units: cooling by evaporation of pressurized liquid CO₂ and cooling by Peltier elements. Repeated experiments indicate that a reliable initialization of crystallization is possible. Measurements showed when temperatures were achieved that were sufficiently low for application with the various SAT composites. Detailed practical experience of initiating crystallization of supercooled SAT composites using these methods has not been reported previously in the literature.

2. Experimental method

2.1. Material cooling tests (freezer)

2.1.1. Materials

We used SAT of food grade (European standard 262i) from industrial supply [35]. The material was delivered in bags of 20 kg, 4 months after its production.

To stabilize the SAT, we used CMC and a prototype of a liquid polymer composition provided by Suzhou Hongde Co., Ltd. Jiangsu, China. Demineralised water was used to increase the water content of composites.

To study their influence on the minimum supercooling (nucleation) temperature, we also added graphite flakes and silicone oils to the samples. Table 1 presents the specifications of the materials used.

Table 1. Material properties.

| | SAT | CMC | Graphite flakes | Liquid polymer | Silicone Oil |
|-----------------------------|---|------------------------------|---------------------------|--|---------------------------|
| Type: | CAS 6131-90-4 | Cekol 30000 | - 10 mesh | HD 310 | CAS 63148-62-9 |
| Supplier: | IG Chemicals GmbH (GER) | CP Kelco (FIN) | Alfa Aesar | Sushou Hongde Co. Ltd. (CN) | Sigma Aldrich |
| Batch: | 18.10.2015 (production date) | 09.09.2013 (production date) | no. 43319 | 2016 (prototype) | - |
| Selected properties: | purity: >98.5%, water content: 36-42%wt., pH-value: 8-9.5 | - | purity: 99% (metal basis) | Solid concentration: 40%, PH-value: 4.0, brookfield viscosity (at 20°C): 1.2 | density: 963 kg/l at 25°C |

After delivery, the exact water content of the SAT material was measured in dry-out tests. Four open glass cups were prepared with a thin layer (~2 mm) of crystalline SAT, resulting in four SAT samples with a weight of 20 g each. The SAT samples were put in a drying oven (Mettler UF55) with a temperature of 120 °C and air exchange to the ambient. Periodic weight measurements were conducted with a precision scale (linearity: +/- 30 mg) outside the drying unit. The dry-out tests were repeated with stored SAT 22 months after delivery.

Finely granulated SAT was melted in a closed glass jars at 90 °C for about 24 hours. To dissolve SA fully, about 1%wt. demineralized water was added to the granulated SAT. As explained in section 3.1, the SAT delivered showed differences from the molecular SA-water ratio (Fig. 8). The fully dissolved SA aqueous solution (40.5%wt. water) was referred to SAT.

Then the additives were added to the opened jars and the jars were weighed using a precision scale for individual material configurations. CMC was added in powder form during stirring, while extra water and liquid polymer were added using pipettes and the materials were thoroughly stirred afterwards. The mass of each additive was set to achieve a certain fraction of the gross-weight of the compositions (Eq.1):

$$\%wt. = \frac{m_{Additive}}{m_{SAT} + m_{Additive}} \quad (1)$$

The resulting compositions were re-heated in closed glass jars for about 12 hours. Then the samples were put into 50 ml glass jars with polymeric lids. Fig. 1 shows some of the SAT composite samples in solid state from the present work.



Fig. 1. SAT composite samples after crystallization (from left: SAT, SAT + water, SAT + CMC, SAT + HD 310).

The resulting sample weight depended on the fraction of additive in the mixed composition, based on 60 g of SAT. Graphite flakes and silicone oil were also added to similarly prepared samples. This approach was chosen to ensure an equal amount of SA in the samples for comparison.

To study the influence of rough metal surfaces, slices of corroded T-profiles of steel (welded connections) were cut with a metal saw and added to samples (Fig. 2b) in 2 batches for separate cooling tests.

An overview of all the samples prepared is presented in Table 2.

Table 2. The material samples investigated, distributed over five batches.

| | Batch 1 | | | Batch 2 | | | | Batch 3 | | | Batch 4 | | | | Batch 5 | | |
|-----------------------------|---------|-------------|-------------|---------|-------------|-------------|-----------|---------|-------------|-------------|---------|-------------|-------------|-----------|---------|-------------|-------------|
| | SAT (g) | Add. 1 %wt. | Add. 2 %wt. | SAT (g) | Add. 1 %wt. | Add. 2 %wt. | Steel (g) | SAT (g) | Add. 1 %wt. | Add. 2 %wt. | SAT (g) | Add. 1 %wt. | Add. 2 %wt. | Steel (g) | SAT (g) | Add. 1 %wt. | Add. 2 %wt. |
| SAT | 60 | - | - | 60 | - | - | 11 | 60 | - | - | 61 | - | - | 9 | 60 | - | - |
| SAT + water | 63 | 9 | - | 60 | 9 | - | 12 | 61 | 9 | - | 60 | 9 | - | 10 | 60 | 10 | - |
| SAT + CMC | 61 | 5 | - | 59 | 5 | - | 13 | 60 | 5 | - | 60 | 5 | - | 9 | - | - | - |
| SAT + CMC + graphite flakes | 60 | 5 | 5 | 60 | 5 | 5 | 13 | 60 | 5 | 5 | 60 | 5 | 5 | 10 | 60 | 5 | 5 |
| SAT + HD 310 | 60 | 3 | - | 61 | 3 | - | 16 | 60 | 3 | - | 60 | 3 | - | 12 | 60 | 3 | - |
| SAT + HD 310 + silicone oil | - | - | - | - | - | - | - | - | - | - | - | - | - | - | 60 | 3 | 4 |

2.1.2. Test procedure

After sample preparation, TT-type thermocouples (copper/constantan) were attached to the outside of the glass jars. They were wrapped 3 times around the glass body and fixed with aluminium tape (Fig. 2a) to ensure good heat transfer. Next, the closed glass jars were evenly insulated with foam insulation (thickness: 15 mm) to avoid fast cooling in a cold environment and to achieve more uniform temperatures in the material samples.

The thermocouples positioned on the outer surfaces of the glass jars should have been able to measure the material temperatures because the thin glass wall (2 mm) had about 20 times greater thermal conductivity ($0.9\text{--}1.5 \text{ W m}^{-1}\text{K}^{-1}$) than the rather thick foam insulation ($0.04 \text{ W m}^{-1}\text{K}^{-1}$). Furthermore, the slow cooling rates ensured a uniform jar temperature, a precise measurement of sample temperatures, and a reduced risk of the glass jars breaking during the expansion and contraction of the samples. The bottom and the mantle insulation (as indicated in Fig. 2a) were glued together, while the cap insulation of the sample containers was fixed with tape.

The thermocouple wires of each batch (5 samples at a time) were connected to a portable 10-channel data logger (HIOKI LR8431-20) to ensure continuous logging of temperatures. The ambient air temperature was logged with an additional thermocouple (the 6th channel on the data logger). Measurements were logged at intervals of one second.

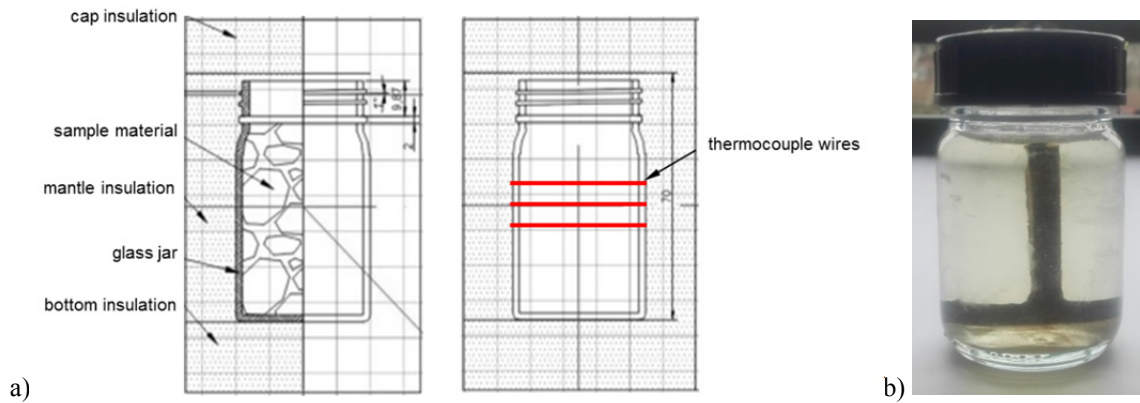


Fig. 2. (a) Sample containment for cooling tests; (b) Glass jar with SAT and sliced steel profile.

To ensure uniform material temperatures, samples were heated in the oven without insulation (placed side-by-side; Fig. 3a) for about 12 hours.

During a cooling down process, the samples were placed in foam insulation and rested, first at room temperature (about 20 °C). Then they were put into a freezer (temperature of about -30 °C) with 10 cm distance to the bottom and the walls, realised using a metal framework (Fig. 3b). The test conditions applied for each batch of samples are given in Table 3.

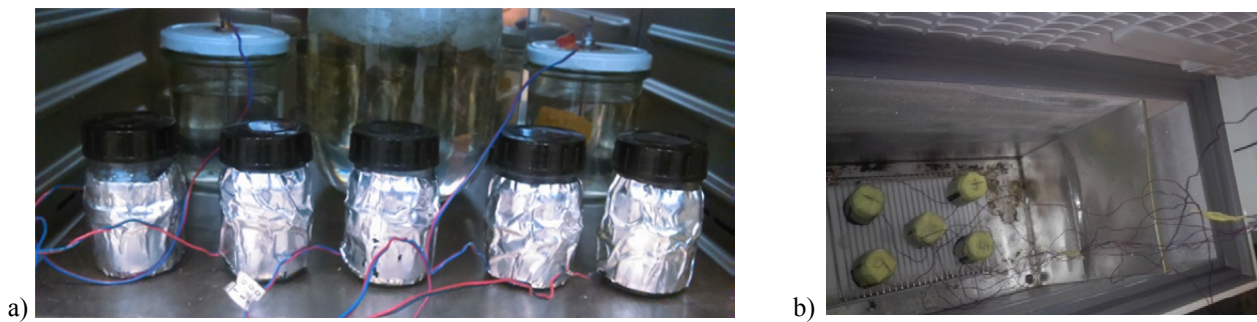


Fig. 3. Photos: (a) Sample placement during heating; (b) Sample placement during cooling.

The cooling process was stopped after 12 hours, when the sample temperatures were no more than 1 K above the air temperature in the freezer. Next, the samples were kept in their insulation for a period of 4 hours at room temperature before the insulation was finally removed.

Table 3. Test conditions.

| | Batch 1 | Batch 2 | Batch 3 | Batch 4 | Batch 5 |
|---------------------------------------|---------|---------|---------|---------|---------|
| Charging temperature (°C) | 90 | 90 | 90 | 90 | 85 |
| Rest period | none | none | 7 days | 8 days | 2 h |
| Temperature at freezer placement (°C) | >60 | >60 | ~20 | ~20 | <30 |
| Steel profile? | no | yes | no | yes | no |
| No. of repetitions | 1 | 1 | 1 | 1 | 4 |

With batches 1–4, we tested various SAT compositions with different rest periods, cooling temperatures, and with and without the presence of a rusty steel profile in the sample. We found that nearly all the glass jars containing a CMC composition broke due to thermal and mechanical stress. So we decided to produce five more samples, to reduce the heating temperature slightly, and to apply a minimum rest period of 2 hours at room temperature (until the samples cooled down to 30 °C) the samples were placed in the freezer. With these samples (Batch no. 5), it was possible to repeat the heating and cooling tests.

2.1.3. Analysis

Minimum supercooling temperatures, i.e. crystallization temperatures, were detected when sample temperatures started to rise due to the release of latent heat. We therefore measured the local temperature minima (T_{CRi}) reached in each sample during the cooling process. The first local minimum (T_{CR1}) was defined as the crystallization temperature. We also measured the increase in the temperature of each sample (ΔT_{CRi}) after each local minimum, so that we could compare the different samples.

The average logged temperature in the freezer during cooling of the supercooled samples was set as the reference (T_{ref}) for the cooling rate calculation. The start of the cooling periods (T_{C1}) was set to 45 K above the reference temperature, while the end of the cooling period (T_{C2}) was set to 20 K above the reference temperature. The resulting temperature difference (25 K) was divided by the duration of cooling in minutes (Eq. 2) to obtain the cooling rate:

$$cool\text{-down rate } (K \text{ min}^{-1}) = \frac{(T_{C1} - T_{ref}) - (T_{C2} - T_{ref})}{t(T_{C1}) - t(T_{C2})} \quad (2)$$

For example, Fig. 4 shows the approach we chose applied to a cooling curve with SAT + 9%wt. water. The characteristic temperature levels are indicated.

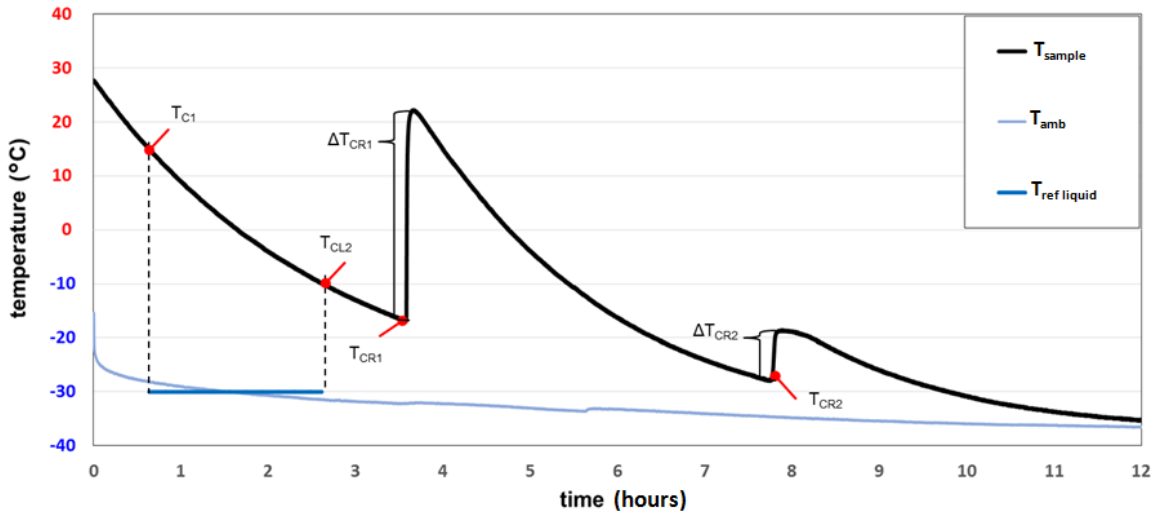


Fig. 4. An example illustrating the evaluation method in the cooling tests (schematic).

2.2. Initialization of crystallization using CO₂ evaporation

Prototype heat storage units with SAT composites were heated up to 90 °C and actively or passively cooled down to ambient temperatures under controlled conditions, as described by Dannemand et al. [10]. The prototype heat storage units were 240 x 120 x 5 cm and contained 200–220 kg of SAT composite. In a series of six experiments (overview in Table 5 and section 3.6), the SAT composites in the units were stable in supercooled state at ambient room temperatures

(about 20 °C), before we initiated crystallization by evaporating CO₂ in a small chamber adjacent to the chamber with the supercooled PCM.

As shown in Fig. 5, a CO₂ cylinder with a dip tube was connected via a rubber tube to the 100 mL CO₂ chamber on one side of the heat storage unit. Another tube was connected to the outlet of the CO₂ chamber with a pressure-regulating valve including a manometer. The pressure-regulating valve was set to maintain a pressure of approximately 5.5 bars in the tubes and the CO₂ chamber. This was to allow the CO₂ to remain in liquid phase in the tubes and the CO₂ chamber.

The temperatures on the outside of the CO₂ chamber (T_{CO_2}), on the side of the PCM chamber ($T_{surface}$), and inside the PCM (T_{PCM}) were measured using thermocouples (TT-type). The temperature in the PCM was measured in the other side of the PCM chamber, approximately 240 cm away from the CO₂ chamber.

To start the crystallization of the supercooled SAT composite in the heat storage unit, the valve for the CO₂ cylinder was opened and the CO₂ was flushed through the CO₂ chamber until a temperature increase (indicating crystallization) was detected by the nearby temperature sensor ($T_{surface}$) on the side of the PCM chamber.

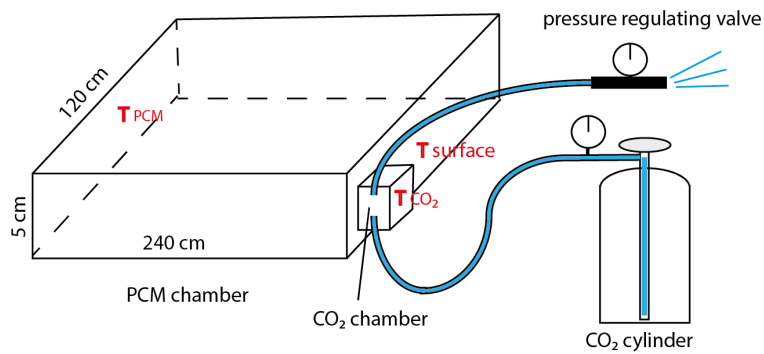


Fig. 5. Principle diagram of the nucleation method using cooling with CO₂.

2.3. Initialization of crystallization using Peltier elements

Based on previous work by Dröscher [36], we built a novel double-element Peltier device with cooling power of 8.8 W and 29.7 W (Fig. 6).

To ensure contact with the PCM, a steel extension pipe with a hole drilled in the bottom was mounted on the Peltier device. The extension pipe was filled with PCM. Rubber sealing ensured air-tightness in the construction. The lower Peltier element was in contact with the pipe via a steel plate. Thermal compound was used to improve the heat transfer to the steel plate. A thermocouple (type K) was placed below the lower Peltier element to measure the temperature of its cold side, which was attached to the steel plate ($T_{steel\ plate}$). Above the upper Peltier element, a heat sink was realised with an air cooler mounted, consisting of an electrically driven fan and aluminium fins. The temperature of the heat sink ($T_{heat\ sink}$) was measured with a thermocouple.

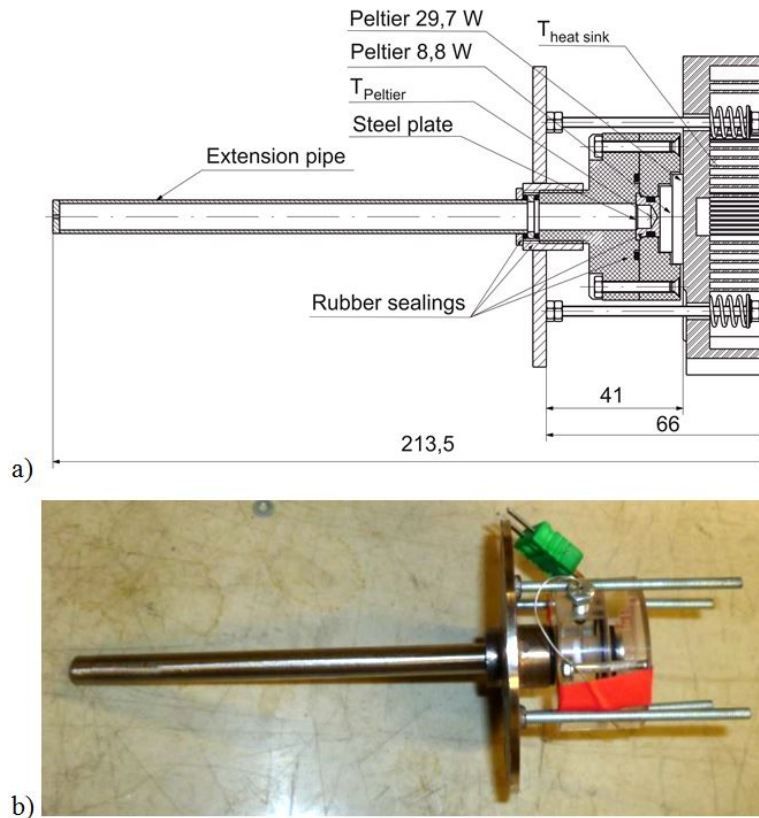


Fig. 6. (a) Drawing of the Peltier device with extension pipe (dimensions in mm); (b) Peltier triggering device with extension pipe (without the heat sink).

The Peltier device was tested with a small-scale flat heat storage prototype, filled with 5.4 kg SAT + 6%wt. extra water. It was attached via a steel plate to the top-left flange of the heat storage unit (Fig. 7). An additional thermocouple was inserted into the opposite side of the heat storage unit to measure the temperature of the SA-water mixture (T_{PCM}).

The SA-water mixture was heated to 85 °C and then passively cooled down to room temperature. The power supplies of the two Peltier elements and the fan were turned on until an increase in the temperature T_{PCM} indicated the crystallization of the SA-water mixture.

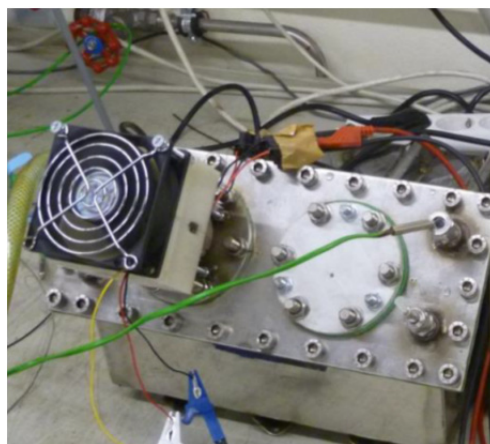


Fig. 7. Photograph of the Peltier device mounted on the small-scale heat storage prototype.

3. Results and discussion

3.1. Water content of SAT from industrial supply

Fig. 8 shows the water loss over time during material dry-out. The various water-loss development characteristics of the samples were caused by differences in local temperature and humidity inside the drying oven:

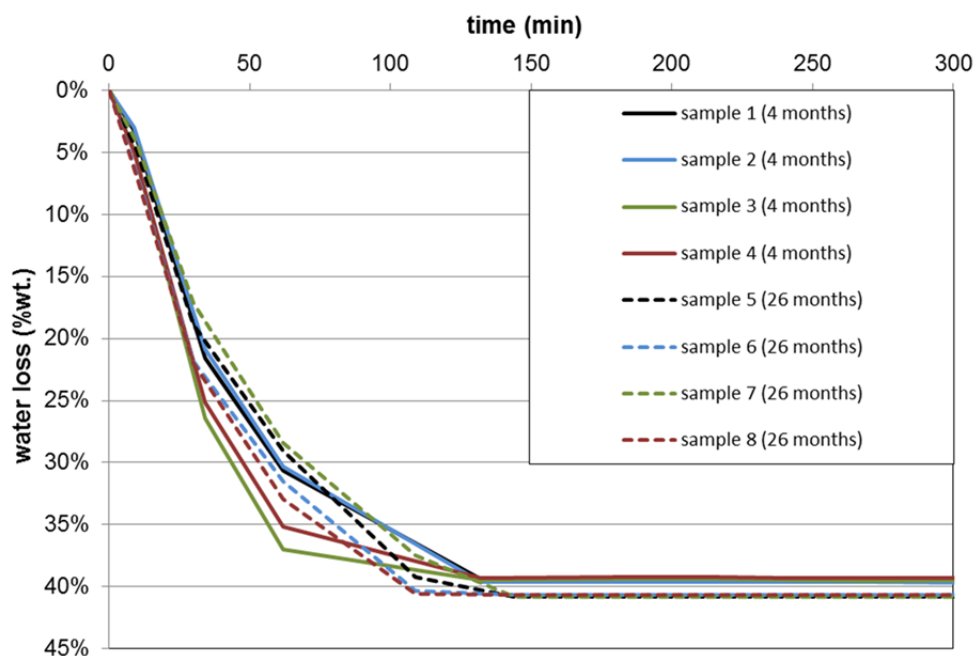


Fig. 8. Drying of SAT samples.

In the case of samples 1–4, the drying tests were conducted after delivery (4 months after production), and they showed an average water loss of 39.5%wt. Based on the molar SA-water ratio, the water content of chemically pure SAT is calculated to be 39.72%wt. Taking the minimal purity of the material into account, the water loss was expected to be 39.12%wt. (lower benchmark). The influence of scale accuracy on the final weight measurement was calculated to be $\pm 0.248\%$ wt. The mass loss measured therefore indicates the complete dry-out of SAT containing impurities.

After a period of 22 months (26 months after production), samples 5–8 were taken from a SAT bag, which was stored in the laboratory. By this time, the material, which was originally finely granulated particles, had clumped together due to its hygroscopic properties. An average water loss of 40.80%wt. was measured. This indicates that the water content of SAT from industrial supply strongly depends on the storage conditions.

In this research, SAT was defined with a water content of 40.5%wt. This value was found to be necessary to fully dissolve SA in water during melting when SAT of food grade (purity >98.5%) was used. The value also includes water vapour losses during the melting of the SA-water mixtures in closed glass jars.

3.2. Crystallization behaviour of SA-water mixtures

In the cooling tests of SAT and SAT with extra water, two stages of heat release were observed. Fig. 9 shows the temperature developments in the SA-water mixtures in four tests with similar conditions. After the initialization of crystallization was detected for the first time (T_{CR1}), the samples cooled down to a temperature below T_{CR1} , until a second temperature increase was measured at T_{CR2} .

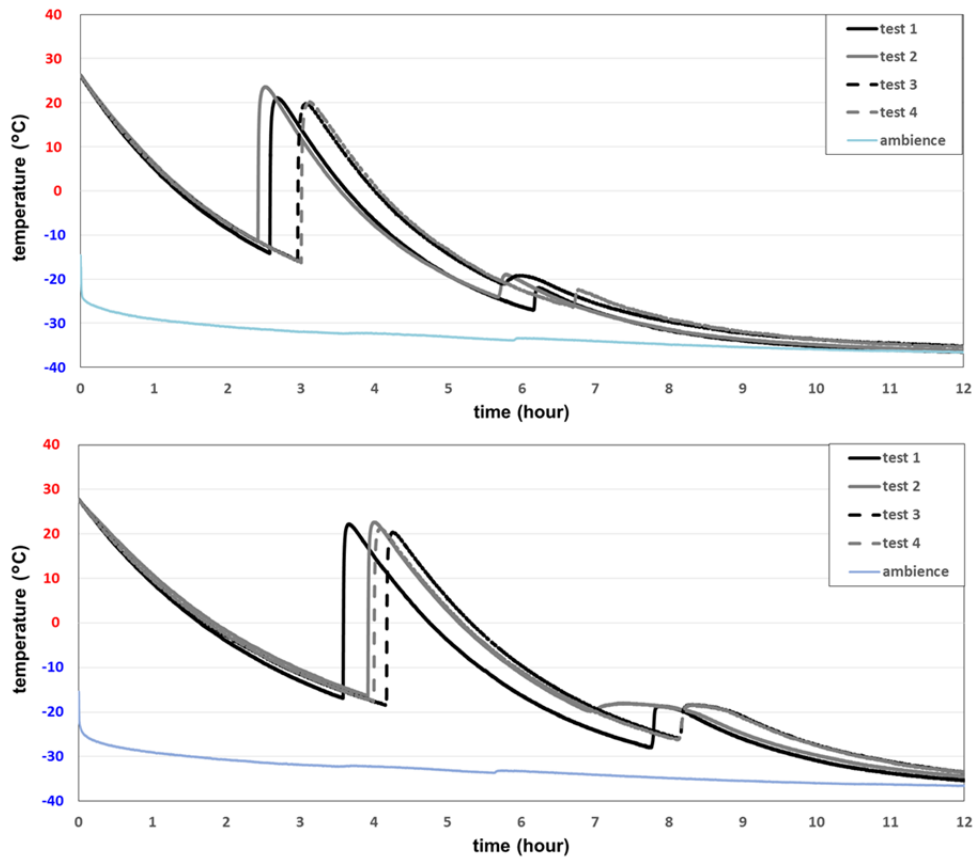


Fig. 9. Crystallization behaviour (sample batch no. 5) in SAT (top) and SAT with extra water (bottom).

As listed in Table 4, with extra water the SA-water mixture cooled down to significantly lower temperatures than any of the other SAT composites (the mean value of T_{CR1} was about 2 K below the T_{CR1} in other samples). So, extra-water did lower the crystallization temperature. Moreover, the second release of latent heat happened at lower temperatures with this SAT composite.

When the second release of latent heat occurred at a temperature around $-25\text{ }^{\circ}\text{C}$, a rapid temperature increase was observed. In some cases, the second reaction was initialised at higher temperatures and ΔT_{CR2} was lower, followed by a longer cooling period. This behaviour indicates that the heat content released during the reaction was similar to when there was a rapid temperature increase.

3.3. Crystallization behaviour of SAT with stabilizers

The composites with CMC or liquid polymer did not have a second temperature peak during the cooling process. Fig. 10 shows, however, that samples containing stabilizers reached significantly higher temperatures after crystallization started (evaluated in Fig. 13). Afterwards, the SAT composites cooled down over a similar time period (about 8 hours) to the freezer temperature.

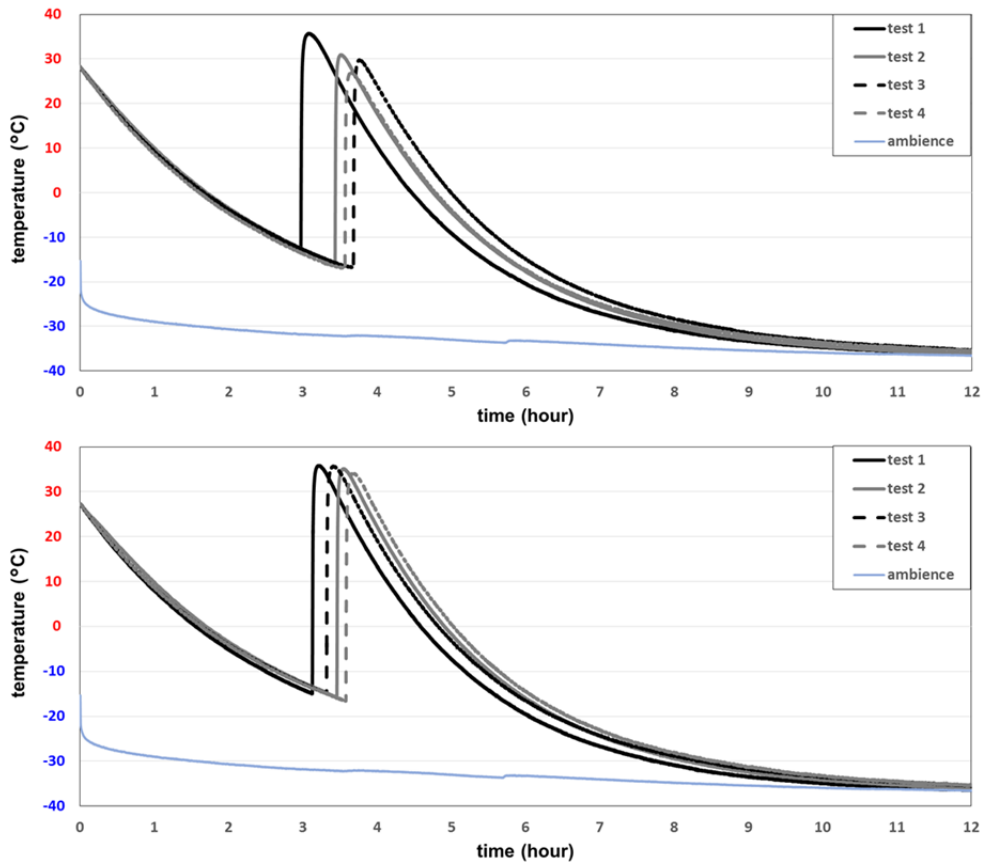


Fig. 10. Crystallization behaviour (sample batch no.5) in SAT +CMC + graphite flakes (top) and SAT +HD 310 (bottom).

The presence of silicone oil in samples containing liquid polymer did not influence temperature developments. As shown in Table 4, four similar heating and cooling cycles revealed no significant tendency for T_{CR1} and T_{CR2} to vary and neither did the type of stabilizer (CMC or liquid polymer) significantly influence T_{CR1} (basis: 12 tests).

3.4. Influence of steel profiles on the crystallization behaviour

In parallel tests with various samples containing steel profiles (Fig. 11 bottom), almost uniform crystallization temperatures were detected. As shown in Table 4, crystallization started at higher temperatures. In contrast, samples without steel profiles (Fig. 11 top) showed a big variation in crystallization temperatures, indicated by the time gaps between the crystallizations.

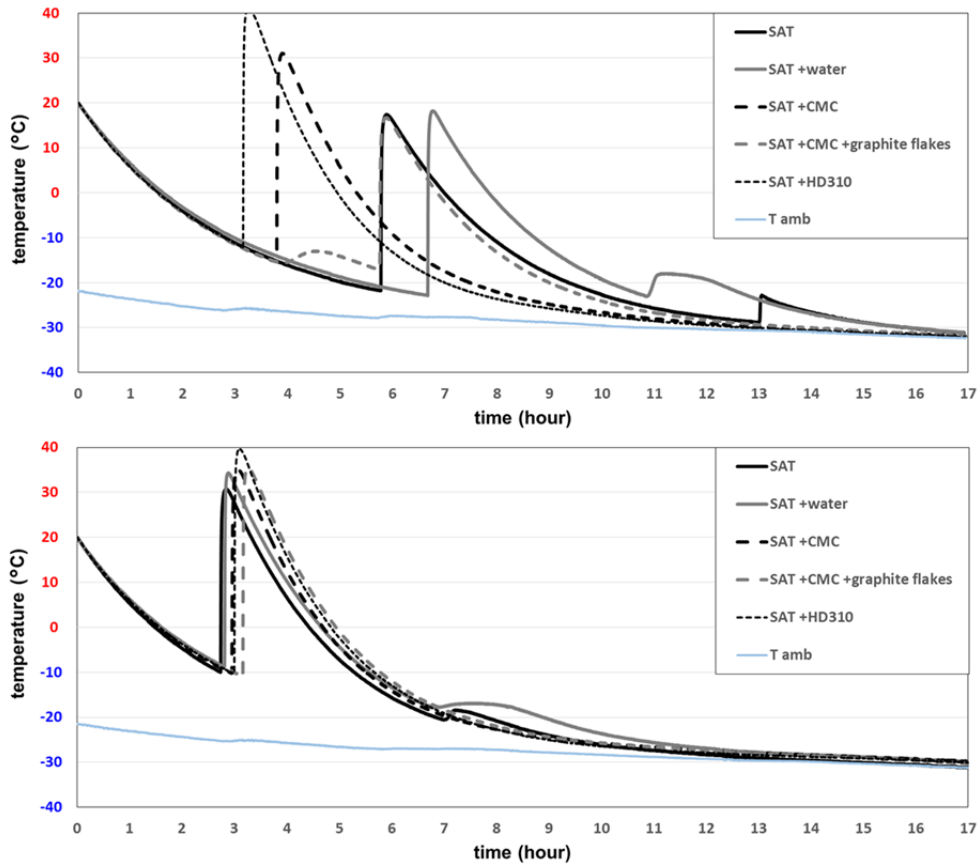


Fig. 11. Crystallization behaviour of sample batch no. 1 (without steel profiles; top) and sample batch no.2 (with steel profiles; bottom).

We found no significant difference in the crystallization behaviour of SAT composites cooled immediately (Fig. 11) and those first given one week of stable supercooling at 20 °C before cooling (Fig. 12). However, as shown in Table 4, lower crystallization temperatures were observed in samples containing rusty steel profiles that were given the rest period before cooling.

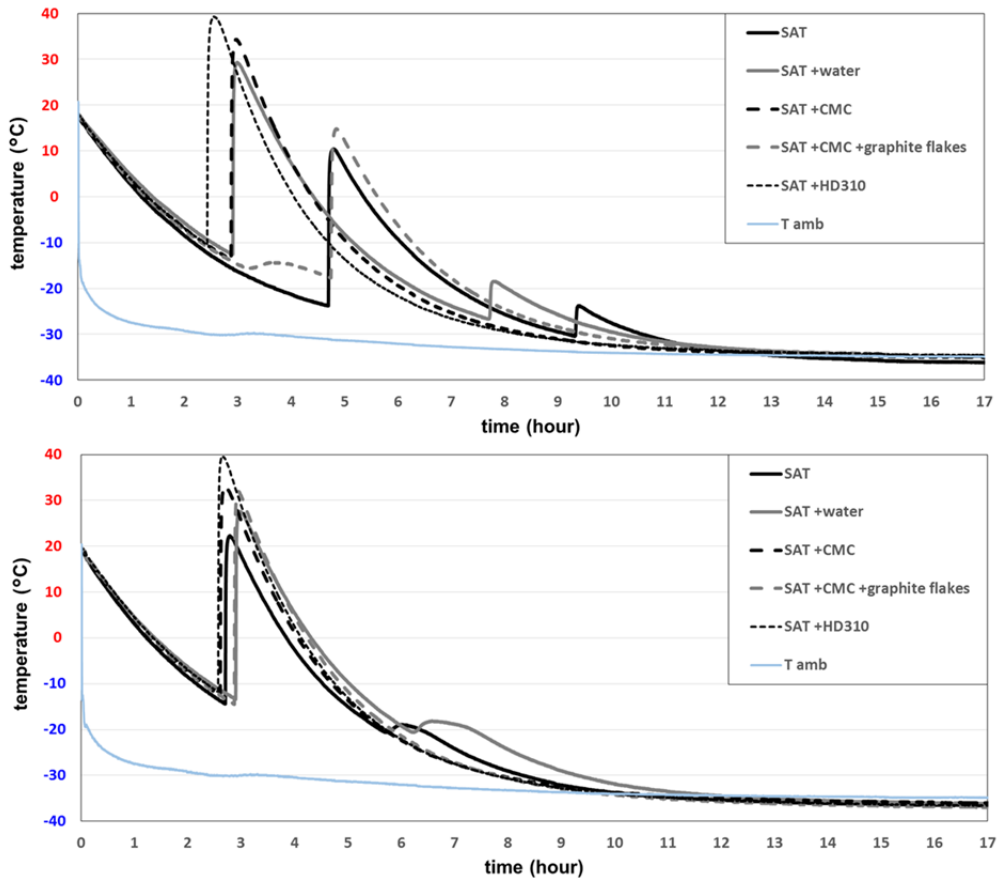


Fig. 12. Crystallization behaviour after one week rest sample batch no. 3 (without steel profiles; top) and sample batch no.4 (with steel profiles; bottom).

3.5. Cooling test analysis

Cooling rates varied only slightly in between 0.2 and 0.24 K min^{-1} . Samples containing extra water cooled down most slowly, while the SAT only samples showed the fastest cooling. Table 4 gives an overview of the local minimum temperatures in all the tests. Temperature values showing a moderate temperature increase are highlighted in grey.

The random measurement error of the thermocouples used was $\pm 0.5 \text{ K}$, assuming a uniform probability distribution. Because measurements were taken every second and the cooling rates were rather low, the temperature measurements are considered to be precise. The position of the sensors means the temperatures measured should be very close to the actual sample temperatures. Moreover, the slow cooling resulted in a graph with a very small slope, which enables us to say that crystallization usually started at about the temperature reported in the literature for pure SA aqueous solutions ($-15 \text{ }^\circ\text{C}$). However, significantly lower temperatures were measured with Batches 1 and 3.

During cooling of the samples without steel profiles present, we observed composite-specific ranges for T_{CR1} (and T_{CR2} where applicable). The crystallization of SAT and SAT + water samples (16 tests) started in the range of -11.5 to $-23.0 \text{ }^\circ\text{C}$, while in the samples with stabilizers (24 tests), T_{CR1} occurred in the range of -10.7 to $-17.2 \text{ }^\circ\text{C}$. The second release of heat for SAT and SAT + water (16 tests) ranged from -17.8 to $-30.4 \text{ }^\circ\text{C}$.

Table 4. Overview of crystallizations temperatures (T_{CR1}) and second local minimum temperatures (T_{CR2}).

| | Batch 1 | Batch 2 | Batch 3 | Batch 4 | Batch 5 | | | |
|-----------------------------|-----------|------------------|---------|---------------|---------|--------|--------|--------|
| | no rest | no rest steel | rest | rest steel | test 1 | test 2 | test 3 | test 4 |
| | (°C) | (°C) | (°C) | (°C) | (°C) | (°C) | (°C) | (°C) |
| | T_{CR1} | | | | | | | |
| SAT | -21.8 | -10 | -23.8 | -14.4 | -14.2 | -11.5 | -15.8 | -16.2 |
| SAT + water | -22.9 | -8.8 | -12.6 | -14.4 | -16.9 | -16.4 | -18.5 | -17.6 |
| SAT + CMC | -15.3 | -10.2 | -13.7 | -12.6 | - | - | - | - |
| SAT + CMC + graphite flakes | -17.2 | -10.9 | -17.6 | -14.5 | -13.1 | -15.9 | -16.8 | -16.9 |
| SAT + HD310 | -12.1 | -10.3 | -10.5 | -11.7 | -15 | -15.8 | -14.9 | -16.6 |
| SAT + HD 310 + silicone oil | n.a. | n.a. | n.a. | n.a. | -14.2 | -16.6 | -13.1 | -10.7 |
| | T_{CR2} | | | | | | | |
| SAT | -28.9 | -20.6 | -30.4 | -20.5 | -27 | -24.1 | -21.1 | -26.3 |
| SAT + water | -23.0 | -17.8 | -26.7 | -20.5 | -27.9 | -19.7 | -25.9 | -26.2 |

The samples with steel profiles (10 tests) showed a clear tendency to more uniform and higher T_{CR1} and T_{CR2} values. Crystallization temperatures between -8.8 and -10.9 °C were measured for samples cooled without a rest period (5 tests). The second local minimum resulted in a moderate temperature increase.

The samples with steel profiles that had a rest period before cooling (5 tests) crystallized at temperatures in a lower range (-11.7 to -14.5 °C). There were no significant differences in the local temperature minima in samples without steel profiles that had a rest period before cooling (5 tests) and those that did not (5 tests).

Several of the glass jars containing CMC broke. The tests were repeated with Batch 5, when the test procedure had been improved.

In Fig. 13, the blue bars show the average temperature increase in samples during the cooling tests. Here we have excluded the two tests with samples containing CMC and graphite flakes (Fig. 11 top and Fig. 12 top) that did not show a sharp temperature increase when crystallization started.

Because the material volumes of the composite samples (based on 60 g SAT) differed, ΔT_{CR1} can only be compared in a qualitative way. Nevertheless, a clear order of average temperature increase can be seen: SAT samples showed 36.6 K; SAT + water samples showed 40.3 K; SAT + CMC showed 46.3 K, and 46.5 K with added graphite; SAT + HD 310 showed 50.9 K, and 49 K with silicone oil added. This order is in good agreement with the heat content for SAT composites measured by Kong et al. [14] using a T-history method. This indicates that CMC and liquid polymer significantly improve the reactivity of SA with water during crystallization.

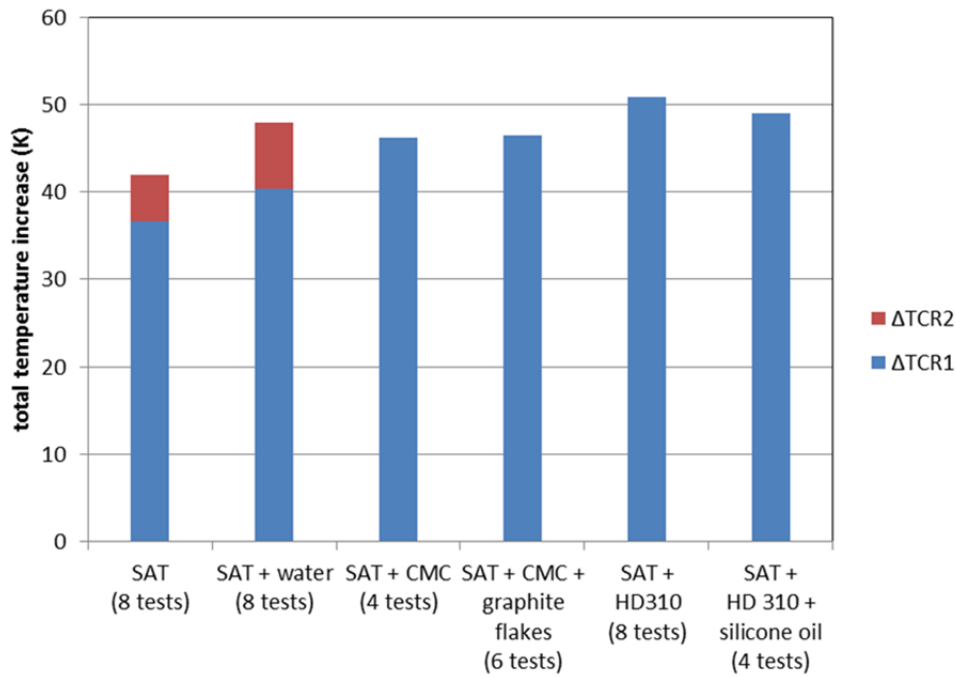


Fig. 13. Comparison of temperature increase during crystallization of material samples.

The second temperature increase (ΔT_{CR2} , red bar segments) was derived from samples that showed a sharp temperature increase (10 tests). In 6 out of 16 tests runs, the second temperature peak was reached slowly. The total temperature increase ($\Delta T_{CR1} + \Delta T_{CR2}$) was 41.6 K for SAT and 48.3 K for SAT + water samples. This indicates that, due to the very low temperature in these samples, further exothermic crystallization was enabled. This further potential of heat release was not observed by Kong et al. [14] when crystallization took place at 20 °C. We conclude that it can be only utilized when the SA-water mixtures (full volume) are exposed to low temperatures, as in the freezer (−30 °C).

The presence of steel profiles (10 tests) and periods of rest before cooling showed no systematic influence on the temperature increases.

3.6. Initialization of crystallization using CO_2 evaporation

Six experiments (Table 5) with the initiation of nucleation using cooling by evaporating CO_2 were carried out with the prototype units. A temperature range of −27 to −44 °C was measured on the outside on the CO_2 chamber. After 1.5–5.0 minutes of releasing CO_2 into the chamber, a temperature increase was detected at the nearby temperature sensor ($T_{surface}$) on the surface of the PCM chamber and the valve on CO_2 cylinder was closed. The crystallization probably started earlier, because it would take some time for the temperature to increase at the point next to the CO_2 chamber where the sensor was. Furbo et al. have reported that supercooled SAT nucleated within 30 seconds of applying the CO_2 evaporation method through a 2 mm metal plate. In their case, the nucleation was observed visually [37].

Table 5. Overview of our experiments with heat storage unit prototypes to initialize crystallization using CO₂ evaporation.

| Experiment | 1 | 2 | 3 | 4 | 5 | 6 |
|---|-----------------|-------------------|-------------------|-----------------|------------------|--|
| PCM | SAT + 1%wt. CMC | SAT + 5%wt. water | SAT + 5%wt. water | SAT + 1%wt. CMC | SAT + 1 %wt. CMC | SAT +1%wt. CMC + 2%wt. graphite powder |
| Cooling method | active | active | active | passive | passive | active |
| Duration of stable supercooling | 1 day | 5 days | 3 days | 14 days | 71 days | 1 day |
| Minimum temperature CO ₂ chamber | -30 °C | -34 °C | -36 °C | -27 °C | -27 °C | -44 °C |
| Maximum PCM temperature during solidification | 58 °C | 53 °C | 53 °C | 58 °C | 58 °C | 58 °C |

Fig. 14 shows the development of T_{PCM} , $T_{surface}$ and T_{CO_2} in the heat storage unit during the initialization of crystallization in the supercooled SAT composite in Experiment 1 (1%wt. CMC). As the PCM composite temperature was measured at the other end of the heat storage unit, approximately 240 cm from the CO₂ chamber, the crystallization and temperature increase occurred there approximately 12 minutes after the nucleation started next to the CO₂ chamber. The maximum temperature reached in the PCM after crystallization is also listed in Table 5.

For each nucleation, 700–900 g CO₂ was used. This could probably be significantly reduced with a faster response in relation to when nucleation actually started and an optimized design of the tube and CO₂ chamber size.

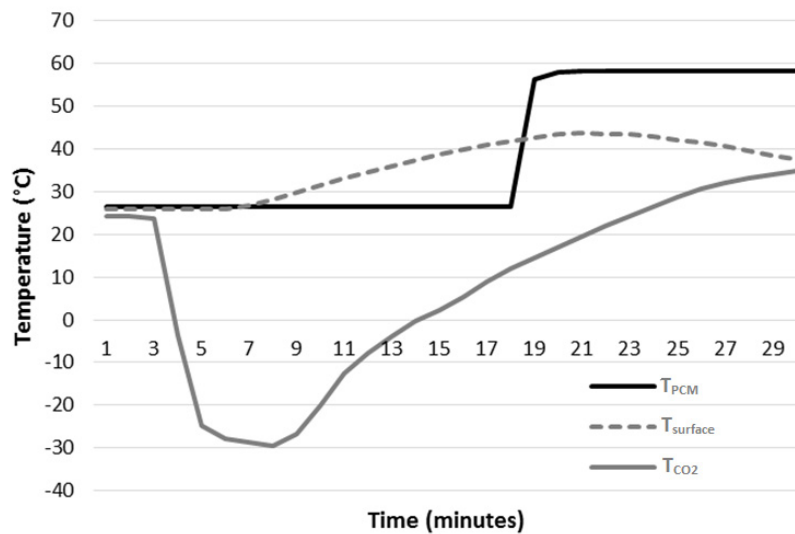


Fig. 14. Temperature development in the PCM, the CO₂ chamber and next to the CO₂ chamber.

3.7. Initialization of crystallization using Peltier elements

Two series of ten experiments each were carried out with the Peltier triggering device. After the SA-water mixture cooled to room temperature, the Peltier device was turned on. The temperature reached in the area of the lower Peltier element ($T_{steel\ plate}$) varied from -31 to -36 °C. Despite the limited cooling power of the Peltier elements, sufficiently low cold-side temperatures were possible when the SA-water mixture supercooled to temperatures below 30 °C.

In the first test series the number of necessary cooling attempts increased till the last experiment, when no crystallization was initiated. The time gap between turning on the Peltier device (first attempt) to measured temperature increase of the PCM varied from 5 minutes to more than six hours at the last experiment. The reason for unsuccessful attempts might be due to the SA-water mixture flowing out of the extension pipe so that no PCM was in contact with

the steel plate. So we reduced the diameter of the bore-hole at the front of the extension pipe from 1mm to 0.4 mm and the PCM filling volume of the extension pipe from 7.5 to 4.5 ml by adding inert material. The second test series showed 10 successful experiments, in each of which the SA-water mixture crystallized 2.5–7.5 minutes after the Peltier device was turned on.

Fig. 15 shows the temperature developments in Experiment 3 of the second test series. $T_{\text{steel plate}}$ decreased as $T_{\text{heat sink}}$ increased. When $T_{\text{steel plate}}$ reached $-33\text{ }^{\circ}\text{C}$, a temperature increase was observed (dotted line in Fig. 15) indicating that the SA-water mixture had started to solidify in the extension pipe. One minute later, the solidification was detected at the temperature sensor in the PCM container (T_{PCM}). During crystallization, the SA-water mixture reached a temperature of $56.5\text{ }^{\circ}\text{C}$ (T_{PCM}).

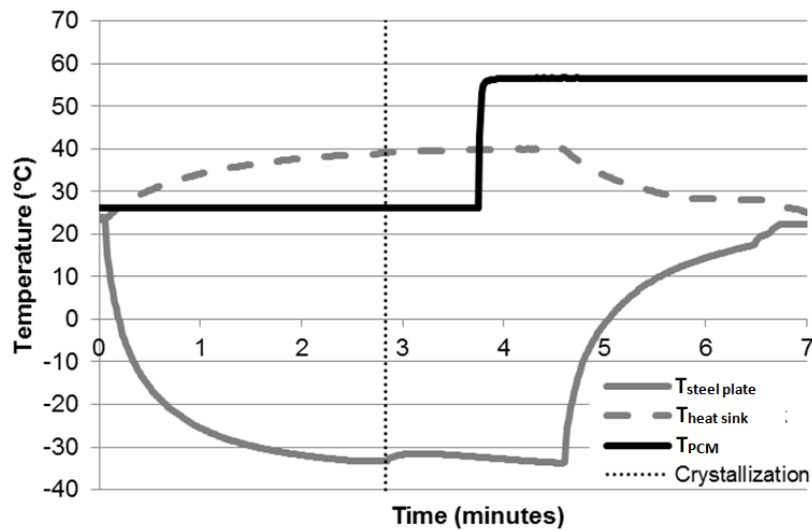


Fig. 15. Crystallization of SA-water mixture by local cooling using Peltier elements.

3.8. Economic aspects

For industrial use SAT is available in large quantities. Market prices depend on its purity and are typically below 0.5 Euros per kilogram. Therefore SAT is potentially an economically attractive heat storage material. For economic assessment of heat storage units additives, container, heat exchanger, hydraulics and devices for controlled activation of crystallization need to be taken into account. Rathgeber et al. [38] made a top-down evaluation of acceptable costs of energy storages. They found that acceptable storage capacity costs ranged from about 1 Euro per kWh for seasonal heat storage to 429 Euros per kWh for daily utilization in buildings. Englmaier et al. [12] demonstrated that flat prototype heat storage units, utilizing stable supercooling of 200 kg SAT composites, enable combined short- and long-term heat storage in domestic solar heating systems. Their total heat storage capacity was 27.4 kWh. 12 storage cycles per year result by assuming monthly utilization. In this case acceptable costs for such heat storage units range from 200 to 460 Euros. Prototype heat storage units and activation devices used in the presented work need to be further developed to achieve this cost range. Cylindrical unit design [11] is expected to allow reduction of container and heat exchanger costs in comparison to flat units. Peltier elements and CO_2 evaporation can potentially initiate SAT composite solidification with inexpensive devices of reduced size.

4. Conclusions

All the SAT composites investigated supercooled to temperatures below $-8\text{ }^{\circ}\text{C}$, which means they can be considered useful for application as heat storage materials in households. The following temperatures were required for initialization of crystallization of SAT composites:

- $-24\text{ }^{\circ}\text{C}$ for SAT and SAT with 9%wt. water added
- $-18\text{ }^{\circ}\text{C}$ for SAT with 5% CMC and 3% of HD 310 added
- $-15\text{ }^{\circ}\text{C}$ for all SAT composites in closed steel containers

Extra water added to the SAT resulted in lower crystallization temperatures in comparison to SAT. Experiments on additional impurities in SAT compositions in the form of rusty steel profiles (which could resemble the metal surfaces of the PCM container) showed that crystallization started at higher and more uniform temperatures for all samples. Letting the samples rest at ambient temperature only affected the crystallization behaviour when steel profiles were present.

The cooling tests proved useful for investigating the supercooling stability of SAT composites:

- A second minor temperature peak occurred below $-20\text{ }^{\circ}\text{C}$ in the SAT composites with no stabilizers added, and the samples cooled further after the first crystallization. When it occurred below $-21.3\text{ }^{\circ}\text{C}$, a sharp temperature rise resulted. Otherwise, the temperature increase was slow.
- SAT with 9%wt. extra water showed higher temperature increases during crystallization than SAT on its own.
- SAT composites with stabilizers (carboxymethyl cellulose and liquid polymer HD 310) showed the highest temperature increase when crystallization was initiated, and there was no second temperature peak as a result of the release of heat.

When a large amount of loose crystalline SAT in paper bags is used to prepare composites for heat storage, its water content must be determined. During melting, 40.5%wt. water content was necessary to fully dissolve SAT of food grade.

To initiate crystallization of SAT composites in heat storage units in a controlled way, evaporating carbon dioxide in a chamber adjacent to a PCM chamber with supercooled SAT composites worked reliably. A device with Peltier elements mounted on a PCM chamber was also able to generate local cooling to sufficiently low temperatures to initiate crystallization for all the SAT composites investigated when the SA-water mixtures had supercooled to temperatures below $30\text{ }^{\circ}\text{C}$. With both methods, local cooling was realised rapidly, so that crystallization was initiated two to five minutes after the experiments were started.

Declaration of interest

None.

Acknowledgements

This research was funded by the European Commission (Grant Agreement N_295568) as part of the Seventh Framework Programme of the European Community for Research, Technological Development and Demonstration Activities under the funding scheme of "Collaborative Project" through the COMTES consortium. The work was also supported by the PhD program of the Sino-Danish Center for Education and Research (SDC).

References

- [1] M. Dannemand, J.M. Schultz, J.B. Johansen, S. Furbo, Long term thermal energy storage with stable supercooled sodium acetate trihydrate, *Appl. Therm. Eng.* 91 (2015) 671–678.
- [2] B. Zalba, J.M. Marín, L.F. Cabeza, H. Mehling, Review on thermal energy storage with phase change: materials, heat transfer analysis and applications, *Appl. Therm. Eng.* 23 (3) (2003) 251–283.
- [3] L.F. Cabeza, G. Svensson, S. Hiebler, H. Mehling, Thermal performance of sodium acetate trihydrate thickened with different materials as phase change energy storage material, *Appl. Therm. Eng.* 23 (13) (2003) 1697–1704.
- [4] N. Araki, M. Futamura, A. Makino, H. Shibata, Measurements of Thermophysical Properties of Sodium Acetate Hydrate, *International J. Thermophys.* 16 (6) (1995) 1455–1466.
- [5] M. Dannemand, M. Delgado, A. Lazaro, C. Penalosa, C. Gundlach, C. Trinderup, J.B. Johansen, C. Moser, H. Schranzhofer, S. Furbo, Porosity and density measurements of sodium acetate trihydrate for thermal energy storage, *Appl. Therm. Eng.* 131 (2018) 707–714.
- [6] A. Sharma, V.V Tyagi, C.R. Chen, D. Buddhi, Review on thermal energy storage with phase change materials and applications, *Renew. Sustain. Energy Rev.* 13 (2) (2009) 318–345.
- [7] J. Pereira da Cunha, P. Eames, Thermal energy storage for low and medium temperature applications using phase change materials – A review, *Appl. Energy* 177 (2016) 227–238.
- [8] J. Xu, R.Z. Wang, Y. Li, A review of available technologies for seasonal thermal energy storage, *Sol. Energy* 103 (2013) 610–638.
- [9] T. Kousksou, P. Bruel, A. Jamil, T. El Rhafiki, Y. Zeraouli, Energy storage: Applications and challenges, *Sol. Energy Mater. Sol. Cells* 120 (A) (2014) 59–80.
- [10] M. Dannemand, J. Dragsted, J. Fan, J.B. Johansen, W. Kong, S. Furbo, Experimental investigations on prototype heat storage units utilizing stable supercooling of sodium acetate trihydrate mixtures, *Appl. Energy* 169 (2016) 72–80.
- [11] M. Dannemand, J.B. Johansen, W. Kong, S. Furbo, Experimental investigations on cylindrical latent heat storage units with sodium acetate trihydrate composites utilizing supercooling, *Appl. Energy* 177 (2016) 591–601.
- [12] G. Englmaier, C. Moser, S. Furbo, M. Dannemand, J. Fan, Design and functionality of a segmented heat-storage prototype utilizing stable supercooling of sodium acetate trihydrate in a solar heating system, *Appl. Energy* 221 (2018) 522–534.
- [13] J. Deng, S. Furbo, W. Kong, J. Fan, Thermal performance assessment and improvement of a solar domestic hot water tank with PCM in the mantle, *Energy Build.* 172 (2018) 10–21.
- [14] W. Kong, M. Dannemand, J.B. Johansen, J. Fan, J. Dragsted, G. Englmaier, S. Furbo, Experimental investigations on heat content of supercooled sodium acetate trihydrate by a simple heat loss method, *Sol. Energy* 139 (2016) 249–257.
- [15] W.F. Green, The ‘Melting-Point’ of Hydrated Sodium Acetate : Solubility Curves, *J. Phys. Chem.* 12 (9) (1908) 655–660.
- [16] H. Kimura, J. Kai, Phase change stability of sodium acetate trihydrate and its mixtures, *Sol. Energy* 35 (6) (1985) 527–534.
- [17] S. Furbo, S. Svendsen, Report on heat storage in a solar heating system using salt hydrates, Thermal Insulation Laboratory, DTU, Kgs. Lyngby, Denmark, Report no.70, 1977.
- [18] M. Dannemand, J.B. Johansen, S. Furbo, Solidification behavior and thermal conductivity of bulk sodium acetate trihydrate composites with thickening agents and graphite, *Sol. Energy Mater. Sol. Cells* 145 (3) (2016) 287–295.
- [19] H.W. Ryu, S.W. Woo, B.C. Shin, S.D. Kim, Prevention of supercooling and stabilization of inorganic salt

hydrates as latent heat storage materials, *Sol. Energy Mater. Sol. Cells* 27 (2) (1992) 161–172.

- [20] M.A. Rogerson, S.S.S. Cardoso, Solidification in heat packs: I. Nucleation rate, *AIChE J.* 49 (2) (2003) 505–515.
- [21] D. Zhou, C.Y. Zhao, Y. Tian, Review on thermal energy storage with phase change materials (PCMs) in building applications, *Appl. Energy*, 92 (2012) 593–605.
- [22] J. Guion, M. Teisseire, Nucleation of sodium acetate trihydrate in thermal heat storage cycles, *Sol. Energy* 46 (2) (1991) 97–100.
- [23] W. Cui, Y. Yuan, L. Sun, X. Cao, X. Yang, Experimental studies on the supercooling and melting/freezing characteristics of nano-copper/sodium acetate trihydrate composite phase change materials, *Renew. Energy* 99 (2016) 1029–1037.
- [24] G.A. Lane, *Solar heat storage latent heat material Vol 1*, Boca Raton, Florida, United States: CRC, 1983.
- [25] J.W. Mullin, *Crystallization*, 4th Edition, Oxford: Butterworth-Heinemann, 2001.
- [26] H. Machida, T. Sugahara, I. Hirasawa, Relationship between supercooling stability and solution structure in sodium acetate aqueous solution, *J. Cryst. Growth* 475 (2017) 295–299.
- [27] P. L. Dietz, J.S. Brukner, C.A. Hollingsworth, Linear crystallization velocities of sodium acetate in supersaturated solutions, *J. Phys. Chem.* 61 (7) (1957) 944–948.
- [28] T. Munakata, S. Nagata, Electrical initiation of solidification and preservation of supercooled state for sodium acetate trihydrate, in *Proceedings of the International Heat Transfer Conference*, 2010.
- [29] Z. Ma, H. Bao, A.P. Roskilly, Study on solidification process of sodium acetate trihydrate for seasonal solar thermal energy storage, *Sol. Energy Mater. Sol. Cells* 172 (2017) 99–107.
- [30] M.A. Rogerson, S.S.S. Cardoso, Solidification in heat packs: III. Metallic trigger, *AIChE J.* 49 (2) (2003) 522–529.
- [31] K. Seo, S. Suzuki, T. Kinoshita, I. Hirasawa, Effect of Ultrasonic Irradiation on the Crystallization of Sodium Acetate Trihydrate Utilized as Heat Storage Material, *Chem. Eng. Technol.* 35 (6) (2012) 1013–1016.
- [32] M.A. Rogerson, S.S.S. Cardoso, Solidification in heat packs: II. Role of cavitation, *AIChE J.* 49 (2) (2003) 516–521.
- [33] M. Dannemand, W. Kong, J. Fan, J.B. Johansen, S. Furbo, Laboratory Test of a Prototype Heat Storage Module Based on Stable Supercooling of Sodium Acetate Trihydrate, *Energy Procedia*, 70 (2015) 172–181.
- [34] L. Wei, K. Ohsasa, Supercooling and Solidification Behavior of Phase Change, *ISIJ Int.* 50 (9) (2010) 1265–1269.
- [35] IG Chemicals, Specification sheet SAT E262i. Bad Salzflun, Germany, 2015.
- [36] H. Dröscher, Master Thesis: The chemical system of sodium acetate/ water as phase change material (PCM) for the use in seasonal energy storage, Graz University of Technology, 2012.
- [37] S. Furbo, J. Dragsted, Z. Chen, J. Fan, E. Andersen, B. Perers, Towards seasonal heat storage based on stable super cooling of sodium acetate trihydrate, in *EuroSun Congress Proceedings*, 2010.
- [38] C. Rathgeber, E. Lävemann, A. Hauer, Economic top-down evaluation of the costs of energy storages- A simple economic truth in two equations, *J. Energy Storage*, 2 (2015) 43–46.

[3] G. Englmair, C. Moser, S. Furbo, M. Dannemand, and J. Fan, “Design and functionality of a segmented heat-storage prototype utilizing stable supercooling of sodium acetate trihydrate in a solar heating system,” *Applied Energy*, vol. 221, pp. 522–534, 2018. <https://doi.org/10.1016/j.apenergy.2018.03.124>

This page is intentionally left blank.

Design and functionality of a segmented heat-storage prototype utilizing stable supercooling of sodium acetate trihydrate in a solar heating system

Gerald Englmaier^{1,*}, Christoph Moser², Simon Furbo¹, Mark Dannemand¹ and Jianhua Fan¹

¹Department of Civil Engineering, Technical University of Denmark, Brovej 118, 2800 Kgs. Lyngby, Denmark

²Institute of Thermal Engineering, Graz University of Technology, Inffeldgasse 25/B, 8010 Graz, Austria

Highlights

- Combined short- and long-term heat-storage prototype for domestic solar heating
 - Interplay of solar collectors, four 200 kg PCM units and a 735 L water tank
 - Functionality of a segmented heat storage utilizing stable supercooling of SAT
 - Solidification of supercooled SAT was started by a seed crystal injection device
 - Supply temperatures and thermal power during PCM charge and discharge were evaluated
-

Abstract

A solar heating system with 22.4 m² of solar collectors, a heat storage prototype consisting of four 200 kg phase-change material (PCM) storage units, and a 735 L water tank was designed to improve solar heat supply in single-family houses. The PCM storage utilized stable supercooling of sodium acetate trihydrate composites to conserve the latent heat of fusion for long-term heat storage. A control strategy directed heat from a solar collector array to either the PCM storage or a water buffer storage. Several PCM units had to be charged in parallel when the solar collector output peaked at 16 kW. A single unit was charged with 27.4 kWh of heat within four hours on a sunny day, and the PCM temperature increased from 20 °C to 80 °C. The sensible heat from a single PCM unit was transferred to the water tank starting with about 32 kW of thermal power after it had fully melted at 80 °C. A mechanical seed crystal injection device was used to initialize the crystallisation of the sodium acetate trihydrate after it had supercooled to room temperature. The unit discharge during solidification peaked at 8 kW. Reliable supercooling was achieved in three of the four units. About 80% of latent heat of fusion was transferred from PCM units after solidification of supercooled sodium acetate trihydrate to the water tank within 5 hours. Functionality tests with practical operation conditions on the novel, modular heat-storage configuration showed its applicability for domestic hot water supply and space heating.

Keywords: Solar heating system; heat storage prototype; phase change material; sodium acetate trihydrate; stable supercooling.

Nomenclature

Dimensional variables

| | |
|-----------|--|
| c_p | specific heat capacity (kJ/kg K) |
| G | global irradiance (W/m ²) |
| m | mass (kg) |
| Q | thermal energy, heat (kWh) |
| \dot{Q} | thermal power, heat transfer rate (kW) |
| ρ | density (kg/m ³) |
| t | time (s) |
| T | temperature (°C) |
| \dot{V} | volume flow rate (l/min) |

Greek letters

| | |
|------------|--|
| Δh | specific latent heat of fusion (kJ/kg) |
| ΔH | latent heat of fusion (kJ) |
| ΔT | temperature difference (K) |

Subscripts

| | |
|------|----------------------------------|
| AMB | ambient |
| B | buffer heat storage (water tank) |
| COLL | solar collector |
| IN | inlet line |
| L | lower |

| | |
|-------|-------------------------------|
| LOSS | losses |
| PCM | phase-change material |
| OUT | outlet line |
| S | surface |
| ST | steel |
| TOTAL | total, on the collector plane |
| U | upper |
| W | water |

Abbreviations

| | |
|------|---------------------------------|
| ABS | acrylonitrile butadiene styrene |
| CMC | carboxymethyl cellulose |
| DHW | domestic hot water |
| EDTA | ethylenediaminetetraacetic acid |
| HTF | heat transfer fluid |
| HX | heat exchanger |
| P | pump |
| PCM | phase-change material |
| SA | sodium acetate |
| SAT | sodium acetate trihydrate |
| SH | space heating |
| V | 2-way valve |

1. Introduction

With the increasing utilization of energy from renewable sources, solar heating has become one of the most promising technologies for reducing the percentage of fossil fuels in future energy systems. Thermal energy storage is a key system component for utilizing renewable energy sources to a greater extent [1]. Solar combisystems are designed to achieve high solar fractions of heat supply for domestic buildings. Their task is to collect energy from the sun and store it until it is used for domestic hot water or for space heating/cooling. The importance of heat storage with small heat loss and good interplay with solar collectors is well known [2], [3]. Andersen and Furbo [4] and Thür and Furbo [5] have conducted detailed investigations on the design and potential of solar combisystems and on efficient heat storage using hot water storage tanks.

Due to insufficient solar radiation during the winter and the high energy requirement for space heating at high latitudes, long-period and even seasonal heat storage technology for solar heating applications has attracted more and more attention in recent decades [6], [7].

1.1. *Novel thermal energy storage concepts*

Materials that might enable more efficient storage of heat over long periods, were investigated by Ristić et al. [8]. Promising heat storage concepts are based on solid sorption materials which utilize the adsorption of water vapour [9]–[11], the principle of absorption (e.g. with sodium-hydroxide and water [12] as demonstrated by Fumey et al. [13] and Daguesnet-Frick et al. [14]), thermochemical reactions (as demonstrated by Zondag et al. [15]), and phase-change materials (PCMs). Salt hydrate reactions have been considered for their high potential energy storage density [16]. The thermophysical properties of several salt hydrates are appropriate for utilization as PCMs in building applications [17].

As reported by Quinnel and Davidson [18], the combined use of material properties, such as reaction enthalpy and sensible heat capacity, is potentially advantageous in new materials for domestic heat storage applications. The stable supercooling of PCMs allows the combined use of the latent heat of fusion and sensible heat capacity. This is one long-term heat storage concept that promises more efficient utilization of solar heat for low-energy buildings in summer and transitional seasons [19]. In addition to salt hydrates, microstructured polyol–polystyrene composites have also been considered for their stable supercooling properties [20].

Sodium Acetate Trihydrate (SAT) is a salt hydrate with a melting point of 58 °C and a relatively high latent heat of fusion (264 kJ/kg) [21]. It contains 60.3%wt of sodium acetate and 39.7%wt of water. If SAT has been fully melted and heated to a temperature higher than ~77 °C (as indicated in the binary phase diagram of sodium acetate and water [22]), it can cool down to ambient temperature in its liquid phase without releasing the heat of fusion; this is called “supercooling”, “subcooling” or “undercooling”. The latent heat is conserved until crystallisation occurs. When a PCM is in the supercooled state and in thermal equilibrium with its surroundings, it can in principle store heat indefinitely, so it could be used for seasonal heat storage [23]. Once crystallisation is activated, the latent heat of fusion is released, and the material temperature increases almost immediately to the melting temperature [24].

On the other hand, the cooling down of liquid material to temperatures substantially below its melting temperature is considered to hinder the conventional use of PCMs for thermal energy storage [25], [26]. Ways of reducing the supercooling of SAT have therefore been investigated [27], [28].

Various designs have been developed for domestic heat storage units using PCMs. The performance of heat

exchangers with large PCM volumes in metal containers with an internal bundle of tubes has been studied by Lopez-Navarro et al. [29]. Shell-and-tube heat exchangers [30] and macro encapsulated PCM in water vessels [31] have been tested for sensible-latent heat storage. Moreno et al. [32] have investigated the corrosion of metal and metal alloy containers in contact with various PCMs. Arteconi et al. [33] argue that the application of PCMs in thermal energy storage systems can help manage the mismatch between the availability of renewable electricity and the demand for electricity, for example in buildings where hot water, heating and cooling are delivered by heat pumps and air conditioning.

1.2. *Sodium acetate trihydrate compositions*

SAT is available in large quantities in food-grade products (E262i), which makes it suitable for application in domestic buildings. To stabilize SAT for heat storage applications, adding water (resulting in a lower SA-water ratio) was first studied by Furbo in 1978 [34]. Later investigations on a heat storage unit containing about 200 kg of an SA-water composition with a water content greater than 40%wt [35] showed a decrease in conserved latent heat of fusion when several cycles of heating and cooling were applied.

To overcome the problem of phase separation in the incongruently melting SAT, various additives can be added to form a more stable composition. One proposed solution is to add Carboxymethyl Cellulose (CMC) as a thickening agent [36]. The main drawback of thickening agents is that they reduce heat transfer by convection. Highly conductive graphite powder can improve the thermal conductivity of a composition with a thickening agent [37]. Paraffin oil, which does not mix with SAT, can be added to increase heat transfer by filling insulating cavities formed during the solidification and contraction of the PCM composition [38] due to density differences during phase change [37]. Another way of reducing the problem of phase separation is to increase the solubility of the crystal water in the melted and supercooled SAT mixture. The heat contents of SAT composites with various concentrations of thickening agents, the chelating agent Disodium Ethylenediaminetetraacetic Acid (EDTA), and polymer additives have been investigated by Kong et al. [39].

1.3. *State of the art*

Experiments with rectangular and cylindrical PCM containers with SA-water and CMC composites have been reported by Zhou and Xiang [40]. Their results show that more stable supercooling could be achieved with longer charging periods (to ensure the full melting of all SAT crystals), a relatively low cooling rate, and a lower inner surface roughness in PCM containers. The bending of rough metal surfaces might be an uncontrolled activation mechanism during cooling [41].

In previous work by the present authors, we tested various heat storage designs [42], each based on a flat box with SAT and additives as the heat storage material. A functioning design was identified as consisting of either steel or stainless steel units with room for PCM expansion in the box. Its thermal behaviour was then further investigated by using numerical models [38], [43]. The actual design and its characteristics with SAT as the heat storage material were investigated by Dannemand et al. under laboratory conditions [35]. It was proved and documented that the stable supercooling of SAT composites in flat boxes and cylindrical vessels [44] is enabled by: a) avoiding pressure changes in the PCM container (e.g. by using a membrane expansion vessel), b) smooth inner container surfaces, and c) heating

up the whole material volume to a minimum temperature of ~ 77 °C.

A numerical model for a solar combisystem for the Danish climate with an ideal seasonal PCM heat storage with SAT has been used to calculate the possible solar fraction of heat supply in a low-energy house [45], [36]. It was calculated that solar fractions in the range of 80–100% can only be achieved if the PCM storage volume is subdivided into segments. Individual control with respect to charging, discharging, and the initialization of solidification makes it possible to utilize a small storage volume to match domestic heat demand while conserving the remaining energy.

In this context, the controlled initialization of crystallization is a key requirement. Several methods have been investigated. Successful initiation of crystallization of supercooled SAT with ultrasonic waves has been reported by Seo et al. [46], but other researchers [47] say that the crystallization failed. Starting solidification by cooling supercooled SAT below its crystallization point (around -15 °C) [48] has been successfully achieved using local evaporation of carbon dioxide on the outside of a container wall in steel [35]. Another way to cool down SAT locally is to use Peltier elements. A set-up with double-staged Peltier elements reached -30 °C and would therefore be able to trigger the crystallization [49]. Adding seed crystals is another common method to initialize crystallization in laboratory set-ups [48], [50]. Crystallization with seed crystals works, if the seed crystals do not melt and become inactive [41]. Electric field nucleation has also been reported to work [24]. Activation methods based on local cooling as well as seed crystal injection seem to be reliable.

1.4. *Storage principles with SAT*

SAT composites in closed containers can be utilized for heat storage with or without stable supercooling. In the temperature range of 20 – 90 °C, SAT has a specific heat capacity of 2.9 kJ/(kg K) in liquid and supercooled state [22] and its density is 1280 kg/m³ in liquid phase [51], [52]. This results in a specific, volumetric heat capacity of 3.71 kJ/(l K) – a value close to that of water (4.18 kJ/(l K) [53]). The thermal conductivity of liquid SAT (0.4 W/(m K) [22]) is lower than for water (0.64 W/(m K) [54]). These material properties make SAT also suitable for sensible heat storage applications.

Operation states are defined by the specific energy content and temperature of SAT at atmospheric pressure. Fig. 1 shows the three different storage principles (a–c) which can be combined for the short-term and long-term storage of heat:

- (a) Its high heat-storage capacity at melting point is utilized (as latent heat storage) when no passivation of nucleation seeds is achieved during the charging of SAT composites.
- (b) Most of the heat of fusion can be transferred to a lower temperature level, reducing heat losses to the environment. When SAT composites supercool at ambient temperature, no heat loss due to heat transfer to the environment occurs until crystallization is initialized. Only changes within the material composition, such as phase separation, can reduce the potential of conserved heat.
- (c) When SAT composites remain in liquid state below their melting point, it is possible to utilize sensible heat storage without phase change.

Storage principles (a) and (c) are relevant for short heat-storage periods (hours, days), while the utilization of stable supercooling (b) is beneficial for long-term storage (weeks, months).

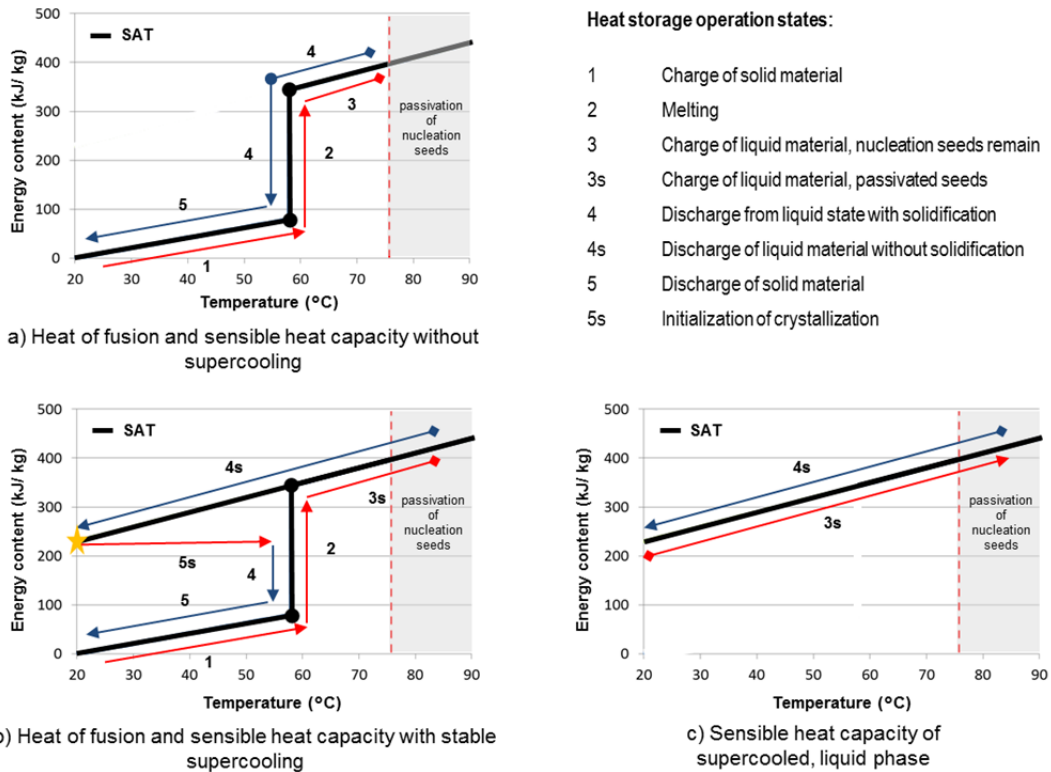


Fig. 1. Heat storage operation states with SAT composites.

1.5. Scope

This article introduces a heat storage system consisting of four heat storage units with PCM comprising a segmented PCM heat storage. The segmented heat storage was connected to a water buffer storage tank and solar collectors in a solar combisystem demonstrator. The combisystem was subject to energy draw-offs representing realistic domestic hot water (DHW) and space heating (SH) demands. An operation strategy for the PCM-solar combisystem was developed (based on numerical studies [36] and design criteria for solar combisystems) and applied to the system. We studied the thermal behaviour of the segmented PCM heat storage while charging with the solar collector and discharging to the water buffer storage. We investigated the ability of PCM units to supercool after being charged with solar heat as the heat source and to operate as long-term and short-term heat storage. We designed a mechanical activation device for the initialization of crystallization, which allowed the injection of seed crystals into the supercooled SAT in closed containers to initialize crystallization when desired.

Investigations on a solar heating system with four heat storage units, each with 200 kg of SAT, and using phase change and stable supercooling for long-term heat storage have not previously been reported in the literature.

Various heat storage operation states (Fig. 1) occurred in the PCM storage during the operation period from August to November 2015. Typical operation modes were analysed and evaluated in relation to the functionality of the heat storage prototype. Temperature developments in the heat transfer fluid (HTF) during the charging and discharging of PCM units in the context of the resulting heat transfer rates were the basic criteria for evaluation. Previous laboratory tests on PCM units [35] have showed that heat transfer rates during charging are rather high in comparison to those during discharging. The discharge behaviour of PCM units is clearly a limiting factor for their functionality and therefore of special interest.

2. Heat storage design

2.1. PCM unit

The flat units (length: 2.4 m; width: 1.2 m) with a height of 5 cm inside the enclosed PCM container (volume: 150 L) were constructed by the Danish company Nilan A/S [35]. A schematic diagram of a unit is shown in Fig. 2a. Parallel channel heat exchangers were attached on the top and the bottom of each flat PCM container. We used water as the HTF, and the volume of the heat exchangers was 32 L per unit. Thermocouples (TT-type) for the channel surface temperature measurements (T_{S1} , T_{S2} and T_{S3}) were installed centralized at a distance of 0.5 m from the front end of the heat exchangers. An air expansion chamber was connected to the expansion vessel to minimize any pressure change during material expansion (about 10% [37]) from solid to liquid state.

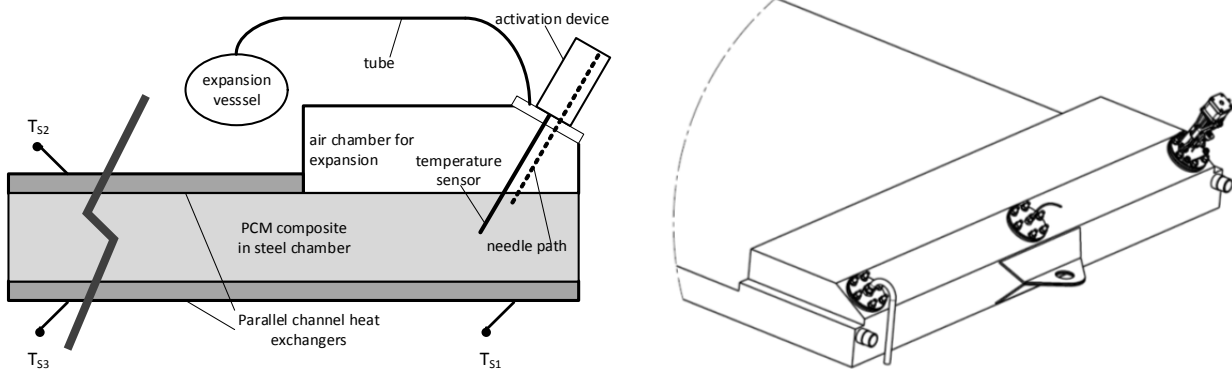


Fig. 2. a) Diagram of PCM unit design (cross-section); b) Perspective drawing of a PCM unit (view with air chamber for expansion).

The activation device was mounted on a flange of the air expansion chamber of each PCM unit (Fig. 2b). Using this device, solid SAT crystals were added to the supercooled SAT composite. A thermocouple inside a hollow metal cylinder (diameter: 3 mm) was mounted on the central flange of the air expansion chamber to allow temperature measurement in the middle of the PCM. The remaining flange was used to connect the air expansion chamber of the unit to a membrane expansion vessel (50 L). Fig. 2b also shows the inlet connections (tubes with a diameter of 3/4") of the two heat exchangers.

2.2. Segmented PCM heat storage

Four flat units were stacked to form the PCM heat storage. Two of the units (units 2 and 4) were made of stainless steel, while the other two were made of steel (units 1 and 3). A two-metre-high assembly (Fig. 3a) with sufficient space for maintenance between the units was built. To make it possible to investigate their performance separately, each PCM unit was insulated with 10 cm of foam and separately connected to the hydraulic circuit (Fig. 3b). Water was used as the HTF. Motor valves (V_1 , V_2 , V_3 , or V_4) were mounted at the inlet for each unit to control the flow through each heat exchanger. This allowed individual charging and discharging for each PCM unit, when both the upper and the lower heat exchanger transferred heat to and from the unit.

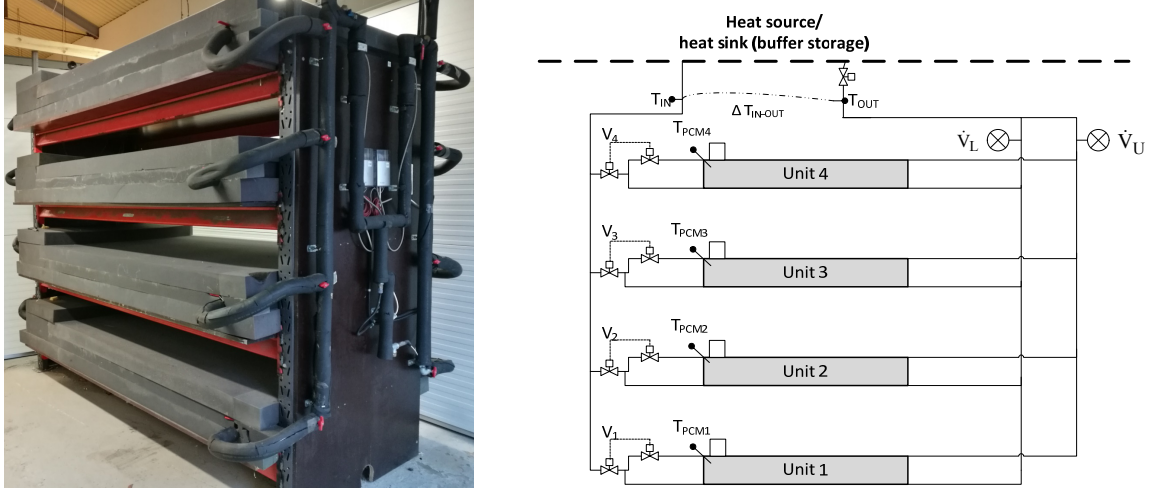


Fig. 3. a) Photograph of the segmented PCM storage; b) Diagram of the hydraulic integration of the PCM units.

The hydraulic layout (Fig. 3b) allowed separate measurement of the flow rates of the lower heat exchangers (\dot{V}_L) and the upper heat exchangers (\dot{V}_U), resulting in an accumulated flow rate (\dot{V}_2 in Fig. 5). Two motor-valves per unit prevented unwanted backflows and thermally driven circulation. Control of charging and discharging of the heat storage units was based on the temperatures (T_{PCM1} , T_{PCM2} , T_{PCM3} or T_{PCM4}) of the PCM layers. The HTF temperatures at the inlet (T_{IN}) to the units and at the outlet (T_{OUT}) from the units were measured with thermocouples. A thermopile was used to measure the temperature difference between T_{IN} and T_{OUT} .

Each PCM unit was filled with a different SAT composite (Table 1), with the aim of investigating their stability in the system demonstration. Previous investigations [39] have shown the highest heat contents (Δh) when 1%wt of CMC (as in units 1 and 2) and 1%wt (unit 3) or 2%wt (unit 4) of EDTA were added to SAT. Unit 3 needed 1%wt extra water to achieve a fully dissolved solution during melting. Moreover, highly conductive graphite powder and paraffin oil were added in unit 1 to study their impact on heat transfer.

The PCM container of unit 4 was damaged and refilled before the installation. During refill no exact weight measurement was carried out.

Table 1. PCM compositions in units.

| | Unit 1 | Unit 2 | Unit 3 | Unit 4 |
|-----------------|---|--------------|-----------------------------|---------------|
| PCM composition | SAT + 1% CMC + 2% graphite + 5 L oil | SAT + 1% CMC | SAT + 1% water + 1% EDTA | SAT + 2% EDTA |
| PCM mass | 202 kg | 220 kg | 202 kg | unknown |
| Δh [39] | 211 kJ/kg* | 211 kJ/kg | 216 kJ/kg** | 215 kJ/kg |
| ΔH unit | 40759 kJ | 46420 kJ | 42004 kJ | - |

*Value for SAT with 1% CMC, added graphite and oil was assumed to be additional non-reactive mass

**Value for SAT with 1% EDTA without extra water in the composition

2.3. Activation device

A mechanism for the initialization of PCM crystallization was realised as a prototype with components in acrylonitrile butadiene styrene (ABS) using a fused filament fabrication method with a 3D-printer. ABS has a relatively high temperature resistance compared to other 3D-printing materials. The activation device consisted of two main parts (Fig. 4a): the sealing unit and the triggering unit.

The sealing unit secured the tightness of the PCM container and allowed the solid SAT crystals to be inserted via a hollow needle into the supercooled SAT. The unit had two different types of sealing membrane. The lower membrane had a low resistance against puncture with a hollow needle and was coated on the bottom with Teflon, which was in direct contact with the expansion chamber. The upper membrane was made of natural rubber, which can resist puncture for longer periods.

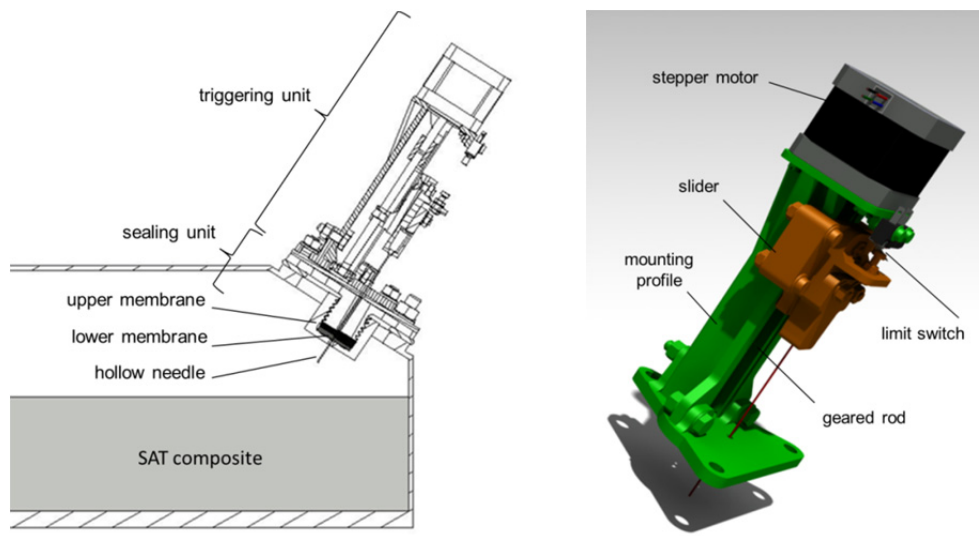


Fig. 4. a) Diagram of the triggering unit (in moving position) mounted on the sealing unit; b) Drawing of the assembled triggering unit.

The triggering unit (Fig. 4) was designed to be detached or mounted without affecting the PCM. The three main parts of the triggering unit were the mounting profile, a slider, and a stepper motor with a geared rod. The mounting profile provided the mounting holes for the stepper, the limit switch, and the fixture to the sealing unit. The slider moved on the sliding surface of the mounting profile. Upward and the downward forces were transferred by means of a nut, which was driven by the geared rod. A hollow needle and an adjusting screw for the limit switch were fixed at the top of the slider.

The hollow needle contained the SAT crystals, and its initial position was outside the PCM box. The membranes ensured that no crystal seeds fell into the PCM before crystallization was triggered. To activate the PCM unit, the needle was injected through the membranes. Control was realised by a microcontroller board (ATMega 2560), a stepper driver (A4988), and an RS323 interface. The following control logic was programmed in the microcontroller: The slider moved upwards, until the limit switch was hit. The slider then moved downward a predefined distance and pushed the hollow needle through the membranes and into the liquid SAT. After a predefined waiting time the slider moved upward again until the limit switch was hit again.

2.4. Heat storage configuration

To apply the concept of a segmented PCM heat storage with water buffer storage to a heat source with fluctuating power, we built a storage configuration for controlled heat transfer. Hydraulic pipework was realised from the heat source to both the PCM units and the water tank. The various hydraulic circuits were set by means of 2-way valves, so that heat could also be transferred from the PCM units to the water tank.

The components of the heat storage prototype configuration, including a solar collector circuit, are shown in Fig. 5. In principle, any heat source utilizing solar energy (such as a solar collector array or an electrical heater supplied by a photovoltaic system) can be integrated via a heat exchanger (HX). To overcome the problem of limited heat transfer to the PCM units [35] and to utilize solar energy for heat supply in periods of sunshine directly, domestic hot water (DHW) and space heating (SH) are supplied via the water tank. The water storage (735 L) was designed as tank-in-tank buffer storage with good thermal stratification behaviour for efficient short-term heat storage. The inner tank (175 L), situated in the centre of the tank) contained domestic water, which entered at the bottom during DHW tapping from the top of the tank. The outer tank volume contained water used as the HTF in a closed hydraulic system with a membrane expansion vessel for compensation for pressure changes. The static HTF pressure was maintained below 1 bar to secure the PCM units. DHW was heated up via the mantle surface of the inner tank from the warmer HTF in the outer tank volume. A space heating circuit (SH) was connected to the outer tank with an inlet at the bottom and draw-off in the middle of the tank. Pipes ($\frac{3}{4}$ " carbon steel), fittings and the plate heat exchanger (HX) were insulated with 19 mm of elastomeric foam.

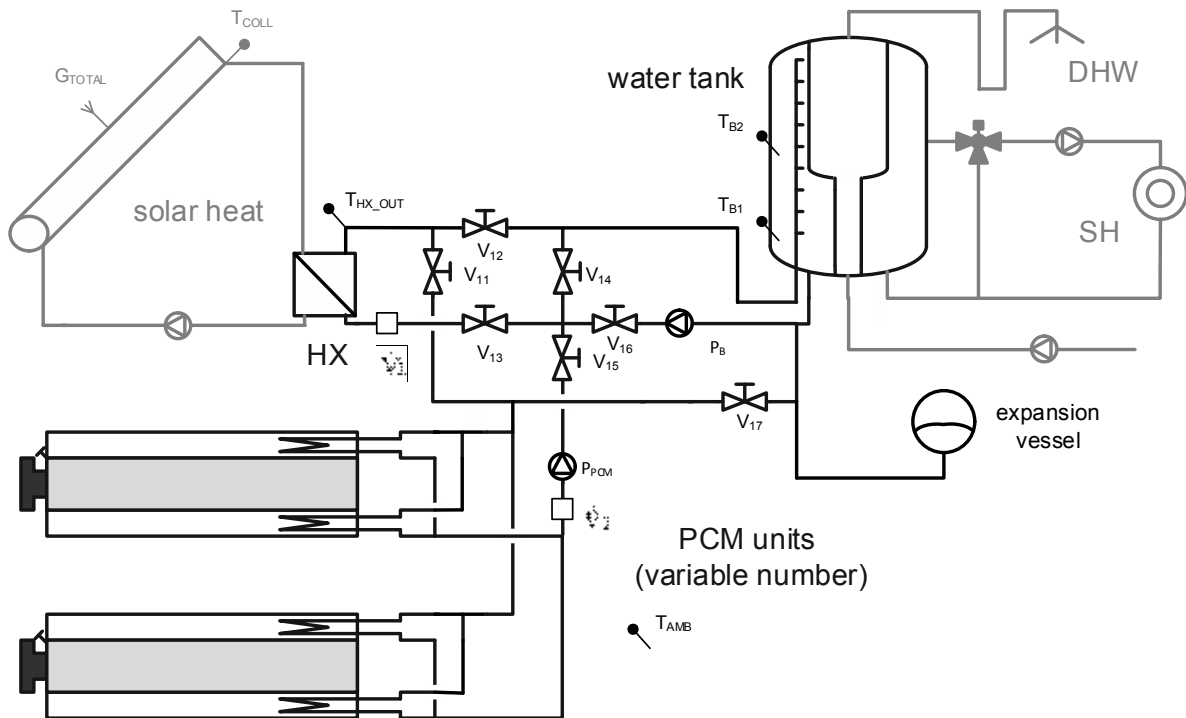


Fig. 5. Diagram of the configuration of the heat storage prototype (heat storage components in black, integrated heat source and heat sink components in grey).

To charge the buffer storage, water from the bottom of the outer tank was circulated, heated up via the HX, and entered the tank via a prototype polymeric inlet stratifier of the same kind as investigated by Dragsted et al. [55]. Three valves (V_{12} , V_{13} and V_{16}) were open during direct charging from a solar heat source and circulation was driven by the buffer storage pump (P_B).

To charge the PCM units, the pump P_{PCM} was used to circulate water via V_{15} , V_{13} , the HX and V_{11} to the segmented PCM heat storage. Heat transfer from the PCM heat storage to the water tank was realized via V_{15} , V_{14} and V_{17} when P_{PCM} was switched on. This configuration (Fig. 5) enables the integration of any number of PCM units. Four PCM units were installed for the heat storage prototype presented here.

3. Experimental investigations and calculations

3.1. Charging with solar heat

A solar collector array (Fig. 6a), consisting of evacuated tubular collectors (type Kingspan Thermomax HP-450, total aperture area of 22.4 m^2), was connected to the HX. It was set up with an inclination angle of 45° and an azimuth angle of 12° towards the east at the solar heating test facility of the Technical University of Denmark (northern latitude of 55.8°). The collectors had an optical efficiency of 0.75, and their heat loss coefficients were $1.18 \text{ W}/(\text{m}^2\text{K})$ and $0.01 \text{ W}/(\text{m}^2\text{K}^2)$. The solar irradiance on the tilted collector plane (G_{TOTAL}) was measured with a pyranometer, as indicated in Fig. 5.

Operation was realised with a LabView program controlling valves and pumps (as described in section 2.4) with a five-minute reaction time for changes. The sequence of tests was based on sensor readings (Fig. 5): The collector circuit pump was started when the outlet temperature (T_{COLL}) of the collector was 10 K higher than the temperature at the bottom of the water storage (T_{B1}). The water tank (Fig. 6b) was charged until a temperature of 60°C was reached in the middle of the water tank (T_{B2}). Charging of the buffer storage stopped when either the lower or the upper threshold value was met. When the upper threshold for the buffer storage was reached, the collector circuit flow stopped until a collector outlet temperature of 70°C and sufficient solar irradiance ($G_{TOTAL} > 150 \text{ W}/\text{m}^2$) was measured, and then the PCM heat storage was charged.



Fig. 6. a) Solar collector array; b) Water tank and graphical LabView interface for live data reading.

The volume flow rate of the HTF in the collector circuit (type: TYFOCOR LS; consisting of propylene-glycol, water and inhibitors) was 5.5 L/min during charging of the buffer storage and 21 L/min during charging of the PCM storage units. On the secondary side of the heat exchanger, connecting the solar collector circuit with the heat stores, a HTF volume flow rate of 16.5 L/min was used in the PCM charging circuit to ensure good heat transfer at the heat exchangers of the PCM units. A flow rate of 5.5 L/min was chosen for charging the water buffer storage to allow build-up of thermal stratification.

Individual PCM unit charging was completed when the temperatures inside the PCM (T_{PCM_i}) reached 80 °C. Because of the fluctuating thermal power from the large solar collector array and the limited heat exchange capacity of PCM units, it was necessary to vary the number of PCM units being charged at the same time to prevent overheating of the HTF. The number of active PCM units was controlled by actuating the motor valves V_1 – V_4 (Fig. 3b) based on the outlet temperature of the heat exchanger T_{HX_OUT} . When this reached 95 °C, the next warmest unit (based on T_{PCM_1} – T_{PCM_4} readings) was opened to the circuit, and both units were charged in parallel. When T_{HX_OUT} dropped below 85 °C, the valve to the circuit for the coldest unit being charged was closed. PCM storage charging for the last unit stopped when $T_{COLL} < 85$ °C and $G_{TOTAL} < 150$ W/m² or when T_{B2} fell below 50 °C so that buffer storage charging was activated.

3.2. Discharging of liquid PCM without solidification

Supercooling of PCM units was tested in parallel by passive cooling to the ambient and individually by active discharging via the water tank. During passive cooling, the heat loss rates (\dot{Q}_{LOSS}) were calculated based on the PCM temperature measured (T_{PCM_i}). The changes in the heat content of the steel container (m_{ST}), of the water in the heat exchangers (m_W), and of the material composite (m_{PCM}) were calculated separately by their temperature-dependent specific heat capacities (c_p). The specific heat capacity of a PCM is highly dependent on the water content of the composite. Calculations were therefore carried out as Araki et al. [9] proposed:

$$\dot{Q}_{loss}(t) = (m_{ST} \cdot c_{pST} + m_W \cdot c_{pW} + m_{PCM} \cdot c_{pPCM}) \cdot \left(\frac{dT_{PCM_i}}{dt} \right) \quad (1)$$

Heat loss coefficients for the PCM units were calculated by dividing the heat loss rate for a specific time step by the temperature difference between the PCM temperature and the ambient temperature (T_{AMB}). T_{AMB} was measured 2 m from the PCM heat storage at the height of unit 2 (as indicated in Fig. 5). Mean values of the heat loss coefficients were calculated from data of two independent cooling periods (5 days each) in August and October 2015. Starting from a temperature of approximately 80 °C, the PCM was cooled down to a temperature of around 30 °C and remained in the liquid phase.

Active discharging of PCM was applied after a rest period (no heat transfer via the hydraulic circuit) of at least two hours after full charge was accomplished. Constant temperatures around 25 °C at the inlet (T_{IN}) to the segmented PCM volume were realised by cooling the water tank via the SH circuit connections. In this way, equal discharge conditions were realised. Volume flow rates of 5 L/min and 10 L/min were applied by manual control of P_{PCM} until the PCM layer temperatures fell below 60 °C.

3.3. Initialization of crystallization and discharge from liquid state with solidification

After full charge ($T_{PCM_i} > 80 \text{ }^\circ\text{C}$) was achieved, the PCM units rested for six days before solidification took place. The PCM supercooled down to ambient temperature ($25 \text{ }^\circ\text{C}$). The crystallization and release of the latent heat of fusion from the supercooled SAT was initialized (activated) when seed crystals were added to the solution. PCM activation was first tested by manual injection of a hollow needle containing SAT crystals via the mounted sealing unit into the PCM chamber (Fig. 4a). Later, mounted triggering units (Fig. 4b) were applied with the previously described activation sequence. Each triggering device was tested individually.

In the first test sequence, heat was discharged to the initially cold buffer storage tank. HTF circulation was started before PCM crystallisation was activated. The HTF volume flow rate was set to 2.13 L/min by manual control of P_B . During crystallization, the PCM temperature increased to approximately $58 \text{ }^\circ\text{C}$ and the discharge was stopped when the PCM temperature fell back to $50 \text{ }^\circ\text{C}$.

In a later test with a volume flow rate of 5 L/min , the discharge was interrupted by automated buffer storage charging from the solar collector array. The water tank was cooled via SH connections during the test.

3.4. Data processing

Thermocouples and thermopiles were connected to a National Instruments 16-channel thermocouple CompactDAQ module (NI9214). Flow meter signals were read via a 32-channel digital input/output CompactDAQ module (NI9403). Data was logged at 10-second intervals. Heat transfer analysis was based on averaged values for 1-minute and 1-hour data. Uncertainties in evaluated measurements resulted mainly from the sensors installed (Table 2).

Table 2. Installed measurement devices.

| Device | Type | Uncertainty |
|---|--|--|
| Thermocouple (T_{Bi} , T_{COLL} , T_{HX_OUT} , T_{PCM_i} , T_{Si}) | TT-type (copper/ constantan) | 0.5 K [56] |
| Thermopile (ΔT_{IN-OUT}) | 5-junction thermopile with TT-type thermocouples | 0.1 K [56] |
| Flow meters (\dot{V}_1 , \dot{V}_L , \dot{V}_U) | Brunata HGQ-1-R3 (class 2) | 2% of reading (according to EN 1434)* |
| Pyranometer (G_{TOTAL}) | Kipp & Zonen CM3 | 15 W/m^2 (below 200 W/m^2) [manufacturer information] |

*The accuracy range was experimentally proved for the applied flow rate range before installation.

Heat transfer rates in the PCM circuit were calculated in the following way (negative temperature difference during discharge):

$$\dot{Q} = \dot{V}_i \cdot c_p \cdot \rho \cdot \Delta T_{IN-OUT} \quad (2)$$

where \dot{V}_i is the measured volume flow rate of the HTF, c_p is the specific heat capacity of the HTF at mean temperature between T_{IN} and T_{OUT} , and ρ is the density of the heat transfer fluid at T_{OUT} , where the volume flow rates were measured.

4. Experimental results and discussion

4.1. Charging with solar heat

During controlled heat storage operation, PCM charging took place after buffer storage charging. This sequence was beneficial because the collector circuit was pre-heated for the charging of PCM units, which require higher HTF flow temperatures. Fig. 7 shows heat transfer rates (hourly averaged values) to the PCM units (red curves) for a representative period. On two sunny days (2nd and 3rd of October), all modules were charged by solar heat (units 1, 2 and 3 already being in supercooled state, and unit 4 from a partially melted state). The development of PCM temperatures in Fig. 7 shows that PCM charging was successfully applied with up to four units (3rd of October) in parallel.

After full charging (a minimum temperature of 80 °C was achieved in all units) the units were passively cooled down. Three units went into supercooled state, while unit 4 solidified in the morning of the 5th of October after supercooling 5 K. The control system detected this PCM unit as the warmest and it was therefore charged again when solar heat was available during the afternoon of the same day.

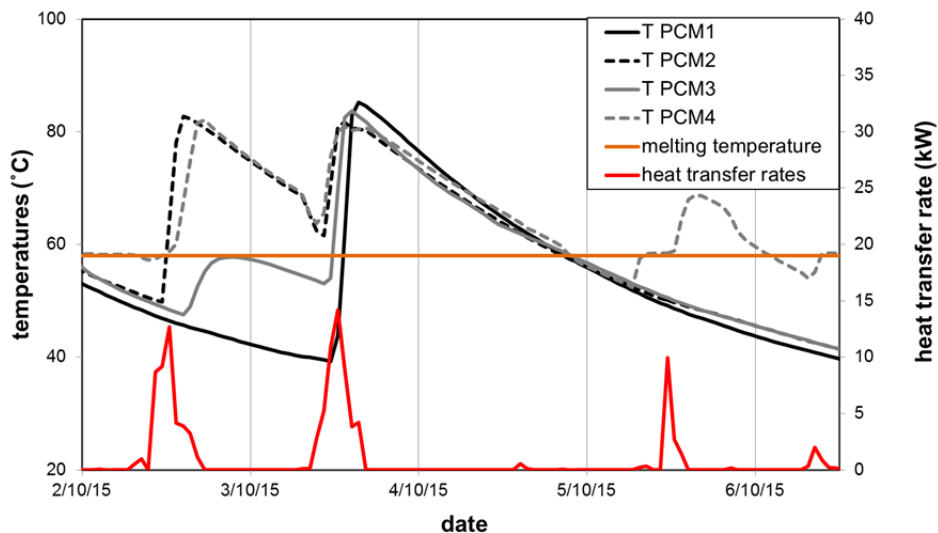


Fig. 7. PCM temperature developments in October 2015.

This test proved that parallel PCM unit charging is necessary on sunny days. With rising PCM temperatures, the heat transfer rates of the units fell. With parallel PCM unit charging, all the heat from the collectors could be transferred to the PCM units and boiling of the HTF was avoided.

PCM unit 4 never achieved stable supercooling during the test period. The SAT composite in this unit was similar to that in unit 3, which successfully supercooled. Even though unit 4 was frequently heated up to a PCM temperature of above 80 °C, no stable supercooling was achieved. We think the supercooling failed because the PCM container was damaged. The failure meant we could not analyse the performance of the composite containing 2%wt EDTA. Our evaluations therefore focused on PCM units 1, 2 and 3.

During the test period, most single PCM unit charging was from an initially solid state. For example, PCM unit no. 1 was charged from ambient temperature (21 °C) in solid state during the afternoon of the 8th of September 2015. Fig. 8

shows the changes in the HTF inlet temperature (T_{IN} , grey curve) and the HTF outlet temperature (T_{OUT} , black curve). As a consequence of the limited heat exchange capacity rate of the unit, the temperature of the charging circuit increased continuously for the first 150 minutes. Then the solar irradiance declined and T_{IN} therefore decreased slightly. Charging of one PCM unit on a sunny afternoon with decreasing solar irradiance matches well with falling heat transfer rates (black dotted curve) during single unit charging when the PCM temperature (orange curve) was increasing.

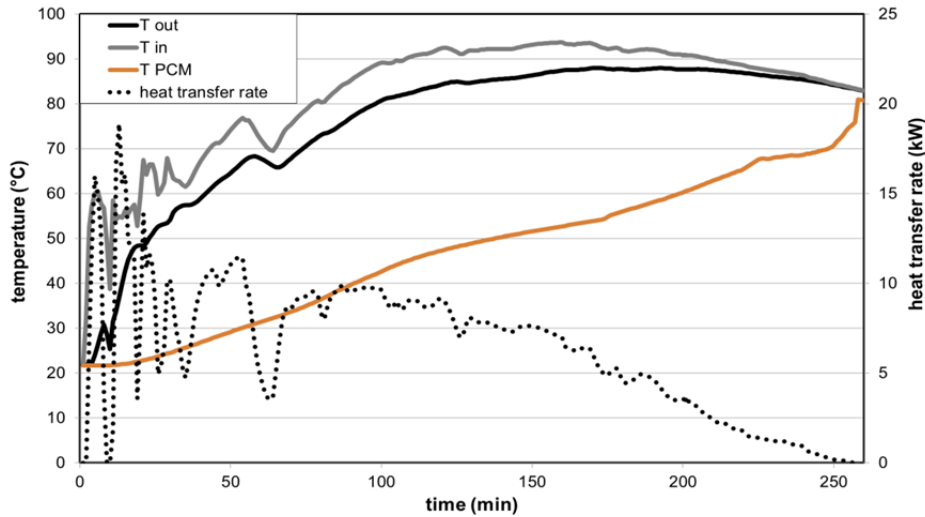


Fig. 8. Temperature and heat transfer rate developments during charging of unit1 from solid state.

Heat was transferred for 250 minutes. Charging (indicated by the heat transfer rate) stopped when T_{PCM} reached 80 °C. During this charging run, 27.4 kWh heat was transferred. The solar irradiance fluctuated due to clouds. The heat transfer rate varied correspondingly. Heat transfer rates of up to 16 kW occurred at the beginning of the test. Later they decreased constantly as G_{TOTAL} decreased.

A sharp increase in the T_{PCM} can be seen after 240 minutes of charge. This indicates that the PCM was fully melted and convection of the liquid phase was taking place at the temperature sensor. Because T_{PCM} is measured in a single location, its reading does not represent the mean material bulk temperature during dynamic charging or discharging.

4.2. Passive discharge of PCM units

Significant heat losses occurred during parallel PCM unit cooling after full charge. Ambient air temperature differences between day and night of up to 7 K were measured. The calculation of heat loss coefficients (Table 3) using data from two independent cooling periods was therefore of benefit.

Table 3. Calculated heat loss coefficients.

| | Unit 1 | Unit 2 | Unit 3 |
|----------------------------------|--------|--------|--------|
| Mean heat loss coefficient (W/K) | 4.5 | 4.3 | 3.9 |

Unit 1 showed the highest heat loss rate, followed by unit 2 and unit 3. This ranking is probably a result of the unit height distribution in the stacked assembly, where unit 1 was lowest (Fig. 3). We did not observe any significant

influence of the different PCM properties on PCM unit heat losses.

The units were installed in such a way that they could be tested individually. The large surface-to-volume ratio of an individual PCM unit resulted in unfavourably high heat loss coefficients.

4.3. Discharge of sensible heat from liquid PCM by heat transfer to the buffer storage

Fig. 9a shows that sensible heat was discharged for 120 minutes from fully charged PCM unit 3. At the beginning, the unit's heat exchangers were still hot (~75 °C), which was indicated by the high initial outlet temperature (black curve). The resulting heat transfer rate (black dotted curve) therefore started at the peak value (15 kW). The heat transfer rate fell steadily, following the development of the decreasing HTF outlet temperature (due to falling T_{PCM}).

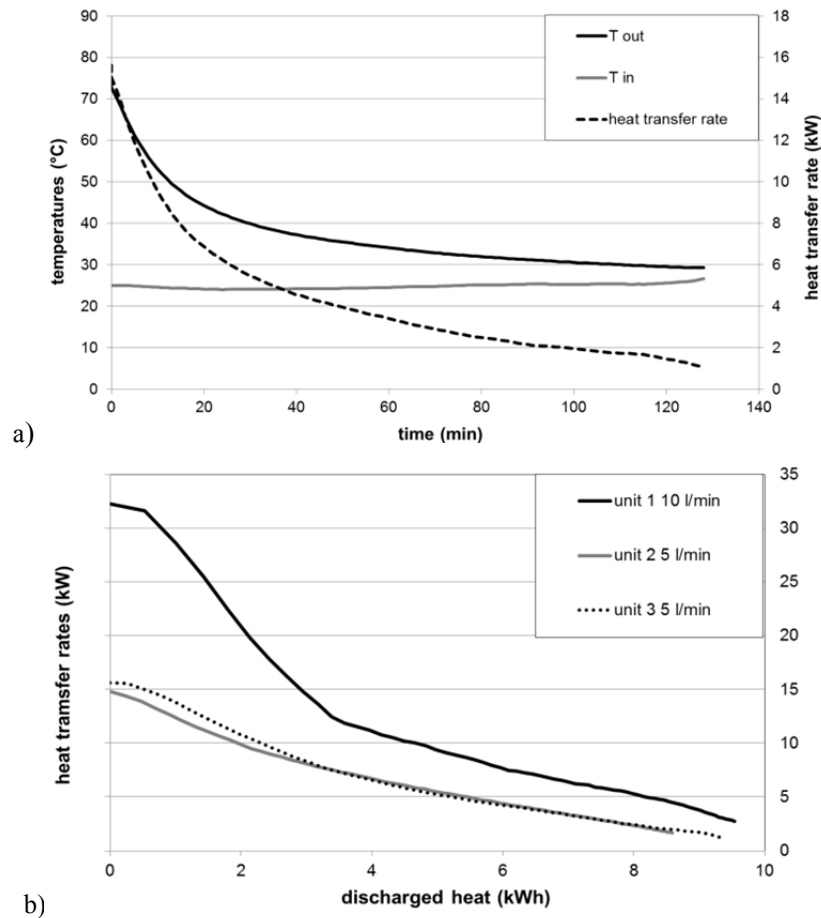


Fig. 9. a) Discharging of unit 3 with a HTF flow rate of 5 L/min; b) Comparison of heat transfer rates (active cooling).

As shown in Fig. 9b, heat transfer rates depended highly on the flow rate and the inlet temperature of the HTF. With the chosen end-criterion ($T_{PCM} = 60$ °C) between 8.5 and 9.5 kWh of heat were discharged from PCM units. For unit 1 (black curve), a flow rate of 10 L/min was applied. Thermal power started at 32 kW, when the hot HTF was pushed out of the unit's channel heat exchangers. The discharge lasted for only 70 minutes. Cooling of unit 2 (grey curve) and unit 3 (black dotted curve) with a HTF flow rate of 5 L/min showed almost similar behaviour, but lasted for more than 130 minutes. This comparison shows that the flow regime in the heat exchangers at flow rates between 5 and 10 L/min are similar and that heat transfer from the liquid PCM to the HTF was not a limiting factor.

4.4. Initialization of crystallization

Fig. 10 shows the development of T_{PCM} (orange curve) and the temperatures on the surface of the unit heat exchangers (sensor distribution scheme in Fig. 2a) after crystallization of the supercooled PCM unit 1 was initialized. A constant HTF flow rate of 2.13 L/min was applied. At initial state ($t=0$ min), T_{PCM} was at 30 °C and the surface temperatures of the heat exchangers were lower due to HTF flow.

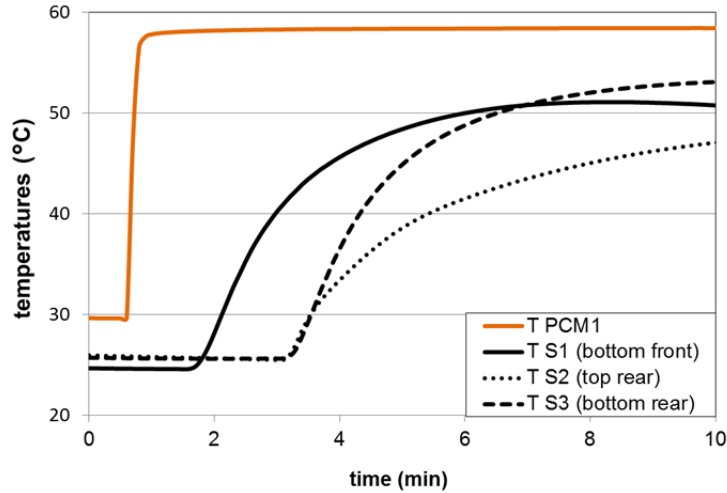


Fig. 10. Temperature developments during activation of PCM unit 1.

After a time delay of 50 seconds, T_{PCM} started to rise sharply to 57.6 °C and reached its maximum value of 58.4 °C after 10 more minutes. It took more than 110 seconds before the front (HTF flow direction) of the lower heat exchanger surface (indicated by T_{S1}) started to heat up. T_{S1} reached its maximum temperature after 7 minutes and then declined slightly. T_{S2} and T_{S3} , which were located about 1.6 m from the activation device, started to rise at $t=3.5$ min. T_{S3} on the lower heat exchanger rose as fast as T_{S1} , while T_{S2} at the rear section of the upper heat exchanger increased more slowly.

Similar surface temperature developments were observed for all PCM units. Time delays in temperature rise indicate that the crystallization expanded at a speed of about 0.7 cm per second, which is comparable to results for crystal growth rates in an SA-to-water (55%wt) mixture from supercooled state [24]. Furthermore, surface temperature developments indicate that the heat transfer from PCM to the lower heat exchanger was better than to the upper heat exchanger. Material contraction and cavities formed on the upper side of the PCM layer could explain this, although unit 1 contained oil to fill cavities and improve the heat transfer during solidification. Solid SAT has a low thermal conductivity, which influences the unit's heat transfer capacity significantly. This should therefore be considered when an improved PCM unit is designed.

The test of the automated needle injection showed that the torque of the stepper motor was sufficient to drive the needle through the membranes into the supercooled SAT mixture and to initialize solidification, but it was too weak to push the hollow needle into a solid PCM bulk. This was indicated by the number of steps detected during the upward movement of the slider. Moreover, the hollow needle got bent and had to be replaced.

The triggering unit was designed and optimized for the 3D-printing process. During PCM charging, the whole assembly was exposed to high temperatures. After repeated heating and cooling of PCM units, the mounting profiles were deformed and showed cracks.

4.5. Discharge during solidification by heat transfer from PCM units to the buffer storage

When the water tank was not cooled during discharge of PCM units (as for tapping of DHW or SH supply), HTF inlet temperatures at the PCM units increased. Fig. 11a shows this behaviour during continuous discharge of unit 2. After one hour, the inlet temperature (black curve) increased and after three hours the outlet temperature (grey curve) stagnated at a constantly low level. The heat transfer was therefore dramatically reduced. After 250 minutes, the temperature difference between inlet and outlet and the heat transfer rate were very small. The peak of thermal power (4.1 kW) was reached after 30 minutes, when the HTF in the unit's heat exchangers reached its maximum temperature. For the first 150 minutes, the T_{PCM} remained at melting temperature, but then it cooled down. Discharge stopped at the chosen end-criterion ($T_{PCM}=50\text{ }^{\circ}\text{C}$).

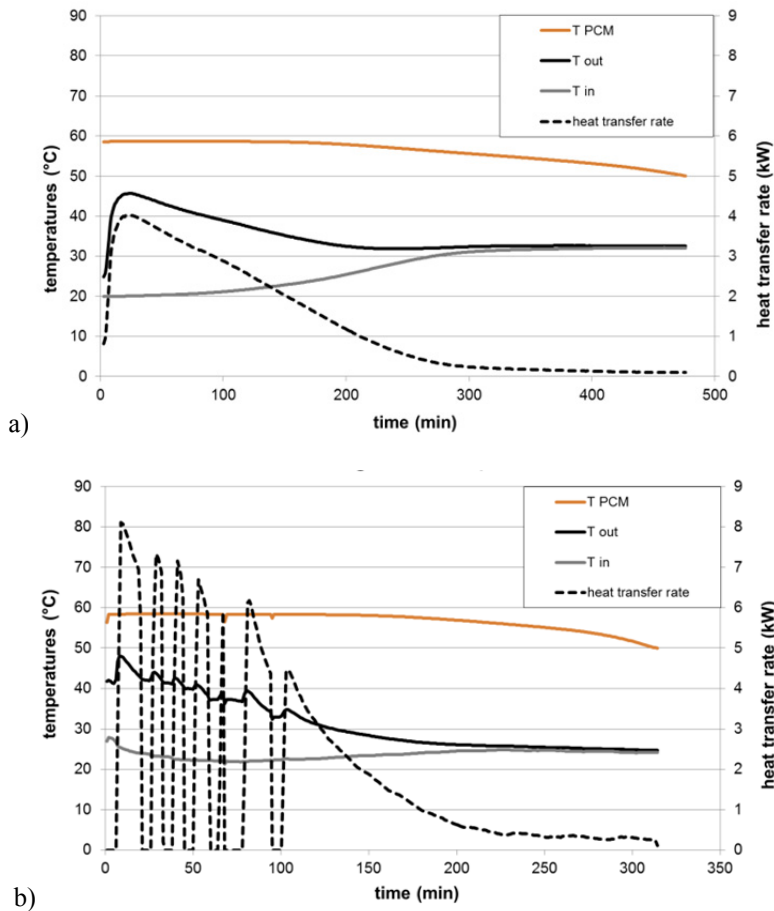


Fig. 11. Discharge after initializing solidification or supercooled PCM: a) Unit 2 with a continuous flow rate of 2.13 L/min; b) Interrupted discharge of unit 1 with a flow rate of 5 L/min.

In contrast, Fig. 11b shows values from the discharge of PCM unit 1 on a cloudy day. During periods of bright sunshine on the collector array, buffer storage charging was frequently activated by the control. The PCM unit discharge was therefore interrupted several times. In these periods, heat was transferred to the HTF in the unit's heat exchangers without flow applied. T_{OUT} and the heat transfer rate therefore decreased more slowly during interrupted discharge. After 100 minutes, there was continuous discharge. Unit discharge stopped 5 hours after solidification was initiated. The higher flow rate applied meant that it took less time than the continuous discharge of unit 2.

Fig. 12a shows heat transfer rate developments for discharged heat during PCM unit discharge runs. A direct comparison of PCM unit performance was possible because all the PCM box geometries were similar. Continuous discharge runs with HTF flow rates of 2.13 L/min showed that higher heat transfer rates were achieved for units with greater heat of fusion (indicated by discharged heat).

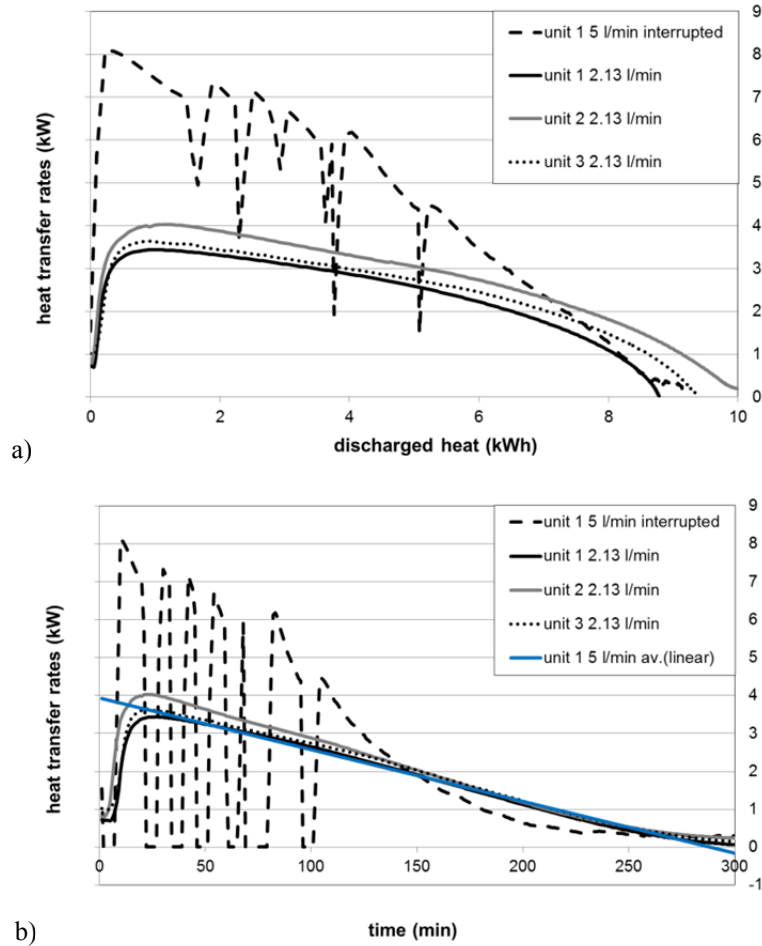


Fig. 12. Comparison of heat transfer rates during discharge with solidification from supercooled state: a) over discharged heat; b) over time.

Unit 2, which had the highest mass of PCM (220 kg) with a high fraction of SAT in the composition, released about 10.3 kWh of heat with a peak power over 4 kW. Unit 1, with a PCM mass of 202 kg and a lower SAT fraction, had the lowest heat release (8.8 kWh) and peak power (3.4 kW). Unit 3, with the same PCM mass as unit 2, released 9.4 kWh with slightly lower thermal power than unit 2.

In general, thermal power continuously declined during discharge after solidification of the PCM, but only dropped below 1 kW when more than 90% of heat had been discharged. Based on calculated ΔH (Table 1), 78% of heat of fusion in unit 1, 80% in unit 2 and 80.5% in unit 3 was utilized before the T_{PCM} dropped to 50 °C. This means that about 20% of the long-term heat storage potential of the PCM units was left.

The interrupted HTF flow in unit 1, combined with a higher volume flow rate led to substantially higher heat transfer rates when there was flow. HTF outlet temperatures were comparable to uninterrupted discharge runs. Based on the total discharge duration including periods without flow (Fig. 12b), the average heat transfer rate with interrupted

flow almost matched the rates achieved during the continuous discharge of the same unit (HTF flow rate of 2.13 L/min). The interrupted flow prevented the rapid lowering of the HTF outlet temperature (Fig. 11b). During solidification, no convection took place in the PCM box. No significant influence on the heat transfer was observed at various different flow rates. This indicates low HTF flow rates in the unit's parallel heat exchangers during all runs. So we can identify conductivity as the critical parameter in the heat transfer process from PCM to HTF, which is why pulsed HTF flow was beneficial.

4.6. Proof of concept

Fig. 13 shows how operation modes were combined for later system demonstration to realise a sequence with combined short-term and long-term heat storage with the PCM heat storage.

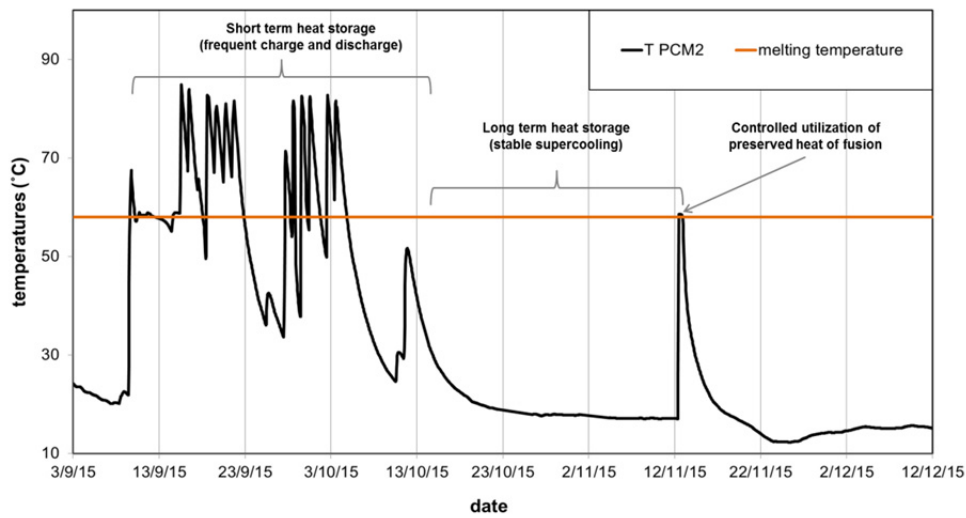


Fig. 13. Operation sequence with PCM unit charging and discharging (data from autumn 2015).

The history of PCM temperature measurements indicated the state of unit charging. In September, starting from initial solid material state, unit 2 melted. On the 9th of September, charging stopped when T_{PCM2} reached 68 °C. As a consequence, crystallization of the SAT composite started at its melting temperature when the unit cooled down. On the 15th of September, full unit charging was achieved: T_{PCM2} exceeded 80 °C. Until the 12th of October, sunny weather resulted in repeated charging. In periods without heat supply from the solar collector array, the unit was partly discharged to heat up the water tank and due to sensible heat losses to the ambient. After the 12th of October, solar irradiation was insufficient to charge PCM unit 2, so it cooled to ambient temperature and remained in a stable supercooled state. The SAT composite's heat of fusion was conserved and no more heat losses occurred. The SAT composite remained in liquid state until crystallization was initiated on the 11th of November (after 57 days) for heat transfer to the water tank. In this way, solar heat from early October was utilized for domestic heat supply in mid-November.

This demonstrates proof of concept for charging by solar thermal collectors and discharge for domestic heat supply via a water tank. The segmented heat storage can also be used for year-round system demonstration by applying a draw-off scenario for DHW and SH supply. This requires a control strategy for the initialization of PCM crystallization depending on the state of water tank charging.

5. Conclusions

The heat storage concept of utilizing stable supercooling of SAT for combined long- and short-term heat storage was proved in system scale. Four PCM units, each containing 200–220 kg of sodium acetate trihydrate composites, and a 735 L water tank formed a segmented heat storage prototype. Hydraulic circuits and controls enabled interaction with a solar heat source and domestic hot water and space heating supply. Tests with the prototype built showed:

- For charging with solar heat, an automated sequence for the combined operation of the water tank and a variable number of PCM units enabled control of heat transfer fluid temperatures in the operation range. PCM melting with heat transfer fluid temperatures above 90 °C was possible. Fluctuating heat transfer rates from a 22.4 m² evacuated tubular collector array peaked at 16 kW. Fast charging (250 minutes) of an individual PCM unit was possible.
- Discharge of sensible heat from liquid and supercooled sodium acetate trihydrate composite was achieved in 3 PCM units without causing solidification. Thermal power during the discharge of a single unit reached 32 kW when discharged from fully heated at 80 °C. Furthermore, rapid unit charging in supercooled state did not cause spontaneous crystallisation. This allowed utilization of the melted PCM as short-term sensible heat storage without compromising its long-term storage potential. Better thermal insulation and a more compact arrangement of PCM units are needed to reduce sensible heat losses.
- Initialization of crystallization with mechanical seed crystal injection worked in initial tests. However, the materials used for the activation device prototype could not withstand repeated cycles of charging and discharging. The triggering unit components must be manufactured in a more temperature-resistant material.
- During continuous discharge after solidification of the supercooled sodium acetate trihydrate composites (at heat transfer fluid flow rates of 2.13 L/min), heat transfer rates reached 4 kW. The thermal power during discharge with a start and stop strategy was up to 8 kW. This kind of “pulsed-flow” was also able to yield higher supply temperatures for domestic hot water supply and space heating via the water tank.

The functionality for typical operation modes was given. Thermal power and the flow temperatures from discharging the PCM units without and during solidification were sufficiently high to cover space heating demands in domestic buildings. However, with the present storage configuration, hot water supply must be realised with a backup heater to ensure supply temperatures above 45 °C. The heat transfer during discharge of PCM units during solidification will need to be improved to avoid this requirement.

This research proved that it is possible to store solar heat in a water tank with the combined application of short- and long-term heat storage utilizing stable supercooling of sodium acetate trihydrate. About 80% of the conserved heat of fusion was utilized during discharge from stable supercooled PCM units.

6. Acknowledgements

This research was funded by the European Commission (Grant Agreement N_ 295568) as part of the Seventh Framework Programme of the European Community for Research, Technological Development and Demonstration Activities under the funding scheme of “Collaborative Project” through the COMTES consortium. The work was also supported by the PhD program of the Sino-Danish Center for Education and Research (SDC). We thank our partners

from Nilan A/S for sharing their knowledge and the DTU research technicians Troels V. Kristensen and Claus Aagaard for their practical assistance.

7. References

- [1] L.F. Cabeza, L. Miró, E. Oró, A. de Gracia, V. Martin, A. Kroenauer, C. Rathgeber, M.M. Farid, H.O. Paksoy, M. Martínez, and A.I. Fernández, “CO₂ mitigation accounting for Thermal Energy Storage (TES) case studies,” *Appl. Energy*, vol. 155, pp. 365–377, 2015.
- [2] Weiss W. (Editor), *Solar Heating Systems for Houses, a Design Handbook for Solar Combisystems*. James & James Ltd., UK, 2003.
- [3] S. Colclough and T. McGrath, “Net energy analysis of a solar combi system with Seasonal Thermal Energy Store,” *Appl. Energy*, vol. 147, pp. 611–616, 2015.
- [4] E. Andersen and S. Furbo, “Solar Combi Systems,” Technical University of Denmark, Department of Civil Engineering report no. R-156, 2007.
- [5] A. Thür and S. Furbo, “Compact solar Combisystem – High Efficiency by Minimizing Temperatures,” Technical University of Denmark, Department of Civil Engineering report no. R-160, 2007.
- [6] S. Furbo and S. Svendsen, “Report on heat storage in a solar heating system using salt hydrates,” Technical University of Denmark, Thermal Insulation Laboratory, report no. 70, 1977.
- [7] M. Telkes, “Thermal energy storage in salt hydrates,” *Sol. Energy Mater.*, vol. 2, no. 4, pp. 381–393, 1980.
- [8] A. Ristić, S. Furbo, C. Moser, H. Schranzhofer, A. Lazaro, M. Delgado, C. Peñalosa, L. Zalewski, G. Diarce, C. Alkan, S.N. Gunasekara, T. Haussmann, S. Gschwander, C. Rathgeber, H. Schmit, C. Barreneche, L. Cabeza, G. Ferrer, Y. Konuklu, H. Paksoy, H. Rammelberg, G. Munz, T. Herzog, J. Jänchen, and E.P. del Barrio, “IEA SHC Task 42 / ECES Annex 29 WG A1: Engineering and Processing of PCMs, TCMs and Sorption Materials,” *Energy Procedia*, vol. 91, no. June, pp. 207–217, 2016.
- [9] B. Mette, H. Kerskes, H. Drück, and H. Müller-Steinhagen, “New highly efficient regeneration process for thermochemical energy storage,” *Appl. Energy*, vol. 109, pp. 352–359, 2013.
- [10] B. Zettl, G. Englmaier, and G. Steinmaurer, “Development of a revolving drum reactor for open-sorption heat storage processes,” *Appl. Therm. Eng.*, vol. 70, no. 1, pp. 42–49, 2014.
- [11] B. Zettl, G. Englmaier, and W. Somitsch, “An Open Sorption Heat Storage Concept and Materials for Building Heat Supply,” *Energy Procedia*, vol. 73, pp. 297–304, 2015.
- [12] R. Weber and V. Dorer, “Long-term heat storage with NaOH,” *Vacuum*, vol. 82, no. 7, pp. 708–716, 2008.
- [13] B. Fumey, R. Weber, and L. Baldini, “Liquid sorption heat storage – A proof of concept based on lab measurements with a novel spiral fined heat and mass exchanger design,” *Appl. Energy*, vol. 200, pp. 215–225, 2017.
- [14] X. Daguene-Frick, P. Gantenbein, J. Müller, B. Fumey, and R. Weber, “Seasonal thermochemical energy storage: Comparison of the experimental results with the modelling of the falling film tube bundle heat and mass exchanger unit,” *Renew. Energy*, vol. 110, pp. 162–173, 2016.
- [15] H. Zondag, B. Kikkert, S. Smeding, R. De Boer, and M. Bakker, “Prototype thermochemical heat storage with open reactor system,” *Appl. Energy*, vol. 109, pp. 360–365, 2013.
- [16] P.A.J. Donkers, L.C. Sögütöglü, H.P. Huinink, H.R. Fischer, and O.C.G. Adan, “A review of salt hydrates for seasonal heat storage in domestic applications,” *Appl. Energy*, vol. 199, pp. 45–68, 2017.
- [17] J. Pereira da Cunha and P. Eames, “Thermal energy storage for low and medium temperature applications using phase change materials – A review,” *Appl. Energy*, vol. 177, pp. 227–238, 2016.
- [18] J.A. Quinnell and J.H. Davidson, “Heat and mass transfer during heating of a hybrid absorption/sensible storage tank,” *Sol. Energy*, vol. 104, pp. 19–28, 2014.

- [19] J.M. Schultz and S. Furbo, "Investigation of heat of fusion storage for solar low energy buildings," *Proc. Sol. World Congr. 2005 Bringing Water To World*, vol. 3, pp. 1833–1838, 2005.
- [20] S. Puupponen, V. Mikkola, T. Ala-Nissila, and A. Seppälä, "Novel microstructured polyol–polystyrene composites for seasonal heat storage," *Appl. Energy*, vol. 172, no. April, pp. 96–106, 2016.
- [21] B. Zalba, J.M. Marín, L.F. Cabeza, and H. Mehling, "Review on thermal energy storage with phase change: materials, heat transfer analysis and applications," *Appl. Therm. Eng.*, vol. 23, no. 3, pp. 251–283, 2003.
- [22] N. Araki, M. Futamura, A. Makino, and H. Shibata, "Measurements of Thermophysical Properties of Sodium Acetate Hydrate," *International J. Thermophys.*, vol. 16, no. 6, pp. 1455–1466, 1995.
- [23] B. Sandnes and J. Rekstad, "Supercooling salt hydrates: Stored enthalpy as a function of temperature," *Sol. Energy*, vol. 80, no. 5, pp. 616–625, May 2006.
- [24] T. Ohachi, M. Hamanaka, H. Konda, and S. Hayashi, I. Taniguchi, T. Hashimoto, and Y. Kotani "Electrical nucleation and growth of $\text{NaCH}_3\text{COO} \cdot 3\text{H}_2\text{O}$," *J. Crystal Growth*, vol. 99, nos. 1–4, pp. 72–76, 1990.
- [25] D. Zhou, C.Y. Zhao, and Y. Tian, "Review on thermal energy storage with phase change materials (PCMs) in building applications," *Appl. Energy*, vol. 92, pp. 593–605, 2012.
- [26] A. Sharma, V.V Tyagi, C.R. Chen, and D. Buddhi, "Review on thermal energy storage with phase change materials and applications," *Renew. Sustain. Energy Rev.*, vol. 13, no. 2, pp. 318–345, Feb. 2009.
- [27] W. Cui, Y. Yuan, L. Sun, X. Cao, and X. Yang, "Experimental studies on the supercooling and melting/freezing characteristics of nano-copper/sodium acetate trihydrate composite phase change materials," *Renew. Energy*, vol. 99, pp. 1029–1037, 2016.
- [28] J. Guion and M. Teisseire, "Nucleation of sodium acetate trihydrate in thermal heat storage cycles," *Sol. Energy*, vol. 46, no. 2, pp. 97–100, 1991.
- [29] A. López-navarro, J. Biosca-Taronger, J.M. Corberán, C. Peñalosa, A. Lázaro, P. Dolado, and J. Payá, "Performance characterization of a PCM storage tank," *Appl. Energy*, vol. 119, pp. 151–162, 2014.
- [30] C. Zauner, F. Hengstberger, B. Mörzinger, R. Hofmann, and H. Walter, "Experimental characterization and simulation of a hybrid sensible-latent heat storage," *Appl. Energy*, vol. 189, pp. 506–519, 2017.
- [31] A. Frazzica, M. Manzan, A. Sapienza, A. Freni, G. Toniato, and G. Restuccia, "Experimental testing of a hybrid sensible-latent heat storage system for domestic hot water applications," *Appl. Energy*, vol. 183, pp. 1157–1167, 2016.
- [32] P. Moreno, L. Miró, A. Solé, C. Barreneche, C. Solé, I. Martorell, and L.F. Cabeza, "Corrosion of metal and metal alloy containers in contact with phase change materials (PCM) for potential heating and cooling applications," *Appl. Energy*, vol. 125, pp. 238–245, 2014.
- [33] A. Arteconi, N.J. Hewitt, and F. Polonara, "State of the art of thermal storage for demand-side management," *Appl. Energy*, vol. 93, pp. 371–389, 2012.
- [34] S. Furbo, "Investigations of Heat Storages with salt hydrate as storage medium based on the extra water principle," Technical University of Denmark, Thermal Insulation Laboratory report no. 80, 1978.
- [35] M. Dannemand, J. Dragsted, J. Fan, J.B. Johansen, W. Kong, and S. Furbo, "Experimental investigations on prototype heat storage units utilizing stable supercooling of sodium acetate trihydrate mixtures," *Appl. Energy*, vol. 169, pp. 72–80, 2016.
- [36] M. Dannemand, J.M. Schultz, J.B. Johansen, and S. Furbo, "Long term thermal energy storage with stable supercooled sodium acetate trihydrate," *Appl. Therm. Eng.*, vol. 91, pp. 671–678, 2015.
- [37] M. Dannemand, J.B. Johansen, and S. Furbo, "Solidification behavior and thermal conductivity of bulk sodium acetate trihydrate composites with thickening agents and graphite," *Sol. Energy Mater. Sol. Cells*, vol. 145, pp. 287–295, 2016.

- [38] M. Dannemand, J. Fan, S. Furbo, and J. Reddi, "Validation of a CFD Model Simulating Charge and Discharge of a Small Heat Storage Test Module based on a Sodium Acetate Water Mixture," *Energy Procedia*, vol. 57, pp. 2451–2460, 2014.
- [39] W. Kong, M. Dannemand, J.B. Johansen, J. Fan, J. Dragsted, G. Englmaier, and S. Furbo, "Experimental investigations on heat content of supercooled sodium acetate trihydrate by a simple heat loss method," *Sol. Energy*, vol. 139, pp. 249–257, 2016.
- [40] G. Zhou and Y. Xiang, "Experimental investigations on stable supercooling performance of sodium acetate trihydrate PCM for thermal storage," *Sol. Energy*, vol. 155, pp. 1261–1272, 2017.
- [41] M.A. Rogerson and S.S.S. Cardoso, "Solidification in heat packs: III. Metallic trigger," *AIChE J.*, vol. 49, no. 2, pp. 522–529, 2003.
- [42] S. Furbo, J. Fan, E. Andersen, Z. Chen, and B. Perers, "Development of seasonal heat storage based on stable supercooling of a sodium acetate water mixture," *Energy Procedia*, vol. 30, pp. 260–269, 2012.
- [43] J. Fan, S. Furbo, E. Andersen, Z. Chen, B. Perers, and M. Dannemand, "Thermal behavior of a heat exchanger module for seasonal heat storage," *Energy Procedia*, vol. 30, pp. 244–254, 2012.
- [44] M. Dannemand, J.B. Johansen, W. Kong, and S. Furbo, "Experimental investigations on cylindrical latent heat storage units with sodium acetate trihydrate composites utilizing supercooling," *Appl. Energy*, vol. 177, pp. 591–601, 2016.
- [45] J.M. Schultz and S. Furbo, "Solar heating systems with heat of fusion storage with 100% solar fraction for solar low energy buildings," in *ISES Solar World Congress 2007 Proceedings*, 2007, pp. 2721–2725.
- [46] K. Seo, S. Suzuki, T. Kinoshita, and I. Hirasawa, "Effect of Ultrasonic Irradiation on the Crystallization of Sodium Acetate Trihydrate Utilized as Heat Storage Material," *Chem. Eng. Technol.*, vol. 35, no. 6, pp. 1013–1016, 2012.
- [47] M.A. Rogerson and S.S.S. Cardoso, "Solidification in heat packs: II. Role of cavitation," *AIChE J.*, vol. 49, no. 2, pp. 516–521, 2003.
- [48] M.A. Rogerson and S.S.S. Cardoso, "Solidification in heat packs: I. Nucleation rate," *AIChE J.*, vol. 49, no. 2, pp. 505–515, 2003.
- [49] L. Wei and K. Ohsasa, "Supercooling and Solidification Behavior of Phase Change," *ISIJ Int.*, vol. 50, no. 9, pp. 1265–1269, 2010.
- [50] P.L. Dietz, J.S. Brukner, and C.A. Hollingsworth, "Linear Crystallization Velocities of Sodium Acetate in Supersaturated Solutions," *J. Phys. Chem.*, vol. 61, no. 7, pp. 944–948, 1957.
- [51] L.F. Cabeza, A. Castell, C. Barreneche, A. de Gracia, and A.I. Fernández, "Materials used as PCM in thermal energy storage in buildings: A review," *Renew. Sustain. Energy Rev.*, vol. 15, no. 3, pp. 1675–1695, 2011.
- [52] G.A. Lane, *Solar heat storage latent heat material, Volume 1: Background and Scientific Principles*. CRC, 1983.
- [53] K.N. Marsh (Editor), *Recommended Reference Materials for the Realization of Physicochemical Properties*. Oxford: Blackwell Scientific Publications, 1987.
- [54] J.V. Sengers and J.T.R. Watson, "Improved International Formulations for the Viscosity and Thermal Conductivity of Water Substance," *Journal of Physical and Chemical Reference Data*, vol. 15, no. 4, pp. 1291–1314, 1986.
- [55] J. Dragsted, S. Furbo, M. Dannemand, and F. Bava, "Thermal stratification built up in hot water tank with different inlet stratifiers," *Sol. Energy*, vol. 147, pp. 414–425, 2017.
- [56] S. Furbo and V. Korsgaard, "Varmelagring til solvarmenanlæg," Technical University of Denmark, Thermal Insulation Laboratory report no. 162, 1984.

[4] G. Englmaier, S. Furbo, W. Kong, M. Dannemand, J. Fan, and Z. Wang, "Performance Evaluation of a Demonstration System with PCM for Seasonal Heat Storage: Charge with Evacuated Tubular Collectors," ISES Solar World Congress - IEA SHC International Conference on Solar Heating and Cooling for Buildings and Industry 2017, Proceedings, 2017. <http://doi.org/10.18086/swc.2017.13.02>

This page is intentionally left blank.

Performance Evaluation of a Demonstration System with PCM for Seasonal Heat Storage: Charge with Evacuated Tubular Collectors

Gerald Englmaier¹, Simon Furbo¹, Weiqiang Kong¹, Mark Dannemand¹, Jianhua Fan¹
and Zhifeng Wang²

¹Department of Civil Engineering, Technical University of Denmark

²Institute of Electrical Engineering, Chinese Academy of Sciences

Abstract

A seasonal heat storage with phase change material (PCM) for a solar space heating and domestic hot water combisystem was tested in automated operation during charge with solar collectors. A water tank was operating as buffer heat storage. Based on measurements during a representative day with sunshine, the storage system performance was evaluated regarding charge with solar heat. It shows the system behavior during typical operation resulting from the control strategy. Heat transfer rates from the solar collector array (22.4 m² aperture area) to the heat stores reached a peak of 19 kW, when PCM was melted. 30 kWh of heat was transferred to the 750 l water volume as it heated up. Afterwards 46 kWh of heat was transferred to the segmented PCM storage. In total 56 % of the total irradiation on the tilted collector plane was utilized to heat the storage units. During PCM charge heat transfer fluid temperatures were increasing with the state of charge. This is in contrast to maximization of solar yield. However, the energy conversion efficiency (65 %) of the collector array was satisfying. By considering pump electricity consumption, an overall performance ratio of 30.8 was obtained.

Keywords: Solar combisystem; Seasonal heat storage; Demonstrator; Performance evaluation; Measurement.

Nomenclature:

| Symbol | Quantity | Unit |
|-----------|---------------------------|----------------------|
| G | global irradiance | [W/m ²] |
| H | global irradiation | [Wh/m ²] |
| P | electrical power | [W] |
| PR | performance ratio (daily) | [-] |
| \dot{Q} | heat transfer rate | [W] |
| Q | heat | [Wh] |
| T | temperature | [°C] |
| W | electrical work | [Wh] |
| η | efficiency | [-] |

| Subscript | Quantity |
|---------------|------------------------------------|
| aperture | aperture area (collector field) |
| charge | buffer charge and PCM charge loops |
| charge buffer | buffer charge loop |
| charge PCM | PCM charge loop |
| coll | solar collector |
| coll loop | solar collector loop |
| P | pump |
| total | tilted surface (collector field) |

1. Introduction

Sodium acetate trihydrate (SAT) can be utilized for heat storage in a solar combisystem for space heating and domestic hot water supply. It can be melted in sunny periods with solar heat, the PCM can cool down to the ambient temperature without solidifying and remain stable in supercooled state. The solidification can be initiated and the heat of fusion released later when heat is in demand. This concept was successfully applied to flat prototype heat storage units (Dannemand et al., 2016). SAT has a melting point of 58°C and a latent heat of fusion of 264 kJ/kg (Meisingset & Grønvold, 1984). The heat content of SAT composites was experimentally investigated by Kong et al. (2016).

A seasonal PCM heat storage demonstration system (Fig. 1) was designed based on calculations with a TRNSYS model (Dannemand et al., 2015). Four 150 l heat storage units have been assembled to a latent heat storage stack. They were tested for their ability to supercool in a stable way after being charged with a fluctuating heat source (Englmair et al., 2016). The system was built at the solar heating test facility of the Technical University of Denmark. Heat from a solar collector array, 7 panels of evacuated tubular collectors with an aperture area of 22.4 m², was used to charge a 750 l water tank (buffer storage). The excess yield of the collector array was utilized to heat up the latent heat storage. This additional storage volume aims to preserve heat for periods with shortage of solar energy supply.

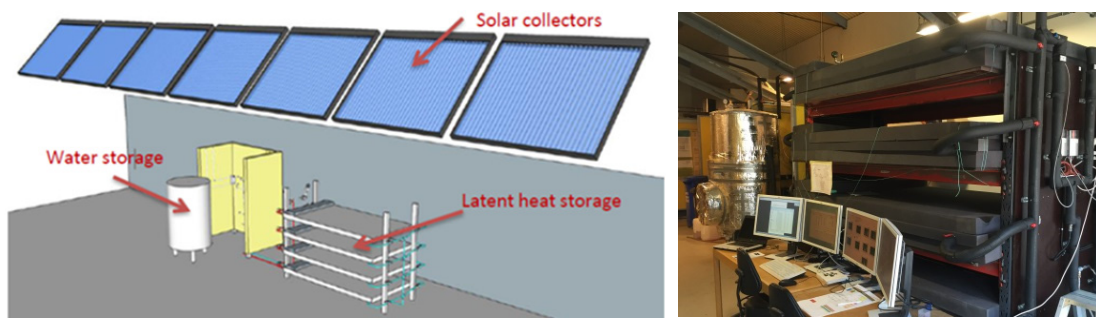


Fig. 1: Overall system design: Schematic drawing (left); Photography of water tank and PCM heat storage (right).

Using evacuated tubular collectors as a heat source for seasonal PCM heat storage is a novel approach. The heat transfer to the buffer storage and the PCM units are of special interest, since the solar source is fluctuating and therefore an optimized control strategy has to be found. Therefore data from a sunny day (9th of September 2015) where the system was operating with the designed control strategy was analyzed. The performance evaluation was based on measured heat transfer rates and monitoring of pump electricity consumption.

2. Method

2.1 Hydraulic configuration

The solar collector array was formed with 7 panels of Thermomax HP 450 (heat pipe evacuated tubular solar collectors) from Kingspan Renewables. Each panel consisted of 30 tubes. The 7 panels were connected in 2 parallel circuits. One circuit with 4 panels in series and one with 3 panels in series as illustrated in Fig 2. Equal fluid flow rate in each collector panel was realized by means of regulation valves. A CM3 pyranometer from Klipp & Zonen was used for G_{total} measurements in between the two parallel collector circuits (location marked with the green star). A copper-constantan thermocouple (TT-type) was used for measurement of the collector outlet temperature (location marked with the red

2.2 Operation sequence

The collector loop pump was activated when the temperature difference between the collector outlet temperature and the temperature at the bottom of the water storage exceeded 10 K (lower threshold value). The water tank was charged until a temperature of 55°C was reached in the middle of the water tank. This value was chosen as the upper threshold value for the control. Buffer storage charge stopped 5 minutes after either the lower or upper threshold value was met.

When the upper threshold for the buffer storage was met, collector loop circulation stopped until a collector outlet temperature of 70°C was measured. Then the PCM charge mode was activated. Melting of SAT composites required higher temperature, therefore previous buffer storage charge was beneficial. In order to achieve the full melting of the PCM, which is required for stable supercooling, inlet temperatures to the PCM units of up to 93 °C and high water flow rates were applied.

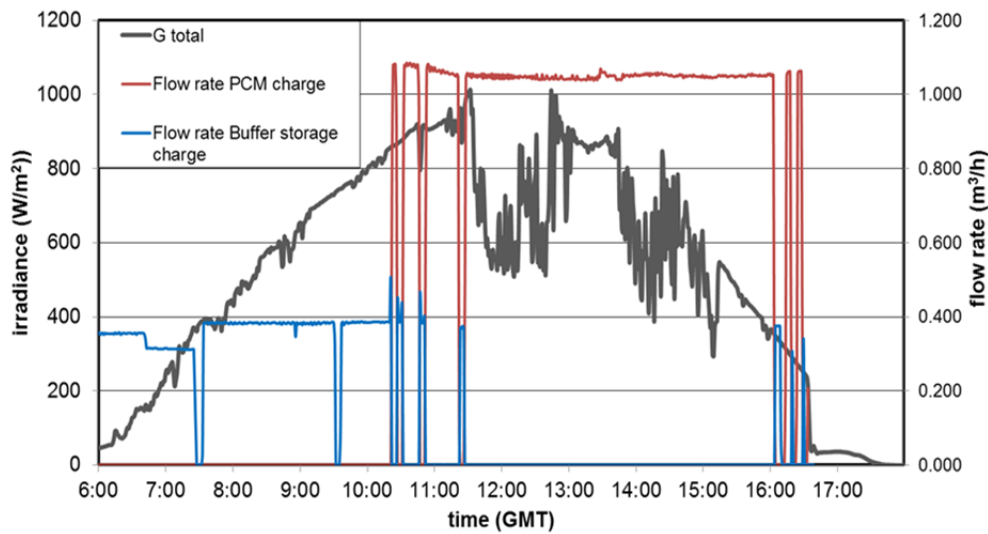


Fig. 4: Development of irradiance on the collector array and water flow rates applied.

Fig. 4 shows the flow rates applied on the secondary side of the plate heat exchanger. At 7:30 h the operation mode was switched from manual to automated control. The buffer storage was charged with a flow rate of 6.3 l/min (blue curve). Although at 10:15 h the buffer storage was already heated up, some periods of additional demand around noon and in the evening were detected by the control system. The collector array was shaded from 16:20 h on. As a consequence, the operation stopped with a short delay. A water flow rate of about 16.5 l/min (red curve) was applied when the PCM storage was charged. Due to the limited heat exchange capacity rates of a single PCM unit (Englmair et al., 2016) the units were charged in parallel.

2.3 Performance evaluation

The evaluation was based on heat transfer rates in the charging loops. In Fig. 5 the thermopiles (TP) mark the location where the heat transfer rates were evaluated. Also inlet-and outlet temperature measurements were located there. Beside temperature difference, measured flow rates, temperature dependent densities and specific heat capacities (resulting from temperature measurements) of the heat transfer fluids (solar collector fluid and water) were used for calculation.

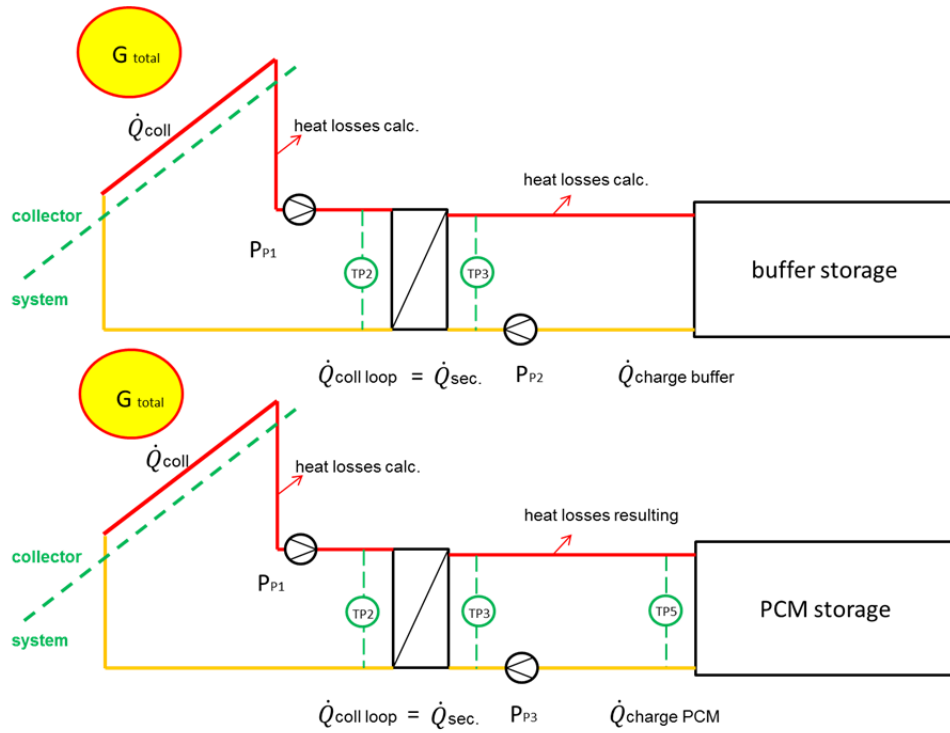


Fig. 5: Schematic evaluation model.

Pipe heat losses between the solar collector and the heat exchanger and between the heat exchanger and the buffer storage are included in the analyses. The heat loss in the solar collector loop was determined by calculations based on length, diameter and insulation thickness for the pipes and on measured temperatures. The heat loss in the PCM charge loop was resulting from the difference of heat transfer rates between TP3 and TP5. Thermal collector power was resulting from adding pipe heat losses to the calculated heat transfer rates at the plate heat exchanger.

Transferred heat was resulting from integration of heat transfer rates over time, considering the duration of each charging period.

As reference for evaluation, the solar potential was defined by the daily solar irradiation ($H_{aperture\ total}$) on the aperture area of the tilted collector surface. The course of the solar irradiance (G_{total}) is drawn in Fig. 4 (grey curve). The overall energy conversion efficiency was defined by the ratio of heat transferred to the sink (Q_{charge}) and the solar potential (formula no. 3).

$$\eta_{collector} = \frac{Q_{coll}}{H_{aperture\ total}} \quad (1)$$

$$\eta_{system} = \frac{Q_{charge}}{Q_{coll}} \quad (2)$$

$$\eta_{overall} = \frac{Q_{charge}}{H_{aperture\ total}} \quad (3)$$

Energy conversion efficiency at the collector (formula no. 1) and heat transfer efficiency in the system (formula no. 2) were based on the system border to the collector array, defined in Fig. 5. This approach enabled a closer look on the dependency of heat losses to the water temperatures during the two charging modes.

In terms of electrical power, control plays a minor role in solar heating systems. Therefore the consumption of pumps (marked in Fig. 5) was evaluated with the following performance ratios:

$$PR_{charge\ buffer} = \frac{Q_{charge\ buffer}}{W_{P1\ charge\ buffer} + W_{P2}} \quad (4)$$

$$PR_{charge\ PCM} = \frac{Q_{charge\ PCM}}{W_{P1\ charge\ PCM} + W_{P3}} \quad (5)$$

$$PR_{charge\ overall} = \frac{Q_{charge\ buffer} + Q_{charge\ PCM}}{W_{P1} + W_{P2} + W_{P3}} \quad (6)$$

As reference, their electrical work was logged during charging periods (indicated by the flow rates in Fig. 4). The collector loop pump (P1) was in operation during all periods, while P2 operated during buffer storage charge and P3 during PCM storage charge.

3. Results and discussion

On the selected day, the system was only in charging operation. Heat transfer rates, the daily energy balance as well as efficiency values were evaluated.

3.1 Heat transfer rates

In Fig. 6 the development of heat transfer rates of the collector loop (black marks), of the buffer storage charge loop (blue marks) as well as of the PCM charge loop (red marks) are drawn over time. The collector loop power followed G_{total} (grey curve in Fig. 4). During PCM charge peak values of up to 19 kW were reached when the mode has been activated (10:15 h), as well as during cascading of the number of PCM units (13:30 h – 14:00 h) in the charging loop.

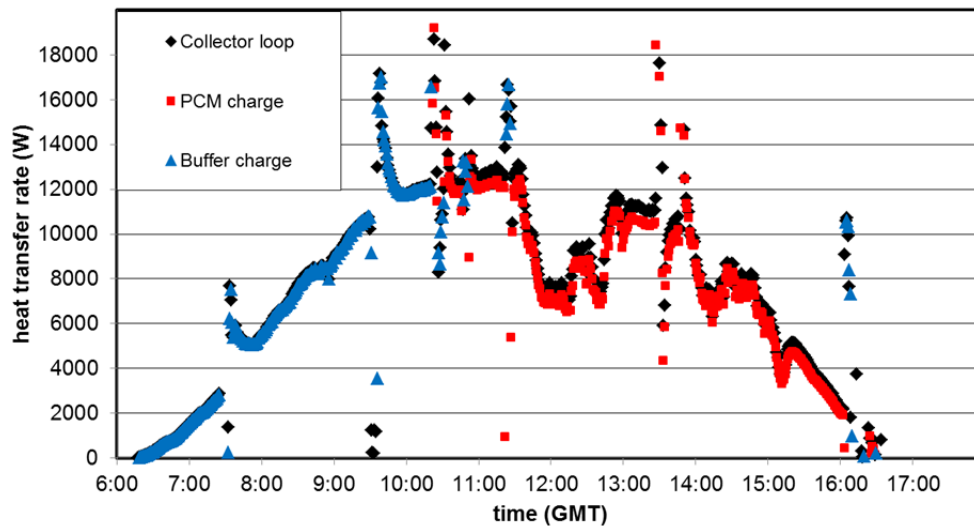


Fig. 6: Heat transfer rates during the course of the day.

Because the buffer storage is situated close to the plate heat exchanger, the collector loop power almost equaled to the heat transferred to the water tank. Buffer storage charge was interrupted two times before noon. Significant heat losses occurred in the PCM charge loop. The total duration of heat transfer was 10 hours.

The data were noisy through to the setting of the control system. Cascading of PCM units during PCM storage charge is

necessary to match the fluctuating collector power with the limited heat transfer capacity of PCM units. In contrast, intermediate buffer storage charge during periods of PCM storage charge only happened due to small internal temperature changes in the water tank. This cooled down the collector array and system components (collector loop, plate heat exchanger, pipework). Therefore a temperature hysteresis for full buffer charge (end criterion: 60°C, start criterion: 50°C) was implemented in the control after the present initial tests.

3.2 Daily energy balance

The energy balance was analyzed by integration of the heat transfer rates over time. Fig. 7 shows the solar potential (black curve) compared to the transferred heat during the course of the day. The difference between the collector loop energy (red curve) and the calculated collector output (red dotted curve) was a result of the pipe heat losses in the collector loop. During the total period of operation, the solar potential was 135 kWh. From this potential 79 kWh of energy was supplied by the collector loop to the heat storage system. 76 kWh (53 % of the solar potential) of heat was stored. Most heat was transferred to the PCM modules (46 kWh) in the period from 10:30 h to 16:00 h. This means an average net heat transfer rate of 9 kW. To the buffer tank (green curve) the highest share of energy (25 kWh) was transferred until 10:00 h, while the rest was transferred later, in four short periods.

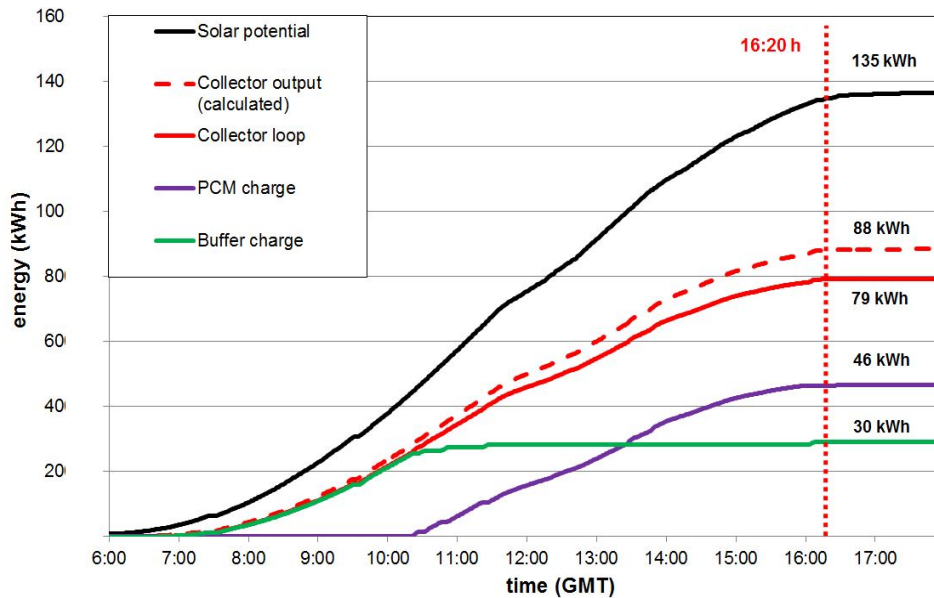


Fig. 7: Development of heat transfer during the course of the day.

During buffer storage charge only minor heat losses occurred in the system (collector loop and charging loop), while significant heat losses (8 kWh) occurred during the charge of the PCM units with high solar collector fluid and water temperatures.

The buffer storage charge means an average temperature increase of 35K in the water tank (750 l), which was considered to be sufficiently high to cover the heat demand of an energy efficient single family house throughout the following day. Full charge of a single PCM unit (from solid state at ambient temperature) required 27.4 kWh (Englmaier et al., 2016). However, since up to 3 PCM units were charged in parallel, 2 consecutive sunny days are assumed to be necessary to ensure full PCM unit heat up to a uniform temperature of 80°C. Only in this way the supercooling ability of charged PCM units can be enabled.

3.3 Energy efficiency

Based on the daily energy balance, average energy efficiency factors are obtained:

$$\eta_{collector} = 0.65; \quad \eta_{system} = 0.86; \quad \eta_{overall} = 0.56$$

As a result of energy conversion of the collector, 65 % of the solar potential was transferred in form of heat to the system. The system efficiency was 86 % on the reference day. 10 % of heat in the collector loop and 4 % of heat in the secondary loop were dissipated via heat losses to the ambience. So, in total 56 % of the solar potential was transferred to the heat sink.

Further information can be seen from the course of energy efficiencies in context to the collector outlet temperature in Fig. 8. The energy conversion efficiency at the collector (grey scattered curve) was low until 9:00 h. During this period and all components of the collector loop as well as the heat transfer fluids were heating up. Peak values occurred due to changes of operation modes. After 9:00 h $\eta_{collector}$ reached a level of above 65 %. Because of rising heat transfer fluid temperatures (indicated by the collector outlet temperature – red curve) $\eta_{collector}$ fell throughout the day. Shifts between buffer and PCM charge modes (Fig. 4) caused collector outlet temperature jumps. During PCM charge the heat transfer fluid temperatures were coupled to the state of PCM unit charge.

After 15:00 G_{total} and the efficiency values fell down dramatically and the heat transfer fluid temperatures remained high. When the operation stopped, heat remained in the hot heat transfer loops and in the solar collector.

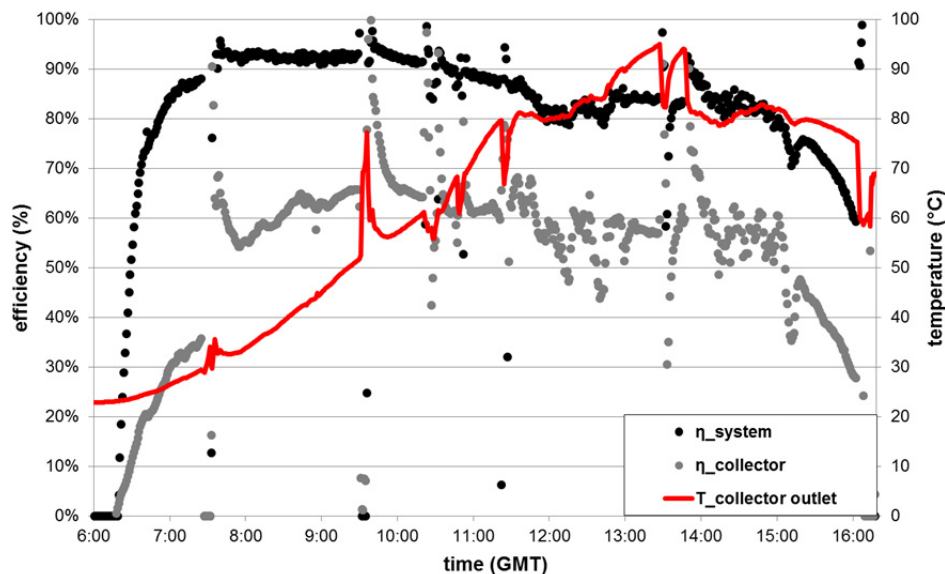


Fig. 8: Development of system efficiency, energy conversion efficiency at the collector and collector outlet temperature during the course of the day.

The system efficiency (black scattered curve) showed similar behavior. After the pipework was heated up (until 7:30 h), η_{system} remained above 90 % during buffer storage charge. During PCM charge, when heat transfer fluid temperatures raised and a longer pipework was used, η_{system} was in the range of 80-90 % for long time. Lower values were observed around noon, when G_{total} was fluctuating at lower level than before noon. Decreasing system efficiency after 15:00 h was a result of lower heat transfer rates at high fluid temperatures. This means that during that period a high share of heat was dissipated to the ambience.

Longer periods of buffer storage charge (lower heat transfer fluid temperatures) at the end of the day (when G_{total} is decreasing) would maximize the daily energy yield. Increased η_{system} and $\eta_{collector}$ values would be resulting. However, PCM unit charge is beneficial after the buffer heat storage is sufficiently heated for domestic heating applications.

3.4 Pump efficiency

The secondary loop pump (P2) was powered with 8 W to achieve the set water flow rate during buffer charge. To match the heat transfer capacity rate of the solar collector fluid at the heat exchanger to the water, a collector loop pump power of 70 W was required. During PCM charge the pumps were set at 90% of their maximum operation speed to enable high fluid flow rates. The collector loop pump power reached 390 W and the secondary loop pump (P3) was operating at 120 W. The resulting electricity consumptions are given in Tab. 1:

| | WP1 | WP2 | WP3 |
|-----------------------|------------|------------|------------|
| | (Wh) | (Wh) | (Wh) |
| Buffer charge | 167 | 22 | none |
| PCM charge | 1716 | none | 548 |
| Overall charge | 1883 | 22 | 548 |

Tab. 1: Pump electricity consumption during charging periods.

The electrical power consumption of pumps during PCM charge (about 5 hours of operation) was 2.5 kWh, while for buffer storage charge only 0.2 kWh were consumed. Based on the previous definitions, the following performance ratios were resulting:

$$PR_{charge\ buffer} = 154; \quad PR_{charge\ PCM} = 19.1; \quad PR_{charge\ overall} = 30.8$$

The highest performance ratio was occurring during buffer storage charge (154), while the performance ratio during PCM module charge was about 8 times lower. The overall charge performance ratio was 30.8. It was found that the electricity consumption for PCM charge can be lowered by application of different pump types. Also, a reduction of flow rates during PCM charge could lower the electricity consumption. However, this would lower the heat transfer in the PCM units.

4. Conclusions

A demonstration system on seasonal heat storage, utilizing the principle of stable supercooling of SAT, was tested for its functionality during charge on a representative sunny day. System control enabled interplay between solar collectors, buffer heat storage and PCM heat storage:

- The applied collector array enabled sufficiently high heat transfer for both, buffer storage and PCM charge. The heat transfer reached peak values of more than 12 kW in both operation modes. When modes were changed or interrupted, heat transfer rates of up to 19 kW occurred.
- During PCM charge the HTF temperatures were increasing with the state of PCM charge. This is in contrast to maximisation of solar yield. Since the number of PCM units in operation was variable, no restrictions for heat transfer from the collector array were observed.

- Regarding to the required high collector outlet temperatures (up to 95°C) during PCM charge, the energy conversion efficiency of the collector array was satisfying. 65 % of the solar potential was converted into heat and transferred to the system.
- 76 kWh (86 %) of available heat was stored. During buffer storage charge only minor pipe heat losses occurred. 46 kWh of heat were charged to the PCM storage when 8 kWh (10% of available heat) were dissipated via hydraulic components to the ambience.
- The PCM charge performance ratio (19.1) and therefore also the overall performance ratio (30.8) were quite low, although standby consumptions of pumps and of the control system were not considered in their calculation.

The resulting operation sequence proved functional system behavior. Significant heat losses due to a long pipework, frequent mode-switches and rather high pump electricity consumption during PCM charge were identified as areas for potential improvements.

5. Acknowledgements

This research was funded by the European Commission (Grant Agreement N_ 295568) as part of the Seventh Framework Programme through the former COMTES project. The work was also supported by the PhD program of the Sino Danish Center for Education and Research (SDC). We thank our partners from Nilan A/S and the Graz University of Technology for sharing knowledge and discussions as well as the research technicians Troels V. Kristensen and Claus Aagaard for their practical support.

6. References

- Dannemand, M., Dragsted, J., Fan, J., Johansen, J. B., Kong, W., & Furbo, S., 2016. Experimental investigations on prototype heat storage units utilizing stable supercooling of sodium acetate trihydrate mixtures. *Applied Energy*, 169, 72–80.
- Dannemand, M., Schultz, J. M., Johansen, J. B., & Furbo, S., 2015. Long term thermal energy storage with stable supercooled sodium acetate trihydrate. *Applied Thermal Engineering*, 91, 671–678.
- Englmair, G., Dannemand, M., Johansen, J. B., Kong, W., Dragsted, J., Furbo, S., & Fan, J., 2016. Testing of PCM Heat Storage Modules with Solar Collectors as Heat Source. *Energy Procedia*, 91, 138–144.
- Kong, W., Dannemand, M., Johansen, J. B., Fan, J., Dragsted, J., Englmair, G., & Furbo, S., 2016. Experimental investigations on heat content of supercooled sodium acetate trihydrate by a simple heat loss method. *Solar Energy*, 139, 249–257.
- Meisingset, K. K., & Grønvold, F., 1984. Thermodynamic properties and phase transitions of salt hydrates between 270 and 400 K III. $\text{CH}_3\text{CO}_2\text{Na}\cdot 3\text{H}_2\text{O}$, $\text{CH}_3\text{CO}_2\text{Li}\cdot 2\text{H}_2\text{O}$, and $(\text{CH}_3\text{CO}_2)_2\text{Mg}\cdot 4\text{H}_2\text{O}$. *The Journal of Chemical Thermodynamics*, 16(6), 523–536.

[5] G. Englmaier, W. Kong, J. B. Berg, S. Furbo, and J. Fan, “Demonstration of a solar combi-system utilizing stable supercooling of sodium acetate trihydrate for heat storage”, submitted to Applied Thermal Engineering, in review.

This page is intentionally left blank.

Demonstration of a solar combi-system utilizing stable supercooling of sodium acetate trihydrate for heat storage

Gerald Englmaier^{1,2}, Weiqiang Kong¹, Jakob Brinkø Berg¹, Simon Furbo¹ and Jianhua Fan¹

¹Department of Civil Engineering, Technical University of Denmark, Brovej 118, 2800 Kgs. Lyngby, Denmark

² Sino-Danish Center, University of Chinese Academy of Sciences, 380 Huaibeizhuang, Huairou district, Beijing, China

Highlights

- System design with combined short and long-term heat storage
 - A control strategy enabling on-demand utilization of heat of fusion
 - System demonstration with 22.4 m² (aperture) tubular collectors
 - Analysis of automated system operation in spring and autumn
-

Abstract

Achieving a high fraction of solar heat in heat supply for domestic buildings would reduce the use of fossil fuels for heat generation and has been a goal for a long time. Combined short and long-term heat storage has been identified as one way of achieving solar fractions higher than 50 percent in heat supply for domestic buildings. To this end, a laboratory solar heating system was built with heat-pipe tubular collectors 22.4 m² in aperture and a heat-storage prototype consisting of a 735 L water tank and four PCM units each containing 200 kg sodium acetate trihydrate (SAT) composite. The SAT composite was utilized as sensible heat storage with the additional ability to release heat of fusion on demand. Operation was demonstrated with the space heating and hot water demand patterns of a standard-size Passive House in the Danish climate. A strategy was developed to control the system. Seven operation modes enabled combined charging of water tank and PCM units, heat transfer from PCM units to the water tank when heat was in demand, and the right timing of auxiliary heating. We present the controller settings identified and the heat transfer fluid flow rates applied. Sequences of water tank charging, and single and parallel PCM unit charging were used to match the collector power available and the heat transfer limitations of the stores. During the charging of PCM units, the flow temperature was kept between 70 and 95 °C to allow continuous heat transfer rates of up to 16 kW. Peaks of up to 36 kW occurred when PCM units were added to the charging circuit. During heat transfer from PCM units to the water tank, flow temperatures were close to the SAT composite temperature and thermal power of up to 6 kW was measured. The heat stores were efficiently utilized in spring and autumn. The developed control strategy and measurement data from system demonstration will form the basis for numerical performance investigations.

Keywords: Solar heating system; system demonstration; control strategy; heat storage prototype; phase change material; stable supercooling.

Nomenclature

Symbols

| | | | |
|------------------|--|---------|-------------------------------|
| A | area (m ²) | eff | effective storage density |
| c _p | specific heat capacity (kJ/kg K) | in | inlet line |
| E _{aux} | electrical heater (auxiliary) | liquid | liquid SAT |
| G | global irradiance (W/m ²) | max | maximum temperature |
| H | height | melting | melting temperature of PCM |
| L | latent heat (kJ/kg) | out | outlet line |
| Q | thermal energy, heat (kWh) | PCM | phase change material |
| \dot{Q} | heat transfer rate (kW) | phy | physical storage density |
| S | Energy storage density (kWh/m ³) | sec | secondary circuit |
| t | time (s) | service | service |
| T | temperature (°C) | SH | space heating |
| Ø | diameter (m) | solid | solidified SAT |
| V | volume (m ³) | total | total, on the collector plane |
| \dot{V} | volume flow rate (l/min) | water | water |

Greek letters

| | |
|------------|------------------------------|
| ΔT | temperature difference (K) |
| ρ | density (kg/m ³) |

Subscripts

| | |
|-------|----------------------------------|
| amb | ambient |
| aux | auxiliary |
| act | actual storage density |
| B | buffer heat storage (water tank) |
| coll | collector outlet |
| cycle | cycles per year |
| DHW | domestic hot water |

Abbreviations

| | |
|---------|---|
| DHW | domestic hot water |
| HTF | heat transfer fluid |
| HX | heat exchanger |
| LabVIEW | laboratory virtual instrument engineering workbench |
| MEV | membrane expansion vessel |
| P | pump |
| PCM | phase change material |
| SAT | sodium acetate trihydrate |
| SH | space heating |
| X | control valve |

1. Introduction

1.1. *Solar combi-systems*

Solar heating is a promising technology for reducing fossil-fuel consumption in the building sector. Solar combi-systems in various designs [1] can help cover domestic hot water and space heating demand. IEA SHC Task 26 evaluated nine solar combi-system designs on the European market [2] and found that the optimal collector tilt, which depends primarily on the latitude, also needs to increase to better utilize the solar irradiation during the heating season if the solar fraction is to be increased. Andersen [3] investigated how to design solar combi-systems that can achieve high solar fractions. Detailed investigations were conducted on storage tanks in terms of discharge from different levels [4], inlet stratifiers [5], and degrees of stratification efficiency [6]. Based on elaborated knowledge, Thür [7] developed a compact system focused on minimizing temperature to reduce heat losses and to increase the efficiency of the solar collector.

Efficient heat storage has been identified as the key component for well-performing solar heating systems [8], [9]. Long-term storage of heat is essential to cover heat demand with solar fractions larger than 50% in central and northern Europe. Water tanks have been used for this purpose [10,11], but large storage volumes were necessary to compensate for sensible heat losses.

1.2. *Combined short and long-term heat storage*

As an alternative to water, the International Energy Agency Solar Heating and Cooling Task 42/ Annex 29 [12] investigated novel materials for more efficient heat storage over long periods. Prototype heat stores have recently been developed that use solid sorption materials in an open system [13,14] or in a closed system [15,16], or that use liquid absorption with sodium-hydroxide [17,18]. Thermochemical long-term heat storage with a salt/zeolite composite has been demonstrated in building scale [19], [20]. Phase change materials (PCMs) have been used in low and medium temperature applications [21], especially building applications [22,23]. Salt hydrate PCMs have been considered because of their relatively high latent heat.

Quinnell and Davidson [24] have showed that the combined use of material properties, such as reaction enthalpy and sensible heat capacity, gives advantages in solar thermal systems in terms of energy supply flexibility. The combined use of latent heat of fusion and sensible heat capacity is possible with the salt hydrate sodium acetate trihydrate (SAT), which can stably supercool to ambient temperatures while preserving its heat of fusion [25], [26], [27]. After melting and heating to a temperature above 77 °C, sensible heat can be discharged until room temperature is reached. Then, the crystallization of the supercooled solution can be initiated by seed crystal injection [28,29] or by local cooling [30], and the heat of fusion will be released as it crystalizes. This heat storage concept dates back to initial research in the late 1920s [31] and was later found to enable more efficient solar heat supply of low-energy buildings in summer and transitional seasons [32].

1.3. *Heat storage prototypes utilizing stable supercooling of SAT*

SAT is attractive for combined short and long-term heat storage due to its relatively high specific heat capacities in liquid and solid phases [28] in combination with its heat of fusion (264 kJ/kg [33]). Its melting point of 58 °C is appropriate for heat supply in buildings. Its density has been determined to be 1.27 kg/L at 90 °C in liquid state and 1.33 to 1.34 kg/L in an open sample after solidification from supercooled state [34].

To overcome phase separation of SAT in supercooled state [35], SAT composites were developed in previous research at the Technical University of Denmark. Promising composites contained extra water, carboxymethyl cellulose and xanthan rubber, as well as ethylenediaminetetraacetic acid and liquid polymeric solutions. When their crystallization is initiated in supercooled state at 20 °C, heat contents above 200 kJ/kg have been measured [36]. In contact with steel, supercooled SAT composites crystallize below –15 °C [30]. A thermal conductivity in the range of 0.5 – 0.65 W/mK has been found for solid composites containing carboxymethyl cellulose and xanthan rubber [37]. As for most PCMs, this is considered as a limitation of heat transfer.

Dannemand et al. addressed the engineering challenges of volumetric change and decreasing conductivity during SAT composite solidification by using flat [38] and cylindrical [39] prototype heat storage units. SAT has also been used in the mantle of hot water tanks [40].

Englmair et al. [41] report the design and the functionality of a heat storage prototype consisting of four flat units containing 200 kg SAT composites each and a 735 L water tank. Stable supercooling was achieved in three out of the four units. The full charge of a single unit from ambient temperature was measured at 27.4 kWh. 14 kWh of sensible heat and 10.2 kWh (80% heat of fusion) of heat during solidification were discharged with PCM temperatures higher than 50 °C. Prototype devices for seed crystal injection worked during initial tests, but were later dismantled, due to deformation by temperature changes.

1.4. *Scope*

A novel solar combi-system with application of a previously developed heat storage prototype utilizing stable supercooling of SAT composite is presented. System tests with an array of evacuated tubular collectors and space-heating and domestic hot water patterns of a standard-size Passive House in the Danish climate were conducted to provide the following outcome:

- A control strategy with operation modes for storage charge and discharge as well as auxiliary heating
- Automated system operation by determination of threshold values for modes, settings of control valves, and optimized heat transfer fluid flow rates
- Validation of control parameter settings by system demonstration
- Analysis of the system behaviour to elucidate how water tank and PCM units can be operated for the efficient utilization of solar collectors in a single-family household.

The generated experimental data will be the basis for further system development by numerical performance investigations. The demonstration of a solar combi-system utilizing stable supercooling of SAT has not been reported before and will provide reference for more efficient solar heating by combined short and long-term heat storage.

2. System design

2.1. Components

A system demonstrator was built in the prototype test facility at the Technical University of Denmark (northern latitude: 55.8°) to apply the domestic hot water (DHW) and space heating (SH) demand patterns. It was designed as a solar combi-system with a solar collector array, a water heat storage, and a segmented PCM heat storage utilizing SAT (Fig. 1 a).

The collector array was formed with 7 panels (totalling 22.4 m² of aperture area) of heat pipe evacuated tubular collectors, type Thermomax HP 450 from Kingspan Renewables. They were chosen due to their relatively low heat loss coefficients (Table 1), which allow good performance during melting of SAT with collector outlet temperatures above 70 °C. The collectors were mounted with an inclination of 45° and an azimuth angle of 12° towards east. Tyfocor LS, a heat transfer fluid (HTF) based on propylene glycol and water, was used to ensure frost protection. The panels were connected in 2 parallel circuits, one circuit with 4 panels and one with 3 panels in series.

The water tank (Fig. 1 b) had a volume of 735 L. It was designed as tank-in-tank heat storage with an electrical resistor (E_{aux}) for auxiliary heating situated at a height of 0.5 m. The outer tank (\varnothing : 0.8 m) had a height of 1.6 m and was insulated with 0.05 m of mineral wool. The inner tank (\varnothing : 0.45 m, V: 175 L), was situated in the top-centre of the outer tank. It covered a height of 1.1 m and included a pipe (\varnothing : 0.16 m) to the bottom of the outer tank. Cold water entered the inner tank from the bottom and DHW was tapped from the top of it. The outer tank contained water as HTF. The SH circuit was connected with an outlet at a height of 1 m and an inlet at the bottom of the outer tank. The charging circuit was implemented with an outlet at the bottom of the outer tank, where there was also a polymeric inlet stratifier [42] to enable good thermal stratification.

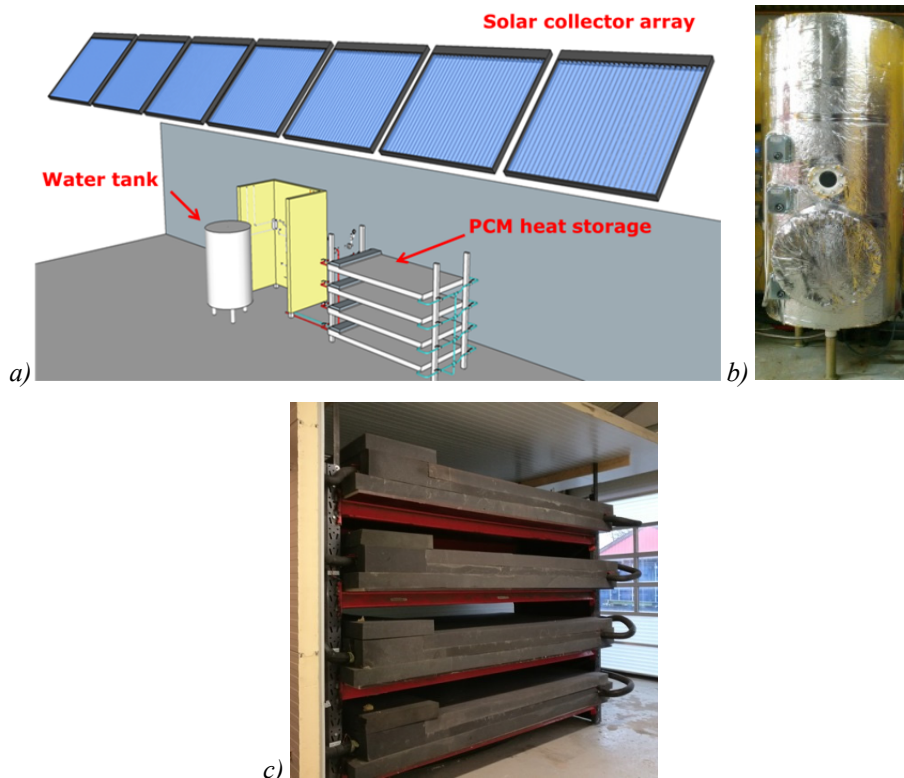


Fig. 1. System demonstrator: a) Component configuration; b) Water tank; c) PCM heat storage.

The segmented PCM heat storage (Fig. 1 c) consisted of four flat units, each containing 150 L of SAT composite. They were insulated with 10 cm of foam insulation. The hydraulic configuration, activation devices applied and the functionality of the heat storage prototype have all been previously reported [41].

The interplay of the collector array, a variable number of PCM units, and the water tank was enabled by hydraulic circuits (Fig. 3). For the collector circuit, 35 m of copper piping (outer Ø: 20 mm, insulation: 19 mm) was installed. Circuits with a length of 9 m for water tank charging and 19 m for heat transfer to/from the PCM heat storage were realized with steel piping (¾", insulation: 19 mm). A plate heat exchanger (HX) connected the collector circuit with pipework for storage charging. Its overall heat exchange capacity rate was calculated to be 1.100 W/K.

Table 1. Data from collector panel certification [43].

| Aperture area (m ²) | Gross area (m ²) | Peak collector efficiency (-) | 1 st order loss coefficient (W/m ² K) | 2 nd order loss coefficient (W/m ² K ²) | Effective heat capacity (kJ/m ² K) |
|---------------------------------|------------------------------|-------------------------------|---|---|---|
| 3.2 | 4.15 | 0.750 | 1.18 | 0.010 | 4.4 |

2.2. Energy storage density

For domestic heat storage, the heat capacity of the SAT applied is limited by the room temperature ($T_{amb}=25\text{ °C}$) and the maximum HTF temperature ($T_{max}=90\text{ °C}$). The physical storage density (S_{phy}) was calculated as follows:

$$S_{phy} = [(T_{melting} - T_{amb}) * c_{p,solid} + L + (T_{max} - T_{melting}) * c_{p,liquid}] * \rho_{liquid} \div 3.6 = 151 \frac{kWh}{m^3} \quad (1)$$

where the specific heat capacities (c_p) of SAT in liquid phase (3 kJ/kgK at 74 °C) and solid phase (2.1 kJ/kgK at 42 °C) [28] and a latent heat of fusion (L) of 264 kJ/kg [33] were applied. The density (ρ) of SAT in liquid phase is lower than in solid phase and must be therefore used. A minimum density of 1.27 kg/L at 90 °C [34] was considered.

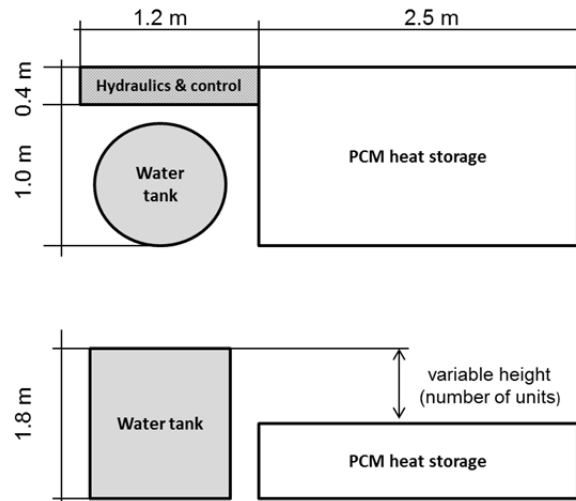


Fig. 2. Dimensions of the heat storage components.

In discharge tests, a minimum SAT temperature of 50 °C was found to be necessary for heat supply. For a single unit, a heat capacity (Q_{PCM}) of 24.2 kWh (14 kWh short-term; 10.2 kWh long-term) was measured under application

conditions. The minimal space demand for the heat stores, hydraulic installations, and monitoring equipment is illustrated in Fig. 2. Instead of the individual insulation of PCM units in the storage prototype, several PCM units could be installed within one insulation layer. The given water tank height (H) allows space for up to 14 PCM units. Including hydraulics and control, an area (A_{PCM}) of 3.89 m² would be necessary. The effective storage density (S_{eff}), related to the necessary installation space of PCM units, would be:

$$S_{eff} = \frac{Q_{PCM} * 14}{A_{PCM} * H} = 48 \frac{kWh}{m^3} \quad (2)$$

of which 28 kWh/m³ are available as sensible heat storage, and 20 kWh/m³ can be used for long-term heat storage.

For the solar heating system, a water tank was also applied. Its storage capacity (Q_{water}) was calculated to be 38 kWh, assuming an average water temperature increase of 45 K. For maintenance access, a distance of 0.5 m from at least two sides was necessary. The occupied area ($A_{service}$) was 8 m², which corresponds to a volume demand of 14.4 m³. The actual storage density (S_{act}) of the heat storage configuration with 4 PCM units was:

$$S_{act} = \frac{Q_{PCM} * 4 + Q_{water}}{A_{service} * H} = 9.4 \frac{kWh}{m^3} \quad (3)$$

With 14 PCM units installed, the actual storage density would be 26.2 kWh/m³.

3. Experimental method

3.1. Monitoring and control

System operation was realized by a LabVIEW-based data acquisition and control program. The LabVIEW program was executed on a National Instruments Compact Rio 9085 industrial computer running a real-time operating system. Thermocouples and thermopiles were connected to a 16-channel thermocouple data acquisition module (NI9214). Flow meter signals were read via a 32-channel digital input/output data acquisition module (NI9403). Uncertainties resulted mainly from the sensors installed (Table 2). Pump speed and valve positions (X) were set by the Compact Rio computer to operate hydraulic circuits (Fig. 3). A digital output module (NI 9476) was used to control valve motors (Honeywell, V4043H) and auxiliary heating. An analogue output module (NI 9263) and a digital output module (NI 9403) were used for HTF flow rate control via pump speed. An operator monitor program, also programmed in LabVIEW, was created to enable operators to monitor the system and operate it manually from an adjacent PC. To estimate SH requirements, outdoor sensors were positioned to gather information about solar radiation levels (G_{total}) and ambient temperature (T_{amb}).

Table 2. Measurement devices installed.

| Measurement device | Type | Uncertainty |
|---|--|--|
| Thermocouple (T_{Bi} , T_{coll} , T_{DHW_in} , T_{DHW_out} , T_{HX_out} , T_{PCMi} , T_{SH_in} , T_{SH_out}) | TT-type (copper/ constantan) | 0.5 K [44] |
| Thermopile with two integrated TT-type thermocouples (ΔT_{coll} , ΔT_{PCM} , ΔT_{sec}) | 5-junction thermopile with TT-type thermocouples | 0.1 K [44] |
| Flow meters (\dot{V}_{coll} , \dot{V}_{DHW} , \dot{V}_{PCM} , \dot{V}_{SH} , \dot{V}_{sec}) | Class 2 | 2% of reading (in accordance with EN 1434)* |
| Pyranometer (G_{total}) | Kipp & Zonen CM3 | 15 W/m ² (below 200 W/m ²) |

*The accuracy range was experimentally proved for the flow rate range applied before installation.

Heat losses from the hydraulic circuit to the PCM storage were evaluated between thermopiles at the heat exchanger (ΔT_{sec}) and at the PCM heat storage (ΔT_{PCM}). Heat losses during water tank charging were calculated based on measured pipework length.

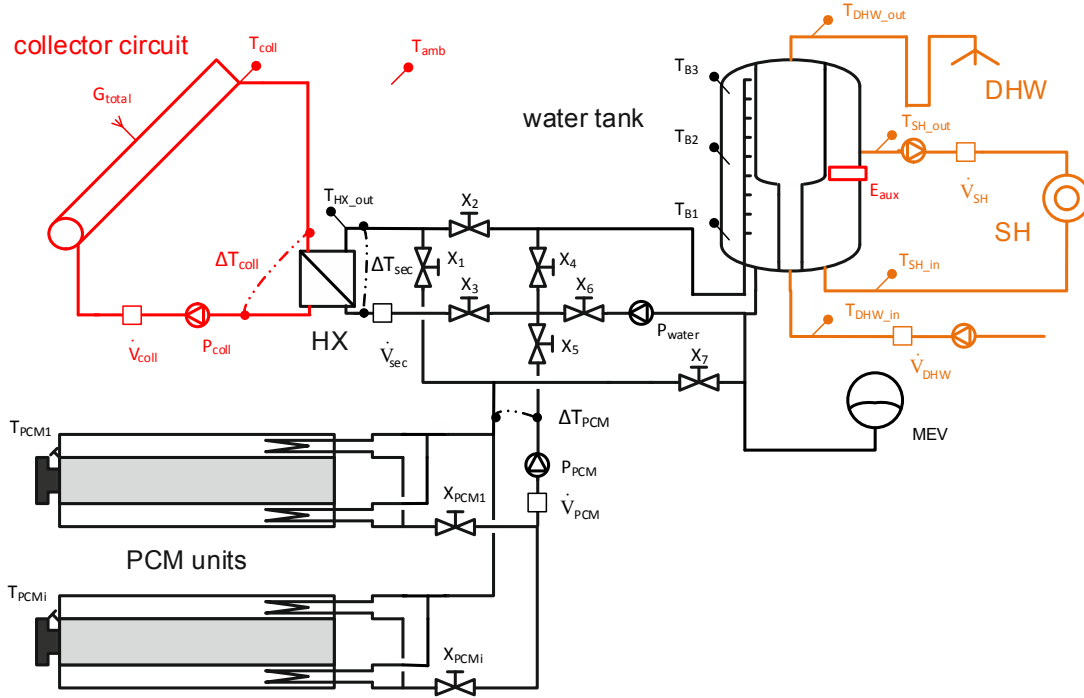


Fig. 3. System layout with heat storage components in black, heat sources in red, and heat sinks in orange.

3.2. Hot water and space heating demand

Characteristic SH patterns were found in a previously conducted simulation of a 130 m² building built to Passive House Standard [45] and using the Danish weather reference year. The annual SH demand was 15 kWh/m². The building model included south-orientated windows. When the hourly average global irradiance (G) was above 200 W/m², there were no heating loads in the simulation. Hourly heating loads, depending on G and ambient temperature (T_{amb}), were fitted with Equations 4–7:

$$0 \text{ W/m}^2 < G < 10 \text{ W/m}^2: \quad \dot{Q}_{SH} = -0.0526 * T_{amb} + 0.7764 \text{ [kW]} \quad (4)$$

$$10 \text{ W/m}^2 < G < 50 \text{ W/m}^2: \quad \dot{Q}_{SH} = -0.0538 * T_{amb} + 0.7196 \text{ [kW]} \quad (5)$$

$$50 \text{ W/m}^2 < G < 100 \text{ W/m}^2: \quad \dot{Q}_{SH} = -0.0503 * T_{amb} + 0.5458 \text{ [kW]} \quad (6)$$

$$100 \text{ W/m}^2 < G < 200 \text{ W/m}^2: \quad \dot{Q}_{SH} = -0.0328 * T_{amb} + 0.2761 \text{ [kW]} \quad (7)$$

Heat-draw for space heating was enabled in intervals of 6 hours (Fig. 9, Fig. 10). In this way, it was possible to calculate heat demand for 6 hours based on measurements from the monitoring system. SH was enabled from 15th October to 31st March and used data collected from outdoor sensors as previously described.

The Danish code of practice for domestic water supply DS 439 [46] recommends a daily DHW consumption of 4.36 kWh in a standard house with 3.5 occupants and a cold water temperature of 10 °C. This consumption does not include hot water for kitchen-use. For system demonstration, the DHW consumption was calculated with 113L of hot water at 45 °C daily, considering the comfort requirements of all users and efficient use of water. This results in daily

loads of 4.6 kWh. Three hot water draw-offs a day (7:00 h, 12:00 h, 19:00 h), with 1.53 kWh of heat each draw-off, were applied to simulate user behaviour (Fig. 9, Fig. 10).

3.3. Demonstration

To match supply from solar collectors and heat demands in an efficient way, a control strategy with modes for charging and discharging the heat storage prototype was applied. Threshold conditions for operation modes and subroutines for PCM discharge were tested until the system was able to operate automatically. Valve settings, optimized HTF flow rate, and temperature settings were identified by manual parameter control in the LabVIEW operator monitoring and control program.

The resulting system behaviour was studied during automated operation from February 2016 until April 2017. From 30th of June until 21st September 2016, the collector array was covered to avoid stagnation conditions. Utilization of SAT crystallization from stable supercooled state was demonstrated with manual system settings. This was necessary because of limitations in the activation devices [41].

The setting of operation modes, heat transfer rates to the water tank and the PCM heat storage, and the state of PCM units were analysed with data from two characteristic periods. The applicability of combined charging of water tank and PCM units and the necessary subroutines during PCM storage charging was evaluated for a spring day with clear sky. Measurements and operation mode settings were logged in 10 second intervals. Data analysis was based on averaged values for 1 minute and 1 hour. Heat transfer rates in the circuits were calculated using Equation 8:

$$\dot{Q} = \dot{V}_i \cdot c_p \cdot \rho \cdot \Delta T_{in-out} \quad (8)$$

where \dot{V}_i is the measured volume flow rate of the HTF, c_p is the specific heat capacity of the HTF at mean temperature between T_{in} and T_{out} , and ρ is the density of the heat transfer fluid at T_{out} where the volume flow rates were measured. ΔT was measured by thermopiles.

DHW-tapping and SH-draw were realized using two cooling circuits at the prototype test facility (Fig. 3). HTF flow started at set times and stopped when previously set heat demands were measured:

$$Q_i = \int (\dot{V}_i \cdot c_p \cdot \rho \cdot (T_{i,in} - T_{i,out})) \cdot dt \quad (9)$$

where \dot{V}_i was the measured volume flow rate of the HTF at either \dot{V}_{DHW} or \dot{V}_{SH} . The temperature differences were calculated between T_{DHW_in} and T_{DHW_out} , and between T_{SH_in} and T_{SH_out} . HTF properties were determined in accordance with Equation 8.

4. Experimental results and discussion

4.1. Control strategy

An overview of the concept is presented in Fig. 4, where operation modes are shown in black boxes and resulting settings in grey boxes. Mode A defines states without collector circuit operation when the water tank charge is sufficient for DHW and SH demand. In this mode, the control system is in standby, with just monitoring system measurements

being taken. The collector circuit starts operating when measurements fulfil threshold conditions, and there are three different modes (B–D) of using its thermal power for storage charging. The water tank has first priority in order to cover DHW and SH demands. Additional solar yield is stored in the PCM. An additional subroutine for charging individual units of the PCM heat storage was found useful during functionality tests [41]. When all PCM units are fully charged, the water tank is charged until the thermal power of the collector circuit can no longer be transferred and the collector circuit returns to standby. There are three other operating modes (E–G) that are triggered by demand when the collector circuit is in standby and the water tank is insufficiently charged. Discharge of sensible heat from all PCM units has priority to minimize heat losses. SAT crystallization, followed by discharge of stored heat of fusion, is then initialized unit by unit. Auxiliary heating of the water tank takes place when all stores have discharged.

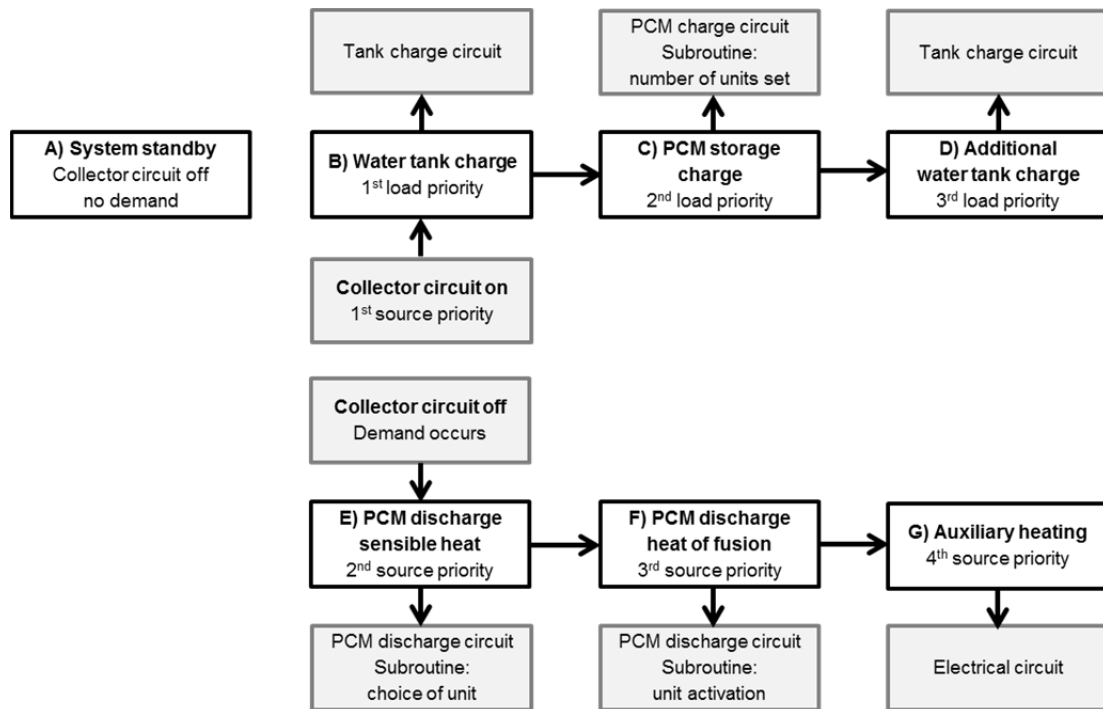


Fig. 3. Diagram of the system control strategy.

4.2. Identified control parameter settings

The applicability of the control strategy was confirmed with data from 4278 hours of automated control in 2016. In 2688 of these hours, measurements were observed in mode A. Operation was set in mode B for 490 hours, in mode C for 500 hours, in mode D for 10 hours, in mode E for 190 hours, and in mode G for 400 hours. Additional water tank charging (mode D) occurred only during sunny periods in summer, while sensible heat discharging from PCM units (mode E) occurred in periods in spring, summer and autumn. Conditions for heat of fusion discharging from PCM units (mode F) were detected in spring and autumn, when sunny periods were followed by several cloudy days.

Threshold conditions and the final configurations of the settings for the 7 modes are presented in Table 3. To avoid too frequent changes of mode, an observation period of five minutes was introduced before mode changes were executed. In this way, activation of auxiliary heating (mode G) resulted in a minimum water tank charge of 0.25 kWh.

All valves (Fig. 3) were closed during system standby. Valves X_1 – X_7 were set in three ways to enable water tank charging, PCM charging, and heat transfer from the PCM to the water tank. HTF flow through the PCM units was enabled by opening valves X_{PCM1} – X_{PCMi} .

Fluctuating collector power and limited heat transfer capacity of individual PCM units were matched by a subroutine. Starting from single unit charging, the next warmest unit was added to the PCM charging circuit when T_{HX_out} exceeded 95 °C. When T_{HX_out} fell below 85 °C, the coldest unit was removed from the PCM charging circuit. Discharging of sensible heat (mode E) and heat of fusion (mode F) were carried out depending on T_{PCM} , i.e. the warmest PCM unit had priority.

For auxiliary heating, the electrical resistor (E_{aux}) was switched on by means of a relay.

Table 3. Summary of threshold conditions and mode settings.

| Operation mode | Threshold conditions | | | Setting |
|---|---|---------------------------------|---|---|
| A) System standby | Tank temperature sufficient | T_{B2} | >45 °C | Valves closed and pumps off |
| | Collector temperature insufficient | T_{coll} | < $T_{B1}+10$ K | |
| B) Water tank charging | Tank temperature insufficient | T_{B2} | ≤50 °C; active mode: ≤60 °C | X_2, X_3, X_6 open $P_{coll} = 7$ L/min $P_{water} = 6.3$ L/min |
| | Collector temperature sufficient | T_{coll} | > $T_{B1}+10$ K; active mode: > $T_{B1}+2$ K; | |
| C) PCM storage charging | Tank temperature sufficient | T_{B2} | >60 °C; active mode: >50 °C; | X_1, X_3, X_5 open $P_{coll} = 19$ L/min $P_{PCM} = 16.5$ L/min Subroutine parallel charge: Warmest unit priority: X_{PCM1} – X_{PCMi} set If $T_{HX_OUT} >95$ °C: next warmest unit open If $T_{HX_OUT} >85$ °C: coldest unit closed When T_{PCM} unit >80 °C: unit closed |
| | Collector temperature sufficient for PCM charge | T_{coll} | >70 °C | |
| | Solar radiation sufficient or Hot collector | G_{total} OR T_{coll} | >150 W/m ² or $T_{coll} >85$ °C | |
| | Modules not fully charged | T_{PCM1} – T_{PCMi} | <80 °C | |
| D) Additional water tank charging | Collector temperature sufficient | T_{coll} | > $T_{B1}+10$ K; active mode: > $T_{B1}+2$ K; | X_2, X_3, X_6 open $P_{coll} = 7$ L/min $P_{water} = 6.3$ L/min |
| | Modules fully charged | T_{PCM1} – T_{PCMi} | >80 °C | |
| E) PCM discharge of sensible heat | Tank temperature insufficient | T_{B2} | <45 °C | X_4, X_5, X_7 open $P_{PCM} = 2$ L/min Subroutine choice of unit: Warmest unit priority: X_{PCM1} – X_{PCMi} set When T_{PCM} unit <50 °C: unit closed Repetition with next warmest unit |
| | Collector temperature insufficient | T_{coll} | < T_6+10 K | |
| | Sensible heat in modules | T_{PCM1} – T_{PCMi} | >50 °C | |
| F) PCM discharge of heat of fusion | Tank temperature insufficient | T_{B2} | <45 °C | X_4, X_5, X_7 open $P_{PCM} = 2$ L/min Subroutine unit activation: Warmest unit priority: X_{PCM1} – X_{PCMi} set When T_{PCM} unit <50 °C: unit closed Repetition with next warmest unit |
| | Collector temperature insufficient | T_{coll} | < $T_{B1}+10$ K | |
| | Sensible heat in modules | T_{PCM1} – T_{PCMi} | <50 °C | |
| G) Auxiliary heating | Tank temperature insufficient | T_{B2} | <45 °C | Valves closed and pumps off E_{aux} on |
| | Collector temperature insufficient | T_{coll} | < $T_{B1}+10$ K | |
| | Sensible heat in modules | T_{PCM1} – T_{PCMi} | <50 °C | |
| | Top tank temperature below | T_{B3} | <50 °C | |

4.3. Combined charge of water tank and PCM units

Data from 11th April 2016, a day with clear sky, shows how mode B and mode C with its subroutines were combined for efficient storage charging. The water tank was charged for 2.5 hours and the PCM heat storage for 7.5 hours.

Fig. 5 shows measurements of G_{total} and HTF flow rates to the water tank and the PCM units over the course of the day. The sun shone on the collector array from 6:10 am to 5:00 pm. At 7:15 am, when the collector outlet temperature was high enough ($T_{B3}+10$ K), water tank charging started. T_{coll} fell immediately, so the circulation stopped after 5 min (observation period for mode changes). From 7:30 am, the water tank was continuously charged until 9:30 am, when T_{B2} reached 60 °C and PCM charging was activated. Flow rates ranged from 0.95 m³/h with one PCM unit to 1.02 m³/h when three units were being charged in parallel. PCM unit charging stopped 10 min after the collector array was shaded, and therefore the charging circuit cooled down ($T_{\text{HX}} < 70$ °C).

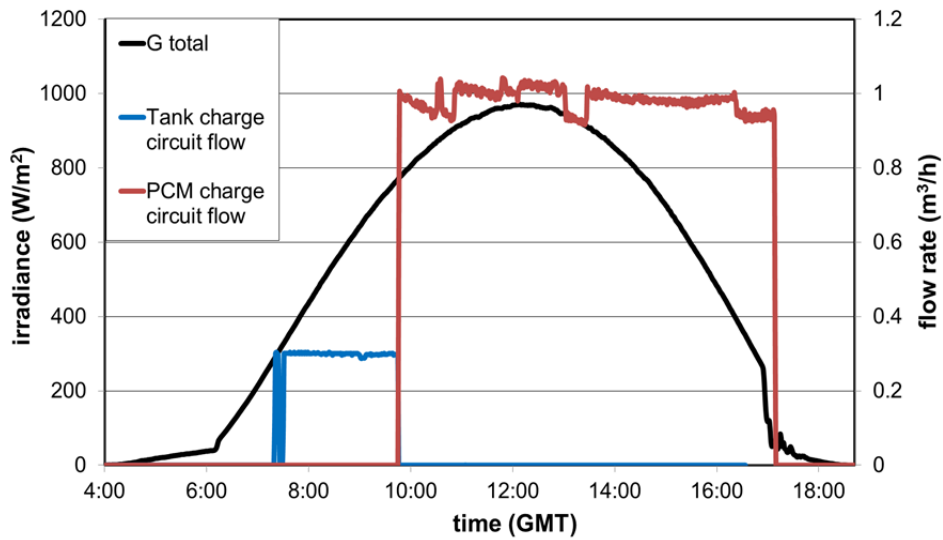


Fig. 4. Dependence of HTF flow to water tank and PCM storage on solar irradiation.

The development of T_{coll} depends on charging settings, as shown in Fig. 6, where periods of water tank charging are marked in blue, charging of a single PCM unit (different ones) in orange, two PCM units in red, and three PCM units in green. Initial water tank charging required a collector outlet temperature of 35 °C ($T_{B3}=25$ °C). After 7:30 am, solar irradiance was high enough to heat the HTF continuously. The water tank was sufficiently charged when T_{coll} reached 65 °C. After the circuit was stopped for 5 min, T_{coll} rose to 70 °C and PCM storage charging mode started. At 10:30 am, T_{HX} reached 95 °C (T_{coll} was at 97 °C) and a second PCM unit was added to the charging circuit. It was removed when T_{HX} fell to 85 °C. In this way the subroutine made sure that the HTF fluid temperature was high enough to achieve stable supercooling of SAT but boiling was avoided. Between 11:00 am and 4:00 pm, merely two PCM units were charged in parallel. Three PCM units were charged only between 12:50 and 1:00 pm. Units 1 and 2 reached full charge at 13:00 h, while the PCM in units 3 and 4 was partly melted at the end of the day.

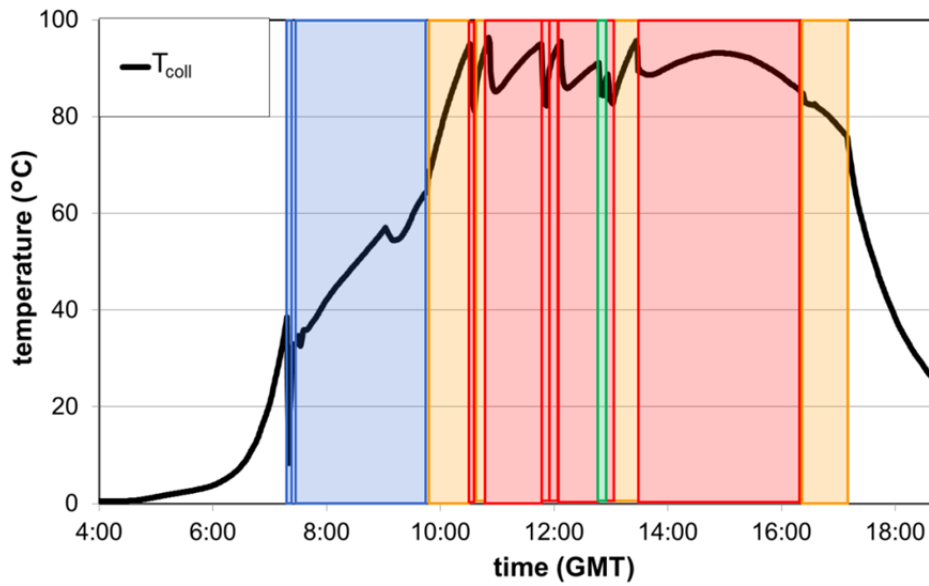


Fig. 5. Dependence of T_{coll} on storage charging configuration.

Fig. 7 shows the thermal power of the collector circuit (black marks), and heat transfer rates to the water tank (blue marks) and to the PCM heat storage (red marks). The collector circuit power reached peak values of up to 22 kW when PCM units were added to the charging circuit. The water tank was situated near the HX, so heat transfer rates to the water tank closely followed the collector circuit's thermal power. During charging of the PCM units, greater heat losses resulted due to higher HTF temperatures and longer pipework. During the course of the day, 82 kWh of heat was transferred from the collector circuit to the heat stores: 13.5 kWh to the water tank and 62 kWh to the PCM storage. Pipe heat losses (from the HX to the stores) amounted to 6.5 kWh.

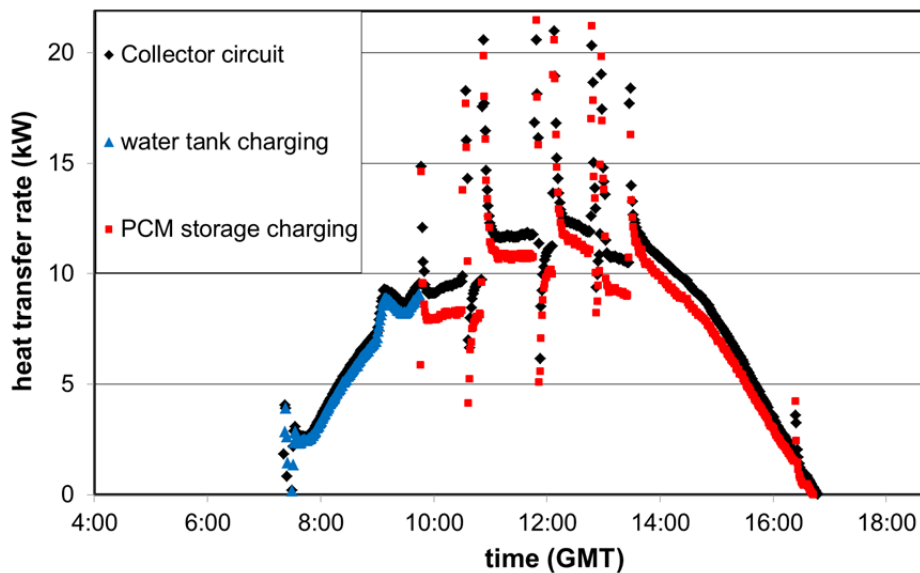


Fig. 6. Heat transfer rated during the course of a day with clear sky.

4.4. Short and long-term heat storage

Fig. 8 presents a test sequence of the combined short and long-term heat storage. It shows hourly averaged values of heat transfer to/from the PCM heat storage and the T_{PCM} for three units. During automated control, the units were frequently charged with solar heat. Heat transfer rates indicated that from 27th to 30th April, and on 5th May, part of the stored heat was transferred to the water tank. On 1st May, the PCM units reached full charge after noon. Over the following three days, heat losses were compensated by re-charging. Negative heat transfer rates resulted when PCM charging (mode C) was activated with $T_{PCM} > 70$ °C. The same situation occurred before mode C was deactivated as the PCM charging circuit cooled down due to decreasing collector power. The threshold values applied were chosen to avoid frequent interruption of PCM charging during partly cloudy days.

The collector array was covered from 6th May. The three PCM units cooled down passively. The units rested for 10, 16 and 17 days respectively before solidification of SAT was manually activated and heat of fusion (mode F) was discharged.

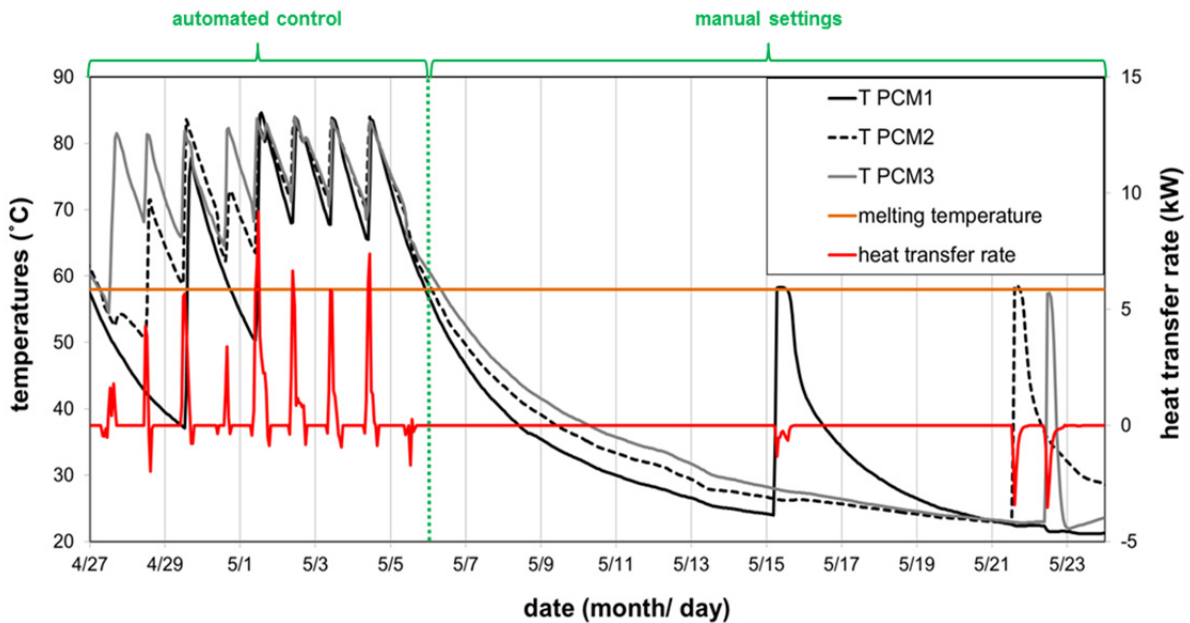


Fig. 7. PCM unit temperatures and heat transfer rates during charging and discharging in May 2016.

4.5. System behaviour during selected periods

Fig. 9 shows system behaviour during a sunny period of eight days in March, when five different operation modes occurred. At the beginning of the period, auxiliary heating was needed to enable DHW and SH supply. On 16th March, T_{B2} reached 60 °C during water tank charging, so mode C was activated. PCM storage charging was interrupted once by repeated water tank charging in the afternoon. During mode shifts, and when PCM units were added or removed from the PCM charging circuit, heat transfer rates of up to 36 kW were measured. During the following days, water tank charging was typically followed by charging of the PCM units. Mode E was activated to transfer heat from the PCM units to the water tank when the collector array could not fully cover the heat demand. On 22nd and 23rd March, the water tank was mainly heated in this way.

Fig. 10 shows system behaviour in October, when only DHW was in demand. Six different operation modes occurred during a rather cloudy period of 12 days. On the 1st and from 4th to 8th October, collector thermal power was sufficient to cover the demand with solar heat. Excess heat was stored in PCM units. On 5th October, additional water storage charging (mode D) implied full PCM unit charge. From 2nd to 4th and from 9th to 11th October, DHW demand was merely covered by heat transfer from PCM units to the water tank. Interrupted flows of 2 L/min ensured high HTF temperatures to the water tank. Heat transfer rates were below 6 kW. On the 4th and from 10th October, auxiliary heating was needed to achieve hot water temperatures above 45 °C. Thanks to the control strategy, the mismatch of heat supply and DHW demand was bridged for several days. It can be assumed that auxiliary heating could have been avoided during the entire period if stored heat of fusion had been used (mode F).

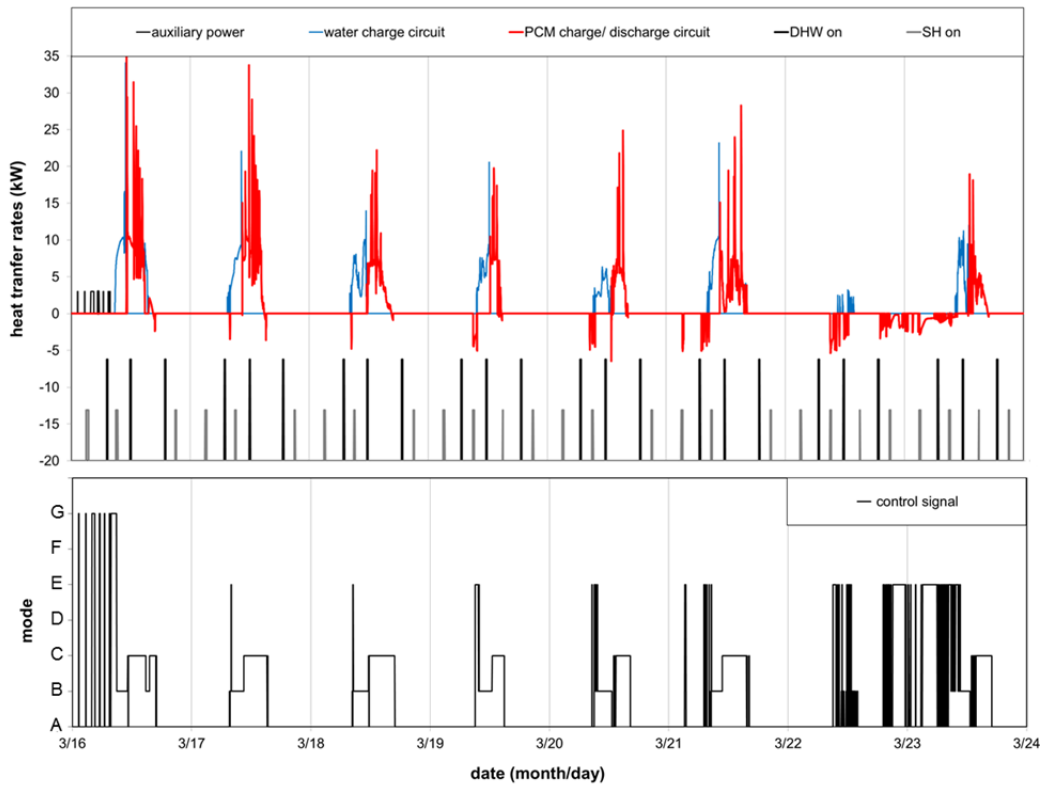


Fig. 8. Storage heat transfer, SH and DHW demand patterns, and system control signals in March 2016.

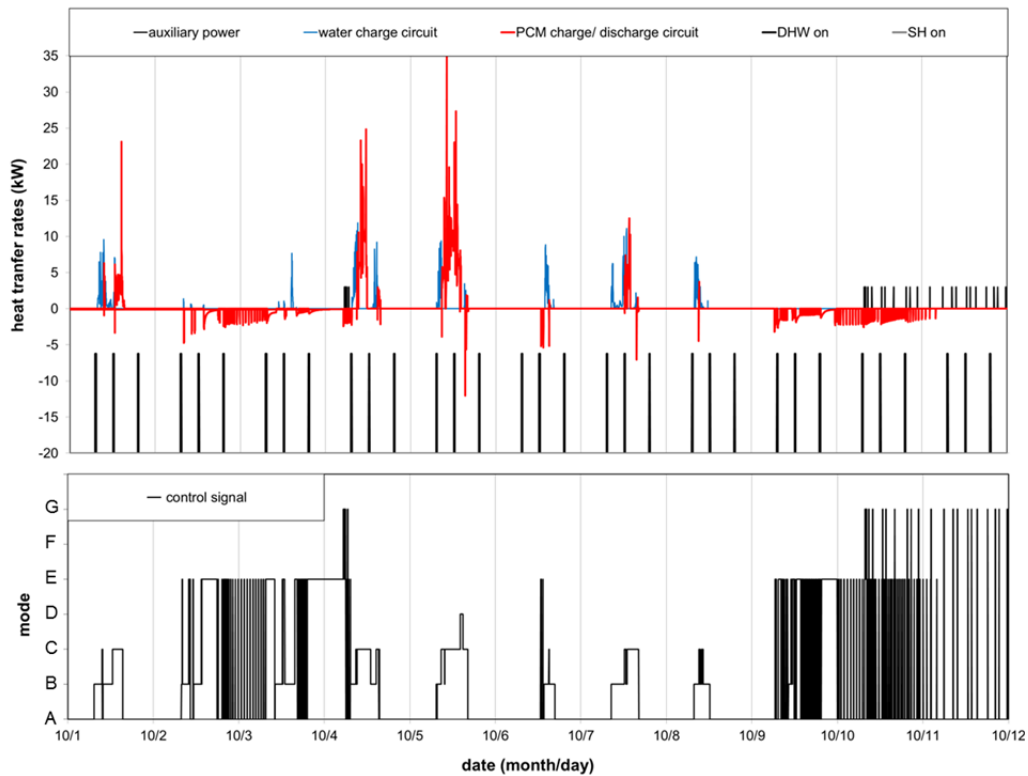


Fig. 9. Storage heat transfer, DHW demand patterns and system control signals in October 2016.

5. Conclusions

For the first time, a laboratory solar combi-system with tubular collectors and a segmented PCM heat storage prototype was successfully demonstrated in a Danish Passive House scenario. The following progress of technology development was achieved:

- a) A control strategy with seven modes enabling automated system operation. With validated control parameter settings, the system worked in the following way:
 - Hydraulic circuits and flow rates were set to charge first the water tank and then the PCM heat storage
 - The number of PCM units was varied during charging to match their limited heat transfer capacity with the fluctuating collector power
 - Additional water tank charging took place once all PCM units were fully charged
 - When heat demands were not covered by the solar collectors, heat was transferred from the PCM units (the warmest first) to the water tank
 - After all the PCM units were discharged below 50 °C, electrical heating of the water tank ensured space heating and hot water supply.

A mode for discharging heat of fusion on demand was included in the control strategy. Automated PCM unit activation (the warmest unit first) is followed by heat transfer to the water tank with a flow rate of 2 L/min.

- b) Automated system operation showed that the PCM units, containing SAT, were frequently charged and discharged in spring and autumn. This proved that compact PCM heat stores for combined short and long-term heat storage can be built with an effective energy storage density of 48 kWh/m³.
- c) The applicability of the system was analysed: Heat transfer fluid temperatures closely followed the collector outlet temperature during water tank charging and were kept between 70 and 95 °C during PCM unit charging to ensure good heat transfer to the SAT composites. During continuous operation, heat transfer rates were below 16 kW, but reached peaks up to 36 kW when PCM units were added to the charging circuit. A flow rate of 2 L/min ensured high HTF temperatures when heat was transferred from PCM units to the water tank. An observation period of five minutes was proved a practical way to avoid frequent mode changes. The system prototype could be improved by shortening pipework lengths to reduce heat losses during heat storage charging and discharging. Control logic to avoid PCM units cooling during charging should be considered.

Based on this work, the full potential of the system could be explored in the future without the restrictions of the demonstrator by using simulation models and calculating the annual thermal performance of the system in a variety of application scenarios.

Acknowledgements

This research was funded by the European Commission (Grant Agreement N_ 295568) as part of the Seventh Framework Programme of the European Community for Research, Technological Development and Demonstration Activities under the “Collaborative Project” funding scheme through the COMTES consortium. The work was also supported by the PhD program of the Sino Danish Center for Education and Research (SDC). We thank Mark Dannemand and the DTU research technicians Troels V. Kristensen and Claus Aagaard for their practical support.

References

- [1] Weiss W. (Ed.), *Solar Heating Systems for Houses, a Design Handbook for Solar Combisystems*, James & James Ltd., UK, 2003.
- [2] W. Streicher, R. Heimrath, C. Bales, *Analysis of System Reports of Task 26 for Sensitivity of Parameters*, 2003 (revised February 2007). <http://www.iea-shc.org/task26>.
- [3] E. Andersen, *Solar Combi Systems*, PhD thesis, Technical University of Denmark, Department of Civil Engineering report no. R-156, 2007.
- [4] S. Furbo, E. Andersen, A. Thür, L.J. Shah, K.D. Andersen, Performance improvement by discharge from different levels in solar storage tanks, *Sol. Energy*. 79 (2005) 431–439. doi:10.1016/j.solener.2005.01.005.
- [5] L.J. Shah, E. Andersen, S. Furbo, Theoretical and experimental investigations of inlet stratifiers for solar storage tanks, *Appl. Therm. Eng.* 25 (2005) 2086–2099. doi:10.1016/j.applthermaleng.2005.01.011.
- [6] M.Y. Haller, E. Yazdanshenas, E. Andersen, C. Bales, W. Streicher, S. Furbo, A method to determine stratification efficiency of thermal energy storage processes independently from storage heat losses, *Sol. Energy*. 84 (2010) 997–1007. doi:10.1016/j.solener.2010.03.009.
- [7] A. Thür, S. Furbo, *Compact solar Combisystem - High Efficiency by Minimizing Temperatures*, Technical University of Denmark, Department of Civil Engineering report no. R-160, 2007.
- [8] L.F. Cabeza, L. Miró, E. Oró, A. de Gracia, V. Martin, A. Krönauer, C. Rathgeber, M.M. Farid, H.O. Paksoy,

- M. Martínez, A.I. Fernández, CO₂ mitigation accounting for Thermal Energy Storage (TES) case studies, *Appl. Energy*. 155 (2015) 365–377. doi:10.1016/j.apenergy.2015.05.121.
- [9] S. Colclough, T. McGrath, Net energy analysis of a solar combi system with Seasonal Thermal Energy Store, *Appl. Energy*. 147 (2015) 611–616. doi:10.1016/j.apenergy.2015.02.088.
- [10] W. Kramer, A. Oliva, G. Stryi-Hipp, S. Kobelt, D. Bestenlehner, H. Drück, J. Bühl, G. Dasch, Solar-active-houses - Analysis of the building concept based on detailed measurements, *Energy Procedia*. 48 (2014) 895–903. doi:10.1016/j.egypro.2014.02.103.
- [11] A. Oliva, G. Stryi-Hipp, S. Kobelt, D. Bestenlehner, H. Drück, G. Dasch, Solar-Active-Houses - Dynamic System Simulations to Analyze Building Concepts with High Fractions of Solar Thermal Energy, *Energy Procedia*. 70 (2015) 652–660. doi:10.1016/j.egypro.2015.02.173.
- [12] A. Ristić, S. Furbo, C. Moser, H. Schranzhofer, A. Lazaro, M. Delgado, C. Peñalosa, L. Zalewski, G. Diarce, C. Alkan, S.N. Gunasekara, T. Haussmann, S. Gschwander, C. Rathgeber, H. Schmit, C. Barreneche, L. Cabeza, G. Ferrer, Y. Konuklu, H. Paksoy, H. Rammelberg, G. Munz, T. Herzog, J. Jänchen, E.P. del Barrio, IEA SHC Task 42 / ECES Annex 29 WG A1: Engineering and Processing of PCMs, TCMs and Sorption Materials, *Energy Procedia*. 91 (2016) 207–217. doi:10.1016/j.egypro.2016.06.205.
- [13] B. Zettl, G. Englmaier, G. Steinmaurer, Development of a revolving drum reactor for open-sorption heat storage processes, *Appl. Therm. Eng.* 70 (2014) 42–49. doi:10.1016/j.applthermaleng.2014.04.069.
- [14] C. Reichl, D. Lager, G. Englmaier, B. Zettl, M. Popovac, Fluid dynamics simulations for an open-sorption heat storage drum reactor based on thermophysical kinetics and experimental observations, *Appl. Therm. Eng.* 107 (2016) 994–1007.
- [15] R. Köll, W. van Helden, G. Engel, W. Wagner, B. Dang, J. Jänchen, H. Kerskes, T. Badenhop, T. Herzog, An experimental investigation of a realistic-scale seasonal solar adsorption storage system for buildings, *Sol. Energy*. 155 (2017) 388–397. doi:10.1016/j.solener.2017.06.043.
- [16] G. Engel, S. Asenbeck, R. Köll, H. Kerskes, W. Wagner, W. van Helden, Simulation of a seasonal, solar-driven sorption storage heating system, *J. Energy Storage*. 13 (2017) 40–47. doi:10.1016/j.est.2017.06.001.
- [17] X. Daguene-Frick, P. Gantenbein, J. Müller, B. Fumey, R. Weber, Seasonal thermochemical energy storage: Comparison of the experimental results with the modelling of the falling film tube bundle heat and mass exchanger unit, *Renew. Energy*. 110 (2016) 162–173. doi:10.1016/j.renene.2016.10.005.
- [18] B. Fumey, R. Weber, L. Baldini, Liquid sorption heat storage – A proof of concept based on lab measurements with a novel spiral fined heat and mass exchanger design, *Appl. Energy*. 200 (2017) 215–225. doi:10.1016/j.apenergy.2017.05.056.
- [19] S. Bonk, H. Drueck, Development and Testing of a Thermo-Chemical Energy Store - Results of a Five-Year Research Project, *Proc. SWC2017/SHC2017*. (2017) 1–10. doi:10.18086/swc.2017.13.01.
- [20] T. Nonnen, S. Beckert, K. Gleichmann, A. Brandt, B. Unger, H. Kerskes, B. Mette, S. Bonk, T. Badenhop, F. Salg, R. Gläser, A Thermochemical Long-Term Heat Storage System Based on a Salt/Zeolite Composite, *Chem. Eng. Technol.* 39 (2016) 2427–2434. doi:10.1002/ceat.201600301.
- [21] J. Pereira da Cunha, P. Eames, Thermal energy storage for low and medium temperature applications using phase change materials - A review, *Appl. Energy*. 177 (2016) 227–238. doi:10.1016/j.apenergy.2016.05.097.
- [22] D. Zhou, C.Y. Zhao, Y. Tian, Review on thermal energy storage with phase change materials (PCMs) in building applications, *Appl. Energy*. 92 (2012) 593–605. doi:10.1016/j.apenergy.2011.08.025.
- [23] A. Sharma, V. V Tyagi, C.R. Chen, D. Buddhi, Review on thermal energy storage with phase change materials and applications, *Renew. Sustain. Energy Rev.* 13 (2009) 318–345. doi:10.1016/j.rser.2007.10.005.
- [24] J. a. Quinnell, J.H. Davidson, Heat and mass transfer during heating of a hybrid absorption/sensible storage

tank, *Sol. Energy*. 104 (2014) 19–28. doi:10.1016/j.solener.2013.07.035.

- [25] J. Xu, R.Z. Wang, Y. Li, A review of available technologies for seasonal thermal energy storage, *Sol. Energy*. 103 (2013) 610–638. doi:10.1016/j.solener.2013.06.006.
- [26] T. Kousksou, P. Bruel, a. Jamil, T. El Rhafiki, Y. Zeraoui, Energy storage: Applications and challenges, *Sol. Energy Mater. Sol. Cells*. 120 (2014) 59–80. doi:10.1016/j.solmat.2013.08.015.
- [27] B. Zalba, J.M. Marín, L.F. Cabeza, H. Mehling, Review on thermal energy storage with phase change: materials, heat transfer analysis and applications, *Appl. Therm. Eng.* 23 (2003) 251–283.
- [28] N. Araki, M. Futamura, A. Makino, H. Shibata, Measurements of Thermophysical Properties of Sodium Acetate Hydrate, *Internatlonal J. Thermophys.* 16 (1995) 1455–1466.
- [29] M.A. Rogerson, S.S.S. Cardoso, Solidification in heat packs: I. Nucleation rate, *AIChE J.* 49 (2003) 505–515. doi:10.1002/aic.690490220.
- [30] G. Englmaier, Y. Jiang, M. Dannemand, C. Moser, H. Schranzhofer, S. Furbo, J. Fan, Crystallization by local cooling of supercooled sodium acetate trihydrate composites for long-term heat storage, *Energy Build.* 180 (2018) 159–171. doi:10.1016/j.enbuild.2018.09.035.
- [31] G.A. Lane, *Solar heat storage latent heat material Vol 1*, CRC, Boca Raton, Florida, United states, 1986.
- [32] J.M. Schultz, S. Furbo, Investigation of heat of fusion storage for solar low energy buildings, *Proc. Sol. World Congr. 2005 Bringing Water To World, Incl. Proc. 34th Ases Annu.* 3 (2005) 1833–1838.
- [33] J.M. Marin, B. Zalba, L.F. Cabeza, H. Mehling, Determination of enthalpy temperature curves of phase change materials with the temperature-history method: improvement to temperature dependent properties, *Meas. Sci. Technol.* 14 (2003) 184–189. doi:10.1088/0957-0233/14/2/305.
- [34] M. Dannemand, M. Delgado, A. Lazaro, C. Penalosa, C. Gundlach, C. Trinderup, J.B. Johansen, C. Moser, H. Schranzhofer, S. Furbo, Porosity and density measurements of sodium acetate trihydrate for thermal energy storage, *Appl. Therm. Eng.* 131 (2018) 707–714. doi:10.1016/j.applthermaleng.2017.12.052.
- [35] H. Kimura, J. Kai, Phase change stability of sodium acetate trihydrate and its mixtures, *Sol. Energy*. 35 (1985) 527–534. doi:10.1016/0038-092X(85)90121-5.
- [36] W. Kong, M. Dannemand, J.B. Johansen, J. Fan, J. Dragsted, G. Englmaier, S. Furbo, Experimental investigations on heat content of supercooled sodium acetate trihydrate by a simple heat loss method, *Sol. Energy*. 139 (2016) 249–257. doi:10.1016/j.solener.2016.09.045.
- [37] M. Dannemand, J.B. Johansen, S. Furbo, Solidification behavior and thermal conductivity of bulk sodium acetate trihydrate composites with thickening agents and graphite, *Sol. Energy Mater. Sol. Cells*. 145 (2016) 287–295. doi:10.1016/j.solmat.2015.10.038.
- [38] M. Dannemand, J. Dragsted, J. Fan, J.B. Johansen, W. Kong, S. Furbo, Experimental investigations on prototype heat storage units utilizing stable supercooling of sodium acetate trihydrate mixtures, *Appl. Energy*. 169 (2016) 72–80. doi:10.1016/j.apenergy.2016.02.038.
- [39] M. Dannemand, J.B. Johansen, W. Kong, S. Furbo, Experimental investigations on cylindrical latent heat storage units with sodium acetate trihydrate composites utilizing supercooling, *Appl. Energy*. 177 (2016) 591–601. doi:10.1016/j.apenergy.2016.05.144.
- [40] J. Deng, S. Furbo, W. Kong, J. Fan, Thermal performance assessment and improvement of a solar domestic hot water tank with PCM in the mantle, *Energy Build.* 172 (2018) 10–21. doi:10.1016/j.enbuild.2018.04.058.
- [41] G. Englmaier, C. Moser, S. Furbo, M. Dannemand, J. Fan, Design and functionality of a segmented heat-storage prototype utilizing stable supercooling of sodium acetate trihydrate in a solar heating system, *Appl. Energy*. 221 (2018) 522–534. doi:10.1016/j.apenergy.2018.03.124.

- [42] J. Dragsted, S. Furbo, M. Dannemand, F. Bava, Thermal stratification built up in hot water tank with different inlet stratifiers, *Sol. Energy*. 147 (2017) 414–425. doi:10.1016/j.solener.2017.03.008.
- [43] TUV Rheinland/DIN CERTCO, Summary of EN 12975 Test Results , annex to Solar KEYMARK Certificate of Kingspan Thermomax solar collectors, 2011.
- [44] S. Furbo, V. Korsgaard, Varmelagring til solvarmenalæg, Technical University of Denmark, Thermal Insulation Laboratory report no. 162, 1984.
- [45] Passive House Institute, “Passive House Institute.” [Online]. Available: <https://passivehouse.com>. [Accessed: 31-Oct-2018].
- [46] DS 439, Norm for vandinstallationer – Code of Practice for domestic water supply, Danish Standards (2009) 75.

[6] G. Englmair, C. Moser, H. Schranzhofer, J. Fan, and S. Furbo, “A solar combi-system utilizing stable supercooling of sodium acetate trihydrate for heat storage: numerical performance investigation”, *Applied Energy*, vol. 242, pp. 1108–1120, 2019.
<https://doi.org/10.1016/j.apenergy.2019.03.125>

This page is intentionally left blank.

A solar combi-system utilizing stable supercooling of sodium acetate trihydrate for heat storage: numerical performance investigation

Gerald Englmaier^{1,2}, Christoph Moser³, Hermann Schranzhofer³, Jianhua Fan² and Simon Furbo²

¹Sino-Danish Center, University of Chinese Academy of Sciences, 380 Huaibeizhuang, Huairou district, Beijing, China

²Department of Civil Engineering, Technical University of Denmark, Brovej 118, 2800 Kgs. Lyngby, Denmark

³Institute of Thermal Engineering, Graz University of Technology, Inffeldgasse 25/B, 8010 Graz, Austria

Highlights

- On-demand crystallization of sodium acetate trihydrate for heat storage
 - A numerical model was validated with data from system demonstration
 - Sensitivity analysis of solar collector area and heat storage volume
 - Annual solar fraction of 71% with 0.6 m³ water and 1 m³ of PCM for heat storage
 - 1000 kWh of heat supplied by PCM units with 5.5 annual heat storage cycles
-

Abstract

To reduce the energy consumption of buildings significantly, a novel solar combi-system with short and long-term heat storage has been developed. A system prototype with 22.4 m² (aperture) evacuated tubular collectors, a 735 L water tank and 4 phase change material (PCM) units each containing 150 L sodium acetate trihydrate composite has been built. Experimental investigation has shown advantages of utilization of stable supercooling of sodium acetate trihydrate in spring and autumn. In this paper, a newly developed numerical model was used to investigate the performance potential of the system with combined utilization of the water tank and the PCM units, including on-demand crystallization of supercooled sodium acetate trihydrate composites. PCM units, the water tank and the collector circuit models were validated with measurement data from system demonstration. Space heating and hot water demand patterns of a Danish single-family Passive House with a yearly heat demand of 3723 kWh were applied. Results showed that a 56% annual solar fraction of heat supply was achieved with the prototype specifications. A 69% solar fraction could be achieved with an optimized scenario including a 15% increased hot water demand. Sensitivity analysis of component sizing showed that PCM units of 200 L can be more efficiently used with a 0.6 m³ water tank. Optimal solar collector array tilt was 70°. Aperture areas between 12.8 and 22.4 m² were found adequate for frequent utilization of a PCM volume up to 1 m³. Thus, the PCM heat storage capacity could be utilized at least 5.5 times a year. With a 22.4 m² collector area and 5 PCM units of 200 L each, a solar fraction of 71% was calculated for the annual heat supply. Assuming full charge of a 0.6 m³ water tank and 2.8 m³ of sodium acetate trihydrate composite by electricity at the beginning of the year, the system could run 18 days without need for auxiliary heating. Thus, in periods without solar collector power available, generation maxima of wind power could be utilized. In conclusion, building heat demand could be covered close to 100% by renewable energy resources.

Keywords: Solar heating system; phase change material; sodium acetate trihydrate; stable supercooling; Passive House; numerical simulation.

Nomenclature

Symbols

| | |
|--------------------|--|
| A | collector array aperture area (m ²) |
| C | heat capacity (kWh) |
| G _{total} | global irradiance; collector plane (W/m ²) |
| I | collector array inclination (°) |
| N _{cycle} | number of storage cycles per year (-) |
| Q | thermal energy, heat (kWh) |
| \dot{Q} | heat transfer rate (kW) |
| \dot{Q}_{coll} | collector power at the heat exchanger (kW) |
| q _{coll} | specific solar yield (kWh/m ²) |
| t | time (s) |
| T | temperature (°C) |
| V | Volume (m ³) |
| \dot{V} | volume flow rate (L/min) |

Subscripts

| | |
|-----------|--------------------|
| aux | auxiliary |
| coll | collector outlet |
| charge | charge |
| cycle | cycles per year |
| DHW | domestic hot water |
| discharge | discharge |
| flow | flow temperature |

| | |
|--------|-------------------------------|
| meas | measured value |
| out | outlet line |
| PCM | phase change material |
| return | return temperature |
| sec | secondary circuit |
| SH | space heating |
| sim | simulation value |
| solar | net utilized solar energy |
| total | total, on the collector plane |
| water | water tank |

Abbreviations

| | |
|--------|----------------------------------|
| DHW | domestic hot water |
| E | electrical heating element |
| HTF | heat transfer fluid |
| IAM | incidence angle modifier |
| PCM | phase change material |
| REF | renewable energy fraction |
| SF | solar fraction of heat supply |
| SAT | sodium acetate trihydrate |
| SH | space heating |
| TRNSYS | transient system simulation tool |

1. Introduction

1.1. Concepts for high solar fractions of building heat supply

In Europe, the energy consumption in buildings accounts for 40% of the total energy supply [1]. Since heating accounts for the largest share of this consumption, a near-zero energy consumption is required from all new buildings by the EU Energy Performance of Buildings Directive in 2010 [2] from 31st December 2020.

Solar combi-systems for space heating (SH) and domestic hot water (DHW) supply can contribute to achieve this goal by heat generation, storage and supply in buildings [3]. The biggest challenge is the mismatch between availability of solar resources and heat demands. Lower operation temperatures of collector circuit and heat storage and low heat storage losses by compact system design have been identified as key factors for well-performing systems [4], [5]. Thus, solar fraction (SF) of heat supply (net utilized solar energy divided by SH and DHW demand) can be improved.

To achieve high SF, energy-efficient building envelopes and optimal DHW supply temperatures are the basis. The Danish code of practice for domestic water supply, DS 439 [6], recommends a hot water temperature of 45 °C as sufficient to fulfil comfort requirements. To utilize solar irradiation during the heating season, a relatively large collector area is required as well as optimization of the collector tilt, which depends on the latitude [7].

In Germany, energy-efficient “solar active houses” with large solar collector arrays and water stores, enabling solar fractions close to 100%, have been reported [8]. To achieve well-performing solar combi-systems with moderate collector area and more compact heat storage, long-term heat storage concepts have been tested: Sorption systems with zeolites or composites of zeolite and salt as storage material could store solar heat during summer for heat supply in winter [9]. Open reactors have been demonstrated in laboratory scale [10]. Zettl et al. have developed a process with solar air collectors for regeneration of zeolite pebbles [11], which can be utilized for heat supply via a rotating drum-reactor [12]. A closed sorption system utilizing flat plate collectors for regeneration of zeolites achieved a solar fraction of 83.5% during laboratory testing in winter [13]. Evacuated tubular solar collectors can be used for regeneration in a liquid sorption heat storage with sodium hydroxide [14], the concept was recently proved by Fumey et al. [15]. Phase change materials (PCM) are applicable in low and medium temperature applications [16], where a high potential for building applications was found [17]. PCM with optimized melting temperatures can be utilized as passive thermal energy storage in the building envelope, leading to notable reduction of heat demand [18]. PCM could be also utilized in a photovoltaic/ thermal system to increase electrical and thermal energy efficiency [19] and to prevent thermal systems from freezing in winter [20].

Sodium acetate trihydrate (SAT), a salt hydrate with a melting temperature of 58 °C, has the ability to supercool stably to ambient temperatures while preserving its heat of fusion [21], [22]. It is therefore considered as PCM for the investigated solar system due to its capability for long-term heat storage.

Rathgeber et al. [23] made a top-down evaluation of acceptable costs of energy stores for buildings, based on their energy storage capacity. Results imply that long-term heat storage concepts are only economically attractive when applications enable a certain number of annual storage cycles. The number mainly depends on costs for storage material, container and heat exchanger.

In general, PCM heat stores and thermochemical processes for long-term heat storage are assumed to be more expensive than heat storage by water tanks. To achieve the optimal number of annual heat storage cycles, integration into a future energy system should be considered. For example, energy storage with PCM can help to overcome the

mismatch between renewable electricity generation and hot water, heating and cooling demand [24]. Wind as the most dominant contributor to renewable power generation is stronger during winter than in summer across Europe [25]. Because of occurring overproduction of wind turbines in windy periods, it is economically attractive to integrate wind power into the heat market in Denmark, so the excess wind power can be consumed for heating of buildings [26]. Solar combi-systems could become more attractive when collector arrays are sized for optimal annual yield, avoiding stagnation periods, and cheap electricity is stored in long-term heat storages, allowing year-round heat supply with renewable energy sources.

1.2. *Heat stores utilizing stable supercooling of SAT*

The latent heat of fusion of pure SAT has been determined to be 264 kJ/kg [27]. To overcome phase separation of the incongruently melting salt, full dissolving of sodium acetate in its crystal water can be achieved by adding extra water [28] and by avoiding water concentration differences in large volumes containing SAT in liquid phase [29]. To achieve stable SAT compositions and to avoid the need for mechanical mixing of melted SAT, thickening agents and liquid additives have been applied and tested for their thermal conductivity [30], porosity and density [31] and heat content in supercooled state [32]. Crystallization of supercooled SAT composites can be either initialized by seed crystal injection [22], [33] or by local cooling to temperatures below $-15\text{ }^{\circ}\text{C}$ [34].

Different concepts have been developed to overcome heat transfer restriction of solid PCM in domestic heat stores. Commercially available heat exchangers for use in PCM heat stores were evaluated by Medrano et al. [35]. Internal tube bundle heat exchangers were tested in a large PCM container [36]. Another way was to realize sensible-latent heat storage with macro-encapsulated PCM in water vessels [37] or shell-and-tube heat exchangers with PCM filling [38].

Zhou and Xiang [39] tested rectangular and slim cylindrical vessels containing SAT composites with extra water and with carboxymethyl cellulose. They reported engineering challenges to achieve stable supercooling. Those challenges have been addressed previously by designing flat [40] and cylindrical [41] heat storage prototypes. Stable supercooling was enabled by avoidance of pressure changes in the PCM container, smooth inner container surfaces and heat up of the whole material volume to a minimum temperature of $77\text{ }^{\circ}\text{C}$. Also application of SAT in the mantle of hot water tanks was tested [42].

1.3. *Development of a novel solar combi-system*

In previous work at the Technical University of Denmark (DTU), it was investigated how heat stores utilizing stable supercooling of SAT could be used for solar heating in buildings (a-c):

- a) As a pre-study in 2015, Dannemand et al. [43] simulated an application in a standard-size Passive House in Danish climate. A simple energy balance model with SAT properties from literature [44], was used for the heat storage. The authors found that a system with several individual flat units, forming a segmented PCM heat storage, would work best. Simulations with 10 units, containing in total 1.5 m^3 of SAT, and 36 m^2 flat plate collectors resulted in annual solar fractions of over 75%.
- b) Based on this promising results, a segmented heat storage prototype with four flat PCM units [40], containing 150 L of different SAT composites each and a 735 L water tank was built and tested for utilization in a solar heating system [45]: Functionality tests with an evacuated tubular collector array proved combined short and long-

term heat storage by PCM units. Starting from solid state at room temperature, 27.4 kWh of solar heat was stored in a single PCM unit. Parallel charging of PCM units was necessary to match their limited heat transfer capacity with fluctuating solar collector power. Stored sensible heat was transferred from PCM units to the water tank. Afterwards, SAT composites supercooled stably to room temperature. SAT composite solidification was then initialized by seed crystal injection and 10.4 kWh (80% of heat of fusion) of heat was discharged. Because of heat transfer restrictions a heat transfer fluid (HTF) flow rate of 2 L/min and a final SAT composite temperature of 50 °C needed to be applied to heat a water tank. Therefore 20% of heat of fusion remained in the warm SAT composite and container.

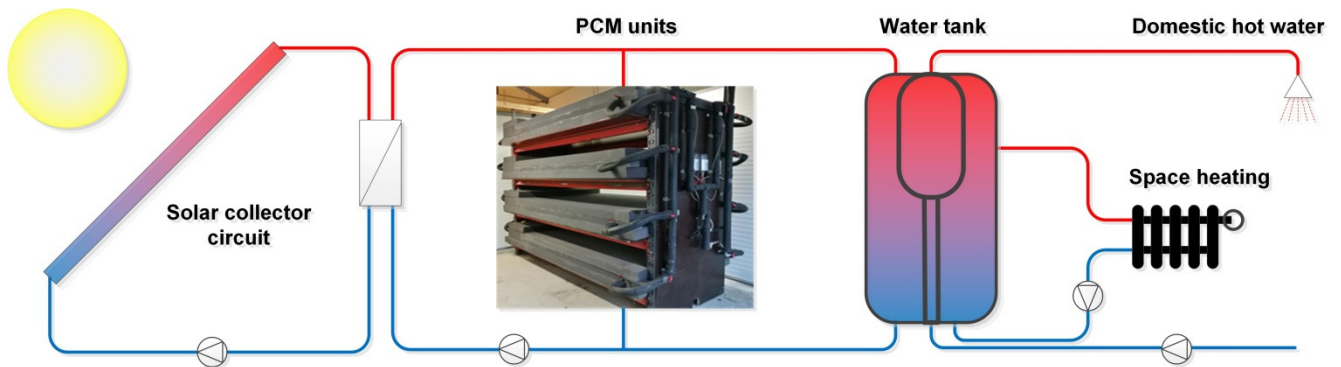


Fig. 1. Diagram of the tested solar combi-system utilizing stable supercooling of SAT.

- c) The prototype was implemented in a solar combi-system with 22.4 m² (aperture) evacuated tubular collectors (Fig. 1). It was demonstrated with SH and DHW demand patterns of a 130 m² Passive House in Danish climate. A strategy for charging [46] and discharging of water tank and PCM units was developed (see section 2). Automated operation was realized by a monitoring system and a control program. Data analysis showed that heat stores were efficiently utilized in spring and autumn 2016. However, SAT composite crystallization needed to be initialized manually, and thus studying the annual system performance was not possible.

1.4. Scope

To the authors' best knowledge, the application potential of recently developed heat stores utilizing stable supercooling of SAT has never been investigated before. Based on the outcome of the previous work (section 1.3), the following gap of knowledge was addressed:

- Annual system performance: On-demand utilization of heat of fusion of SAT has not been possible during automated operation of the developed solar heating system. Full-performance investigation, including possible solar fraction of heat supply, must be thus conducted with a numerical model.
- Development of a realistic system model: In contrary to the pre-study, solar collector array, water tank and PCM units were modelled and validated using data from experimental work. SAT composite properties were implemented in the PCM unit model. System simulation was conducted with an experimentally developed control strategy, considering a hot water supply temperature of 45 °C.
- Sizing of system components: The optimal solar collector area and heat storages volumes are determined by means of sensitivity analysis considering economic aspects.

- Integration into a future energy system: By power-to-heat conversion, buildings will serve as one possible source of demand flexibility in future electrical grids [47]. The demand flexibility of systems utilizing stable supercooling of SAT composites was never investigated before.

Numerical simulation results for full potential analysis of a solar combi-system utilizing stable supercooling of SAT are presented. For this purpose specification of the first system demonstrator of its kind as well as characteristic space heating and hot water demand patterns of a standard-sized Danish Passive House were applied. The performance potential of the system was studied in a scenario without identified restrictions of the system demonstrator.

The goals were to investigate how component sizing influences the solar fraction of the system and which system configurations would be economically attractive. The potential for integration in a future energy system was elucidated in a scenario assuming full storage charge by wind power at the beginning of the year, when no solar collector power was available.

2. Layout and applied control strategy of the system

Settings of seven operation modes (A-G) have been developed and their applicability has been previously demonstrated. Fig. 2 illustrates how the solar combi-system was operated in modes B-F. The following control strategy was applied in the numerical system model:

- System standby (mode A): Water tank coverage is sufficient for DHW and SH supply.
- Water tank charging (mode B, Fig. 2 a): The mode starts when the collector outlet temperature (T_{coll}) is 10 K higher than T_1 and the temperature in the middle of the water tank (T_2) is below 50 °C. During operation, T_{coll} must be at least 2 K higher than the temperature at the bottom of the water tank (T_1). Water tank charging stops when T_2 reaches 60 °C.
- PCM heat storage charging (mode C, Fig. 2 b): A total irradiance on the tilted collector plane (G_{total}) of at least 150 W/m² must be measured or T_{coll} must be at least at 70 °C. The mode starts when T_2 is above 60 °C and it is interrupted by water tank charging (mode B) when T_2 falls below 50 °C. Units with a PCM temperature (T_{PCM}) below 80 °C are subject to charge, where the warmest unit has priority. Charging starts with a single unit, the next warmer unit is charged in parallel if the flow temperature ($T_{\text{sec flow}}$) exceeds 95 °C. When $T_{\text{sec flow}}$ falls below 85 °C, the coldest unit is removed from the charging circuit. The mode stops when the PCM in all units reaches a temperature of at least 80 °C.
- Additional water tank charging (mode D, Fig. 2 a): When all PCM units are fully charged and T_{coll} is 10 K higher than T_1 , additional water tank charging takes place. It stops when T_{coll} is less than 2 K higher than T_1 , or if stagnation conditions occur.
- PCM discharge of sensible heat (mode E, Fig. 2 c): Without collector power available and a temperature at the middle of the tank (T_2) below 45 °C, heat from the warmest PCM unit is transferred to the water tank. When T_{PCM} falls below 50 °C the next warmest unit is discharged. The mode stops when either T_2 reaches 45 °C, or all PCM temperatures become too low.

- PCM discharge of heat of fusion (mode F, Fig. 2 c): When threshold conditions for mode E are reached, but PCM unit temperatures are too low, SAT composite solidification of the warmest, supercooled unit is initialized by means of seed crystal injection. Heat transfer fluid flow starts when T_{PCM} rises to 58 °C. When T_{PCM} is lower than 50 °C, the procedure is repeated with the next warmest, supercooled unit. The mode stops when either T_2 reaches 45 °C, or when all PCM temperatures become too low.
- Auxiliary heating (mode G): When no collector power is available, T_2 and T_3 (top of the tank) are below 45 °C, PCM temperatures are below 50 °C and SAT composites are in solid state, an auxiliary heating element (E_{aux}) is switched on in the water tank. The mode stops when T_3 reaches 45 °C.

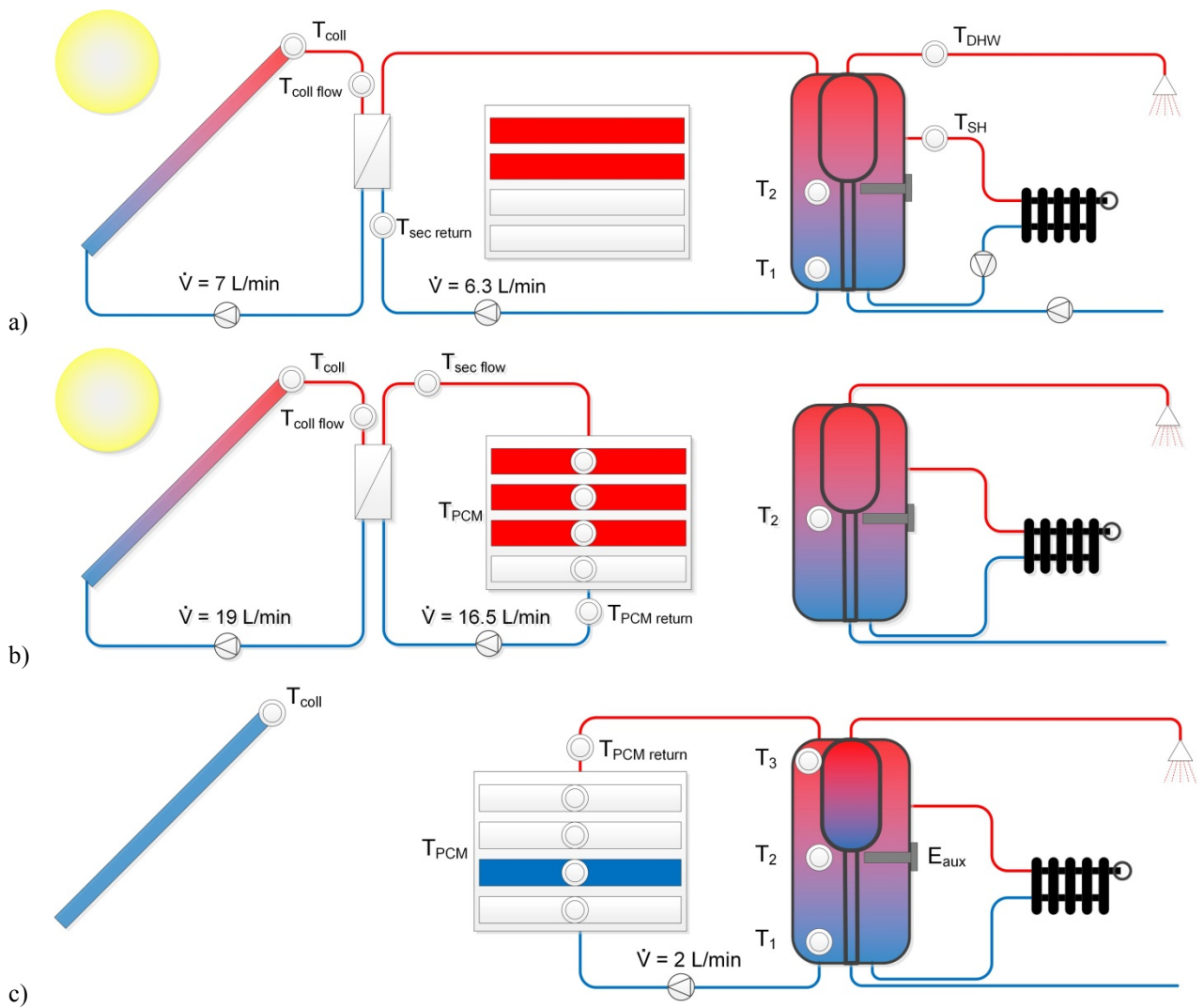


Fig. 2. Diagram of operation schemes: a) Modes B and D; b) Mode C; c) Modes E and F.

3. Method

3.1. System model

A numerical model was built in TRNSYS 17 environment. The water tank model, type 8893, the multiple flat PCM unit model, type 8888 and the controller of PCM units, type 8889, have been previously developed by authors of this article. The system control strategy (section 2) was implemented via the newly developed controller type 8896.

The collector array was modeled with type 538, using specifications of 7 evacuated tubular collector panels, type Thermomax HP 450 from Kingspan Renewables, see Table 1. The parameters in the table are based on the aperture area of the collector.

Table 1. Data from collector panel certification [48].

| | Aperture area (m ²) | Gross area (m ²) | Peak collector efficiency (-) | 1 st order loss coefficient (W/m ² K) | 2 nd order loss coefficient (W/m ² K ²) | Effective heat capacity (kJ/m ² K) |
|----------------------------|---------------------------------|------------------------------|-------------------------------|---|---|---|
| | 3.2 | 4.15 | 0.750 | 1.18 | 0.010 | 4.4 |
| Angle (°) | 10 | 20 | 30 | 40 | 50 | 60 |
| IAM for transversal angle | 1.01 | 1.02 | 1.04 | 1.04 | 0.99 | 0.90 |
| IAM for longitudinal angle | 1.00 | 0.99 | 0.97 | 0.95 | 0.91 | 0.83 |

The water tank model was based on a one-dimensional node approach. An immersed tank, containing domestic water and the outer tank, containing water as heat transfer fluid, were integrated. Domestic hot water tapping was modelled by ports at the bottom and top of the immersed tank. The space heating circuit was integrated via ports at the bottom and at a relative height of 0.67 of the water tank. The total water tank volume varied in simulation scenarios, while the immersed tank volume was fixed with 175 L to ensure sufficient hot water supply. Auxiliary heating was set to a power of 3 kW, located at a relative tank height of 0.5 of the water tank.

The PCM units were modelled with differential equations for heat transfer as well as for enthalpies, solved by an explicit method. A one-dimensional node approach included vertical nodes for SAT composites, steel container, water in heat exchangers and insulation material. HTF flow distribution in PCM unit heat exchangers and initialization of SAT composite solidification was handled by the PCM unit controller model.

The annual space heating profile was loaded from a data file, which was based on hourly heating load calculation, resulting from the weather conditions during system demonstration in 2016. Three times a day (3:00 h, 9:00 h, and 21:00 h), calculated loads were discharged. The dependency of heating loads on solar irradiation and ambient temperature of a 130 m² building in Passive House Standard [49] in Denmark has been previously determined by B. Johansen et al. [50] by simulation of a space heating system.

Daily DHW load profiles (see section 3.3) were implemented via time-dependent forcing functions.

Experimental HTF flow rates were used to simulate heat transfer via hydraulic circuits (Fig. 2). Initial temperature of the outer water tank volume was 45 °C. Inner tank volume, PCM units, and hydraulic components were set to 25 °C. At the beginning of the year, one PCM unit was set to liquid, while the other units were set to solid state. To run system simulations close to application conditions, the following parameter approximations have been made:

- Phase change temperature interval of 55 to 58 °C

- Simulation time-step of one minute
- An observation period of five minutes before mode changes were executed
- Conditions for collector circuit stagnation: $T_{\text{coll}}=130\text{ }^{\circ}\text{C}$; $T_{\text{flow}}=100\text{ }^{\circ}\text{C}$

Minute-based weather data from 2016, measured at the DTU climate station [51], was used for annual system simulation. The collector loop model and the behavior of the system controller were validated with experimental data from system operation in 2016. The annual, global irradiation on a horizontal plane was measured to 1010 kWh/m^2 , similar to the Danish reference year (1038 kWh/m^2). All system simulations were conducted for a year (January 1st – December 31st). Yearly energy balances of the collector circuit heat exchanger, water tank and the PCM heat storage were checked for each simulation.

3.2. Model validation

System tests have been conducted in accordance to the methodology used in functionality tests of the heat storage prototype [39]. Test data have been used to validate the TRNSYS component types used in the current study. For validation, experimental HTF flow rates were applied for system simulation. Resulting HTF temperatures during system tests and simulation were compared in each hydraulic circuit of the system (Fig. 2). Transferred heat, and the development of HTF temperatures were evaluated as follows:

- Collector circuit validation: Measurement data from March 17th – April 28th 2016 were used. During this period the water tank and the PCM heat storage were daily charged with solar heat. Thus, HTF flow rates in the collector circuit and in the charging circuits varied in accordance to the mode B and the mode C (Fig. 2a and Fig. 2b). HTF temperatures close to the heat exchanger ($T_{\text{coll flow}}$) were compared. As for the annual system simulation, weather data of the DTU climate station, located in 150 m distance from the collector array, were applied. As in the prototype scenario (section 3.3), shading of the collector array by surrounding buildings and trees was considered implementing the angular obstruction heights with type 67.
- Water tank model validation: Measurement data from March 15th – March 16th 2016 were used, where only the second day was evaluated to ensure equivalent temperature profiles in the tank. Charging was conducted via the collector circuit in accordance to the mode B (Fig. 2a), where $T_{\text{sec return}}$ was compared based on measured flow temperatures. During discharging T_{SH} and T_{DHW} were compared. Pipe heat losses of each line were considered. DHW consumption, as described in the prototype scenario (section 3.3), was conducted with a flow rate of 5 L/min. For SH consumption (section 3.1) a HTF flow rate of 7 L/min was applied.
- PCM model validation: Measurement data of charge and discharge of a single PCM unit was used. HTF temperatures were compared in the return line of the PCM heat storage ($T_{\text{PCM return}}$). HTF flow rates were approx. 16.5 L/min during charging and 2 L/min during discharging. Pipe heat losses were considered. For charging, heat was supplied from the solar collector circuit, which heated the HTF via the plate heat exchanger (Fig. 2b). Before charge and discharge the unit was in temperature equilibrium with the room. Charging stopped at $T_{\text{PCM return}} = 88\text{ }^{\circ}\text{C}$. During discharging, cold HTF from the bottom of the water tank was heated from the PCM unit during SAT composite solidification (Fig. 2c).

3.3. Investigated scenarios

The prototype scenario was based on system demonstrator specifications (Table 2). Collector array shading at the prototype test facility, due to buildings and trees, was considered. A daily consumption of 113 L of hot water at 45 °C and a cold water temperature of 10 °C was considered. User behaviour was simulated using three hot water draw-offs a day (7:00 h, 12:00 h, 19:00 h) with 1.545 kWh of heat each draw-off.

A scenario with optimized operation conditions was defined by neglecting the limitations of the system demonstrator. Component parameters were varied in accordance to Table 2. Ideal orientation of the collector array and no shading were considered, where an inclination of 70° was found in sensitivity analysis of the system performance (section 4.3). Compact PCM heat storage design was assumed by increased insulation of the PCM units. A PCM unit size of 150 L was used for direct comparison with the prototype scenario, whereas a PCM unit size of 200 L was found to increase the annual system performance and was therefore applied for further scenario calculations. Reduced water tank heat losses were considered by reduced tank dimensions and increased insulation. A daily DHW consumption of 130 L at 45 °C was applied. With regards to the Danish code of practice [6], a cold water temperature of 10 °C and increased use of hot water in the kitchen were assumed. 1.725 kWh per draw-off, meaning 5.175 kWh of daily loads were resulting, which was 15% higher than in the prototype scenario. The optimized scenario was applied to analyse the sensitivity of component sizing regarding the solar fraction of heat supply. Realistic variations of collector array aperture area and PCM volume were used to evaluate the performance potential of the system.

Table 2. Overview of applied parameters.

| | Prototype scenario | Optimized scenario |
|---|---------------------|-----------------------------|
| Collector array | | |
| Aperture area: | 22.4 m ² | 9.6 – 28.8 m ² |
| Inclination: | 45° | 70° |
| Azimuth: | 12° | 0° |
| Shading: | on | off |
| PCM heat storage | | |
| Volume: | 0.6 m ³ | 0.15 – 2.8 m ³ |
| Insulation thickness: (top; sides; bottom) | 0.1; 0.1; 0.1 m | 0.15; 0.5; 0.15 m |
| Thermal conductivity of insulation: | 0.04 W/mK | 0.02 W/mK |
| Unit size: | 150L | 150 / 200L |
| Water tank | | |
| Volume: | 0.74 m ³ | 0.6 / 1 m ³ |
| Height: | 1.6 m | 1.6 / 2 m |
| Heat loss coefficient: (top; mantle; bottom) | 4.5; 2; 0.25 W/K | 1; 1; 0.25 / 1; 2; 0.25 W/K |
| Annual heat demand | | |
| Space heating: | 2031 kWh | 2031 kWh |
| Hot water: | 1692 kWh | 1946 kWh |

Finally, the demand-side flexibility of the system was investigated by simulating full storage charge from electricity at the beginning of the year, when almost no solar heat was available. This was realized by an initial temperature of 90 °C for both the PCM units and the outer volume of the water tank. The time duration of system operating without auxiliary heating was determined as well as the effect on annual coverage of heat demands including solar heat supply.

3.4. Performance evaluation

Simulation results were evaluated by yearly and monthly energy balances, calculated by periodic integration of heat transfer rates in the hydraulic circuits. The following indicators were used to analyse system performance:

$$Q_{solar} (kWh) = \int (\dot{Q}_{SH} + \dot{Q}_{DHW} - \dot{Q}_{aux}) * dt \quad (1)$$

$$SF \text{ or } REF (\%) = \left[1 - \frac{\int (\dot{Q}_{aux}) * dt}{\int (\dot{Q}_{SH} + \dot{Q}_{DHW}) * dt} \right] * 100 \quad (2)$$

where the net utilized solar heat (Q_{solar}) is the sum of the domestic hot water and space heating minus auxiliary energy use. The solar fraction (SF) was calculated in scenarios without and the renewable energy fraction (REF) in scenarios with full storage charge at the beginning of the year. Both indicators were calculated as the fraction of annual net utilized solar energy divided by SH and DHW demand. Q_{solar} , SF and REF were determined at the water tank.

The specific solar yield per square meter aperture area (q_{coll}) of the collector circuit and the number of storage cycles per year (N_{cycle}) of water tank and PCM heat storage were calculated to analyse the sensitivity of component sizing:

$$N_{cycle} = \frac{\int (\dot{Q}_{out}) * dt}{C} \quad (3)$$

$$q_{coll} \left(\frac{kWh}{m^2} \right) = \frac{\int (\dot{Q}_{coll}) * dt}{A} \quad (4)$$

where the capacity (C) of single PCM unit, containing 150 L of SAT composite, was considered with 27 kWh [45]. PCM heat storage capacities were scaled according to the set volumes in the calculation. Water tank capacities were calculated to be 34 kWh for 0.6 m³, 45 kWh for 0.8 m³ and 57 kWh for 1 m³. For heat draw (\dot{Q}_{out}), heat supply from the PCM to the water tank, respectively from the water tank to the SH and DHW circuits were considered.

4. Results and discussion

4.1. Model validation

Table 3 presents a comparison of measured and simulated heat transfer in collector circuit, water tank and PCM heat storage. All component models were found to be valid with minor deviations:

- Solar yield (Q_{coll}) was 1.9% higher in the simulation than during the testing period from March 17th – April 28th 2016. This period is crucial for annual system performance because solar heat was directly utilized for heat supply via the water tank and the PCM units were charged.

- Water tank simulation resulted in 1.7% higher charge (Q_{charge}) during March 15th – March 16th. Simulated SH consumption (Q_{SH}) was 1.9% lower, and simulated DHW consumption (Q_{DHW}) was 1.5% higher than in measurements. Measured Q_{DHW} and therefore also simulated Q_{SH} deviated from the prototype scenario. This is not the case in later scenario calculation, where time-dependent forcing functions were used.
- Simulated PCM unit charge ($Q_{\text{PCM charge}}$) was only 0.6% lower than in measurements. Measured $Q_{\text{PCM charge}}$ and therefore also simulated Q_{PCM} was higher than in functionality tests [45], because initial temperatures of the PCM unit were lower. Simulated PCM unit discharge ($Q_{\text{PCM discharge}}$) was 2.6% higher than in measurements, therefore less heat remained in the PCM unit when discharge stopped.

Table 3. Simulated and measured heat transfer in collector circuit, water tank and PCM heat storage.

| | Measurement (kWh) | Simulation (kWh) | Deviation (kWh) | Deviation (%) |
|---|-------------------|------------------|-----------------|---------------|
| Q_{coll} (March 17 th – April 28 th 2016) | 1146 | 1168 | 22 | 1.9 |
| Q_{charge} | 25.2 | 25.6 | 0.4 | 1.7 |
| Q_{SH} | 10.4 | 10.2 | 0.2 | 1.9 |
| Q_{DHW} | 4.76 | 4.83 | 0.07 | 1.5 |
| $Q_{\text{PCM charge}}$ | 28.09 | 27.91 | 0.18 | 0.6 |
| $Q_{\text{PCM discharge}}$ | 8.87 | 9.09 | 0.23 | 2.6 |

Fig. 3 presents a comparison of the development of measured and simulated $T_{\text{coll flow}}$ and Q_{coll} from the March 30th – April 1st 2016. During each day, water tank charging before noon was followed by PCM heat storage charging with a varying number of PCM units. HTF temperatures fluctuated due to changes of solar irradiance as well as during mode changes. Measured and simulated $T_{\text{coll flow}}$ approximately matched. Minor deviations in morning and evening hours corresponded to periods with partial shading of the collector array. Because of the relatively large collector area partial shading occurred in tests, this could not be considered in the shading model. Overall, developments of $T_{\text{coll flow}}$ and Q_{coll} showed a high degree of similarity.

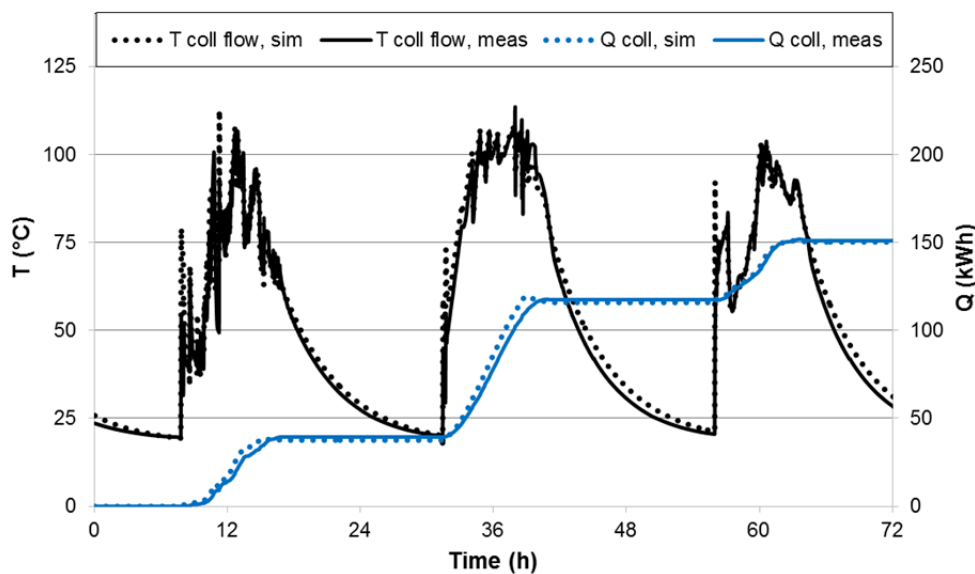
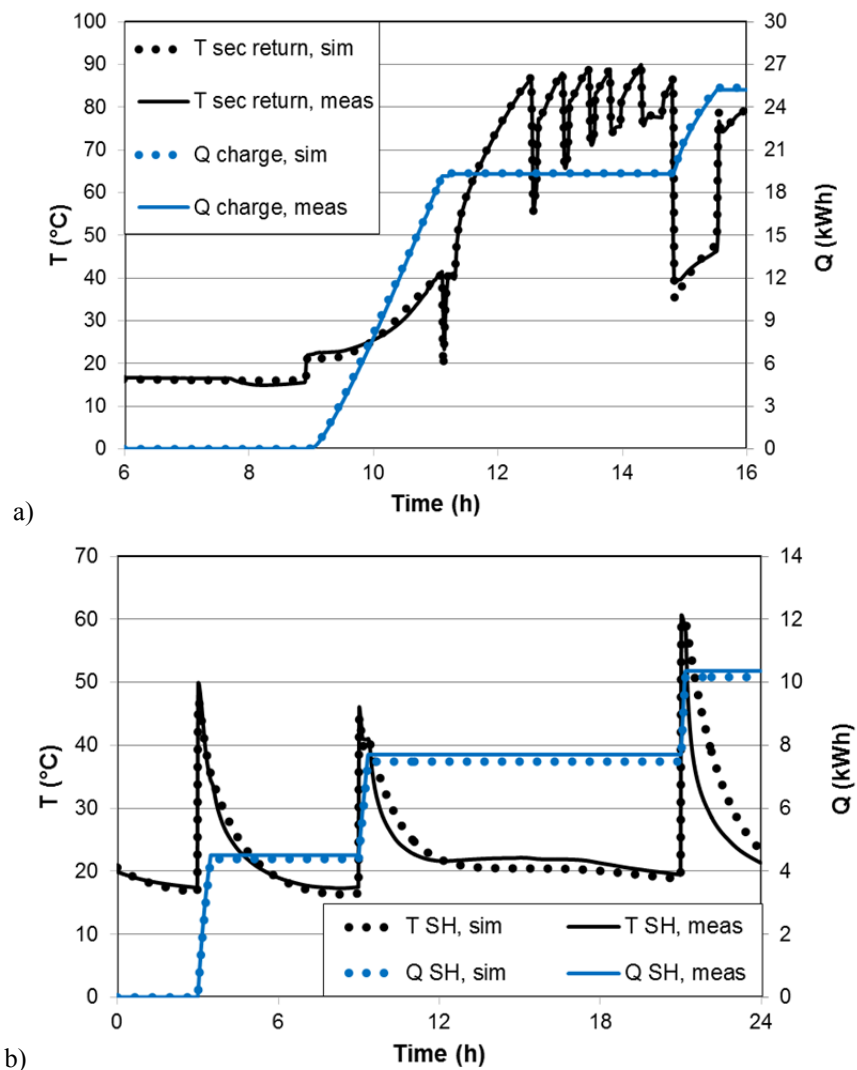


Fig. 3. Collector circuit validation.

Fig. 4 presents results of water tank model validation with experimental data from March 16th 2016. Charging took place in two periods from approximately 9:00 h–11:00 h and from 15:00 h–14:00 h. As presented in Fig. 4a, $T_{\text{sec return}}$ was slightly lower at the beginning and slightly higher towards the end of each charging period, in comparison to measured values. Measurement values in between those periods are resulting from PCM charging, which was employed via the same hydraulic line. Overall, $T_{\text{sec return}}$ had a high degree of similarity and the development of Q_{charge} matched. As presented in Fig. 4b, T_{SH} matched at the beginning and at the end of SH consumption. Deviations during cool-down of the pipework did not compromise the simulation. Q_{SH} had a sufficient degree of similarity. As presented in Fig. 4c, DHW consumption also started with precise HTF temperatures. Towards the end of the first draw-off T_{DHW} was approximately 3 K lower and towards the end of the second draw-off approximately 3 K lower than in tests, whereas values matched during the third draw-off. This is considered as sufficient degree of similarity, because the development of Q_{DHW} approximately matched.



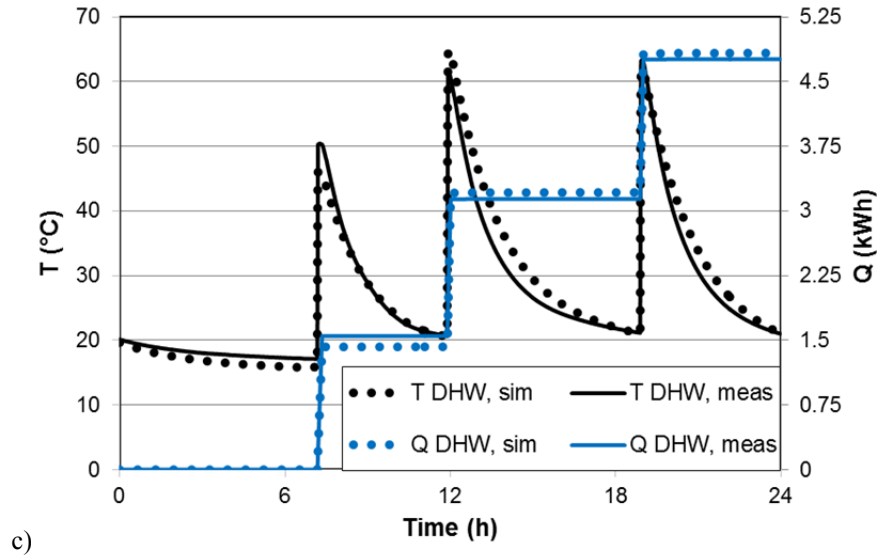
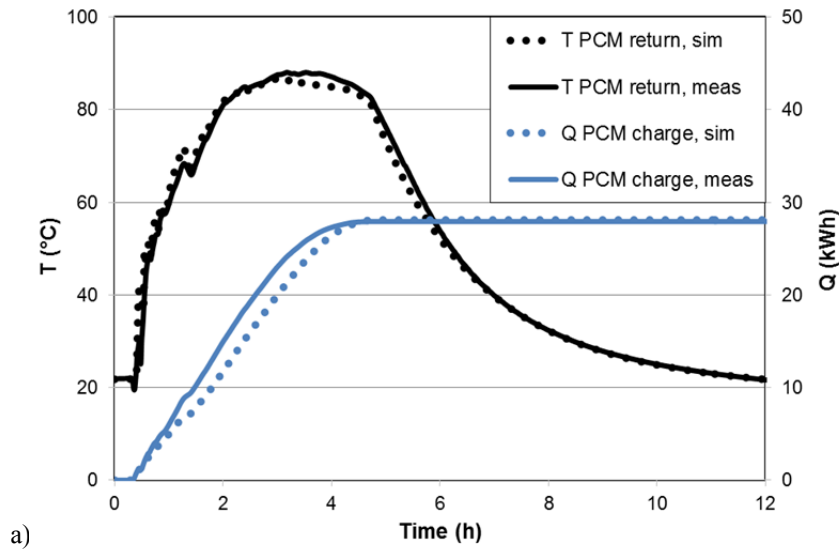


Fig. 4. Water tank model validation: a) Charging circuit; b) SH consumption; c) DHW consumption.

Fig. 5a presents a comparison of the developments of $T_{PCM\ return}$ and of $Q_{PCM\ charge}$. $T_{PCM\ return}$ had a high degree of similarity, whereas simulated $Q_{PCM\ charge}$ rose with time delay. The developments of $T_{PCM\ return}$ and of $Q_{PCM\ discharge}$ are shown in Fig. 5b. Simulated $T_{PCM\ return}$ deviated, whereas $Q_{PCM\ discharge}$ had a high degree of similarity. The described deviations are considered to be the result of idealized modelling of SAT composite phase change, where a temperature interval of 55–58 °C was applied.



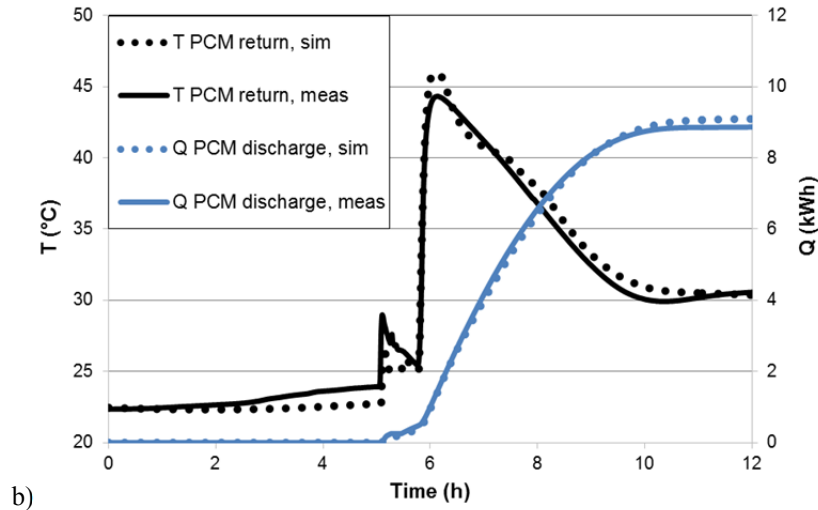


Fig. 5. PCM heat storage model validation: a) Charge; b) Discharge.

4.2. Annual system performance

The system performance was calculated for the prototype scenario with a water volume of 0.74 m^3 and for the optimized scenario with $V_{\text{water}}=0.6 \text{ m}^3$. Results are shown in Table 4 and in Table 5. In both scenarios the DHW demand was fully covered by solar heat from April to September (indicated by a solar fraction of 100%) due to the relatively large collector array ($A=22.4 \text{ m}^2$). During this period the water tank was directly heated by the collector array and also collector circuit stagnation occurred. From October to March space heating caused higher heat demand, which was partly covered by heat transfer from the PCM heat storage. The electrical heater covered the missing load by heating the water tank. With the prototype configuration the PCM store was utilized during four months, while with the optimized configuration the PCM store was used during the whole heating season.

Table 4. Heat supply in the prototype and in the optimized scenario with $A=22.4 \text{ m}^2$ and $V_{\text{PCM}}=0.6 \text{ m}^3$ with 4 units of 150 L.

| | SH (kWh) | DHW (kWh) | | Q_{aux} (kWh) | | Q_{solar} (kWh) | | SF (%) | |
|---------------|----------------|--------------------|--------------------|------------------------|--------------------|--------------------------|--------------------|--------------------|--------------------|
| | Both scenarios | Prototype scenario | Optimized scenario | Prototype scenario | Optimized scenario | Prototype scenario | Optimized scenario | Prototype scenario | Optimized scenario |
| January | 512 | 143 | 165 | 518 | 454 | 137 | 211 | 21% | 31% |
| February | 344 | 129 | 149 | 287 | 237 | 186 | 259 | 39% | 52% |
| March | 324 | 143 | 165 | 151 | 137 | 316 | 354 | 68% | 72% |
| April | 0 | 139 | 160 | 0 | 0 | 139 | 160 | 100% | 100% |
| May | 0 | 144 | 166 | 0 | 0 | 144 | 166 | 100% | 100% |
| June | 0 | 140 | 161 | 0 | 0 | 140 | 161 | 100% | 100% |
| July | 0 | 144 | 166 | 0 | 0 | 144 | 166 | 100% | 100% |
| August | 0 | 144 | 166 | 0 | 0 | 144 | 166 | 100% | 100% |
| September | 0 | 140 | 161 | 0 | 0 | 140 | 161 | 100% | 100% |
| October | 173 | 143 | 165 | 96 | 23 | 220 | 319 | 69% | 93% |
| November | 321 | 139 | 160 | 171 | 55 | 289 | 425 | 63% | 88% |
| December | 358 | 143 | 165 | 400 | 320 | 101 | 203 | 20% | 38% |
| Annual | 2031 | 1692 | 1946 | 1623 | 1227 | 2100 | 2750 | 56% | 69% |

Table 5. Heat transfer in the prototype and in the optimized scenario with $A=22.4 \text{ m}^2$ and $V_{\text{PCM}}=0.6 \text{ m}^3$ with 4 units of 150 L.

| | Q_{coll} (kWh) | | q_{coll} (kWh/m ²) | | Buffer charge (kWh) | | PCM charge (kWh) | | PCM to buffer (kWh) | |
|---------------|----------------------------|--------------------|--|--------------------|------------------------|--------------------|---------------------|--------------------|------------------------|--------------------|
| | Prototype scenario | Optimized scenario | Prototype scenario | Optimized scenario | Prototype scenario | Optimized scenario | Prototype scenario | Optimized scenario | Prototype scenario | Optimized scenario |
| January | 192 | 235 | 9 | 11 | 157 | 136 | 32 | 94 | 14 | 89 |
| February | 259 | 298 | 12 | 13 | 181 | 175 | 71 | 116 | 40 | 98 |
| March | 547 | 531 | 24 | 24 | 262 | 244 | 269 | 275 | 106 | 150 |
| April | 548 | 297 | 24 | 13 | 200 | 221 | 322 | 55 | 6 | 4 |
| May | 769 | 322 | 34 | 14 | 282 | 239 | 440 | 53 | 0 | 0 |
| June | 681 | 298 | 30 | 13 | 233 | 224 | 405 | 47 | 0 | 0 |
| July | 635 | 305 | 28 | 14 | 217 | 227 | 380 | 51 | 0 | 0 |
| August | 685 | 308 | 31 | 14 | 240 | 229 | 409 | 53 | 0 | 0 |
| September | 665 | 292 | 30 | 13 | 231 | 217 | 393 | 48 | 0 | 0 |
| October | 360 | 348 | 16 | 16 | 191 | 198 | 156 | 139 | 61 | 127 |
| November | 350 | 437 | 16 | 20 | 274 | 218 | 67 | 209 | 39 | 224 |
| December | 153 | 212 | 7 | 9 | 141 | 130 | 8 | 77 | 0 | 83 |
| Annual | 5844 | 3884 | 261 | 173 | 2608 | 2459 | 2953 | 1216 | 265 | 775 |

An annual SF of 56% was calculated for the prototype scenario. Although higher DHW demand was simulated in the optimized scenario (Table 3), the annual SF increased to 69%.

Improved PCM unit insulation, optimized collector array tilt (see also section 4.3) and a smaller water tank with improved insulation resulted in significantly better annual system performance (Table 5). As a consequence of the reduced system heat losses, the specific yield of the solar collector (q_{coll}) decreased from 261 to 173 kWh/m². Direct charge of the water tank (buffer charge) decreased slightly from 2608 to 2459 kWh, while PCM charge dropped from 2953 to 1216 kWh. On the contrary, in the prototype scenario only 265 kWh of stored heat in the PCM units was transferred to the water tank when there was a heat demand. The transferred heat was increased to 775 kWh in the optimized scenario. This means an increase of utilized storage cycles per year from 2.5 to 7.2. The number of annual storage cycles (N_{cycle}) of the water tank increased from 82 to 116, due to decreased size and higher DHW demand. The PCM store was mainly utilized for heat supply from January to March and in October and November.

4.3. System performance sensitivity

The influences of collector area, PCM volume (200 L units) and water tank volume on the solar fraction are shown in Table 6. The investigated SF (equation 2) ranged from 47.5% ($V_{\text{water}}=0.6 \text{ m}^3$, $A=9.6 \text{ m}^2$; $V_{\text{PCM}}=0.2 \text{ m}^3$) to 76.7% ($V_{\text{water}}=1 \text{ m}^3$, $A=25.6 \text{ m}^2$; $V_{\text{PCM}}=2.8 \text{ m}^3$). SF changed moderately (about 4%) by variation of V_{PCM} . Collector area increase from $A=9.6 \text{ m}^2$ to $A=25.6 \text{ m}^2$ increased SF by approximately 25% points throughout all storage sizes. The performance difference was most significant between $A=9.6 \text{ m}^2$ and $A=12.8 \text{ m}^2$ respectively, between 3 and 4 collector panels. For $A=9.6 \text{ m}^2$ the maximal number of PCM units in use was identified to 9 (1.8 m³), smaller collector areas were therefore not included in evaluations.

With a water tank volume of 1 m³, aperture areas above 12.8 m² were required to increase the solar heat supply. Otherwise, the solar fraction of heat supply was lower than with a water tank volume of 0.6 m³ (negative values in

Table 5). This means that the system was not able to compensate additional storage heat losses with smaller collector arrays. Thus, it was found that bigger water tanks would be only beneficial when its heat losses could be reduced.

Table 6. Parametric study on SF of the optimized scenario:

| V_{PCM} (m ³) | 0.2 | 0.4 | 1 | 2 | 2.8 |
|-----------------------------|---|------|------|------|------|
| No. of units | 1 | 2 | 5 | 10 | 14 |
| A (m ²) | SF (%) with 0.6 m ³ water | | | | |
| 9.6 | 47.5 | 47.9 | 49.1 | 50.3 | 50.3 |
| 12.8 | 54.8 | 55.2 | 56.5 | 57.8 | 59.3 |
| 16 | 60.2 | 60.4 | 62.2 | 63.7 | 64.3 |
| 19.2 | 64.8 | 64.8 | 66.2 | 67.7 | 68.5 |
| 22.4 | 68.9 | 68.9 | 71.2 | 72 | 72.7 |
| 25.6 | 72.7 | 73.8 | 74.2 | 75.1 | 76.1 |
| | Change of SF (%) with 1 m ³ water | | | | |
| 9.6 | -0.4 | -0.3 | -0.5 | -0.7 | -0.7 |
| 12.8 | 0.0 | -0.1 | -0.2 | -0.1 | -0.3 |
| 16 | 0.5 | 0.5 | 0.1 | 0.3 | 0.3 |
| 19.2 | 1.5 | 1.3 | 1.1 | 0.9 | 0.8 |
| 22.4 | 2.1 | 2.2 | 1.0 | 1.0 | 0.9 |
| 25.6 | 1.5 | 0.6 | 0.7 | 0.6 | 0.6 |

Fig. 6 shows the influence of PCM heat storage and collector area specifications on the annual net utilized solar heat (equation 1). As reference, a scenario was defined as: $A=16$ m², $I=70^\circ$, $V_{PCM}=1$ m³ and 200 L PCM units. Collector array sizing had the highest impact on solar heat supply, where relative changes of $\pm 20\%$ were calculated with a 60% larger and respectively 40% smaller aperture area. A collector inclination of 70° was found as optimum. A tilt-change of $\pm 20^\circ$ reduced solar heat utilization by 3%. Relatively small changes of net utilized solar heat ($\pm 3\%$) were observed for PCM heat storage sizes 180% larger and 80% smaller. A halving of PCM unit size revealed a significant effect (-2.6%), while with units of 333 L the solar heat supply increased by only 0.5%. Therefore, it was found a PCM unit size of 200 L or larger should be applied. In the reference scenario, full storage charge at the beginning of the year increased the solar heat supply by 5%. An increase of 14% was observed with $V_{PCM}=2.8$ m³.

It was not possible to simulate heat transfer in between the units. Thus, increased insulation of PCM units (Table 2) was set to model an optimized, stacked storage of several units with a lower surface-volume ratio. No scaling factor was used. However, the conducted sensitivity analysis is correct assuming smaller PCM volumes can be obtained with more compact unit design. For example, cylindrical prototype units [40] were reported with a smaller surface-volume ratio than flat plate prototype units [45].

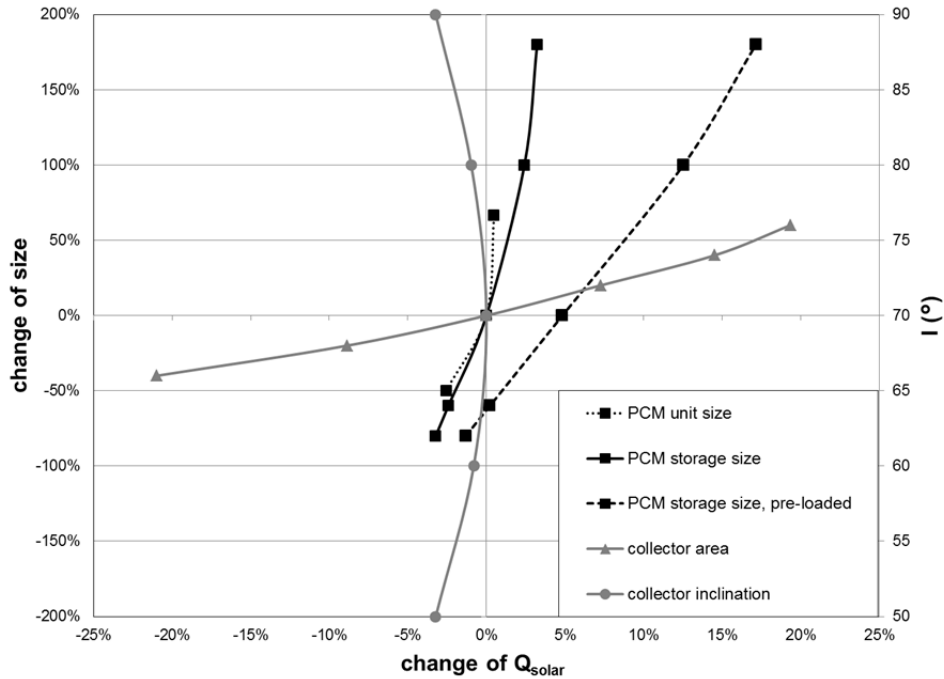


Fig. 6. Annual net utilized solar heat in dependency of PCM heat storage and collector array parameters.

4.4. PCM heat storage

Fig. 7 a shows the heat transfer from the PCM units to water tanks of 0.6 and 1 m³ in dependency of PCM volume and collector area. Increased water tank size reduced the gain from the PCM units but did not significantly change SF (Table 6). A tank volume of 0.4 m³ decreased the heat transfer to the same extent as a 6.4 m² smaller collector aperture area. Then, the annual PCM heat supply with A=22.4 m² and V_{PCM}=0.2 m³ dropped by 200 kWh, illustrating that the annual number of storage utilization cycles N_{cycle} (equation 3) was reduced from 15.6 to 10. For V_{PCM}=2.8 m³ heat supply dropped by 260 kWh, respectively N_{cycle} was reduced from 2 to 1.5. Thus, heat storage utilizing stable supercooling of SAT is more attractive for a solar combi-system with small water tanks (see also section 4.5).

Fig. 7 b shows that initial full-charge of heat stores increased PCM heat supply by 120 – 175 kWh for V_{PCM}=1 m³; 240 – 300 kWh for V_{PCM}=2 m³ and 340 – 360 kWh for V_{PCM}=2.8 m³. As investigated by Englmaier et al. [45] a minimal PCM temperature above 50 °C is needed when heat is discharged during SAT composite solidification. Thus, only 80 % of heat of fusion could be used. The maximal discharge-to-charge ratio would be 0.91, assuming full utilization of stored sensible heat during discharge from 90 °C in liquid SAT composite state (55% of charge) and 80% heat of fusion (36% of charge). Calculated ratios ranged from 1.17 with PCM volumes below 1 m³ to 0.7 with volumes of 2.8 m³. This indicates that 1-2 PCM units were additionally charged by solar heat at the beginning of the year, due to higher PCM temperatures. Larger PCM volumes provided heat over a longer period, resulting in sensible heat losses.

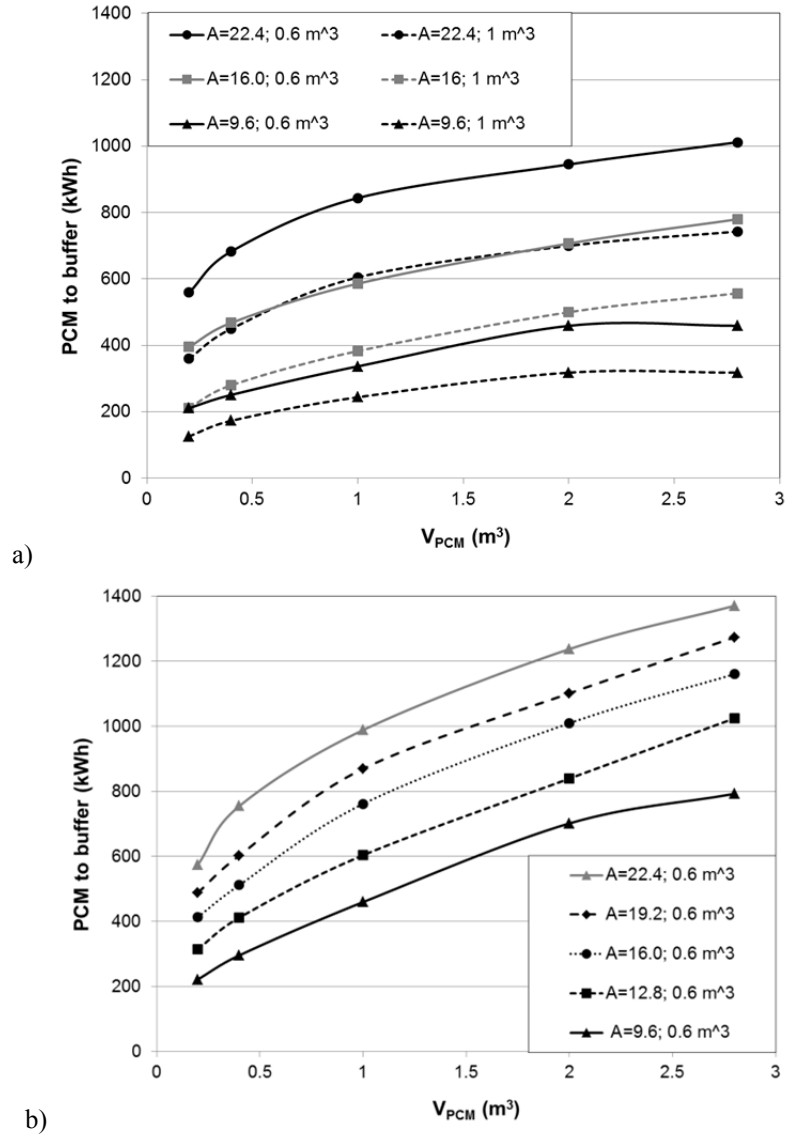


Fig. 7. Heat transfer from the PCM heat storage to the water tank: a) With variation of water tank volume; b) With initial full-charge of stores.

4.5. System sizing aspects

A full charged water tank of 0.6 m³ provided sufficient storage capacity for SH and DHW supply for at least one winter day. The PCM heat storage and the collector circuit are considered to cause the largest share of system costs, accordingly their sizing is pivotal.

Specific solar yields (equation 4; Fig. 8) ranged from 134 kWh/m² (A=28.8 m²; V_{PCM}=0.2 m³) to 330 kWh/m² (A=9.6 m²; V_{PCM}=2 m³). Increase of PCM volume increased the solar yield. Highest impact was identified for A=12.8 m², whereas additional 104 kWh/m², respectively 1331 kWh of heat have been yielded annually with V_{PCM}=2.8 m³ in comparison to V_{PCM}=0.2 m³. The impact of V_{PCM} on the solar yield was lower with larger collector arrays.

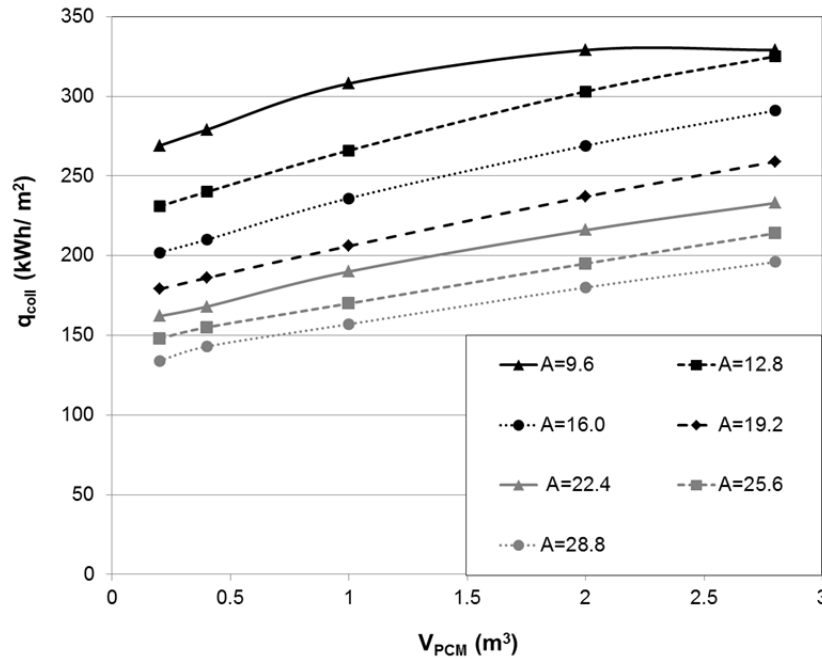


Fig. 8. Solar yield in dependency of collector area and PCM volume ($V_{\text{water}}=0.6 \text{ m}^3$).

Fig. 9 presents the number of storage cycles per year (N_{cycle}) in dependency of the collector area. As suggested by Rathgeber et al. [23], N_{cycle} should be used as basis for decision on PCM heat storage size. High N_{cycle} were calculated for relatively large collector areas and a small number of PCM units. Throughout the year 1-3 PCM units were subject to repeated charge and discharge, while the additional PCM units were utilized seasonally. Larger collector arrays enabled more frequent recharge of a larger PCM volume. Therefore, additional collector panels ($A=3.2 \text{ m}^2$) increased N_{cycle} by about 2 when a single PCM unit was used. This effect was reduced to an increase of 0.35 cycles per year with $V_{\text{PCM}}=2 \text{ m}^3$.

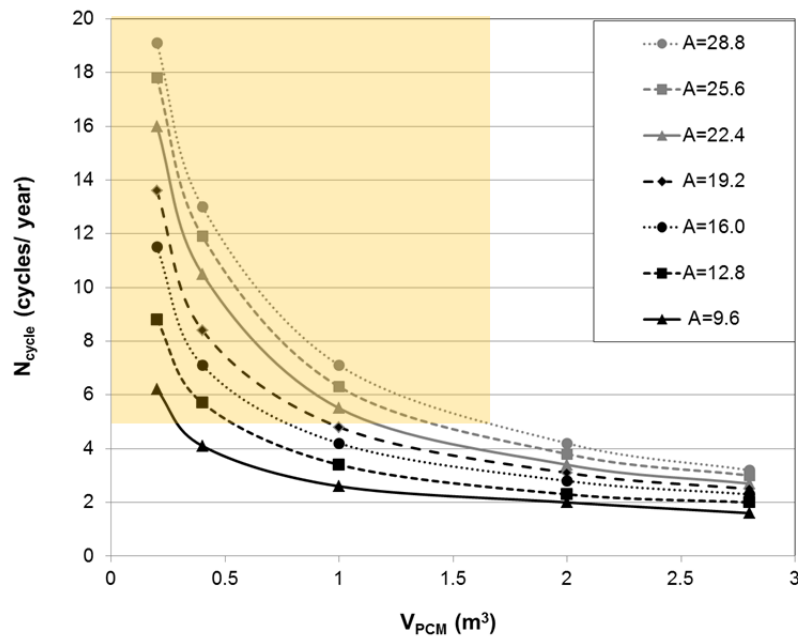


Fig. 9. N_{cycle} in dependency of collector area and PCM volume ($V_{\text{water}}=0.6 \text{ m}^3$, initial full-charge of stores).

Since an increase of the collector area results in better utilization of the PCM volume (V_{PCM}) but in lower specific yield, an optimum is warranted. The calculation of attractive system configurations could be based on two assessments:

1. The available roof area of a single-family house is assumed to be 30 m^2 enabling the installation of 7 panels ($A=22.4 \text{ m}^2$) of the used collector type.
2. Industrial SAT market prices are typically below 0.5 €/kg . Considering a PCM unit of 200 L ($C=36 \text{ kWh}$) could be produced with a cost of 250 €, specific storage capacity costs of 7 €/kWh could be achieved. This value meets the maximal acceptable storage costs in building application [23] with $N_{cycle}=5$. The area of relevant system settings is marked in Fig. 9.

With full storage charge by wind power at the beginning of the year, it was found that attractive combinations would be $V_{PCM}=0.4 \text{ m}^3$ with $A=12.8 - 22.4 \text{ m}^2$, resulting in renewable energy fractions from 57% to 71%. With a PCM volume of 1 m^3 a collector area of 22.4 m^2 would be attractive, resulting in a REF of 75%.

4.6. Application potential

In the solar combi-system, auxiliary heating has to take place when heat is in demand and cannot be covered by stored heat. By simulating full storage charge at the beginning of the year, the heat demand was covered for 2 days with $V_{PCM}=0.2 \text{ m}^3$ and for 18 days with $V_{PCM}=2.8 \text{ m}^3$ before auxiliary heating was activated for the first time, where first sensible heat from the water tank and the PCM units and finally latent heat of fusion from the PCM units was utilized for SH and DHW supply. Power-to-heat conversion during these periods could avoid on-demand charging. So, with large PCM heat stores, solar heat and electricity could be utilized with a high degree of flexibility in time.

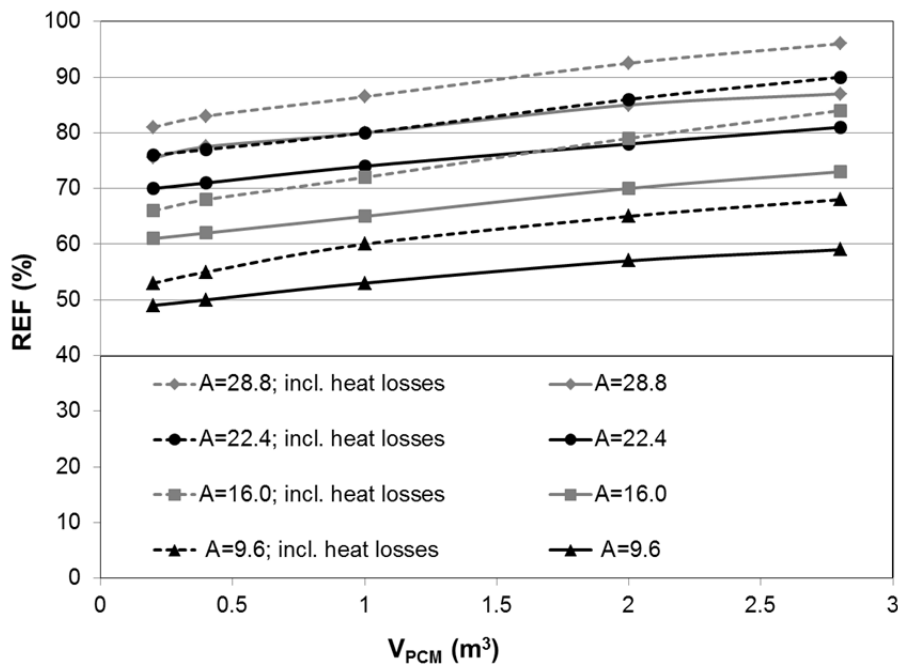


Fig. 10. Renewable energy fractions of the system assuming full storage charge by wind power at the beginning of the year ($V_{water}=0.6 \text{ m}^3$).

Annual renewable energy fractions with full storage charge at the beginning of the year (Fig. 10) would be in between 1% ($V_{PCM}=0.2 \text{ m}^3$) and 8% ($V_{PCM}=2.8 \text{ m}^3$) higher than calculated solar fractions (Table 6). Placing heat stores in the living area of the house, storage heat losses could be utilized to cover SH demand. Then, REFs could be 6% ($V_{PCM}=0.2 \text{ m}^3$) to 18% ($V_{PCM}=2.8 \text{ m}^3$) higher than calculated SFs. However, this would also require measures to avoid overheating of the building during summer.

In Fig. 11 calculated heat quantities for the potentially attractive system setting with $A=22.4 \text{ m}^2$, $V_{\text{water}}=0.6 \text{ m}^3$ and $V_{PCM}=1 \text{ m}^3$ are presented. A SF of 71% was calculated, which could result in a REF of 80% by full storage charge at the beginning of the year and by utilizing storage heat losses. System simulation indicated that full heat supply could be achieved by five times of storage re-charge from end-November to the beginning of March. This would potentially enable use of periodically available, cheap electricity from renewable energy sources, such as wind power (section 1.1).

The investigations performed in this paper were based on properties of previous experimental development of prototype stores [40]. These contained SAT composites allowing combined long- and short-term heat storage. Subsequently, functionality tests employing an integrated water tank proved that the storage concept could be applied into a solar combi-system. The presented numerical study of a Danish Passive House employing a solar combi-system with optimized heat storage utilizing on-demand crystallization of SAT showed promising results. It will provide a reference for building heat supply with a solar fraction larger than 70 % using a relatively small storage volume. This system may be applicable for decentralized electrical grid stabilization in regions with a large wind power generation capacity in winter. Further development of heat stores containing SAT composites, emphasizing improved heat transfer, low manufacturing costs and cyclic stability is therefore desirable.

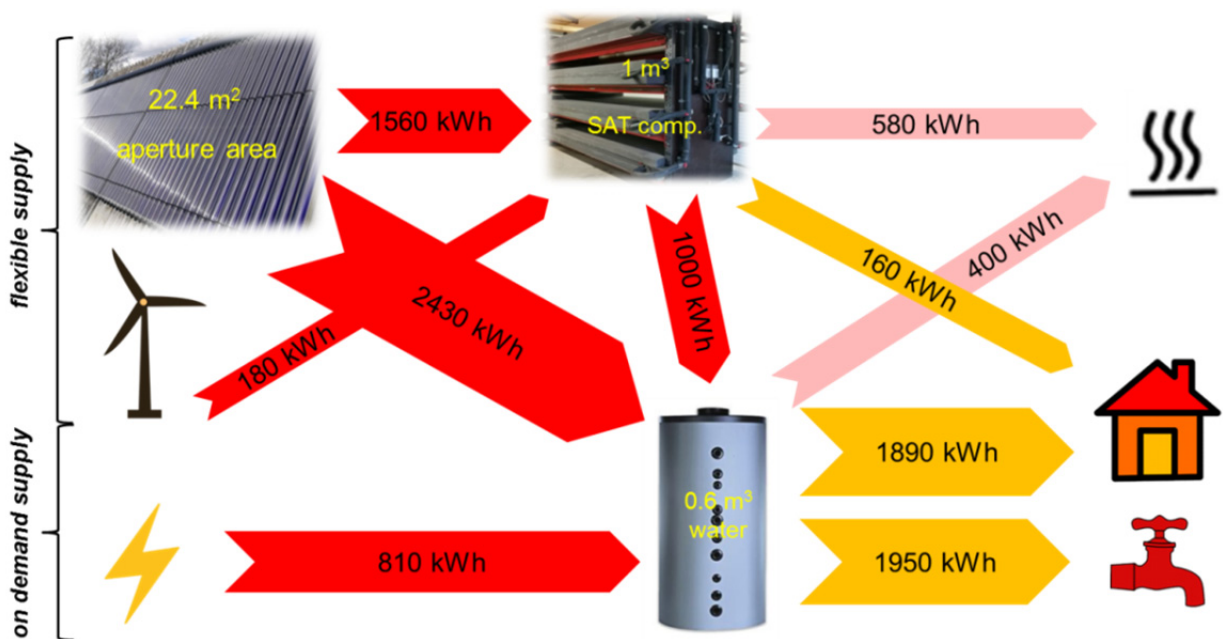


Fig. 11. Annual heat flux (supply in red, demand in orange, heat loss in pink) in a system scenario with a REF of 80%.

5. Conclusions

For the first time, the performance of a solar combi-system with evacuated tubular collectors, water tank and PCM units utilizing stable supercooling of sodium acetate trihydrate was investigated. The validation results of the component models revealed a high degree of similarity with measured data from previous system demonstration. The control strategy included on-demand utilization of heat of fusion of sodium acetate trihydrate composites. Annual simulations showed high potential of the system in a Danish Passive House scenario:

- In spring and autumn, when simulating space heating and domestic hot water patterns, up to three PCM units were subject to repeated charge and discharge, while additional PCM units were utilized as seasonal storage from summer to winter. In this way, combined short and long-term heat storage led to high solar fractions of heat supply.
- With prototype component specification, an annual solar fraction of 56% was calculated for a yearly, total heat demand of 3723 kWh. A scenario with optimized component specifications and a 15% higher hot water demand (3977 kWh of total heat demand) resulted in a solar fraction of 69%.
- Sensitivity analysis showed an optimal collector array inclination of 70° with PCM units of 200 L and a 0.6 m³ water tank. The system was found to perform best with collector aperture areas in between 12.8 and 22.4 m², with PCM volumes below 1 m³ and when additional storage charge at the beginning of the year was assumed. With 22.4 m² (aperture) tubular collectors, approximately 1000 kWh heat demand would be covered by 1 m³ sodium acetate trihydrate composite and its heat storage capacity would be utilized 5.5 times per year, those of the water tank 116 times per year respectively.
- Full-charge of a single 200 L PCM unit and a 0.6 m³ water tank enabled heat supply of 2 days in January, which increased to 18 days when 2.8 m³ of sodium acetate trihydrate composite was charged.
- The heat storage of the system could be charged several times during winter in periods with surplus of wind energy and in summer, spring and autumn by solar collectors. Thus, the system could reveal a renewable energy fraction close to 100% and would only require a relatively small storage volume.

Application of PCM units with a high number of annual storage cycles is needed due to economic reasons. In contrast, reduction of necessary collector area lowers system costs. Further studies elucidating optimal application of heat stores employing stable supercooling of SAT are warranted. For instance, investigations could be done for different climates, different collector types and cylindrical heat storage units with improved heat transfer properties, etc..

Acknowledgements

This research was funded by the PhD program of the Sino Danish Center for Education and Research (SDC). The work was also supported by the European Commission (Grant Agreement N_295568) as part of the Seventh Framework Programme of the European Community for Research, Technological Development and Demonstration Activities under the “Collaborative Project” funding scheme of through the COMTES consortium.

References

- [1] European Parliament, Directive 2012/27/EU of the European Parliament and of the Council of 25 October 2012 on energy efficiency, amending Directives 2009/125/EC and 2010/30/EU and repealing Directives 2004/8/EC and 2006/32/EC. Official Journal of the European Union, 315, pp. 1-56, 2012.
- [2] European Parliament, Directive 2010/31/EU of the European Parliament and of the Council of 19 May 2010 on the energy performance of buildings. Official Journal of the European Union, 153, pp. 13–35, 2010.
- [3] Weiss W. (Ed.), Solar Heating Systems for Houses, a Design Handbook for Solar Combisystems. James & James Ltd., UK, 2003.
- [4] A. Thür, “Compact solar Combisystem – High Efficiency by Minimizing Temperatures,” PhD thesis, Technical University of Denmark, Department of Civil Engineering report no. R-160, 2007.
- [5] S. Colclough and T. McGrath, “Net energy analysis of a solar combi system with Seasonal Thermal Energy Store,” *Appl. Energy*, vol. 147, pp. 611–616, 2015.
- [6] DS 439, “Norm for vandinstallationer – Code of Practice for domestic water supply,” Danish Standards, 75 pp., 2009.
- [7] W. Streicher, R. Heimrath, and C. Bales, “Analysis of System Reports of Task 26 for Sensitivity of Parameters,” December 2003 (revised February 2007).
- [8] W. Kramer, A. Oliva, G. Stryi-Hipp, S. Kobelt, D. Bestenlehner, H. Drück, J. Bühl, and G. Dasch, “Solar-active-houses – Analysis of the building concept based on detailed measurements,” *Energy Procedia*, vol. 48, pp. 895–903, 2014.
- [9] B. Mette, H. Kerskes, H. Drück, and H. Müller-Steinhagen, “New highly efficient regeneration process for thermochemical energy storage,” *Appl. Energy*, vol. 109, pp. 352–359, 2013.
- [10] T. Nonnen, S. Beckert, K. Gleichmann, A. Brandt, B. Unger, H. Kerskes, B. Mette, S. Bonk, T. Badenhop, F. Salg, and R. Gläser, “A Thermochemical Long-Term Heat Storage System Based on a Salt/Zelite Composite,” *Chem. Eng. Technol.*, vol. 39, no. 12, pp. 2427–2434, 2016.
- [11] B. Zettl and H. Kirchsteiger, “An open sorption heat storage application,” in *Proceedings of the International Sustainable Energy Conference (ISEC) 2018*, pp. 605–611, 2018.
- [12] B. Zettl, G. Englmaier, and G. Steinmaurer, “Development of a revolving drum reactor for open-sorption heat storage processes,” *Appl. Therm. Eng.*, vol. 70, no. 1, pp. 42–49, 2014.
- [13] R. Köll, W. van Helden, G. Engel, W. Wagner, B. Dang, J. Jänchen, H. Kerskes, T. Badenhop, and T. Herzog, “An experimental investigation of a realistic-scale seasonal solar adsorption storage system for buildings,” *Sol. Energy*, vol. 155, pp. 388–397, 2017.
- [14] R. Weber and V. Dorer, “Long-term heat storage with NaOH,” *Vacuum*, vol. 82, no. 7, pp. 708–716, 2008
- [15] B. Fumey, R. Weber, and L. Baldini, “Liquid sorption heat storage – A proof of concept based on lab measurements with a novel spiral fined heat and mass exchanger design,” *Appl. Energy*, vol. 200, pp. 215–225, 2017.
- [16] J. Pereira da Cunha and P. Eames, “Thermal energy storage for low and medium temperature applications using phase change materials – A review,” *Appl. Energy*, vol. 177, pp. 227–238, 2016.
- [17] D. Zhou, C. Y. Zhao, and Y. Tian, “Review on thermal energy storage with phase change materials (PCMs) in building applications,” *Appl. Energy*, vol. 92, pp. 593–605, 2012.
- [18] M. Saffari, A. de Gracia, C. Fernández, and L. F. Cabeza, “Simulation-based optimization of PCM melting temperature to improve the energy performance in buildings,” *Appl. Energy*, vol. 202, pp. 420–434, 2017.
- [19] A. Kazemian, A. Salari, A. Hakkaki-Fard, and T. Ma, “Numerical investigation and parametric analysis of a photovoltaic thermal system integrated with phase change material,” *Appl. Energy*, vol. 238, pp. 734–746, 2019.

- [20] W. Yuan, J. Ji, M. Modjinou, F. Zhou, Z. Li, Z. Song, S. Huang, and X. Zhao, "Numerical simulation and experimental validation of the solar photovoltaic/thermal system with phase change material," *Appl. Energy*, vol. 232, pp. 715–727, 2018.
- [21] N. Araki, M. Futamura, A. Makino, and H. Shibata, "Measurements of Thermophysical Properties of Sodium Acetate Hydrate," *International J. Thermophys.*, vol. 16, no. 6, pp. 1455–1466, 1995.
- [22] M.A. Rogerson and S.S.S. Cardoso, "Solidification in heat packs: I. Nucleation rate," *AIChE J.*, vol. 49, no. 2, pp. 505–515, 2003.
- [23] C. Rathgeber, E. Lävemann, and A. Hauer, "Economic top-down evaluation of the costs of energy storages -A simple economic truth in two equations," *J. Energy Storage*, vol. 2, pp. 43–46, 2015.
- [24] A. Arteconi, N.J. Hewitt, and F. Polonara, "State of the art of thermal storage for demand-side management," *Appl. Energy*, vol. 93, pp. 371–389, 2012.
- [25] D. Heide, L. von Bremen, M. Greiner, C. Hoffmann, M. Speckmann, and S. Bofinger, "Seasonal optimal mix of wind and solar power in a future, highly renewable Europe," *Renew. Energy*, vol. 35, no. 11, pp. 2483–2489, 2010.
- [26] F. Hvelplund, P. A. Østergaard, and N. I. Meyer, "Incentives and barriers for wind power expansion and system integration in Denmark," *Energy Policy*, vol. 107, pp. 573–584, 2017.
- [27] B. Zalba, J.M. Marín, L.F. Cabeza, and H. Mehling, "Review on thermal energy storage with phase change: materials, heat transfer analysis and applications," *Appl. Therm. Eng.*, vol. 23, no. 3, pp. 251–283, 2003.
- [28] S. Furbo and S. Svendsen, "Report on heat storage in a solar heating system using salt hydrates," Technical University of Denmark, Thermal Insulation Laboratory, report no. 70, 1977.
- [29] W. Kong, M. Dannemand, J.B. Berg, J. Fan, G. Englmaier, J. Dragsted and S. Furbo, "Experimental investigations on phase separation for different heights of sodium acetate water mixtures under different conditions," *Appl. Therm. Eng.*, vol. 148, pp. 796–805, 2019.
- [30] M. Dannemand, J.B. Johansen, and S. Furbo, "Solidification behavior and thermal conductivity of bulk sodium acetate trihydrate composites with thickening agents and graphite," *Sol. Energy Mater. Sol. Cells*, vol. 145, Part 3, pp. 287–295, 2016.
- [31] M. Dannemand, M. Delgado, A. Lazaro, C. Penalosa, C. Gundlach, C. Trinderup, J.B. Johansen, C. Moser, H. Schranzhofer, and S. Furbo, "Porosity and density measurements of sodium acetate trihydrate for thermal energy storage," *Appl. Therm. Eng.*, vol. 131, pp. 707–714, 2018.
- [32] W. Kong, M. Dannemand, J.B. Johansen, J. Fan, J. Dragsted, G. Englmaier, and S. Furbo, "Experimental investigations on heat content of supercooled sodium acetate trihydrate by a simple heat loss method," *Sol. Energy*, vol. 139, pp. 249–257, 2016.
- [33] P.L. Dietz, J.S. Brukner, and C.A. Hollingsworth, "Linear Crystallization Velocities of Sodium Acetate in Supersaturated Solutions," *J. Phys. Chem.*, vol. 61, no. 7, pp. 944–948, 1957.
- [34] G. Englmaier, Y. Jiang, M. Dannemand, C. Moser, H. Schranzhofer, S. Furbo, and J. Fan, "Crystallization by local cooling of supercooled sodium acetate trihydrate composites for long-term heat storage," *Energy Build.*, vol. 180, pp. 159–171, 2018.
- [35] M. Medrano, M. O. Yilmaz, M. Nogués, I. Martorell, J. Roca, and L. F. Cabeza, "Experimental evaluation of commercial heat exchangers for use as PCM thermal storage systems," *Appl. Energy*, vol. 86, no. 10, pp. 2047–2055, 2009.
- [36] A. López-navarro, J. Biosca-Taronger, J.M. Corberán, C. Peñalosa, A. Lázaro, P. Dolado, and J. Payá, "Performance characterization of a PCM storage tank," *Appl. Energy*, vol. 119, pp. 151–162, 2014.
- [37] A. Frazzica, M. Manzan, A. Sapienza, A. Freni, G. Toniato, and G. Restuccia, "Experimental testing of a hybrid sensible-latent heat storage system for domestic hot water applications," *Appl. Energy*, vol. 183, pp. 1157–1167, 2016.

- [38] C. Zauner, F. Hengstberger, B. Mörzinger, R. Hofmann, and H. Walter, "Experimental characterization and simulation of a hybrid sensible-latent heat storage," *Appl. Energy*, vol. 189, pp. 506–519, 2017.
- [39] G. Zhou and Y. Xiang, "Experimental investigations on stable supercooling performance of sodium acetate trihydrate PCM for thermal storage," *Sol. Energy*, vol. 155, pp. 1261–1272, 2017.
- [40] M. Dannemand, J. Dragsted, J. Fan, J.B. Johansen, W. Kong, and S. Furbo, "Experimental investigations on prototype heat storage units utilizing stable supercooling of sodium acetate trihydrate mixtures," *Appl. Energy*, vol. 169, pp. 72–80, 2016.
- [41] M. Dannemand, J.B. Johansen, W. Kong, and S. Furbo, "Experimental investigations on cylindrical latent heat storage units with sodium acetate trihydrate composites utilizing supercooling," *Appl. Energy*, vol. 177, pp. 591–601, 2016.
- [42] J. Deng, S. Furbo, W. Kong, and J. Fan, "Thermal performance assessment and improvement of a solar domestic hot water tank with PCM in the mantle," *Energy Build.*, vol. 172, pp. 10–21, 2018.
- [43] M. Dannemand, J. M. Schultz, J. B. Johansen, and S. Furbo, "Long term thermal energy storage with stable supercooled sodium acetate trihydrate," *Appl. Therm. Eng.*, vol. 91, pp. 671–678, 2015.
- [44] W. Streicher, J. Bony, S. Citherlet, A. Heinz, P. Pusching, H. Schranzhofer, and J. M. Schultz, "Simulation Models of PCM Storage Units, Report C5, IEA Solar Heating and Cooling programme - Task 32 "Advanced storage concepts for solar and low energy buildings", 2008.
- [45] G. Englmaier, C. Moser, S. Furbo, M. Dannemand, and J. Fan, "Design and functionality of a segmented heat-storage prototype utilizing stable supercooling of sodium acetate trihydrate in a solar heating system," *Appl. Energy*, vol. 221, pp. 522–534, 2018.
- [46] G. Englmaier, S. Furbo, W. Kong, M. Dannemand, J. Fan, and Z. Wang, "Performance Evaluation of a Demonstration System with PCM for Seasonal Heat Storage: Charge with Evacuated Tubular Collectors", *Proceedings of the ISES Solar World Congress 2017 - IEA SHC International Conference on Solar Heating and Cooling for Buildings and Industry*, 2017.
- [47] C. Finck, R. Li, R. Kramer, and W. Zeiler, "Quantifying demand flexibility of power-to-heat and thermal energy storage in the control of building heating systems," *Appl. Energy*, vol. 209, pp. 409–425, 2018.
- [48] TÜV Rheinland/DIN CERTCO, "Summary of EN 12975 Test Results, annex to Solar KEYMARK Certificate of Kingspan Thermomax solar collectors," 2011.
- [49] Passive House Institute, "Passive House Institute." [Online]. Available: <https://passivehouse.com>. [Accessed: 31-Oct-2018].
- [50] J. B. Johansen, G. Englmaier, M. Dannemand, W. Kong, J. Fan, J. Dragsted, B. Perers, and S. Furbo, "Laboratory Testing of Solar Combi System with Compact Long Term PCM Heat Storage," *Energy Procedia*, vol. 91, pp. 330–337, 2016.
- [51] Department of Civil Engineering, "DTU Climate Station Data, climate data from the Technical University of Denmark." [Online]. Available: <http://climatestationdata.byg.dtu.dk/> [Accessed: 30-Sept-2018].

[7] G. Englmair, S. Furbo, M. Dannemand, and J. Fan, “Experimental investigation of a tank-in-tank heat storage unit utilizing stable supercooling of sodium acetate trihydrate”, submitted to Applied Thermal Engineering, in review.

This page is intentionally left blank.

Experimental investigation of a tank-in-tank heat storage unit utilizing stable supercooling of sodium acetate trihydrate

Gerald Englmaier^{1,2*}, Simon Furbo¹, Mark Dannemand¹ and Jianhua Fan¹

¹Department of Civil Engineering, Technical University of Denmark, Brovej 118, 2800 Kgs. Lyngby, Denmark

²Sino-Danish Center for Education and Research, 380 Huaibeizhuang, Huairou district, Beijing, China

Highlights

- Heat storage built with standard components for water heat stores
 - SAT composite provided an energy storage capacity 76 % higher than water
 - Demonstration of combined short and long-term heat storage
 - Sensitivity analysis of heat transfer via mantle and spiral heat exchangers
 - Discontinuous discharge as solution for heat supply in buildings
-

Abstract

A cylindrical heat storage prototype was designed to utilize sodium acetate trihydrate (SAT) composite with 2%wt. extra water and 3%wt. of liquid polymeric solution for combined short and long-term heat storage. It was manufactured with inexpensive standard components of water stores. It contained 150 L of SAT composite in the inner tank and 59 L of water in the mantle surrounding the inner tank and in a spiral heat exchanger going through the inner tank. The concept of stable supercooling of SAT and the heat transfer properties of the store filled with water or the SAT composite were studied. Results showed that 27 kWh of heat was stored between 25 °C and 90 °C, where the energy storage capacity of the composite was determined to be 21.3 kWh. This was 76 % higher than for a water heat store of the same volume. After a storage period in supercooled state at ambient temperature, 11.5 kWh (long-term capacity) of heat was discharged when the SAT composite solidified. This value corresponds to a heat of fusion of 207 kJ/kg. During charge and discharge in periods with solidification, the heat exchange capacity rates did not change with increase of flow rates. With discharge flow rates of 2 L/min applied in the mantle surrounding, thermal stratification was utilized. Thus, flow temperatures higher than the average SAT composite temperature resulted in liquid state. By additional use of the spiral, the discharge power reached 15 kW. During solidification the heat transfer was constantly decreasing, which resulted in a rather low discharge power. In building applications, heat transfer limitation could be overcome by discontinuous discharge via the mantle with intervals of 2 – 24 hours. Thus, thermal power of up to 4 kW was achieved and the outlet temperature was close to the average temperature of the SAT composite.

Keywords: Heat storage testing; Phase change material; Stable supercooling; Performance evaluation; Domestic heating.

Nomenclature

Symbols

| | |
|-------------|--|
| c_p | specific heat capacity (kJ/kg K) |
| C | energy storage capacity (kWh) |
| E | instant effectiveness (-) |
| HXCR | heat exchange capacity rate (W/K) |
| Δh | specific heat of fusion during solidification from supercooled state (kJ/kg) |
| k | heat loss coefficient (W/K) |
| L | latent heat (kJ/kg) |
| \emptyset | diameter (m) |
| Q | thermal energy, heat (kWh) |
| \dot{Q} | thermal power (kW) |
| t | time (h) |
| T | temperature ($^{\circ}\text{C}$) |
| \bar{T} | average temperature ($^{\circ}\text{C}$) |

| | |
|------------|----------------------------|
| ΔT | temperature difference (K) |
| \dot{V} | volume flow rate (L/min) |

Greek letters

| | |
|----------|-----------------------------|
| ρ | density (kg/m^3) |
| σ | standard deviation (% , K) |

Abbreviations

| | |
|---------|---|
| DHW | domestic hot water |
| HTF | heat transfer fluid |
| LabVIEW | laboratory virtual instrument engineering workbench |
| PCM | phase change material |
| SAT | sodium acetate trihydrate |
| SH | space heating |

1. Introduction

1.1. Sodium acetate trihydrate composites for heat storage

Sodium acetate trihydrate (SAT) has a melting point of $58\text{ }^{\circ}\text{C}$ and a latent heat of fusion of 264 kJ/kg [1]. It was identified as a suitable phase change material (PCM) for heat storage in households for space heating and domestic hot water supply [2]. SAT can cool down to the ambient temperature without solidifying and remain stable in supercooled state. The solidification can be reliably initiated by local cooling [3] or a seed crystal [4] and the heat of fusion released later when heat is in demand. The density of solid SAT in a closed sample solidified from supercooled state has been determined to be $1.24\text{--}1.28\text{ kg/L}$ [5].

Supercooling is considered to hinder the conventional use of PCMs. Ways of reducing the supercooling of SAT have therefore been investigated [6,7]. Recently, a review on nucleation triggering methods for PCMs was conducted by Beaupere et al. [8].

Additives are needed to prevent separation of dissolved and undissolved sodium acetate when SAT is supercooled below its melting temperature [9]. SAT composites with thickening agents and graphite were reported to overcome this problem with increased thermal conductivity [10], which is advantageous for heat transfer during solidification. During supercooling of SAT however, liquid additives are considered to be better because natural convection improves the heat transfer of heat exchangers. Kong et al. [11] investigated different stabilizers and concluded that SAT composites with HD 310, a liquid polymer prototype solution, had high heat of fusion after supercooling to room temperature.

1.2. PCM heat stores

PCMs are applicable in low and medium temperature applications [12], where a high potential for building applications was found [2]. PCMs with optimized melting temperatures can be utilized as passive thermal energy storage in the building envelope, leading to notable reduction of heat demand [13]. Among PCMs, salt hydrates are attractive due to their relatively high reaction enthalpies [14].

Because of heat transfer restrictions during PCM solidification, different heat exchangers have been investigated. Liu and Groulx [15] studied the heat transfer inside a horizontal cylindrical latent heat storage. The performance of internal bundle heat exchangers was investigated by Lopez-Navarro et al. [16]. Shell-and-tube heat exchangers [17] and macro encapsulated PCM in water vessels [18] were tested for sensible-latent heat storage. The solidification process of supercooled SAT was first modelled by Ma et al. [19], based on measured thermos-physical properties.

At the Technical University of Denmark, the concept of utilizing stable supercooling of SAT has been first applied to flat [20] and cylindrical [21] prototype heat storage units. Deng et al. [22] have assessed the thermal performance of a hot water tank that makes use of the stable supercooling of SAT in the mantle. A segmented PCM heat storage, consisting of four flat prototype units each containing approximately 200 kg SAT composite, was designed for application in a solar heating system and tested in combination with a water tank [23]. It was later applied for demonstration of a novel solar combi-system, utilizing stable supercooling of SAT [24]. The potential annual system performance in a Danish Passive House scenario was studied by system simulation, considering application of evacuated tubular collectors [25]. It was found that heat storage units could be charged several times during winter with surplus of wind energy and in summer, spring and autumn by solar collectors.

Rathgeber et al. [26] have found that acceptable energy storage capacity costs of heat stores in buildings ranged from about 1 €/kWh for seasonal heat storage to 429 €/kWh for daily utilization. For industrial use SAT is available in large quantities, market prices are typically below 0.5 €/kg. For heat storage units containing 200 kg SAT composites in solar combi-systems, monthly utilization of a heat storage capacity in the range of 15 – 27.4 kWh could be assumed. Then, acceptable costs would be in the range of 100 – 460 € per heat storage unit. Thus, inexpensive heat exchanger and PCM container design is required.

1.3. Scope

In this article, a cylindrical tank-in-tank heat storage with an internal spiral heat exchanger is presented. It is the first heat store utilizing stable supercooling of SAT composites built with low-cost standard components from industry, which were designed for water tanks. Experimental investigations were conducted to clarify the following aspects:

- Can stable supercooling of SAT be utilized with this heat store?
- Energy storage capacities for full charge, short and long-term heat storage based on a series of test cycles
- How does the SAT composite perform in comparison to water?
- Comparison of spiral- and mantle heat exchanger performance with different flow rates
- Is the heat transfer from the SAT composite to water sufficient to enable domestic hot water (DHW) and space heating (SH) supply in terms of flow temperature and power?

The presented results are valuable knowledge in pursue of developing economically attractive compact thermal energy storages that are more efficient than water storages. The investigation shows the potential differences in water and PCM storages and elucidates the way of operating a low cost PCM heat storage for optimal performance.

2. Energy storage capacity calculation

For energy storage capacity calculation of the heat store (C_{store}) the masses of pure SAT, additives, container, and heat transfer fluid (HTF) must be considered. The heat capacities of additives, the container and the HTF were calculated by the temperature-dependent specific heat capacity (c_p) multiplied with the temperature difference at the start and at the end of the heat transfer process. C_{store} results from the sum of the capacity of storage components:

$$C_{store} (kWh) = C_{SAT} + C_{additive} + C_{container} + C_{HTF} \quad (1)$$

For c_p -calculation of water (as HTF) the IAWPS standard [27] was used. The specific heat capacity of pure SAT has been determined by Araki et al. [28], where for solid state from 30 °C to 58 °C Equation 2 and for the liquid state from 30 °C to 80 °C Equation 3 was found:

$$c_{p,solid} \left(\frac{kJ}{kgK} \right) = 0.811 + 4.06 * 10^{-3} * T_{absolute} \quad (2)$$

$$c_{p,liquid} \left(\frac{kJ}{kgK} \right) = 1.56 + 4.27 * 10^{-3} * T_{absolute} \quad (3)$$

Where $T_{absolute}$ is the temperature of SAT in K. To the best knowledge of authors this is the most comprehensive study of SAT's heat capacity, it was therefore assumed that Equations 2 – 3 are applicable in the temperature range of 20–90 °C.

For SAT, three energy storage capacities are relevant:

$$C_{SAT} (kWh) = m_{SAT} * \left[\int_{T_{ambient}}^{T_{phase\ change}} c_{p,solid} dT + L + \int_{T_{phase\ change}}^{T_{final}} c_{p,liquid} dT \right] / 3600 \quad (4)$$

$$C_{SAT\ short-term} (kWh) = m_{SAT} * \int_{T_{ambient}}^{T_{final}} c_{p,liquid} dT / 3600 \quad (5)$$

$$C_{SAT\ long-term} (kWh) = m_{SAT} * \Delta h = m_{SAT} * \left[L - \int_{T_{ambient}}^{T_{phase\ change}} (c_{p,liquid} - c_{p,solid}) dT \right] / 3600 \quad (6)$$

The total energy storage capacity of SAT (C_{SAT}) is calculated for the full operation range, from ambient temperature ($T_{ambient}$) to the temperature at full charge (T_{final}), by employing Equation 4. Its short-term capacity ($C_{SAT\ short-term}$) results from supercooling to ambient condition and is calculated according to Equation 5. Its long-term capacity ($C_{SAT\ long-term}$) is the remaining heat of fusion after supercooling, calculated according to Equation 6. The latent heat of fusion (L) at 58 °C ($T_{phase\ change}$) has been determined to be in the range of 240 kJ/kg [29] to 264 kJ/kg [1]. The specific heat of fusion during solidification from supercooled state (Δh) is temperature-dependent. Δh is based on L , reduced by the difference of c_p in between liquid and solid states during supercooling. Experimental investigations on Δh have been conducted by Kong et. al [11], where heat contents of well-performing SAT composites have resulted in values between 200 and 220 kJ/kg at 20 °C.

Specific energy contents of SAT in calculated states are shown in Fig. 1. For passivation of nucleation seeds the liquid phase of SAT needs to exceed a temperature of 77 °C [28] to be able to supercool to ambient temperature.

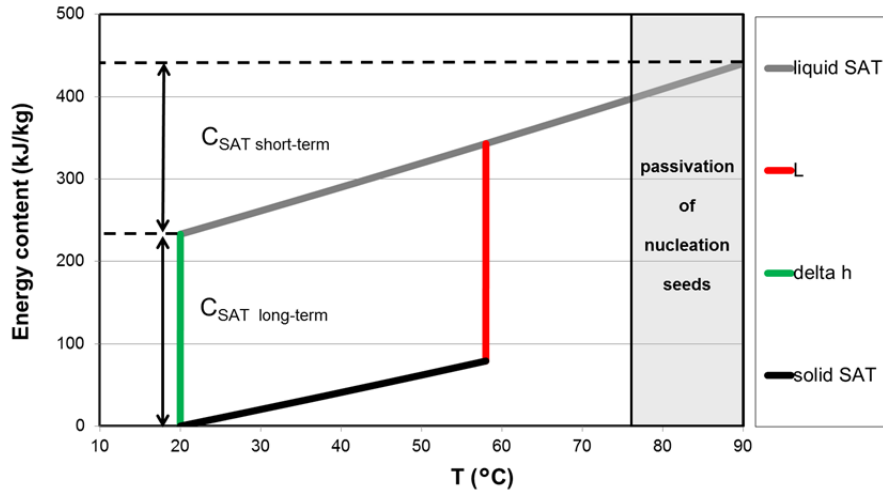


Fig. 1. Specific energy contents of SAT.

3. Method

3.1. Heat storage design

Inexpensive heat stores are needed for building application, which has to be addressed when utilizing SAT composites for heat storage. Therefore, a cylindrical heat storage prototype was built with standard components of water heat stores (scheme in Fig. 2 a). It was manufactured by the Danish company NILAN A/S. A steel tank with an outer diameter of 0.45 m contained the SAT composition and a spiral heat exchanger. It was situated in the centre of another steel tank with a diameter of 0.5 m, to realize heat exchange via its outer surface. By filling the volume between the two tanks with water, used as HTF a mantle heat exchanger was formed. An installer friendly, modular design was realized by rectangular shaped foam insulation and a metal cabinet with sufficient space for piping (Fig. 2 b).

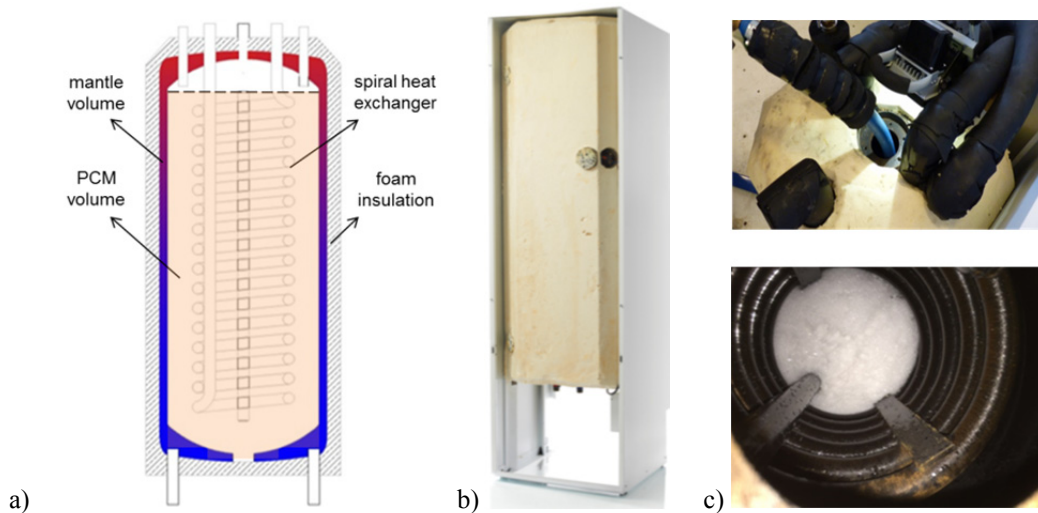


Fig. 2. a) Schematic drawing (intersection); b) Diagram of the cylindrical heat storage; c) Filling of melted SAT composite in the inner tank of the store.

For this work, a composite containing food-grade SAT (European standard 262i) from the German supplier IG Chemicals GmbH, 3 %wt. of the liquid polymer solution HD 310 from the Chinese company Suzhou Hongde Co. Ltd. and 2%wt. of extra water was chosen as PCM.

Crystalline SAT and additives were mixed in two closed vessels of 100 L, which were then placed for 72 hours in an oven at 90 °C. Afterwards, the melted SAT composite was filled into the pre-heated inner tank by means of a tube (Fig. 2 c). The melted SAT composite covered a height of 1.12 m, measured after the first full storage charge to a temperature of 90 °C. The resulting specifications of the heat store are presented in Table 1.

Table 1
Specification of the heat store.

| Container | | Spiral heat exchanger | | SAT composite | |
|----------------------------|--------------------|----------------------------|--------------------|-------------------------|------------------------------|
| Inner tank height: | 1.20 m | Outer coil Ø: | 0.35 m | Maximal volume at 90°C: | approx. 158 L* |
| Outer tank height: | 1.25 m | Number of windings: | 15.5 | Mass: | 200 kg |
| Mass including coil: | 140.8 kg | Coil height: | 0.8 m (centred) | SAT purity: | >98.5%wt. [30] |
| HTF volume: | 59 L | Outer tube Ø: | 0.032 m | $C_{p,solid}$ | 2.09 kJ/kg K at 41.5 °C [28] |
| Heat transfer area mantle: | 1.6 m ² | Heat transfer area spiral: | 1.8 m ² | $C_{p,liquid}$ | 3.04 kJ/kg K at 74° C [28] |

* Considering a density of 1.27 kg/L

3.2. Test setup

The layout of the test setup is presented in Fig. 3. A hydraulic circuit with two parallel lines for spiral- and mantle heat exchangers was built. For charging, an electrical heater with a power of 9 kW was used. Heat was discharged via a heat exchanger to a laboratory cooling circuit, where the cooling power was controlled via flow rate settings. In this way, inlet temperatures (T_{in}) around 25 °C for cooling the heat store were realized. Valves and pumps were set manually for either charging or discharging operation. A membrane vessel was connected to the top of the inner tank to avoid built-up of pressure due to volume changes of the SAT composite [5].

Each line was equipped with volume flow meters. Flow rates to the spiral- (\dot{V}_{spiral}) and to the mantle heat exchanger (\dot{V}_{mantle}) were controlled via string-valves. 5-junction thermopiles were installed to measure temperature differences (ΔT) between inlets and outlets of both lines, where additional thermocouples measured inlet- and outlet temperatures. The temperature of the inner tank was measured by thermocouples in 12 locations, where $T_1 - T_6$ were distributed evenly in a centred line and $T_7 - T_{12}$ were distributed in a distance of 0.19 m from the centre.

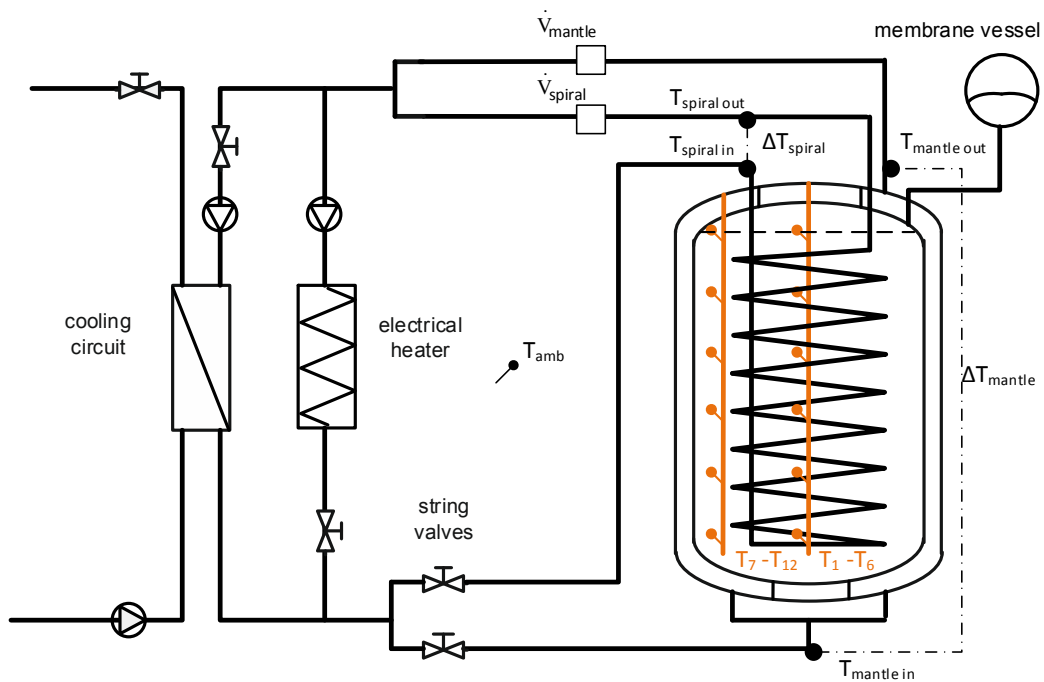


Fig. 3. Diagram of the test setup.

Initially, two glass rods (Fig. 4 a) were used to separate thermocouples and wires from the SAT composite. During the 3rd test cycles the central rod broke. It was therefore removed later and the thermocouples were reinstalled in direct contact to the SAT composite (Fig. 4 b). The ambient temperature was measured one meter from the heat store. Thermocouples and thermopiles were connected to a 16-channel thermocouple data acquisition module (NI9214). Flow meters were connected to a 32-channel digital input/output data acquisition module (NI9403). A LabVIEW program was used to read and to convert the signals every second into measurement values. Instant values were displayed on a monitor and the measurements were logged with minute-averaged values.

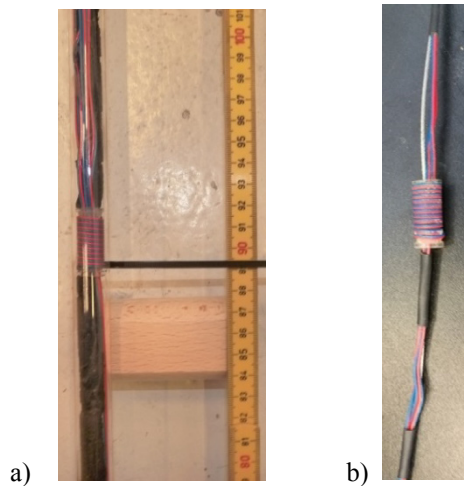


Fig. 4. Thermocouple installment in the inner tank: a) In glass rods; b) In contact with SAT composite alongside a steel rope.

An overview of measurements is given in Table 2, where the random variations of readings have been estimated in accordance to the guide to the expression of uncertainty in measurement [31]. The variation represents the half value of the confidence-interval of a measurand in normal distribution, in which 95.4% (2σ) and 68.2% (σ) of measured values occur.

Table 2
Measurements and their random variation.

| Measurand | Measurement device | Variation including data acquisition | Distribution | Source |
|--|--|--------------------------------------|----------------------|--|
| $\dot{V}_{\text{mantle}}, \dot{V}_{\text{spiral}}$ | Kamstrup Ultraflow 54, class 2 (EN 1434) | 0.5 (%) | normal (σ) | Calibration in accordance to manufacturer information [32] |
| $T_{\text{mantle in}}, T_{\text{mantle out}}, T_{\text{spiral in}}, T_{\text{spiral out}}, T_{\text{amb}}, T_1 - T_{12}$ | TT-type thermocouple (copper/ constantan) | 0.3 (K) | normal (2σ) | Experimental data analysis |
| $\Delta T_{\text{spiral}}, \Delta T_{\text{mantle}}$ | 5-junction thermopile with TT-type thermocouples | 0.15 (K) | normal (2σ) | Experimental data analysis |

3.3. Experimental investigations

Since the heat store was developed for SH and DHW supply in buildings, the following temperatures were considered for application:

- $T_{\text{ambient}} = 25 \text{ }^\circ\text{C}$ (room temperature)
- $T_{\text{in}} = 25 \text{ }^\circ\text{C}$ (space heating return flow in temperature equilibrium with the room; optimum)
- $T_{\text{final}} = 90 \text{ }^\circ\text{C}$ (maximum temperature from heat source; e.g. solar heating system)

The energy storage capacity of the container and the HTF was determined by charging with empty inner tank. Then, the heat store was tested with water, filled to a height of 1.12 m in the inner tank. Its heat content was tested as reference by charging and discharging via spiral- and mantle heat exchangers, applied combined and individually with HTF flow rates of 2 – 10 L/min.

The heat content and the heat transfer were tested with the SAT composite in a similar way. Fig. 5 shows the schematic development of the heat content during a test cycle, where the following test sequence was applied:

- Charging from ambient temperature with an initial thermal power of 9 kW and SAT composite in solid state. Full charge was reached when T_{in} reached $90 \text{ }^\circ\text{C}$ and T_{out} remained constant for about one hour. The charged heat (heat losses were deducted in the calculation) was defined as C_{store} .
- Next, the sensible heat of the storage was discharged while the SAT composite supercooled in liquid state. The storage was discharged to ambient temperature. The discharged sensible heat (storage heat losses were included in the calculation), was defined as the short-term energy storage capacity of the store ($C_{\text{short-term}}$).
- A resting period without heat losses followed, where the SAT composite remained in supercooled state.
- Afterwards, solidification of the SAT composite was initiated by a seed crystal inserted via a flange on top of the inner tank. Stored heat of fusion was then discharged. The long-term energy storage capacity of the storage ($C_{\text{long-term}}$) was defined as the discharge heat, including heat losses.

Several test cycles with combined and individual application of spiral- and mantle heat exchangers and variation of HTF flow rates have been conducted (Table 3). The following tests cycles differed from above mentioned procedure:

- During test cycle 2 supercooled SAT was recharged to 70 °C and then discharged to study $C_{\text{short-term}}$ without supercooling of the SAT composite.
- During test cycle 8, charging was interrupted when T_{out} fell to 30 °C and continued when T_{out} reached the average PCM composite temperature (\bar{T}_{PCM}). Manual seed injection was therefore conducted at $\bar{T}_{\text{PCM}} = 33$ °C.

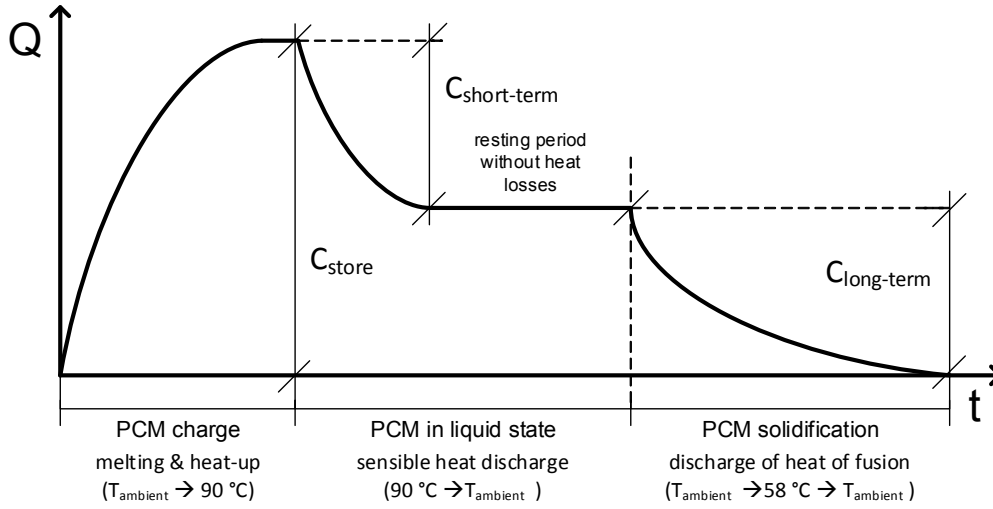


Fig. 5. Applied test cycle.

3.4. Performance evaluation

Thermal power of the heat exchangers was calculated by employing Equation 7:

$$\dot{Q}(\text{W}) = \dot{V} \cdot c_p \cdot \rho \cdot \Delta T \quad (7)$$

Where \dot{V} is the measured volume flow rate of the HTF, c_p is the specific heat capacity of the HTF at mean temperature between T_{in} and T_{out} , and ρ is the density of the HTF at T_{out} .

To determine heat losses, the store was charged by spiral- and mantle heat exchangers with $T_{\text{in}}=70$ °C a HTF flow rate of 2 L/min. A steady state was reached when the heat inflow was equal to the heat losses, resulting in a constant outlet temperature. It lasted for about 12 hours, where the data of the last 2 hours was used to calculate the heat loss coefficient (k) by employing Equation 8:

$$k \left(\frac{\text{W}}{\text{K}} \right) = \frac{\dot{Q}_{\text{spiral}} + \dot{Q}_{\text{mantle}}}{\frac{T_{\text{mantle in}} + T_{\text{mantle out}}}{2} - T_{\text{amb}}} \quad (8)$$

To reduce measurement uncertainty, T_{in} was calculated with the following relation:

$$T_{\text{in}} (\text{°C}) = T_{\text{out}} - \Delta T \quad (9)$$

The instant effectiveness (E) of the heat transfer during charging and discharging was determined with Equation 10:

$$E = \frac{T_{\text{in}} - T_{\text{out}}}{T_{\text{in}} - \bar{T}_{\text{PCM}}} \quad (10)$$

Where \bar{T}_{PCM} is the average SAT composite temperature. E expresses the ratio of actual to ideal heat transfer. Assuming a constant inlet temperature of 25 °C during discharge, E can be understood as the fraction of $\bar{T}_{PCM} - 25$ °C.

The heat exchange capacity rate (HXCR) was used to evaluate the ability to transfer thermal energy between the HTF and the SAT composite:

$$HXCR \left(\frac{W}{K} \right) = \dot{V} * c_p * \rho * \ln \left(\frac{T_{in} - \bar{T}_{PCM}}{T_{out} - \bar{T}_{PCM}} \right) \quad (11)$$

\bar{T}_{PCM} was calculated with a volume-based weight-model for inner tank measurements ($T_1 - T_{12}$). Fig. 6 shows the distribution and the weight of temperature readings, where the inner tank volume was idealised with a central cylinder and two annular spaces, divided into vertical segments (0.2 m in height). Segments of the central cylinder corresponded to $T_1 - T_6$, those of the outer annual space corresponded to $T_7 - T_{12}$ and the central annual space corresponded to the mean temperature value of the central cylinder and the outer annual space. Because the upper segments were filled half, their temperatures were considered with half weight.

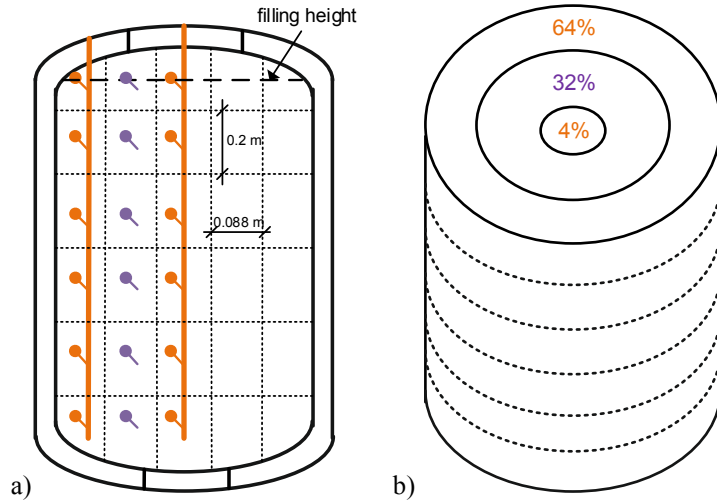


Fig. 6. Determination of \bar{T}_{PCM} : a) Distribution of temperature values (measured in orange, calculated in purple) over the intersection of the heat store: b) Weight of temperature readings corresponding to the volume.

To compare heat transfer properties of different tests, average values of E and HXCR were calculated. The integration of E and HXCR over the heat content of the store (Q_{store}) is illustrated for E:

$$E_{average} = \frac{\int_{\bar{T}_{PCM,1}}^{\bar{T}_{PCM,2}} E dQ_{store}}{\int_{\bar{T}_{PCM,1}}^{\bar{T}_{PCM,2}} Q_{store}} \quad (12)$$

Intervals of \bar{T}_{PCM} were chosen in order to exclude the effect of heat-up and cool-down of heat exchangers: a) charge from 30 °C to 80 °C; b) discharge in liquid state from 80 °C to 30 °C; c) discharge during solidification from 58 °C to 35 °C.

4. Results and discussion

4.1. Proof of concept

The development of stored heat (Q_{store}) and the thermal power (\dot{Q}) during the 5th test cycle is presented in Fig. 7. The orange area marks data measured during charging (solid and liquid phases of SAT), the grey area marks data with SAT in liquid state and the blue area marks data during discharge after SAT composite solidification was initialized.

During charging from initially solid PCM state 27 kWh of heat was stored. Thermal power started at 8 kW and fell below 7.5 kW after 2 hours. After 6 hours \bar{T}_{PCM} reached 88 °C. It took additional 4 hours to reach a steady state with \bar{T}_{PCM} at 90 °C. Then the sensible heat of the store was discharged and cooled down to ambient temperature within 2 hours. Thermal power peaked at 34 kW when the cooling circuit was activated. The high discharge power was mainly due to discharging the 59 L heated HTF in the mantle. Then a resting period of 15 hours was followed by manual seed crystal insertion. As consequence, \bar{T}_{PCM} rose to 58°C. Heat of fusion was discharged with thermal power peaking at 5.9 kW. It took about 13 hours until \bar{T}_{PCM} reached ambient conditions.

In liquid SAT state, the prototype worked as sensible heat storage with a capacity of 15.5 kWh. After a period without heat losses, which in theory can be extended to several months, 11.5 kWh of heat was discharged. This proved that the storage unit could be used for combined short and long-term heat storage.

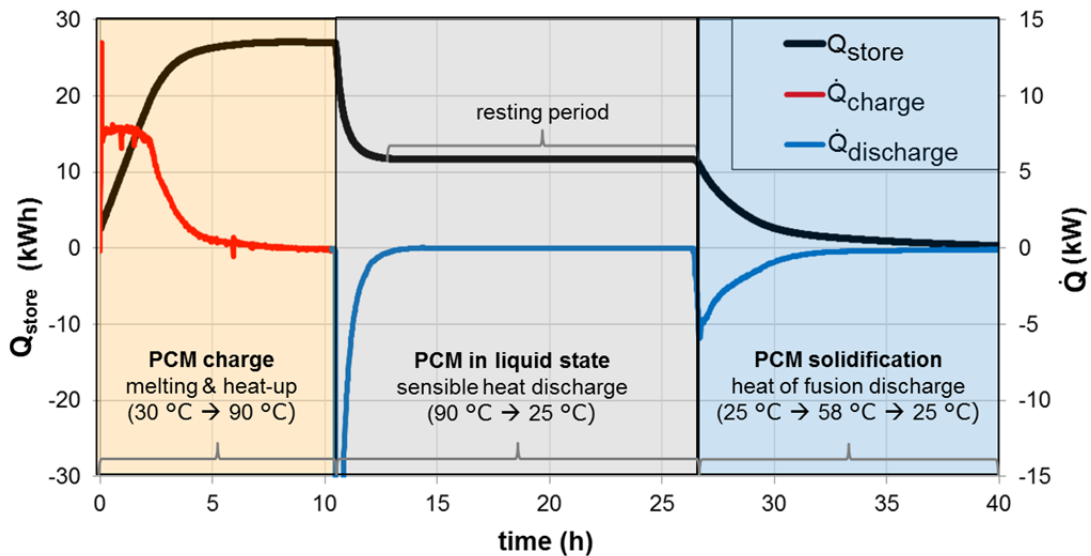


Fig. 7. Development of \dot{Q} and Q_{store} during the 5th test cycle.

4.2. Supercooling stability

Table 3 presents supercooling temperatures and set flow rates during test cycles. In all 12 cycles, low supercooling temperatures were achieved. However, supercooling was only stable in test cycles 1, 2, 5, 7 and 8 where solidification was manually initiated. In other tests uncontrolled crystallization occurred, potentially due to the following reasons:

- In cycle 3 and 4 one of the installed glass rods for internal temperature measurements (Fig. 4 a) was defect. Data analysis showed that SAT crystallization started from the bottom of the inner tank volume, where the rod was broken and therefore ambient air (containing nucleation seeds) could enter the inner tank.

- During cycle 6 and 9 – 12 SAT crystallization started from the top of the inner tank volume. Later inspection showed a corroded top surface of the inner tank with traces of salt, which was not in contact with the SAT composite. It can be assumed that nucleation seeds could remain there and eventually fall on the supercooled SAT composite during cool-down. Other explanations could be that open thermocouple wires (Fig. 4 b) were not suitable for testing and that one of the top-flanges of the inner tank became un-tight.

Despite the open thermocouple wires and corroded inner tank surfaces low supercooling temperatures were achieved. Data of all tests could therefore be used for energy storage capacity and heat transfer analysis. For an improved heat store, the above mentioned problems could potentially be avoided by:

- Using oil instead of air in the expansion volume in the inner tank to avoid corrosion
- Design of the inner tank with a single, well-sealed opening for filling and pressure compensation
- No internal temperature measurements

Table 3

Test cycles with SAT composites.

| Test cycle | Starting date | Supercooling temperature (\bar{T}_{PCM}) | Resting period | HTF flow rates (spiral/ mantle heat exchanger) | | |
|------------|---------------|--|----------------|--|---------------------------|---------------------------------|
| | | | | Charge | Discharge in liquid state | Discharge during solidification |
| 1 | 12.06.2016 | 24 °C | 24 h | 3/ 3.5 L/min | 6.5/ 6.5 L/min | 2/ 1.6 L/min |
| 2 | 16.06.2016 | 25 °C | 10 h | 7/ 7 L/min | 5.5/ 5.5 L/min | 2/ 2 L/min |
| 3 | 6.02.2017 | 33 °C | 0 h | 5/ 5 L/min | 5/ 5 L/min | 5/ 5 L/min |
| 4 | 13.02.2017 | 34 °C | 0 h | 5/ 5 L/min | 5/ 5 L/min | 5/ 5 L/min |
| 5 | 20.03.2017 | 24 °C | 14 h | 5/ 5 L/min | 5/ 5 L/min | 2/ 2 L/min |
| 6 | 30.03.2017 | 30 °C | 0 h | 5/ 5 L/min | 2/ 2 L/min | 2/ 2 L/min |
| 7 | 11.07.2017 | 26 °C | 6 h | 10/ 10 L/min | 5/ 5 L/min | 5/ 5 L/min |
| 8 | 14.07.2017 | 33 °C | 0 h | 10/ 10 L/min | 0/ 2 L/min | 0/ 2 L/min |
| 9 | 19.07.2017 | 24 °C | 0 h | 7/ 7 L/min | 0/ 2 L/min | 0/ 2 L/min |
| 10 | 27.07.2017 | 27 °C | 0 h | 0/ 5 L/min | 2/ 0 L/min | 2/ 0 L/min |
| 11 | 23.01.2018 | 30 °C | 0 h | 5/ 5 L/min | 2/ 2 L/min | 2/ 2 L/min |
| 12 | 24.01.2018 | 26 °C | 0 h | 5/ 5 L/min | 3/ 3 L/min | 3/ 3 L/min |

4.3. Thermal capacities

Determined energy storage capacities are presented in Table 4. The capacity of the container and the filled spiral- and the mantle heat exchangers was 5.7 kWh. C_{store} was 27 kWh with SAT composite. The storage capacity of the SAT composite (C_{PCM}) was calculated to be 21.3 kWh, which was 76 % higher than for water ($C_{water} = 12.1$ kWh). After heat-up to 90 °C, 15.5 kWh ($C_{short-term}$) of sensible heat was discharged as the PCM cooled down to supercooled state and 11.5 kWh ($C_{long-term}$) were discharged after solidification was initialized at 25 °C. This means that 43 % of C_{store} could be stored over long periods without sensible heat losses. The heat loss coefficient of the store was determined to be of 2.4 W/K.

By heat-up to 70 °C, it was ensured that nucleation seeds remained in the liquid SAT composite. The store

provided then 21.8 kWh of heat for short-term usage, utilizing SAT crystallization at 58 °C. $C_{\text{short-term}}$ was then 81 % of C_{store} , which was higher than the capacity of the storage filled with water (66 % of C_{store} at 90 °C).

Referring to the SAT composite mass, Δh was determined to be 207 kJ/kg. This value is 7 kJ/kg higher than found by a heat loss method [11] for a composition with 2 % HD 310 and 2 % extra water, where a lower supercooling temperature (20 °C) was applied.

Table 4
Energy storage capacities with water and SAT composite.

| Temperature range | Capacity (kWh) | | % | Reference |
|------------------------|--|------|-----|---|
| Charge: 25→90 °C | $C_{\text{container}} + C_{\text{HTF}}$: | 5.7 | 21 | heat-up of empty store* |
| | $C_{\text{store with water}}$: | 17.8 | 66 | 3 charging tests (spiral, mantle and combined) with $\dot{V}_{\text{HTF}} = 10 \text{ L/min}^*$ |
| | C_{water} | 12.1 | 45 | $C_{\text{store}} - C_{\text{container}} - C_{\text{HTF}}$ |
| | $C_{\text{store with SAT composite}}$: | 27 | 100 | test cycles: 2 – 11* |
| | C_{PCM} | 21.3 | 79 | $C_{\text{store}} - C_{\text{container}} - C_{\text{HTF}}$ |
| Discharge: 90→25 °C | $C_{\text{short-term with supercooling}}$: | 15.5 | 57 | test cycles: 2,5** |
| Discharge: 70→25 °C | $C_{\text{short-term without supercooling}}$: | 21.8 | 81 | test cycle: 2* |
| Discharge: 25→25 °C | $C_{\text{long-term}}$: | 11.5 | 43 | test cycles: 1 – 12* |

* Values from test cycles were adapted to the given temperature range (according to section 2)

** Exact temperature range applied

4.4. Storage temperature development

Fig. 8 shows the development of the average temperatures of water (\bar{T}_{water} , blue curves) and SAT composite (\bar{T}_{PCM} , black and grey curves) in the inner tank over measured Q_{store} during charge. Charging of water stopped at various temperatures, while PCM charge finished above 85 °C. The store was initially at ambient temperature, and then the average tank filling temperature (\bar{T}) rose with delay due to heat-up of HTF and heat exchangers. From about 2 kWh on, \bar{T}_{water} was directly proportional to the heat content, independent from heat exchanger and flow rate selection. The method for determination of \bar{T} was therefore valid.

\bar{T}_{PCM} rose non-linear, due to combined sensible heat-up and phase change of SAT composite. The temperature of heat exchangers exceeded the melting temperature of SAT (58 °C) around a heat content of 5 kWh, when a phase of liquid SAT composite started to be formed around the heat exchanger surfaces. Higher HTF flow rates correspond to slightly lower \bar{T}_{PCM} . Slower increase of \bar{T}_{PCM} was observed in the ranges of 45 – 55 and 70 – 75 °C when transferred heat was merely consumed to melt SAT composite. This happened at significantly higher temperatures (60 – 75 °C) when only the mantle heat exchanger was applied, which means that the core of the PCM was melted significantly later. During all tests the bottom of the inner tank remained coldest, the melting process was therefore accomplished around $\bar{T}_{\text{PCM}} = 75 \text{ °C}$ and $Q_{\text{store}} = 24 \text{ kWh}$. For more homogenous charging the spiral heat exchanger should be located at a lower position.

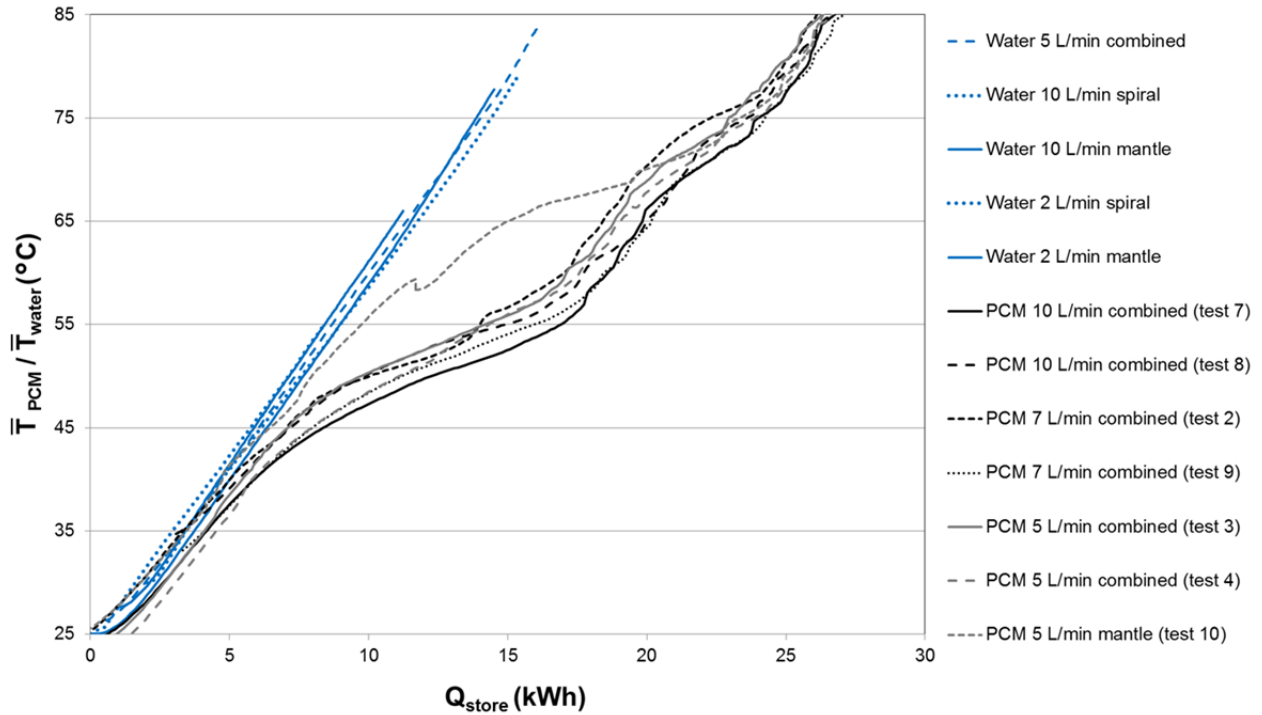


Fig. 8. Development of average water and SAT composite temperatures during charging.

Fig. 9 shows the development of \bar{T}_{PCM} over Q_{store} during charging and discharging for selected cycles. The measured energy contents were compared with calculated values according to Equations 1 – 4 (black curves), using experimentally determined C_{store} , $C_{container}$ and C_{HTF} as reference.

Data from combined charge tests (Fig. 8) was averaged and the resulting curve differed significantly from calculated energy content until phase change was accomplished at 75 °C. SAT solidification was initialized at 26 °C during the 7th and the 12th test cycle and at 30 °C during the 6th test cycle. Their heat storage capacities showed a high degree of similarity, indicating that the heat content did not significantly change after 12 test cycles, conducted over a time-span of 19 months.

From 75 °C to 85 °C the charge tests curve was slightly above the calculated states, because the HTF in the heat exchangers was warmer than \bar{T}_{PCM} . Discharge curves started below calculated values because the HTF in the heat exchangers was at ambient temperature, the curves therefore converged to calculated heat contents with falling \bar{T}_{PCM} .

In the temperature range of 86 – 90 °C (blue marked area) data was incomplete, due to heat storage cool-down before HTF flow was applied. Measurement data in the green marked area showed deviations to calculated states due to warmer HTF during charging and colder HTF during discharging, in comparison to \bar{T}_{PCM} .

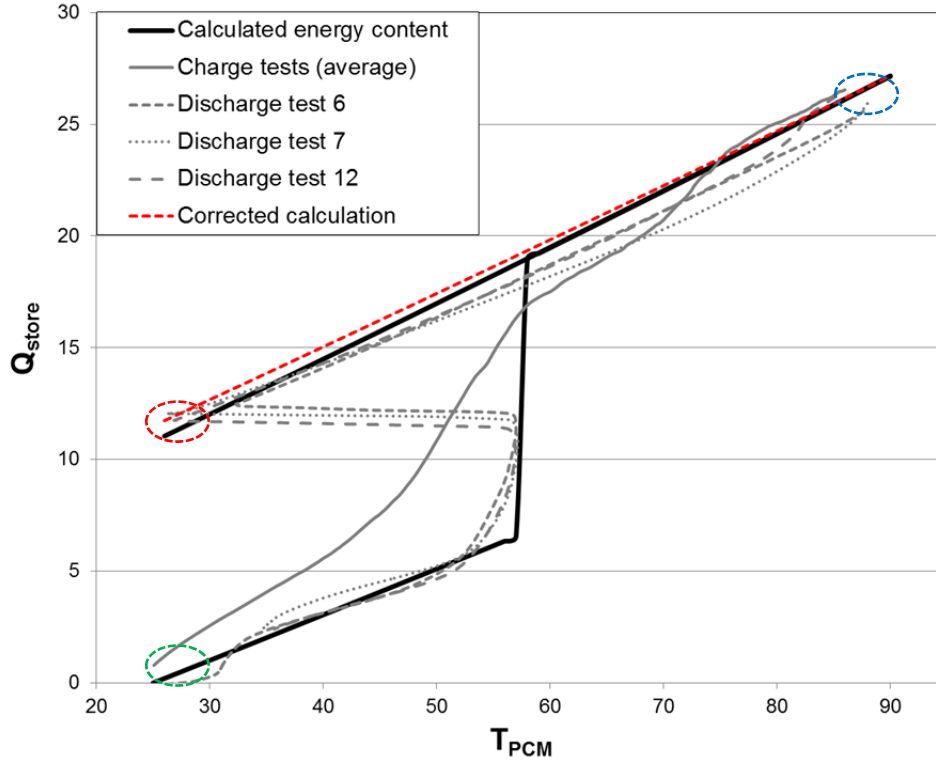


Fig. 9. Comparison of calculated and measured states during charging and discharging.

Data in the red marked area showed that measured $C_{\text{long-term}}$ (11.5 kWh at 25 °C) was higher than calculated (10.8 kWh at 25 °C). This indicated that Equation 3 is not valid for liquid SAT composites. Instead, Equation 13 should be applied:

$$c_{p,\text{liquid}} \left(\frac{\text{kJ}}{\text{kg K}} \right) = 1.56 + 3.65 * 10^{-3} * T_{\text{absoute}} \quad (13)$$

By corrected calculation L was determined to be 238 kJ/kg SAT, which had a minimal purity of 98.5% (Table 1). This result corresponds to reference investigations of SAT containing 1%wt. of nucleating agents as impurity where L was found to be 237 – 243 kJ/kg SAT [29].

4.5. Heat transfer analysis

Fig. 10 presents the development of HXCR and E during charging of water (blue curves) and SAT composites (black curves) over Q_{store} . At the beginning ($Q_{\text{store}} < 2$ kWh) the HTF was heated up and values were therefore not representative.

The development of curves with SAT composite of both parameters was related to the melting behaviour (Fig. 8), values were therefore lowest in between 5 and 15 kWh, when PCM was merely melted and raised when PCM was merely heated up. The HXCR (Fig. 10 a) did not change in the flow rate range of 5 – 10 L/min. This indicated that the flow regime of the HTF did not change and the heat transfer was limited by the SAT composite. Values ranged in between 250 and 400 W/K and were highest when SAT was merely heated up and convection of the melted SAT composite increased. As a consequence, E (Fig. 10 b) was highest with $\dot{V}_{\text{HTF}} = 5$ L/min (0.32 – 0.4) and lowest with $\dot{V}_{\text{HTF}} = 10$ L/min (0.2 – 0.25). This indicated that higher flow rates led to more homogeneous heat exchanger temperatures and higher return temperatures resulted.

During test with water, individual use of the mantle heat exchanger showed rather constant HXCR and E values throughout the whole process, while individual use of the spiral heat exchanger showed slightly decreasing values until 12 kWh, followed by a sharp decrease until fully charged. This shows that the spiral heat exchanger could not efficiently heat the bottom of the heat store. Combined application of heat exchangers resulted in raising HXCR and E until 15 kWh, followed by a decrease until fully charged. E ranged from 0.5 to 0.6 during combined charge with $\dot{V}_{HTF} = 10$ L/min, which was about a factor of three higher than with SAT composite.

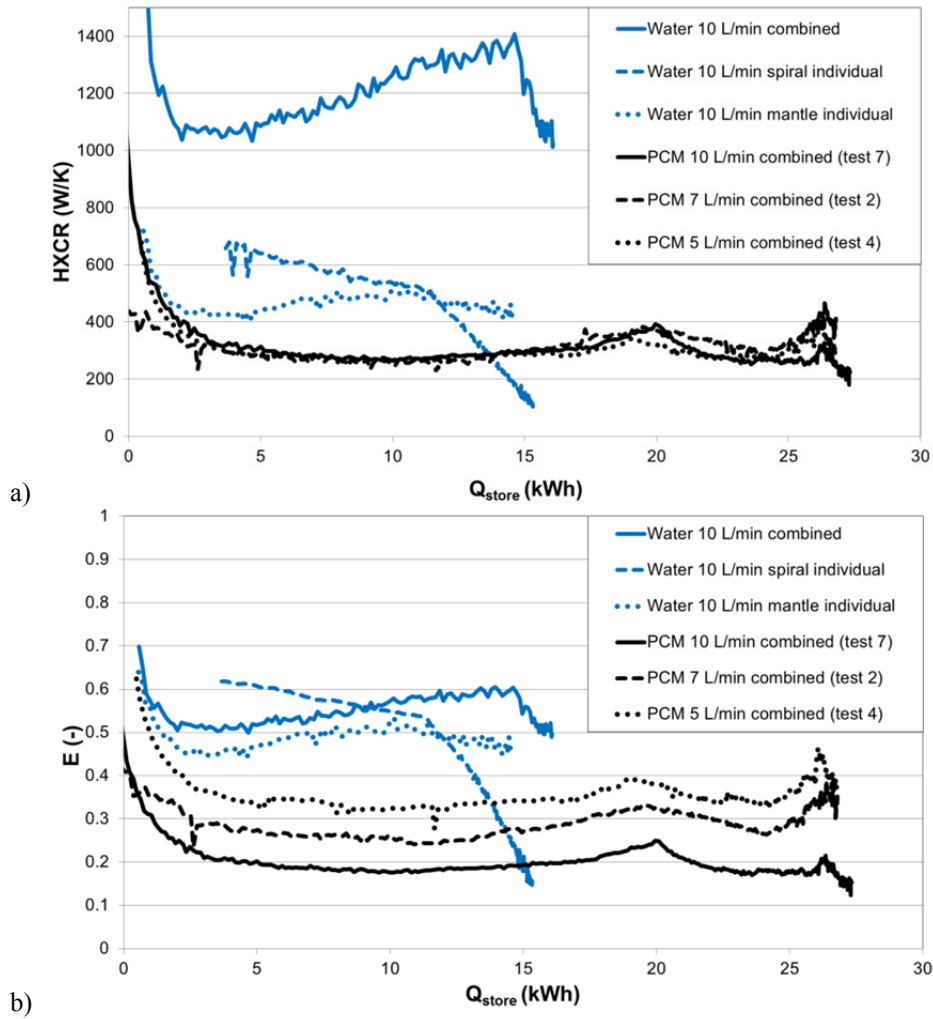


Fig. 10. Development of heat transfer during charging: a) HXCR; b) E.

Fig. 11 presents the development of E over Q_{store} with SAT composite and water filling during discharge. Because of different supercooling degrees (Table 3) values were not comparable in between 11 and 13 kWh.

With liquid SAT composite individual application of spiral- and mantle heat exchangers with $\dot{V}_{HTF} = 2$ L/min was more effective than with water. The mantle heat exchanger achieved $E > 1$ throughout cool-down of the PCM because of thermal stratification in the mantle HTF volume. When $\dot{V}_{HTF} = 2$ L/min was applied to both heat exchangers the development of E almost matched with the mantle heat exchanger. Like during charge of SAT composites, higher flow rates lead to significant lower E, indicating heat transfer restriction. Therefore, with $\dot{V}_{HTF} = 5$ L/min the instant effectiveness was higher with water than with SAT composite throughout discharge.

During SAT composite solidification E was significantly lower. No convection was possible and a growing layer of solid SAT composite, which had a low thermal conductivity, covered heat exchanger surfaces. With both heat exchangers in use, more heat could be discharged with a thinner solid PCM layer on their surfaces, in relation to individual heat exchanger application. With $\dot{V}_{HTF} = 2$ L/min individual heat exchanger operation performed therefore worse than combined operation. E was more than halved when \dot{V}_{HTF} was raised from 2 L/min to 5 L/min in solid SAT composite state.

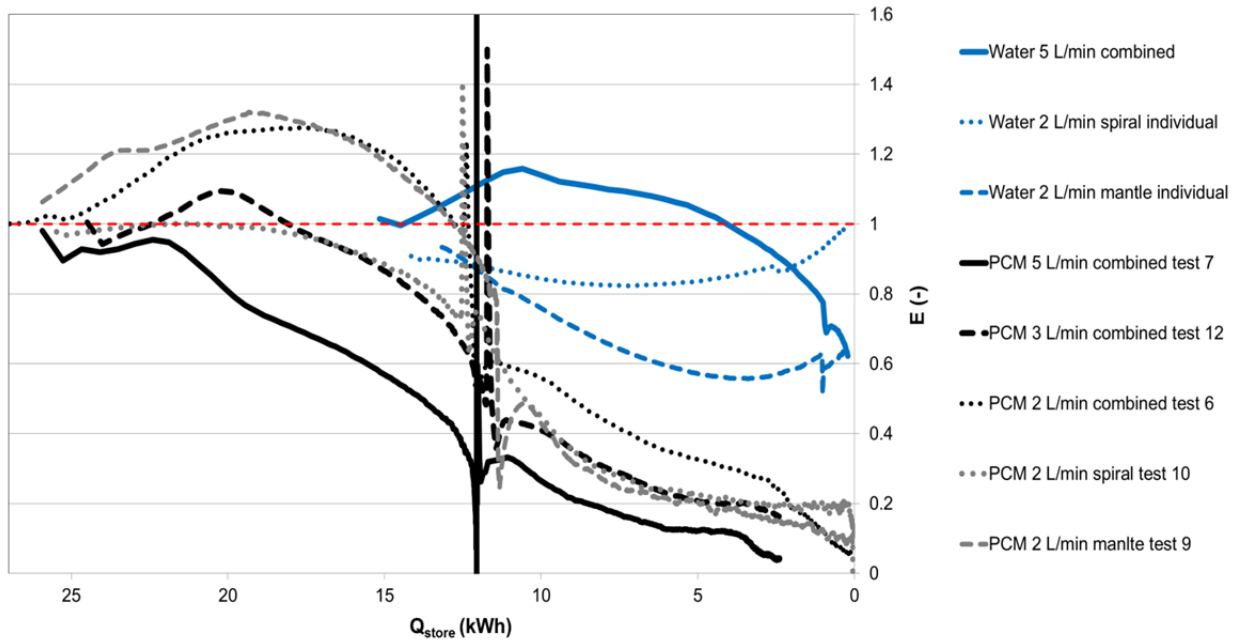


Fig. 11. Development of E during discharge.

Because of thermal stratification ($E > 1$) HXCR calculation was not possible for SAT composite in liquid state. Fig. 12 presents therefore HXCR of discharge tests with SAT composite during solidification and with water. As during charging, change of HTF flow rate did not cause significant changes when both heat exchangers were applied. HXCR started between 250 and 300 W/K, which was as high as during charge. Afterwards, they steadily decreased to a value of about 90 W/K. At the end of discharge ($Q_{store} \sim 3$ kWh) HXCRs dropped rapidly to about 20 W/K, which was due to the geometry of the store: The core of the inner tank remained at around 55 °C, while the outer volume was close to the HTF temperature.

HXCR values during discharge with individual heat exchangers ($\dot{V}_{HTF} = 2$ L/min) started above 100 W/K and decreased steadily to 20 W/K. This means that a reduction of factor 3 in comparison to combined discharge.

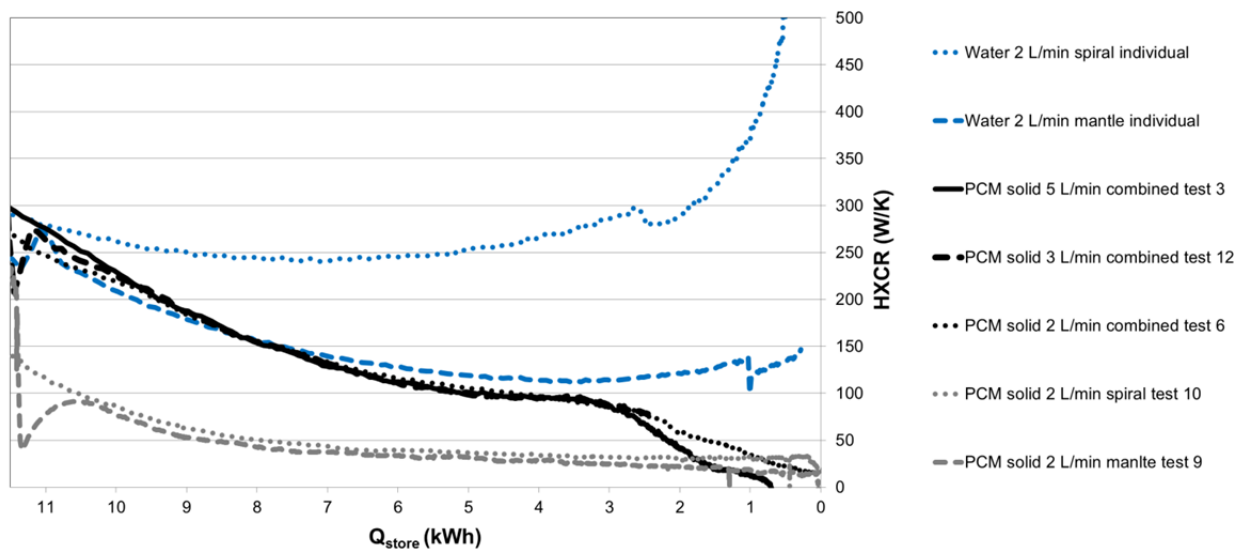


Fig. 12. Development of HXCR during discharge.

Table 5 presents an overview of average HXCR and E during charge and discharge with both heat exchangers. The following settings have been advantageous with SAT composites:

- For charging, a HTF flow rate of 10 L/min ensured homogeneous heat exchanger temperatures, which is needed for reliable passivation of nucleation seeds. The average HXCR was a factor of four and E a factor of 2.8 lower than during charge of water.
- Tests with 2 L/min performed best during discharge of PCM. In liquid state heat was discharged with an effectiveness of 1.23, which was higher than during discharge of the water tank with 5 L/min. However, during solidification of SAT composite E was a factor of 3 lower than in liquid state and the average HXCR about half in comparison to charge.

Table 5

Average HXCR and effectiveness and during selected tests.

| Interval of \bar{T}_{PCM} | SAT composite | | Water | |
|-----------------------------|---|-------------------------------|--|----------|
| 30 → 80 °C | average HXCR with $\dot{V}_{HTF} = 10$ L/min during charge | 298 W/K (combined, test 7) | average HXCR with $\dot{V}_{HTF} = 10$ L/min during charge | 1215 W/K |
| 30 → 80 °C | average E with $\dot{V}_{HTF} = 10$ L/min during charge | 0.20 (combined, test 7) | average E with $\dot{V}_{HTF} = 10$ L/min during charge | 0.56 |
| 80 → 30 °C | average E with $\dot{V}_{HTF} = 2$ L/min in liquid state | 1.23 (combined, test 6) | average E with $\dot{V}_{HTF} = 5$ L/min during discharge | 1.10 |
| 58 → 35 °C | average HXCR with $\dot{V}_{HTF} = 2$ L/min during solidification | 156 W/K (combined, test 6) | | |
| 58 → 35 °C | average E with $\dot{V}_{HTF} = 2$ L/min during solidification | 0.43 (combined, test 6) | | |

4.6. Discharge power

Fig. 13 presents the developments of thermal power (\dot{Q}) over \bar{T}_{PCM} and \bar{T}_{water} during discharge in liquid state. With \dot{V}_{HTF} in the range of 1.5 – 2 L/min a high degree of similarity for SAT composite and water was found. With only spiral- or mantle heat exchanger applied, \dot{Q} was 7 – 9 kW at $\bar{T} = 80$ °C and 1 – 2 kW at $\bar{T} = 30$ °C, whereas with both heat exchangers \dot{Q} reached approximately 15 kW at $\bar{T} = 80$ °C. With flow rates of 3 – 5 L/min the development of \dot{Q} did not change significantly with SAT composite, whereas with water significantly higher discharge power resulted. However, \dot{Q} was considered to be sufficient to enable heat supply in households during all tests.

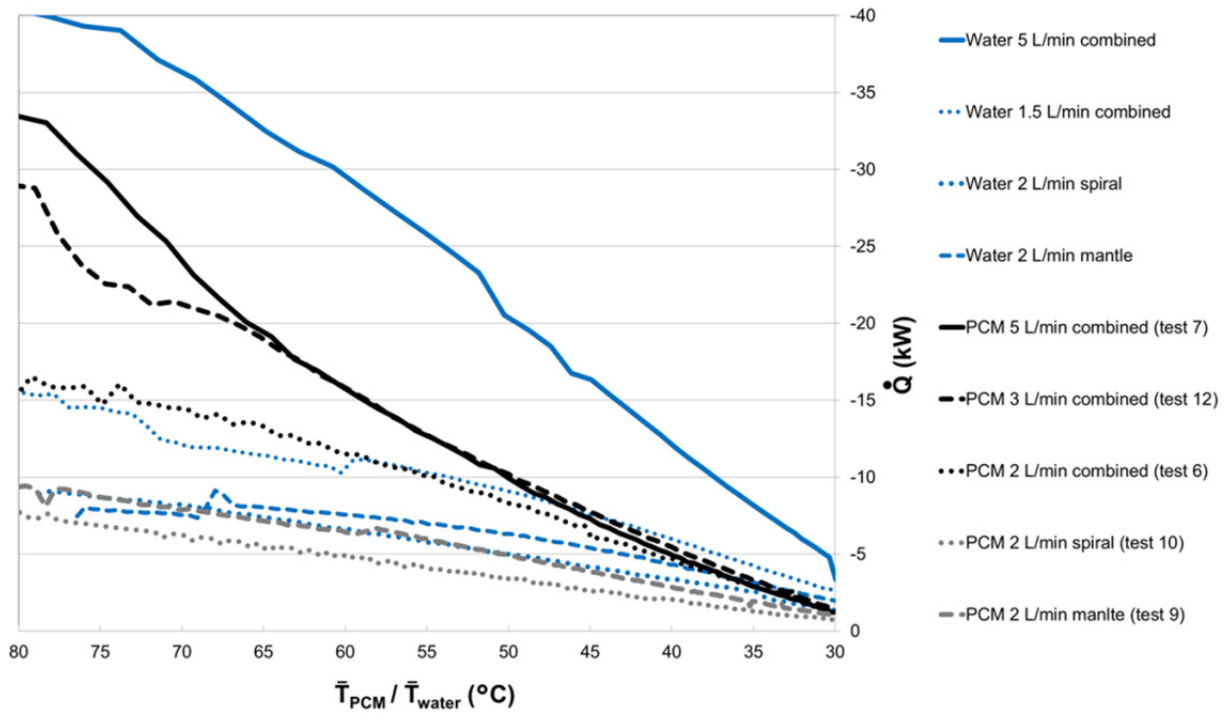


Fig. 13. \dot{Q} during discharge in liquid state.

Fig. 14 presents the development of \dot{Q} over \bar{T}_{PCM} during solidification of the SAT composite. As indicated by analysis of HXCR, no significant influence of HTF flow rates on thermal power was found. Instead, the curves differed due to variation of the inlet temperature (T_{in}), where lower T_{in} resulted in higher \dot{Q} . During test 6 and 12 T_{in} remained almost constant at the set temperature (25 °C), while it increased to 28 °C during test 7 and it decreased to 22 °C during test 6.

The shape of the curves had a high degree of similarity: During combined discharge \dot{Q} started above 5 kW, followed by a sharp decrease to 1.5 – 2.2 at 50 °C and decreased afterwards steadily. Thermal power dropped below 1 kW at $Q_{store} \sim 3$ kWh during tests 1, 6 and 12 and at $Q_{store} \sim 4$ kWh during test 7. Individual heat exchanger application reduced thermal power to approximately less than half, in comparison to tests 6 and 12.

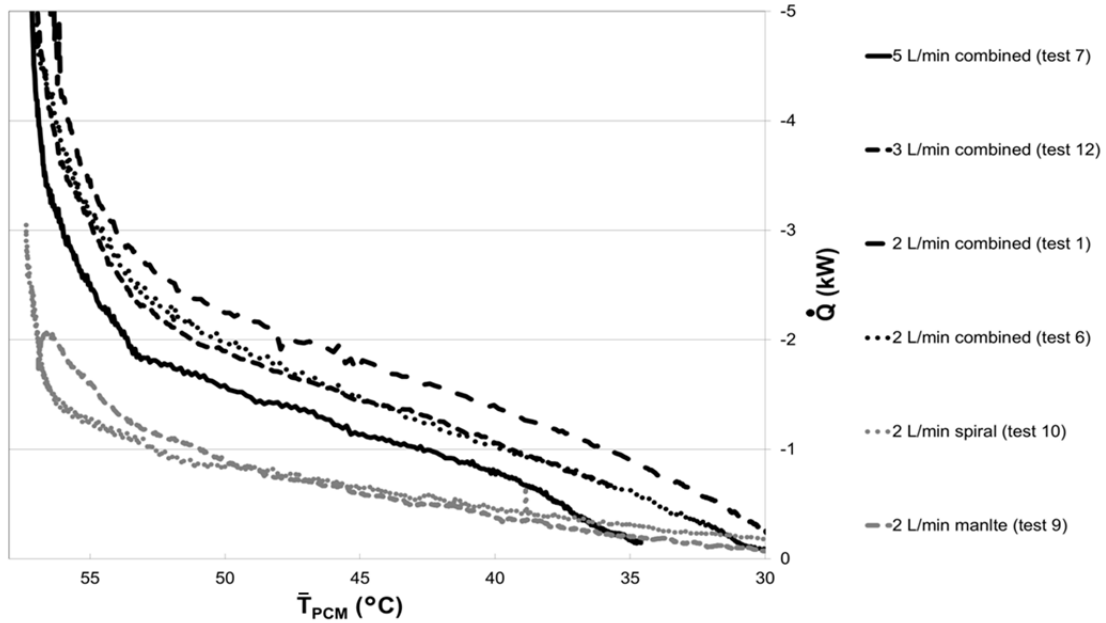


Fig. 14. \dot{Q} during discharge during solidification.

4.7. Discontinuous discharge

Fig. 15 presents data from the 8th test cycle, in which continuous charge was followed by discontinuous discharge via the mantle heat exchanger with a flow rate of 2 L/min. After full charge was achieved (orange area), the store remained hot for about 10 hours, while its heat content was reduced due to sensible heat losses in liquid state (grey area). Then, it was discharged twice in liquid state and interrupted when T_{out} fell to the value of \bar{T}_{PCM} . Crystallization of the SAT composite was initiated at $\bar{T}_{PCM} = 33$ °C. Discharge of the latent heat (blue area) was conducted in seven parts, with intervals of 2 – 24 hours. Thermal power reached around 4 kW during six discharge events, and heat-draws ranged between 1 and 2 kWh for each part discharge.

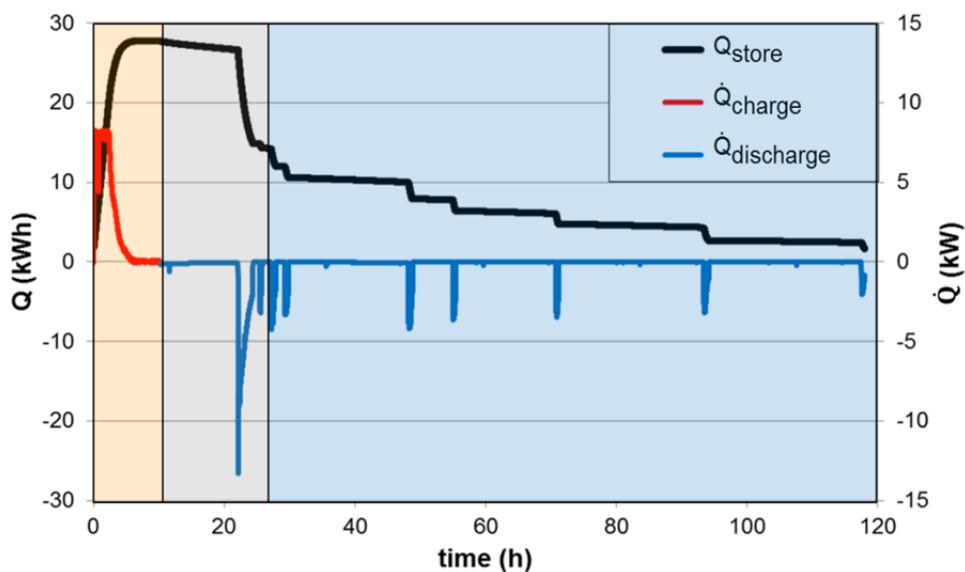


Fig. 15. Development of \dot{Q} and Q_{store} during the 8th test cycle.

As shown in Fig. 16, it was possible to utilize thermal stratification and therefore increased flow temperatures during the entire discharge. In liquid state, E was above one and therefore $T_{out} > \bar{T}_{PCM}$. During solidification E was close to one during the first five discharge events, while during the last two discharge events E exceeded one, because the intervals were 24 hours and the HTF had therefore sufficient time to build up maximal stratification in the mantle volume. T_{out} exceeded 30 °C during all discharges, which is considered as requirement for SH and DHW supply in domestic dwellings. However, for a single-family household the necessary time intervals between discharge events would be too long to cover heat demands. Therefore, a storage system consisting of several tank-in-tank stores would be needed. This would be an economically attractive solution to utilize stable supercooling of SAT composites without need for (potentially expensive) enhancement of the thermal conductivity.

After the last discharge event, \bar{T}_{PCM} remained at 30 °C, which corresponds to a heat content of 1.2 kWh. Since recharge would be needed for further heat supply, the applicable energy storage capacity was determined to be 25.8 kWh.

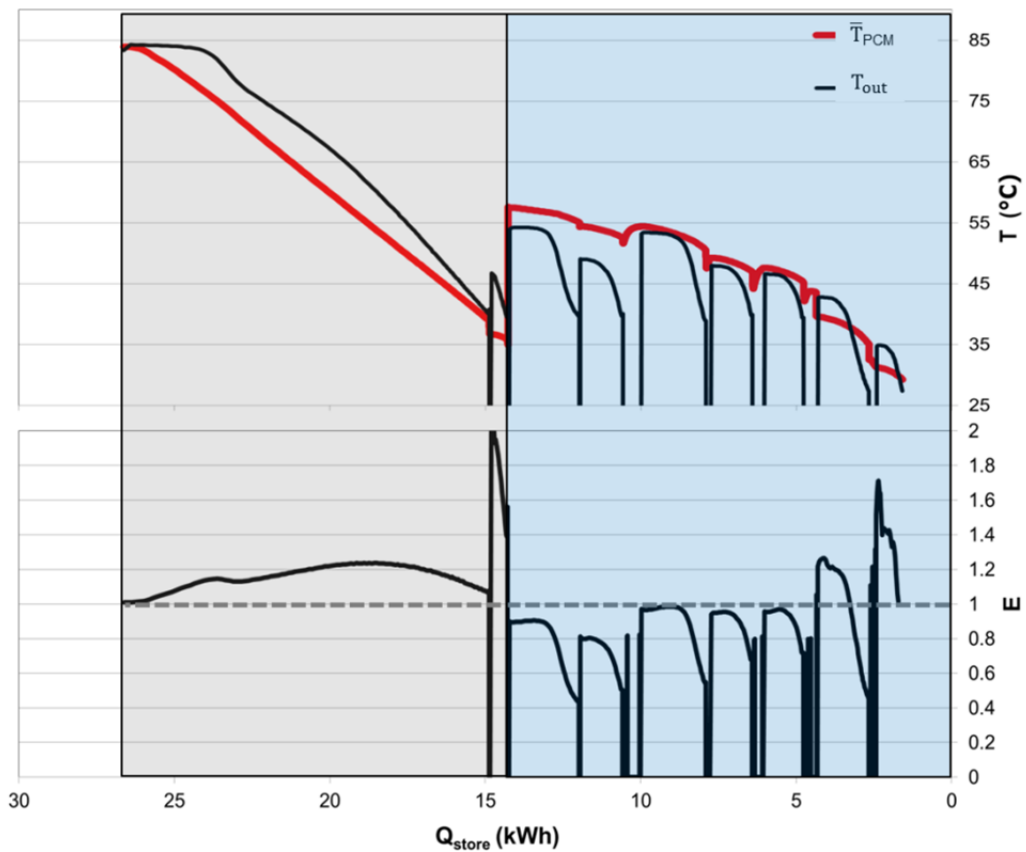


Fig. 16. T_{out} and E during discontinuous discharge.

5. Conclusions

Utilization of stable supercooling of SAT composites for combined short- and long term heat storage was demonstrated with a tank-in-tank store which was built with standard components for water heat stores. Evaluation of test cycles resulted in the following findings:

- During all 12 test cycles low supercooling temperatures were achieved although temperature measurement devices and corrosion on the inner tank surface influenced supercooling stability.
- The energy storage capacity of the store was measured to be 27 kWh for heat-up from 25 to 90 °C, whereas 15.5 kWh of heat was discharged in liquid state and 11.5 kWh of heat was stored in the supercooled PCM. The capacity of the composite was determined to be 21.3 kWh, which was 76 % higher than with water filled in the tank. Based on these capacities, the latent heat of fusion of the composite was calculated to be 238 kJ/kg, whereas 207 kJ/kg could be utilized during solidification from supercooled state at 25 °C.
- Heat exchange capacity rates during charging and discharging of SAT composite did not change in the flow rate range of 3 – 10 L/min, which means that the heat transfer was limited by the SAT composite. Heat-up from 30 °C to 80 °C resulted in an average heat exchange capacity rate of 298 W/K, which was a factor of four lower than for water with a flow rate of 10 L/min.
- During discharging, increase of flow rate increased thermal power only significantly below 3 L/min in liquid state, whereas during solidification no dependency of thermal power on the flow rate was found. As a result, the effectiveness and therefore the outlet temperature decreased with higher flow rates in liquid and solid PCM state.
- The mantle heat exchanger performed best with 2 L/min during discharge in liquid state. The effectiveness from 80 °C to 30 °C was 1.247, which means that the outlet temperature was higher than the average PCM temperature due to stratification.
- Combined use of spiral- and mantle heat exchanger with a flow rate of 2 L/min is considered advantageous for continuous discharge, because it provided rather high thermal power and outlet temperatures were above the corresponding SAT composite temperature in liquid state. However, during solidification thermal power was rather low and effectiveness was reduced by a factor of 3 in comparison to liquid state.

By discharge via the mantle heat exchanger in intervals of 2 – 24 hours it was possible to utilize heat of fusion with thermal power up to 4 kW (flow rate of 2 L/min) and with outlet temperatures close to those of the SAT composite. Application of several stores in parallel could enable heat supply in buildings utilizing discontinuous discharge of single stores. In this way, heat transfer restrictions during solidification of SAT composite could be solved and economically attractive heat stores could be applied for long-term heat storage.

Acknowledgements

This research was supported by the PhD program of the Sino Danish Center for Education and Research (SDC). The work was also supported by the European Commission as part of the Seventh Framework Programme of the European Community for Research, Technological Development and Demonstration Activities under the funding scheme of “Collaborative Project” through the COMTES consortium, Grant Agreement N° 295568. We thank our partner NILAN A/S for the good collaboration. Further we would like to thank the DTU research technician Claus Aagaard as well as Jakob Brinkø Berg, Yiliang Jiang and Andrea Hernandez Pedrero for their practical support.

References

- [1] B. Zalba, J.M. Marín, L.F. Cabeza, H. Mehling, Review on thermal energy storage with phase change: materials, heat transfer analysis and applications, *Appl. Therm. Eng.* 23 (2003) 251–283.
- [2] D. Zhou, C.Y. Zhao, Y. Tian, Review on thermal energy storage with phase change materials (PCMs) in building applications, *Appl. Energy*. 92 (2012) 593–605. doi:10.1016/j.apenergy.2011.08.025.
- [3] G. Englmaier, Y. Jiang, M. Dannemand, C. Moser, H. Schranzhofer, S. Furbo, J. Fan, Crystallization by local cooling of supercooled sodium acetate trihydrate composites for long-term heat storage, *Energy Build.* 180 (2018) 159–171. doi:10.1016/j.enbuild.2018.09.035.
- [4] M.A. Rogerson, S.S.S. Cardoso, Solidification in heat packs: I. Nucleation rate, *AIChE J.* 49 (2003) 505–515. doi:10.1002/aic.690490220.
- [5] M. Dannemand, M. Delgado, A. Lazaro, C. Penalosa, C. Gundlach, C. Trinderup, J.B. Johansen, C. Moser, H. Schranzhofer, S. Furbo, Porosity and density measurements of sodium acetate trihydrate for thermal energy storage, *Appl. Therm. Eng.* 131 (2018) 707–714. doi:10.1016/j.applthermaleng.2017.12.052.
- [6] W. Cui, Y. Yuan, L. Sun, X. Cao, X. Yang, Experimental studies on the supercooling and melting/freezing characteristics of nano-copper/sodium acetate trihydrate composite phase change materials, *Renew. Energy*. 99 (2016) 1029–1037. doi:10.1016/j.renene.2016.08.001.
- [7] J. Guion, M. Teisseire, Nucleation of sodium acetate trihydrate in thermal heat storage cycles, *Sol. Energy*. 46 (1991) 97–100.
- [8] N. Beaupere, U. Soupremanien, L. Zalewski, Nucleation triggering methods in supercooled phase change materials (PCM), a review, *Thermochim. Acta.* 670 (2018) 184–201. doi:10.1016/j.tca.2018.10.009.
- [9] W. Kong, M. Dannemand, J. Berg Johansen, J. Fan, S. Furbo, Experimental investigations on phase separation for different heights of sodium acetate water mixtures under different conditions, *Appl. Therm. Eng.* (2019). doi:10.1016/j.applthermaleng.2018.10.017.
- [10] M. Dannemand, J.B. Johansen, S. Furbo, Solidification behavior and thermal conductivity of bulk sodium acetate trihydrate composites with thickening agents and graphite, *Sol. Energy Mater. Sol. Cells.* 145 (2016) 287–295. doi:10.1016/j.solmat.2015.10.038.
- [11] W. Kong, M. Dannemand, J.B. Johansen, J. Fan, J. Dragsted, G. Englmaier, S. Furbo, Experimental investigations on heat content of supercooled sodium acetate trihydrate by a simple heat loss method, *Sol. Energy*. 139 (2016) 249–257. doi:10.1016/j.solener.2016.09.045.
- [12] J. Pereira da Cunha, P. Eames, Thermal energy storage for low and medium temperature applications using phase change materials - A review, *Appl. Energy*. 177 (2016) 227–238. doi:10.1016/j.apenergy.2016.05.097.
- [13] M. Saffari, A. de Gracia, C. Fernández, L.F. Cabeza, Simulation-based optimization of PCM melting temperature to improve the energy performance in buildings, *Appl. Energy*. 202 (2017) 420–434. doi:10.1016/j.apenergy.2017.05.107.
- [14] P.A.J. Donkers, L.C. Sögütöglü, H.P. Huinink, H.R. Fischer, O.C.G. Adan, A review of salt hydrates for seasonal heat storage in domestic applications, *Appl. Energy*. 199 (2017) 45–68. doi:10.1016/j.apenergy.2017.04.080.
- [15] C. Liu, D. Groulx, Experimental study of the phase change heat transfer inside a horizontal cylindrical latent heat energy storage system, *Int. J. Therm. Sci.* 82 (2014) 100–110. doi:10.1016/j.ijthermalsci.2014.03.014.
- [16] A. López-navarro, J. Biosca-taronger, J.M. Corberán, C. Peñalosa, A. Lázaro, P. Dolado, J. Payá, Performance characterization of a PCM storage tank, *Appl. Energy*. 119 (2014) 151–162. doi:10.1016/j.apenergy.2013.12.041.
- [17] C. Zauner, F. Hengstberger, B. Mörzinger, R. Hofmann, H. Walter, Experimental characterization and simulation of a hybrid sensible-latent heat storage, *Appl. Energy*. 189 (2017) 506–519. doi:10.1016/j.apenergy.2016.12.079.
- [18] A. Frazzica, M. Manzan, A. Sapienza, A. Freni, G. Toniato, G. Restuccia, Experimental testing of a hybrid sensible-latent heat storage system for domestic hot water applications, *Appl. Energy*. 183 (2016) 1157–1167. doi:10.1016/j.apenergy.2016.09.076.

- [19] Z. Ma, H. Bao, A.P. Roskilly, Study on solidification process of sodium acetate trihydrate for seasonal solar thermal energy storage, *Sol. Energy Mater. Sol. Cells*. 172 (2017) 99–107. doi:10.1016/j.solmat.2017.07.024.
- [20] M. Dannemand, J. Dragsted, J. Fan, J.B. Johansen, W. Kong, S. Furbo, Experimental investigations on prototype heat storage units utilizing stable supercooling of sodium acetate trihydrate mixtures, *Appl. Energy*. 169 (2016) 72–80. doi:10.1016/j.apenergy.2016.02.038.
- [21] M. Dannemand, J.B. Johansen, W. Kong, S. Furbo, Experimental investigations on cylindrical latent heat storage units with sodium acetate trihydrate composites utilizing supercooling, *Appl. Energy*. 177 (2016) 591–601. doi:10.1016/j.apenergy.2016.05.144.
- [22] J. Deng, S. Furbo, W. Kong, J. Fan, Thermal performance assessment and improvement of a solar domestic hot water tank with PCM in the mantle, *Energy Build.* 172 (2018) 10–21. doi:10.1016/j.enbuild.2018.04.058.
- [23] G. Englmaier, C. Moser, S. Furbo, M. Dannemand, J. Fan, Design and functionality of a segmented heat-storage prototype utilizing stable supercooling of sodium acetate trihydrate in a solar heating system, *Appl. Energy*. 221 (2018) 522–534. doi:10.1016/j.apenergy.2018.03.124.
- [24] G. Englmaier, W. Kong, J.B. Berg, S. Furbo, J. Fan, Demonstration of a solar combi-system utilizing stable supercooling of sodium acetate trihydrate for heat storage, submitted to *Appl. Therm. Eng.*, in review.
- [25] G. Englmaier, C. Moser, H. Schranzhofer, J. Fan, S. Furbo, A solar combi-system utilizing stable supercooling of sodium acetate trihydrate for heat storage: numerical performance investigation, *Appl. Energy*. 242 (2019) 1108–1120. doi:10.1016/j.apenergy.2019.03.125.
- [26] C. Rathgeber, E. Lävemann, A. Hauer, Economic top-down evaluation of the costs of energy storages -A simple economic truth in two equations, *J. Energy Storage*. 2 (2015) 43–46. doi:10.1016/j.est.2015.06.001.
- [27] The International Association for the Properties of Water and Steam, The IAPWS Industrial Formulation 1997 for the Thermodynamic Properties of Water and Steam, IAPWS R7-97 (2012).
- [28] N. Araki, M. Futamura, A. Makino, H. Shibata, Measurements of Thermophysical Properties of Sodium Acetate Hydrate, *International J. Thermophys.* 16 (1995) 1455–1466.
- [29] L.F. Cabeza, G. Svensson, S. Hiebler, H. Mehling, Thermal performance of sodium acetate trihydrate thickened with different materials as phase change energy storage material, *Appl. Therm. Eng.* 23 (2003) 1697–1704. doi:10.1016/S1359-4311(03)00107-8.
- [30] IG Chemicals, Specification sheet SAT E262i, Bad Salzufflen, Germany, 2015.
- [31] JCGM. Joint committee for guides in metrology: evaluation of measurement data – Guide to the expression of uncertainty in measurement (GUM), JCGM 100, 2008.
- [32] Kamstrup A/S, Technical Description of Ultraflow sensors, [Online]. Available: <https://products.kamstrup.com/index.php>. [Accessed: 27-Feb-2019]

The sensible heat capacity of melted sodium acetate trihydrate (SAT) can be utilized, while its heat of fusion is preserved loss-free at room temperature for on-demand supply. This heat storage concept was demonstrated for the first time with flat prototype units in a solar heating system using 22.4 m² (aperture) evacuated tubular solar collectors. The experimental findings were then used in system simulation with 1 m³ of SAT composite and a 0.6 m³ water tank in a Danish Passive House, resulting in a yearly solar fraction of 71%. Material tests showed that SAT composites crystallize in the range of -9 °C to -15 °C in contact with steel. The heat of fusion, available in supercooled state at 20 °C, was determined to be in the range of 205-216 kJ/kg. Further, inexpensive tank-in-tank units and nucleation by local cooling devices were proved to be applicable.

DTU Civil Engineering

Brovej Building 118
2800 Kongens Lyngby
Tlf. 45251700

www.byg.dtu.dk

8778775078